ERDC TR-11-8

Engineering Research and Development Center

US Army Corps of Engineers®
Engineer Research and Development Center

Risks to Navigation at the Matagorda Ship Channel Entrance, Texas, Phase 2: Evaluation of Significant Risk Factors

Stephen T. Maynord, Lihwa Lin, Nicholas C. Kraus,
Dennis W. Webb, Gary Lynch, Ronald E. Wahl,
Daniel A. Leavell, Don E. Yule, and Joseph B. Dunbar

August 2011

ERDC TR-11-8
August 2011

Risks to Navigation at the Matagorda Ship Channel Entrance, Texas, Phase 2: Evaluation of Significant Risk Factors

Stephen T. Maynord, Lihwa Lin, Nicholas C. Kraus, Dennis W. Webb, and Gary Lynch

Coastal and Hydraulics Laboratory
U.S. Army Engineer Research and Development Center
3909 Halls Ferry Road
Vicksburg, MS 39180-6199

Ronald E. Wahl, Daniel A. Leavell, Don E. Yule, and Joseph B. Dunbar

Geotechnical and Structures Laboratory
U.S. Army Engineer Research and Development Center
3909 Halls Ferry Road
Vicksburg, MS 39180-6199

Final report

Prepared for U.S. Army Corps of Engineers
Washington, DC 20314-1000

Abstract: The Phase 1 Matagorda study (Maynord et al. 2007) examined eight factors to identify which pose a significant risk of disrupting navigation at the Matagorda Ship Channel (MSC) entrance. Three factors were identified that warranted further study of the risk of disrupting navigation. These three factors were flanking of the jetty and slope protection, strong and asymmetric currents on the bay side of the peninsula and in the bottleneck (constricted portion of the entrance channel), and slope failures that constrict the channel, create adverse currents for navigation, or lead to shoaling of the channel. The risk factor of flanking and breaching of the jetty and slope protection was found to have a minimal risk of disrupting navigation because the cross current through the breach is weak compared to the longitudinal current in the navigation channel. The risk factor of slope failure from the continuing scour of the channel bottom will have a minimal risk of disrupting navigation because the size of the slope failures are not large enough to disrupt currents or cause shoaling problems. However, slope failures will increase in frequency and severity due to the continuing scour of the bottleneck. The risk factor of strong and asymmetric currents poses a significant risk of grounding in the existing navigation channel. In the bottleneck, surface currents at the center of the channel equal or exceed 3 knots more than 60 percent of the time and equal or exceed 5 knots 20 percent of the time. Based on expert elicitation of the pilots, the reach between the bottleneck and Sundown Island (B SI) is the reach most likely to experience a powered grounding. A ship simulator was used to evaluate the effects of removal of the bottleneck.

The Phase 2 MSC study recommends use of a “current window” that limits navigation to periods when current in the bottleneck is less than 5 knots. Daylight restricting all deep draft navigation should be considered. If the 5-knot current window and daylight restriction of all navigation cause unacceptable restrictions on navigation, the structural alternative of bottleneck removal will significantly reduce the likelihood of a powered grounding at the MSC Entrance. Relocation of Sundown Island should reduce adverse cross current effects in the bay.

Contents

Figures and Tables

Figures

Tables

Preface

This report documents a study performed to evaluate three factors that were identified as posing a potential risk of disrupting navigation at the Matagorda Ship Channel entrance, TX. The work reported herein was conducted for the U.S. Army Engineer District, Galveston.

This study was performed by the U.S. Army Engineer Research and Development Center, Coastal and Hydraulics Laboratory, during 2007. John J. Otis was the SWG Project Manager. The report was written by Dr. Stephen T. Maynord and Gary C. Lynch, Navigation Branch; Dr. Lihwa Lin, Coastal Engineering Branch; Dr. Nicholas C. Kraus, Senior Scientists Group; Dennis W. Webb, Chief of the Navigation Branch, CHL; and Ronald E. Wahl, Don E. Yule, Daniel A. Leavell, and Joseph B. Dunbar, Geotechnical and Structures Laboratory. J. Holley Messing, CEB, completed final formatting of the report. Work was performed under the general administrative supervision of Dr. Jack E. Davis, Acing Chief of the Navigation Division, CHL; Dr. M. Rose Kress, Deputy Director, CHL; and Dr. William D. Martin, Director, CHL.

COL Gary E. Johnson was Commander and Executive Director of ERDC. Dr. Jeffery P. Holland was Director.

Unit Conversion Factors

Multiply	By	To Obtain
cubic feet	0.02831685	cubic meters
cubic yards	0.7645549	cubic meters
degrees (angle)	0.01745329	radians
feet	0.3048	meters
inch	2.54	centimeters
knots	0.5144444	meters per second
miles (nautical)	1,852	meters
miles (U.S. statute)	1,609.347	meters
miles per hour	0.44704	meters per second
pounds (force)	4.448222	newtons
pounds (force) per square foot	47.88026	pascals
pounds (mass)	0.45359237	kilograms
pounds (mass) per cubic foot	16.01846	kilograms per cubic meter
pounds (mass) per square foot	4.882428	kilograms per square meter
slugs	14.59390	kilograms
square feet	0.09290304	square meters
tons (force)	8,896.443	newtons
yards	0.9144	meters

1 Introduction

The U.S. Army Engineer District, Galveston (hereafter, the Galveston District), requested that the Coastal and Hydraulics Laboratory (CHL), U.S. Army Engineer Research and Development Center (ERDC), U.S. Army Corps of Engineers (USACE) conduct an evaluation of the risks to navigation for the Matagorda Ship Channel (MSC) entrance, TX. The MSC entrance passes through Matagorda Peninsula and connects the Gulf of Mexico to Matagorda Bay to provide deep-draft navigation. The area of concern in this study was the jettied entrance, the bottleneck portion (constricted channel) through the peninsula, and the portion of the channel subject to modifications of the tidal current by Sundown (Bird) Island on the bay side of the peninsula (Figure 1). The study does not include traffic in the Gulf Intracoastal Waterway (GIWW) or the intersection of the GIWW and the MSC. The assessment of risks of navigation disruption is limited to the Federal deep-draft navigation project. ERDC conducted a Phase 1 Study (Maynord et al. 2007) that examined the following eight potential risks to navigation.

1. Jetty failure from hurricanes.
2. Shoaling from hurricanes.
3. Asymmetric currents from partial jetty failure.
4. Long-term deterioration of jetties.
5. Breaching of peninsula away from MSC.
6. Flanking of jetties of jetties or slope protection.
7. Strong and asymmetric current on the bay side of the peninsula and in the bottleneck.
8. Channel bottom scour leading to slope failures that constrict the channel, create adverse currents for navigation, or lead to shoaling of the channel.

The phase 1 study identified three factors requiring further study:

1. Flanking of the jetties or slope protection.
2. Strong and asymmetric current on the bay side of the peninsula and in the bottleneck.
3. Slope failures that constrict the channel that creates adverse currents for navigation or lead to shoaling of the channel.

Figure 1. MSC entrance reach (Top of photo is North).

The Phase 2 Matagorda study documented herein separates these three risk factors into operational risk factors (adverse current) and structural risk factors (flanking and slope failure). This Phase 2 study evaluated in detail the three factors identified in the Phase 1 Study. The MSC entrance study by Kraus et al. (2006) for the Galveston District was depended upon herein and provides background and history of the project.

In evaluating the various components of the MSC entrance, this study makes the distinction between the section with dual jetties that extends into the Gulf of Mexico and the slope-protection section that stabilizes the cut through Matagorda Peninsula. The slope protection channel through Matagorda Peninsula is also referred to as the bottleneck because of its lesser channel width. The bottleneck has a top width of about 950 ft compared to 2,000 ft between the jetties. Because the MSC has a north-

west to southeast alignment, the jetties and shorelines have been referred to as either north and south or east and west. As used herein, the jetty and shoreline on the northeast side of the channel are referred to as the north jetty and north shoreline. The jetty and shoreline on the southwest side of the channel are referred to as the south jetty and south shoreline. The segments on both the north and south sides of the channel joining the jetty channel to the slope protection channel and bottleneck are referred to as spurs.

After evaluating the risks related to navigation, two non-structural alternatives and the structural risk reduction alternative of bottleneck removal are evaluated. Bottleneck removal was proposed in Kraus et al. (2006) and is evaluated therein.

Water level is presented as either mean sea level (MSL) or the Galveston District navigation datum mean low tide (MLT). Numerical results are presented in MSL, and and bathymetry data are presented in MLT. Based on the 2007 bathymetry data collected by SURVCON, Inc., elevation in North America Vertical Datum (NAVD) is equal to elevation in MLT minus 1.0 ft in the study reach. The two water level gages in the study area, Port Lavaca and Port O'Connor, do not presently have acceptable ties between NAVD and MSL. The gage at Rockport, located approximately 40 miles southwest of Port O'Connor, has a published relationship between MSL and NAVD. Elevation in MSL is equal to elevation in NAVD minus 0.75 ft. Based on combining these two relationships, elevation in MSL = elevation in MLT minus 1.75 ft. For example, a channel bottom elevation of -40 ft MLT would be -41.75 ft MSL.

The following three chapters individually examine the three identified risks of flanking of the jetty or slope protection, strong and asymmetric current on the bay side of the peninsula and in the bottleneck, and channel bottom scour leading to slope failures that constrict the channel, creates adverse currents for navigation, or leads to shoaling of the channel. Chapter 5 provides a summary and conclusions of this study. The appendices contain further technical documentation described in the main text of this report.

2 Structural Risk to Navigation- Flanking of Jetties and Slope Protection

General

The landward ends of the MSC jetties are deteriorating. As a result of this deterioration and lowered beach and dunes adjacent to the jetties, there are overwash occurrences during times of high water level during cold front passage, tropical storms, and hurricanes. The impoundment of water at the south jetty and overwash channels on both south and north sides of the bottleneck, as observed in aerial photographs (Figures 2 and 3) taken over the past several years, indicate the potential risk of major breaches in the next tropical storm or hurricane. Once open, such breaches may not close, compromising the navigation project due to stranding of the jetty, a large increase in sand shoaling in the channel, and a possible crosscurrent.

Figure 2. Overwash channels and ponds landward of north jetty.

Figure 3. Overwash channels and impoundment of water landward of south jetty.

Storm conditions

In this risk assessment study, evaluation of the consequences of flanking at the jetties was based on numerical simulations for the 50-year life-cycle storm, a most likely severe storm to occur at MSC based on historical observation (Table 1). Thirty-five historical tropical storms with calculated or observed storm surges greater than 0.1 m at the MSC were selected from 1886 to 2005 for the life-cycle risk analysis. Table 1 presents the storm category (based on the wind strength and center pressure data on Saffir-Simpson Hurricane Wind Scale, http://www.nhc.noaa.gov/aboutsshs.shtml) and surge information, and Table 2 presents the tropical storm parameters. Figure 4 shows the storm track map. For the 35 analyzed cyclones, the mean and standard deviation of the storm moving speeds are 12 and 4 mph, respectively. The mean and standard deviation of the effective storm surge duration, defined as the time interval corresponding to the water level greater than 95 percent of the peak surge, are 6 and 2 hr, respectively. Using a stationary hurricane model and the Empirical Simulation Technique (Scheffner et al. 1999), the storm surge, maximum wind speed, and central pressure deficit were calculated for the return periods between 50 and 1,000 years. The Empirical Simulation Technique

Table 1. Tropical storms from 1886-2005 affecting MSC.

Storm No.	Year/Month	Name	Category	Storm Surge (m)	Source*
1	1886/Aug	None	4	1.3	a
2	1886/Sep	None	2	1.0	a
3	1900/Aug	None	4	0.8	b
4	1909/Jun	None	2	0.3	a
5	1909/Jul	None	3	0.4	a
6	1916/Aug	None	4	1.2	a
7	1919/Sep	None	4	2.8	b
8	1929/Jun	None	1	1.2	a
9	1933/Sep	None	3	0.5	a
10	1934/Jul	None	1	1.3	b
11	1936/Jun	None	1	0.8	b
12	1941/Sep	None	1	0.5	c
13	1942/Aug	None	3	2.5	b
14	1945/Aug	None	4	2.1	a
15	1957/Jun	Audrey	4	0.3	a
16	1959/Jul	Debra	1	0.4	a
17	1961/Sep	Carla	5	3.8	a, c
18	1970/Aug	Celia	3	3.5	a, c
19	1971/Sep	Fern	5	0.4	a
20	1971/Sep	Edith	1	1.4	a
21	1973/Sep	Delia	0	0.4	a
22	1980/Aug	Allen	5	1.5	a
23	1983/Aug	Alicia	3	0.6	d
24	1998/Aug	Charley	0	0.6	d
25	1998/Sep	Frances	0	0.8	d
26	2001/Jun	Allison	0	0.3	d
27	2002/Aug	Bertha	0	0.2	d
28	2002/Sep	Fay	0	0.4	d
29	2002/Sep	Lili	4	0.3	d
30	2003/Jul	Claudette	1	2.2	d
31	2003/Aug	Erika	1	0.1	d
32	2003/Aug	Grace	0	0.2	d
33	2004/Sep	Ivan	5	0.4	d
34	2005/Jul	Emily	5	0.5	d
35	2005/Sep	Rita	5	0.7	d

NOTE: a: numerical simulation (Scheffner et al. 1994) ; b: historical data; c: post-storm report (U.S. Army Engineer District Corps of Engineers, Galveston, TX); d: Texas Coastal Ocean Observation Network (http://lighthouse.tamucc.edu/TCOON/HomePage).

Table 2. Properties of tropical storms from 1986-2005 affecting MSC.

Storm No.	Storm Radius (km)	Max Wind Speed (knot)	Central Pressure (mb)	Storm Forward Speed (m/sec)	Peak Surge Duration (hr)
1	34.5	135	925	5.5	4.2
2	35.7	85	973	2.7	8.8
3	37.0	125	936	6.0	4.2
4	38.0	85	972	3.7	7.0
5	40.0	100	959	5.0	5.5
6	34.0	115	932	9.0	2.5
7	34.0	125	931	4.6	5.0
8	39.0	75	979	5.2	5.0
9	35.0	110	958	6.0	4.0
10	41.0	65	985	6.0	5.0
11	40.0	70	982	3.0	9.0
12	40.0	75	977	4.5	6.0
13	35.0	100	964	7.0	3.5
14	37.0	120	955	2.5	10.0
15	38.0	125	946	7.2	3.5
16	42.0	75	979	2.0	14.0
17	32.0	150	931	3.0	7.0
18	38.0	110	945	7.0	3.7
19	41.0	85	977	6.7	4.1
20	41.0	75	979	3.0	9.5
21	41.0	60	986	5.0	6.0
22	28.0	155	909	6.0	3.0
23	41.0	100	963	2.5	10.0
24	41.0	60	1001	6.0	4.5
25	41.0	55	990	5.5	5.0
26	43.0	50	1002	5.3	5.3
27	44.0	35	1008	3.1	9.5
28	41.0	50	998	1.5	20.0
29	34.0	125	940	7.6	3.0
30	41.0	75	982	4.5	6.0
31	38.0	65	988	8.5	3.0
32	44.0	35	1007	8.0	3.5
33	43.0	50	998	7.5	3.8
34	33.5	110	944	5.0	4.5
35	36.0	115	924	5.0	5.0

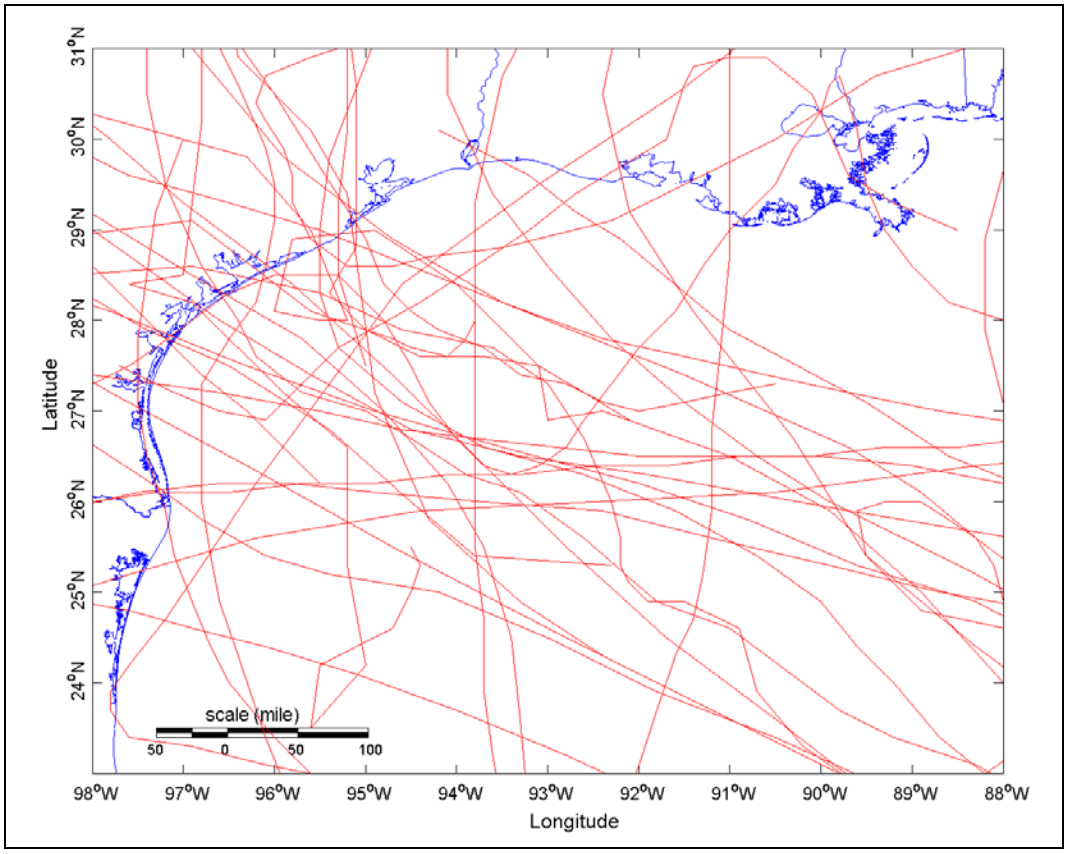

Figure 4. Tropical cyclone tracks.

is a conventional method for simulating multiple life-cycle sequences of multiparameter systems such as hurricanes and their environmental impacts. It generates frequency-of–occurrence relationships to ensure that the future events are statistically similar in magnitudes and frequency to past events. It is by far the most applied, computationally inexpensive, and accepted method for any frequency-related phenomena. The use of a stationary hurricane model over a non-stationary hurricane is to eliminate the randomness of storm movement to reduce the uncertainty in the frequency-0f-occurrence analysis. The corresponding significant wave height and peak period were calculated as a function of the maximum wind speed by the deepwater formulas described in the *Coastal Engineering Manual* (2002). Table 3 presents the calculated storm surge, maximum wind speed, and significant wave height and peak period for the life cycles between 50 and 1,000 years. Appendix A summarizes the methodologies and calculations in the life-cycle risk analysis.

Table 3. Hurricane surge, maximum wind, maximum wave life-cycle predictions.

Return Period (year)	50	100	200	300	400	500	600	700	800	900	1,000
Storm surge (m)	3.5	4.2	5.0	5.4	5.7	6.0	6.1	6.3	6.5	6.6	6.7
Max wind speed* (mph)	139	149	155	158	160	161	162	163	164	165	165
Max wind speed** (mph)	151	161	167	170	172	173	174	175	176	177	177
Sig. wave height** (m)	12.9	14.7	15.8	16.4	16.8	17.0	17.1	17.3	17.5	17.6	17.7
Dominant period** (sec)	13.8	14.7	15.2	15.5	15.7	15.8	15.9	16.0	16.1	16.1	16.1

* Stationary hurricanes.

** Moving hurricanes with an average forward speed = 12 mph.

Storm wave simulation

Two two-dimensional (2D) numerical models, CMS-Flow and CMS-Wave from the Coastal Inlets Research Program's (CIRP) Coastal Modeling System (CMS) (Buttolph et al. 2006; Lin et al. 2008) were applied to simulate the flanking of the jetties. The CMS calculates changes in water level and current by tide, waves, and wind, and this information was fed to a sediment transport calculation and resultant morphology (depth) change. CMS-Flow (Militello et al. 2004) is a finite-difference model that solves 2D depth-integrated continuity and momentum equations of water motion for current and water level fields on a rectangular grid. The CMS grid can have variable cell sizes in the Cartesian coordinates. The CMS contains integrated calculations of sediment transport and morphology change through transport rate formulation, the advection-diffusion equation, and the sediment continuity equation. It can be driven by ocean tides, river flow, surface wind, as well as wave forcing.

Three sediment transport formulations are available in CMS: the Watanabe (1987), the Lund-CIRP (Camenen and Larson 2005, 2007), and the Advection-Diffusion (AD) equation (Buttolph et al. 2006). The Watanabe formula produces a total transport rate whereas the Lund-CIRP and AD equations compute both bed load and suspended load. Transport rates are applied in the sediment continuity equation to calculate the morphology change. The sediment calculation was recently upgraded to a finite-volume, non-equilibrium transport model to better simulate the natural sediment transport process.

CMS-Wave (Mase et al. 2005; Lin et al. 2008) is a wave spectral model that uses a forward-marching, finite-difference implicit-scheme to solve the wave action balance equation for the spatial variation of wave energy in the near shore around coastal structures. It calculates wave spectral transformation in a half-plane rectangular grid (e.g., wave energy is moved from offshore toward the coastline within a 0-to-180 degree sector of the primary incident wave direction at deepwater). The model contains theoretically developed approximations for both wave diffraction and reflection and is suited to wave simulations at coastal structures. Incident wave conditions are specified either as parameters (significant wave height, peak period, and peak wave direction) or 2D spectra (energy densities in frequency and direction spaces) at the seaward boundary. The primary output parameters are the wave height, period, and direction. The 2D wave spectra at special output locations, radiation stresses, and wave breaking fields may also be output.

CMS-Flow and CMS-Wave are coupled for the sediment transport and morphology change calculations. CMS-Flow calculates the water level, current, and sediment transport to update the morphology as input to CMS-Wave. Because waves, interacting with tidal currents and breaking in the nearshore, are considered as the main driving forces for the longshore current and sediment processes, the CMS-Wave calculates and outputs wave parameters and radiation stresses as the main driving forces to the CMS-Flow. Coupling CMS-Flow and CMS-Wave is accomplished on desktop computers in the Surface-water Modeling System (SMS) interface (Zundel 2006). The interface allows the generation of grids and the visualization of model results, and allows specification of the numerical parameters required for a simulation.

The CMS-Wave simulations were conducted on a regional grid and a local grid. The regional grid was used for the storm wave generation in the Gulf of Mexico, and the local grid was used for the nearshore wave transformation at the MSC. The simulation from the regional grid supplies the wave spectrum input to the local grid. The regional grid covered a rectangular area of 150 km × 150 km, with a constant cell size of 100-m × 100-m, that extended seaward from the Texas south central coast to the 1,000-m depth contour in the Gulf of Mexico. The size of the regional grid was so designed for CMS-Wave to generate all of the shoreward wave components from an approaching hurricane. CMS-Wave can simulate the full-plane wave generation but will require covering the entire Gulf of Mexico in the model, which seems

unnecessary in the present study. The local grid extends 4.4 km north and 3.8 km south of the MSC and 5.5 km seaward to the 12-m depth contour. It consisted of variable rectangular cell sizes, with the smallest cell of approximately 20 m × 20 m in the entrance channel to the largest cell of 150 m × 150 m at the seaward boundary. The bathymetry in the region grid was supplied by the Geophysical Data System for Hydrographic Survey Data (GEODAS) (http://gcmd.nasa.gov/records/ GEODAS.html). The bathymetry in the local grid was extracted from a grid developed in a previous study (Kraus et al. 2006) and incorporated with recent hydrographic and land surveys conducted in May 2008 and LiDAR data collected in August 2008 that covered the bottleneck and entrance channel area. Figure 5 shows the regional and local wave bathymetry grids where the depth contours are relative to MSL. The CMS-Flow grid covers a 10.6-km-long and 8.4-km-wide area that extended the local wave grid bayward to the south perimeter of GIWW in the bay (Figure 6). The bathymetry in the CMS-Flow grid incorporated the hydrographic survey conducted in January 2009 that covered the bay and the Bird Island area east of the navigation channel.

The CMS was configured to simulate a 50-year life-cycle hurricane, which corresponds to a 3.5-m storm surge (Category 3) with the maximum wind speed of 151 mph (Category 4) and significant waves of 12.9 m and 13.8 sec in the Gulf of Mexico. For the hurricane wave simulation in the regional grid, the average shoreward wind component was required and it was equal to 61 mph, as obtained by multiplying a conversion factor of 0.4051 to the maximum wind speed as part of a standard averaging technique. Three wave directions of east, southeast, and south were simulated for the direct impact of storm waves to the north jetty, the entrance channel, and the south jetty, respectively. Figure 7 is an example of a calculated wave height field for a hurricane incident from the south. The simulation result from the regional wave grid supplies the wave spectrum input to the local grid for the nearshore wave transformation at the MSC entrance.

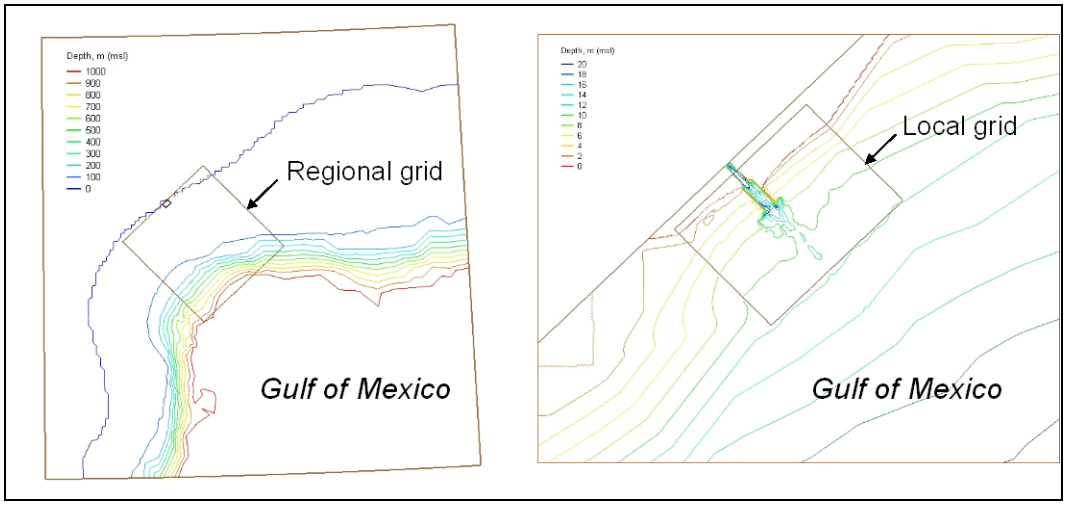

Figure 5. CMS-Wave regional and local bathymetry grids (MSL datum).

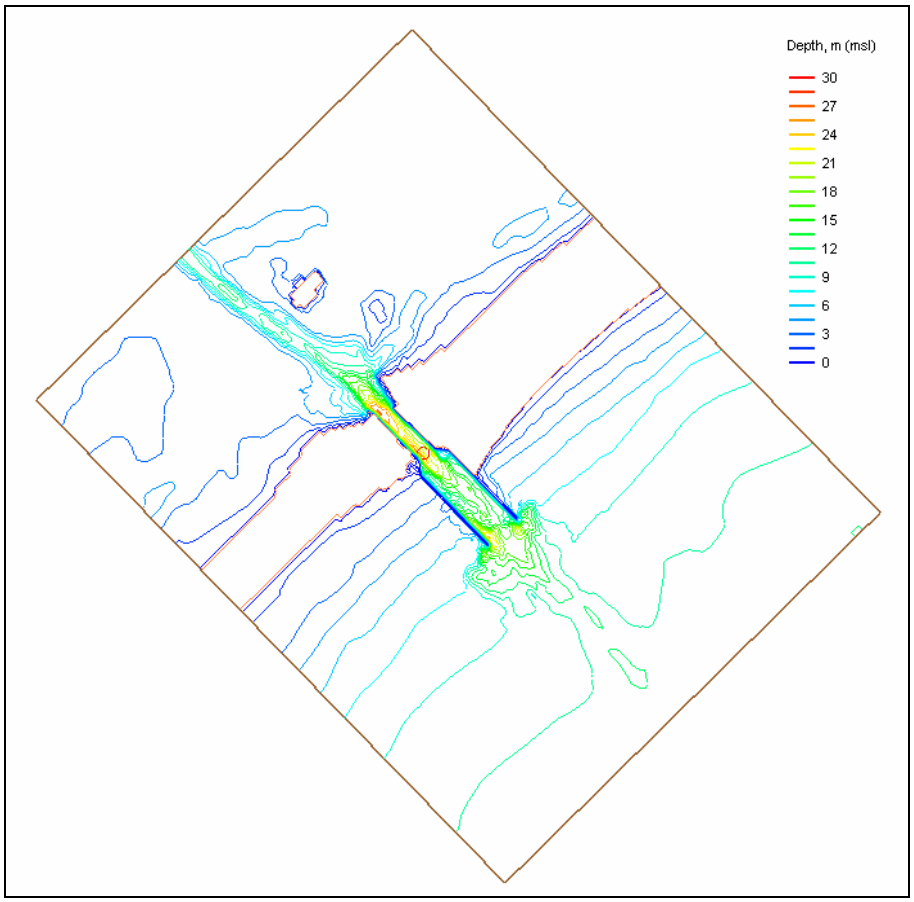

Figure 6. CMS-flow bathymetry grid (MSL datum).

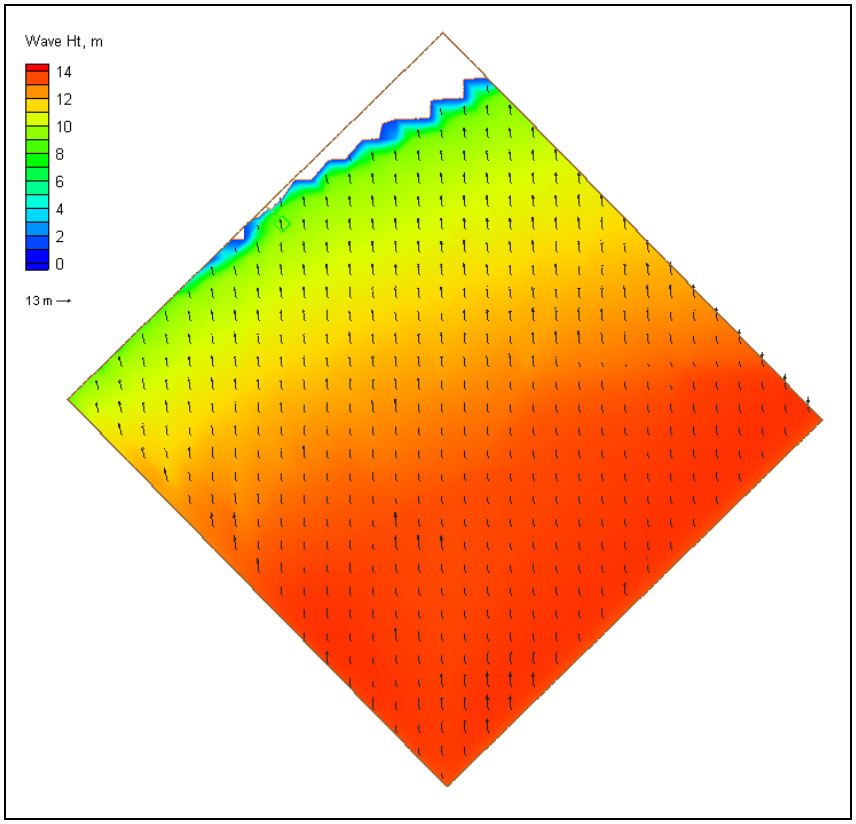

Figure 7. Calculated regional wave field for hurricane from south.

Breaching simulation

Breaching potential is great for elevated water level, because a high level allows waves and water flow to penetrate higher on land. The breaching simulations were conducted for a 50-year Category 3 storm surge in the local CMS grids for hurricanes from the east, southeast, and south using the incident waves calculated in the regional wave grid. The incident wave heights extracted from the regional grid for the local CMS grid are equal to 8.1, 9.3, and 7.5 m for hurricanes from the east, southeast, and south, respectively. The simulation run corresponded to a 12-hr period for which the water level was specified to increase linearly from 0 m to 3 m (MSL) in the first 3 hr and continued to rise to the maximum level of 3.5 m, including the normal tide in the next 1-hr period. The storm surge remained at the peak level of 3.5 m for 4 hr before receding gradually to 0 m at the end of the 12-hr simulation.

The CMS is capable of simulating a breach through coupled sediment transport and morphology change forced by combined waves and current. CMS-Wave was recently upgraded to calculate wave run-up and over-topping on beaches and jetties, which allows a realistic representation of

the extreme water levels that accompany storms. For the coupled wave and flow simulations, the current field was updated at 1-hr intervals after the current field was calculated. Sediment transport and morphology change were calculated at 1-min intervals. Local wave properties and radiation stresses computed by CMS-Wave were input to CMS-Flow, and the water level, current, and morphology change were calculated by CMS-Flow and fed back to CMS-Wave.

Wave run-up, with the water level rising at the beginning of the surge, promoted flow over the existing overwash channel and low crest segment of the jetties to initiate breaching. The jetty section presently residing on sand was allowed to be erodible, whereas the offshore end of the jetty was not erodible. As the water level continued to rise, erosion and scour occurred, and the breach expanded and deepened as a result of sediment transport calculated from higher waves and strong current. The breaching calculation terminated after the storm surge receded, because the breached area became dry.

A hydrodynamic time step of 0.5 sec was specified in CMS-Flow to satisfy the Courant criterion for stable numerical solutions. The sediment transport and morphology time step were specified as 0.5 and 9 sec, respectively. The AD equation was selected in the sediment transport calculation.

Figures 8 and 9 show calculated storm wave height contours during the peak surge for incident waves from the south and southeast, respectively, in the local CMS-Wave grid. Because the nearshore bottom slope was steeper along the beach east of the MSC entrance, waves broke closer to shore on the north beach than on the south beach. The calculated wave heights were slightly greater in the outer channel as waves coming from an oblique angle refracted across the deeper channel. Figures 10 and 11 show calculated current fields as input to CMS-Wave during the peak surge for incident waves from southeast and south, respectively. Hurricane waves approaching from the south generated a strong longshore current as a result of wave breaking in the nearshore. For a hurricane from the southeast, the waves were almost normal to the shoreline, providing a weak longshore current at the MSC entrance.

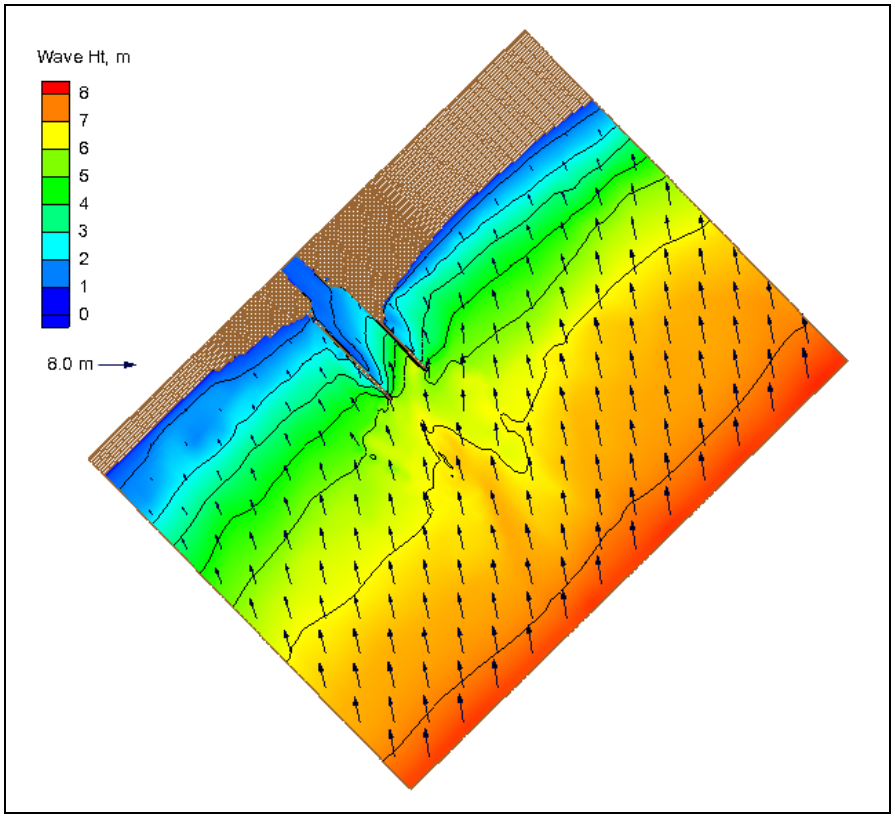

Figure 8. Calculated local wave field for hurricane from south.

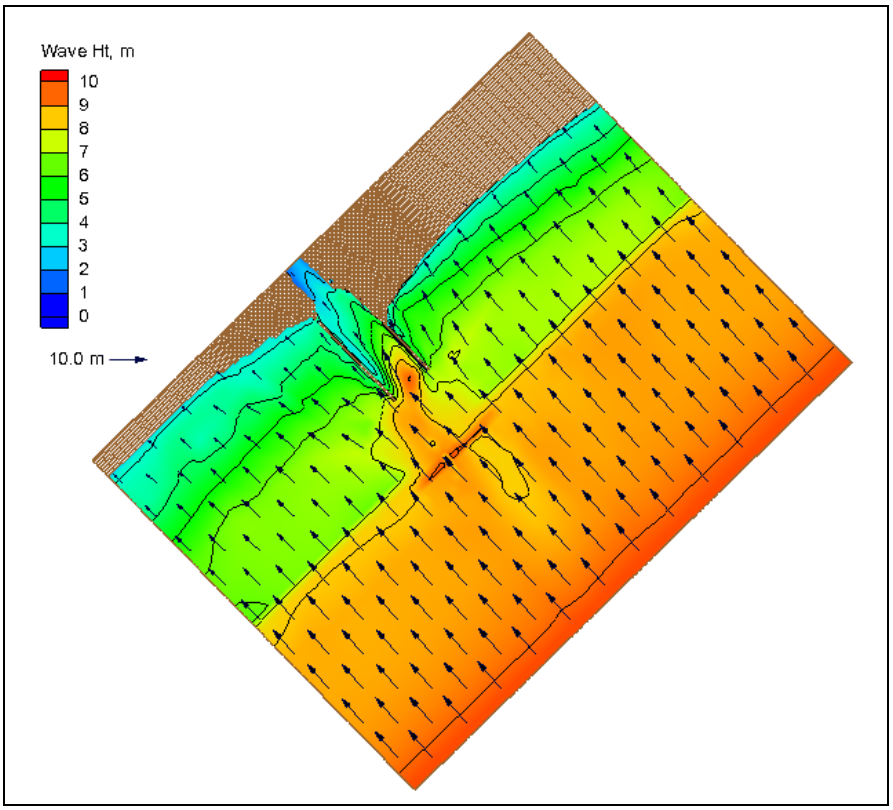

Figure 9. Calculated local wave field for hurricane from southeast.

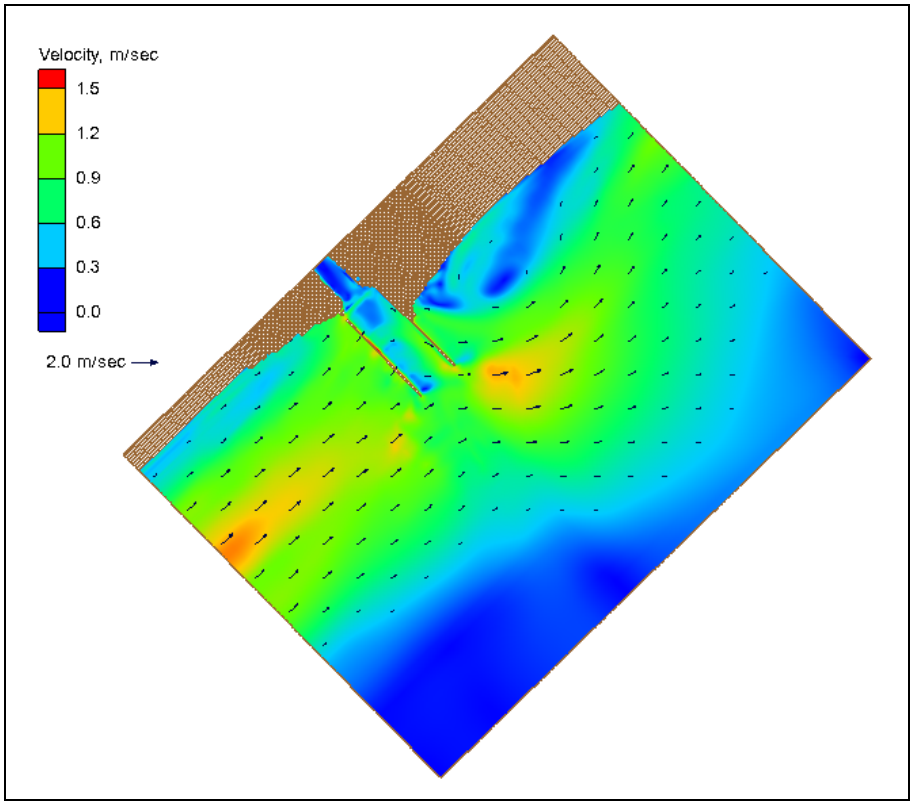

Figure 10. Calculated local current field for hurricane waves from south.

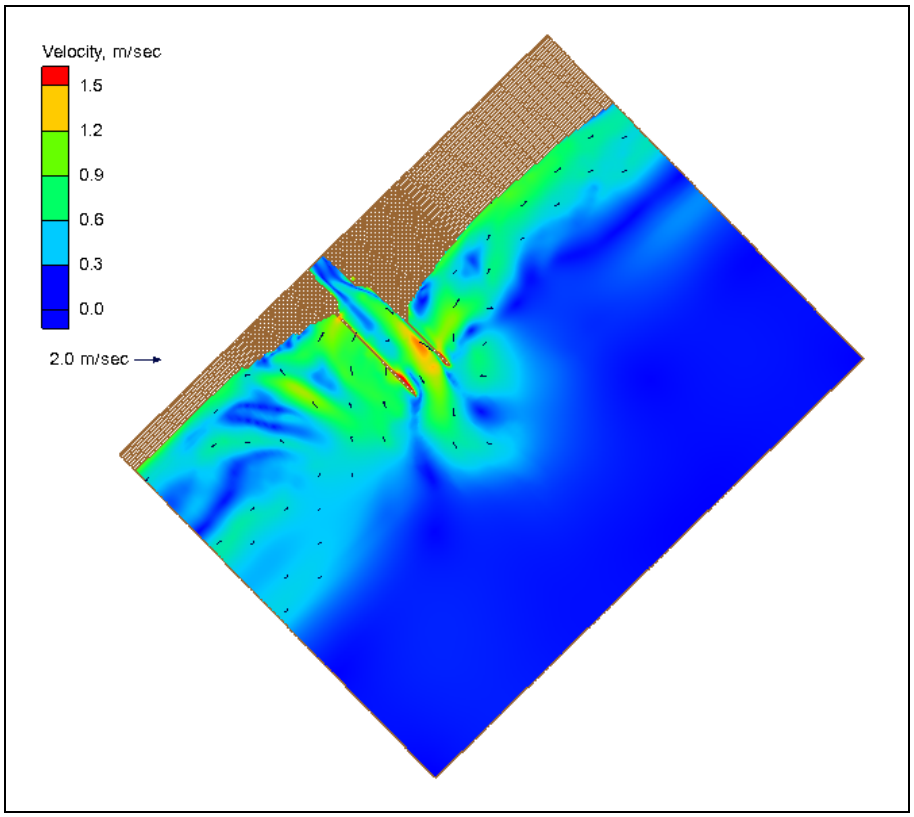

Figure 11. Calculated local current field for a hurricane waves from southeast.

Figures 12 to 14 show calculated morphology changes at the end of 12-hr simulations for hurricane waves from the east, south, and southeast, respectively. Positive values denote accretion (warm colors), and negative values denote erosion (cool colors). There is more channel scour in the bottleneck and between the two jetties for storm waves from the southeast, and more channel infilling between the two jetty tips. Figures 15 to 17 show the morphology changes in the enlarged area at the landward ends of jetties for waves from the east, south, and southeast, respectively. The model simulations showed the erosion on the beach and channel bank as a result of inundation from the higher water level and overwash and breaching at the landward end of jetties during the storm surge. Figures 18 and 19 show the three-dimensional (3D) view of depth contours and current fields corresponding to the 2nd and 12th hr, respectively, representing the pre- and post-storm surge conditions in the 12-hr simulation for hurricane waves from the south. The breaching at the south jetty and the scour on the channel bank in the bottleneck, which occurred during the storm surge, is clearly shown in Figure 19.

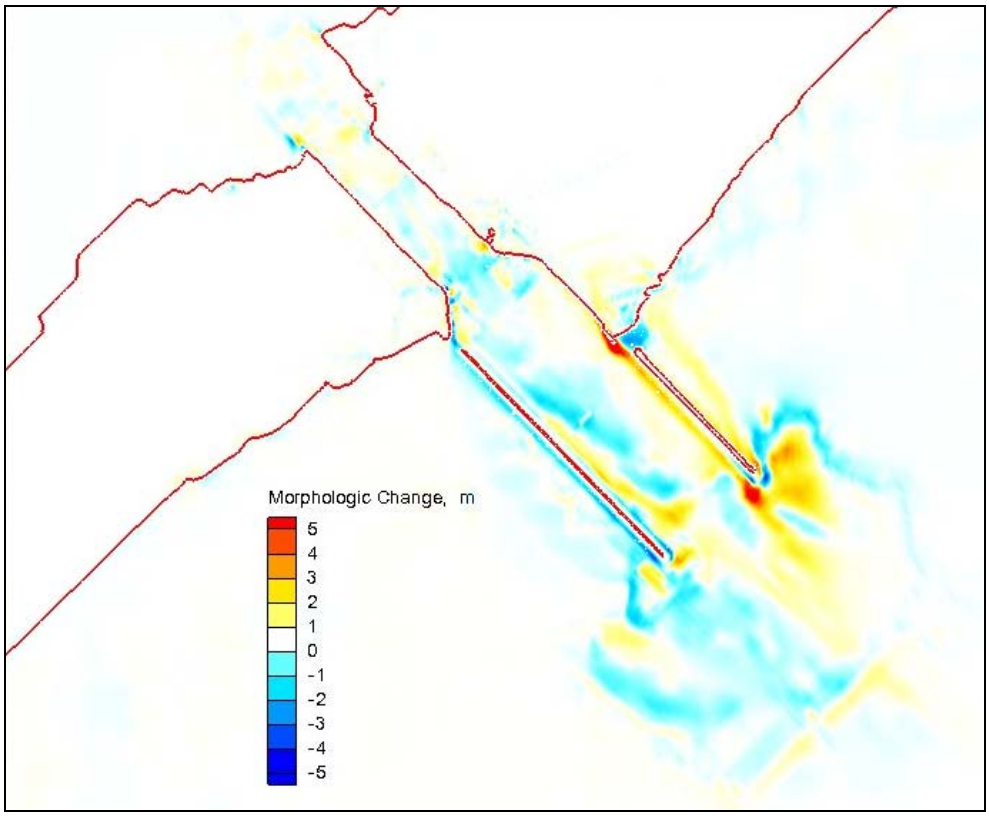

Figure 12. Calculated morphology change for hurricane waves from north.

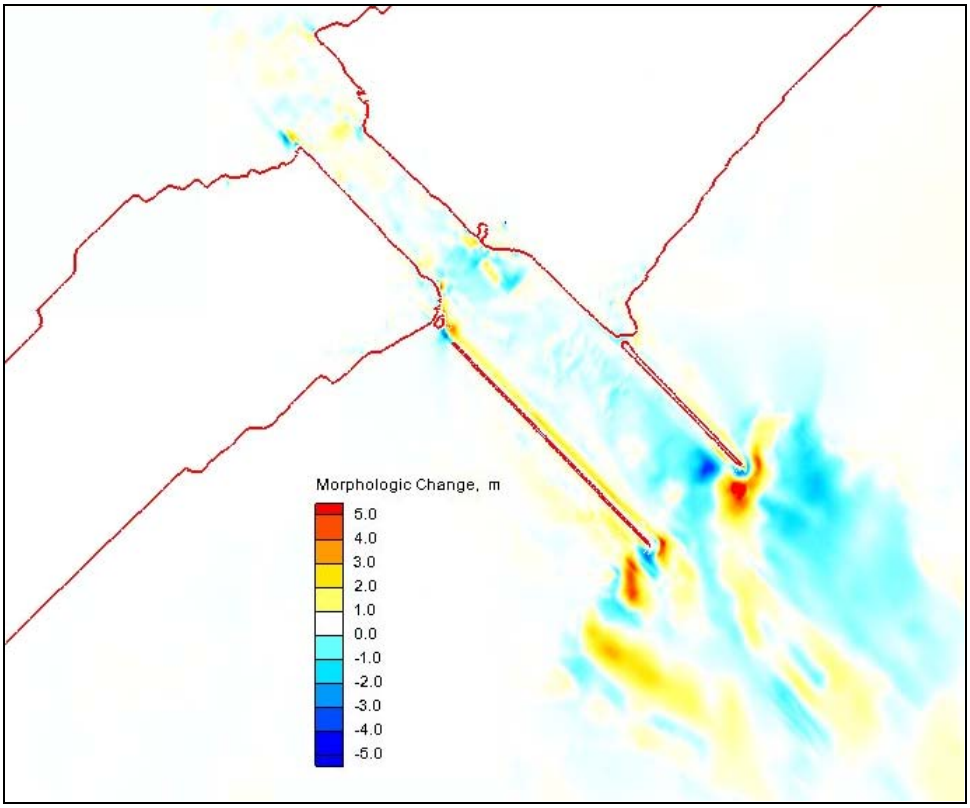

Figure 13. Calculated morphology change for hurricane waves from south.

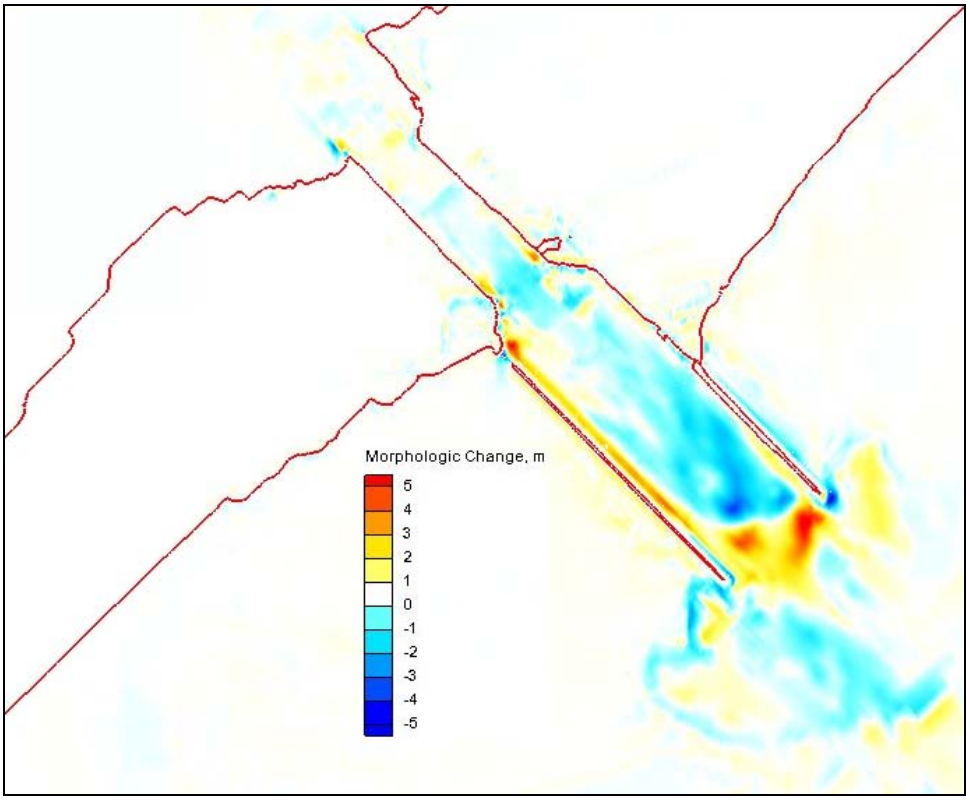

Figure 14. Calculated morphology change for hurricane waves from southeast.

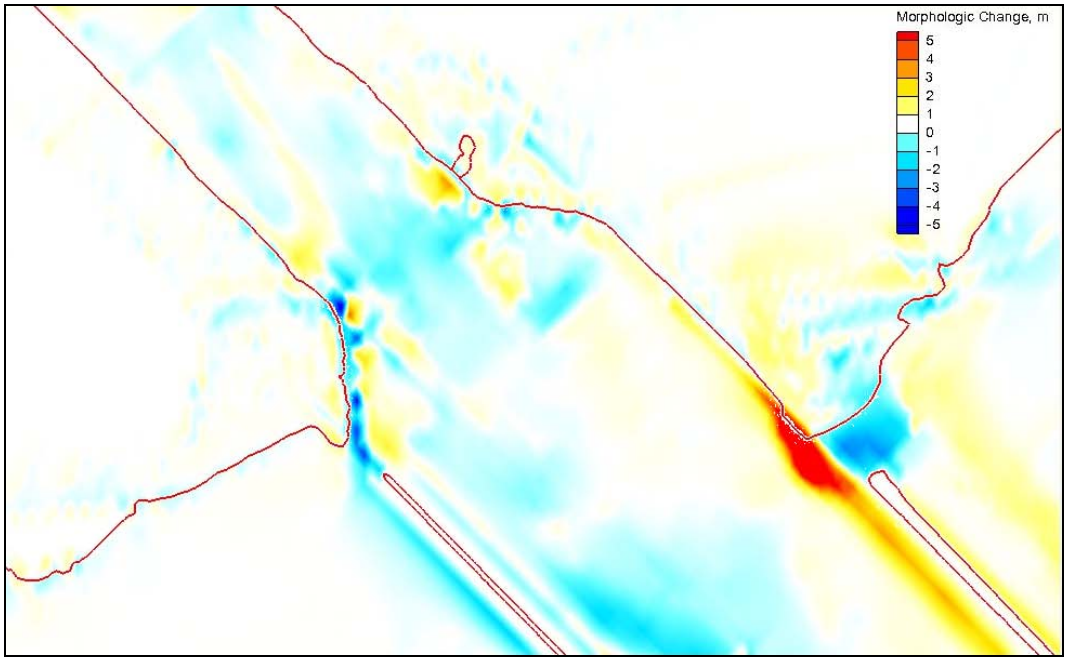

Figure 15. Calculated breaching for hurricanes waves from east.

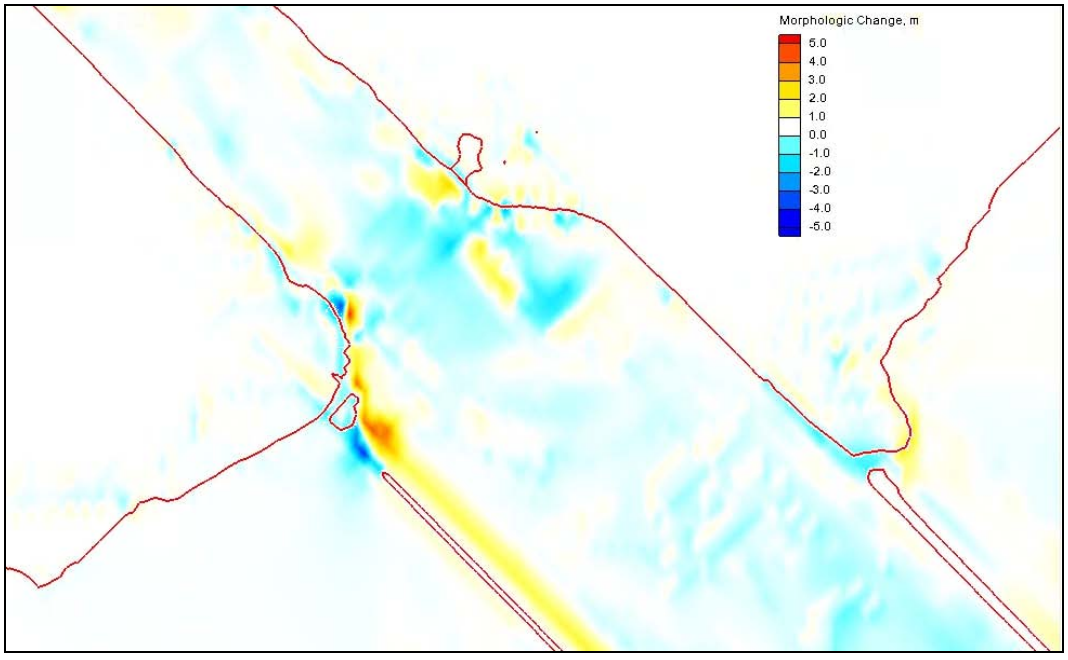

Figure 16. Calculated breaching for hurricanes waves from south.

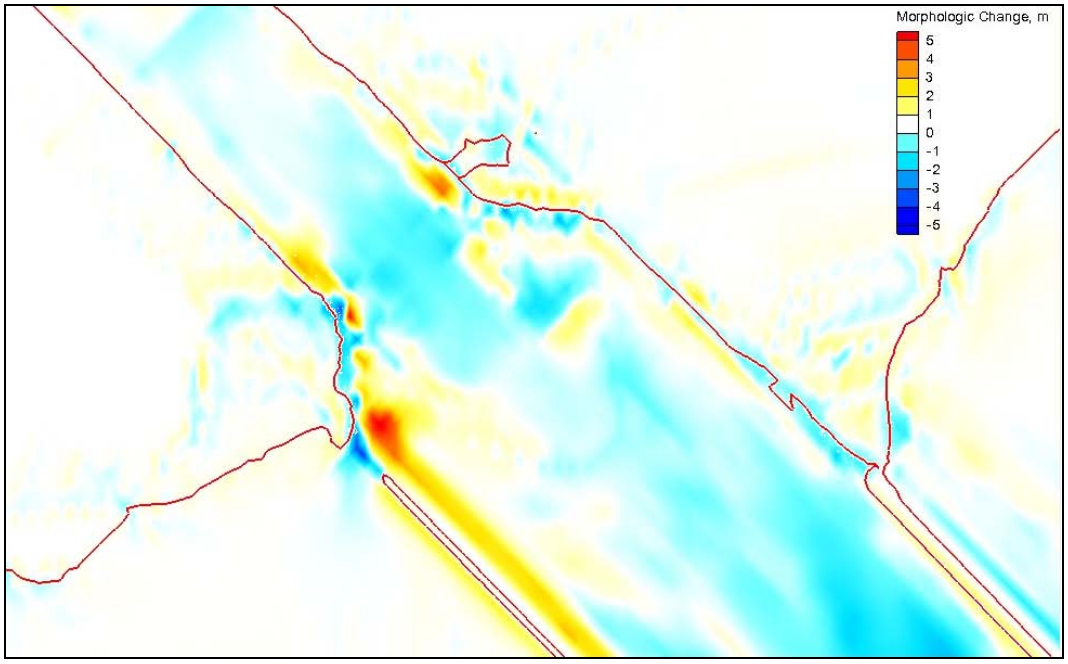

Figure 17. Calculated breaching for hurricanes waves from southeast.

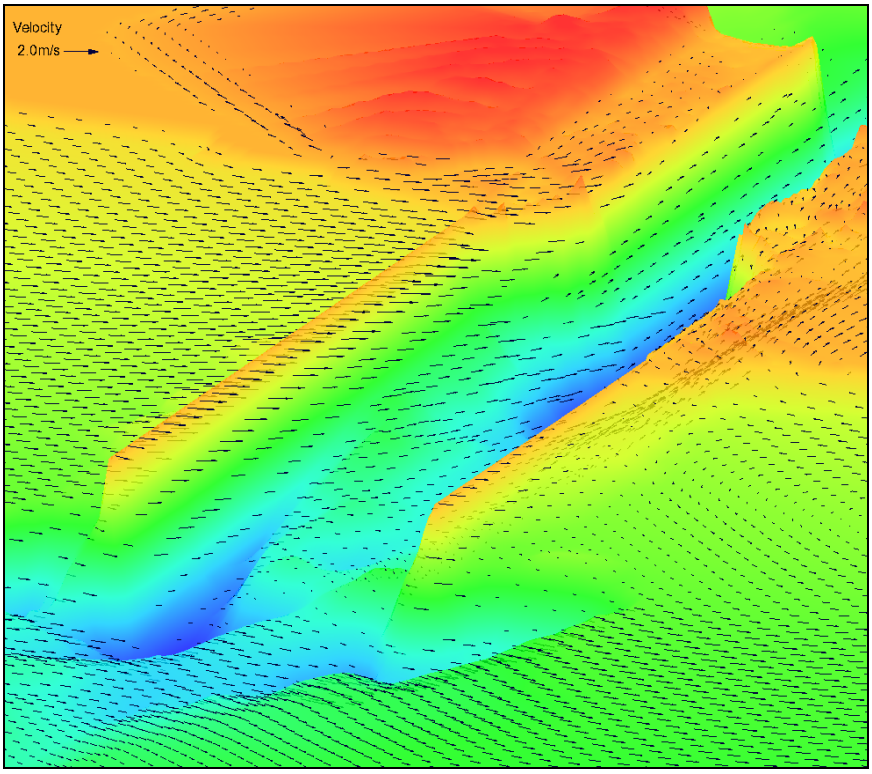

Figure 18. 3D view of calculated water depth and current field before peak storm surge for hurricane waves from south.

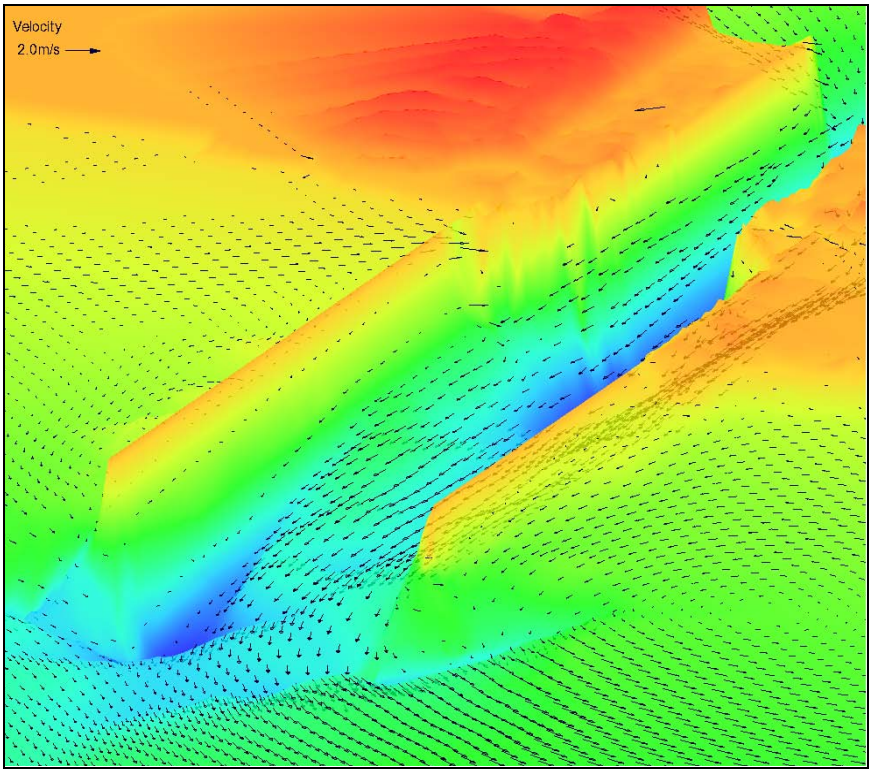

Figure 19. 3D view of calculated water depth and current field after peak storm surge for hurricane waves from south.

The CMS predicted a breach at the landward end of both jetties in the case of storm waves from the east or south. For storm waves from the south, a larger 150-m-wide and 3.5-m-deep breach occurred at the south jetty for waves from the south. For storm waves from the east, a larger 110-m-wide and 2.5-m-deep breach occurs at the north jetty. For the storm waves from southeast, only a 110-m-wide and 3-m-deep breach occurred at the south jetty. Sediment can enter the MSC entrance channel through the breach under combined storm wave and current actions. However, because of the strong current in the bottleneck during the hurricane, the sediment that enters the MSC through the breach tended to deposit near the breach along the jetty or in the channel bank area.

Post-hurricane simulation

The impact of breaching and flanking at the landward ends of the jetties during hurricane passage was evaluated by the simulation of post-storm conditions. The new bathymetry from the Category 3 hurricane surge simulation was specified as the initial bathymetry for the post-storm condition. Two different periods were modeled: (1) 1-14 January 2004 and, (2) 1-10 June 2008. The period of 1-14 January 2004, covered a spring tide

and a winter cold front passage with small river discharges from the Colorado River and Lavaca River. The period of 1-10 June 2008 represented a typical summer condition with prevalent southeasterly winds and a daily sea breeze, also with small river discharges into the bay. Figures 20 and 21 show the water level, wind, and river flow data collected in these two periods. For each, the hydrodynamics in the regional domain covering the entire Matagorda Bay and East Matagorda Bay was calculated by a regional model forced by the water level in the Gulf of Mexico, river discharges in the bay, and wind fields over the model domain. Figure 22 shows the regional grid. The regional model was run for January 2004 in the previous study (Kraus et al. 2006). The calculated water levels and current vectors from the regional model served as input to CMS in the local grid that covers the MSC entrance.

For the period of 1-14 January 2004, three CMS runs were conducted: (1) a large south jetty breach (from the simulation of Category 3 hurricane waves from the south) and a constant 1-m, 6-sec incident wave from the south, representing the winter average wave condition from the south, (2) a large north jetty breach (from the simulation of Category 3 hurricane waves from the east) and a constant 2-m, 8-sec incident wave from the east, representing the winter average wave condition from the east, and (3) the existing configuration (no breach) and a constant 2-m, 8-sec wave from the east. These 14-day simulations showed that the initial breach from the hurricane waves can become slightly deeper, with the maximum depth increased approximately by 0.5 m, but not wider in the post-storm condition. Sediment from the longshore transport can enter the MSC entrance through the breach, but it was quickly carried away by the strong tidal currents. The current magnitude in the MSC entrance increases only a little from the breaching at the landward ends of the jetties. Figure 23 shows the morphology change from the post-storm simulation for the breach with constant incident waves from the south. Figure 24 shows the morphology change for the existing configuration with incident waves from the east. The flow fields shown in Figures 23 and 24 represent a typical flood condition in the simulations. Figure 25 shows the comparison of current speeds at the bay entrance, gulf entrance, and in the middle of the bottleneck from the post-storm simulations for 1-January 2004.

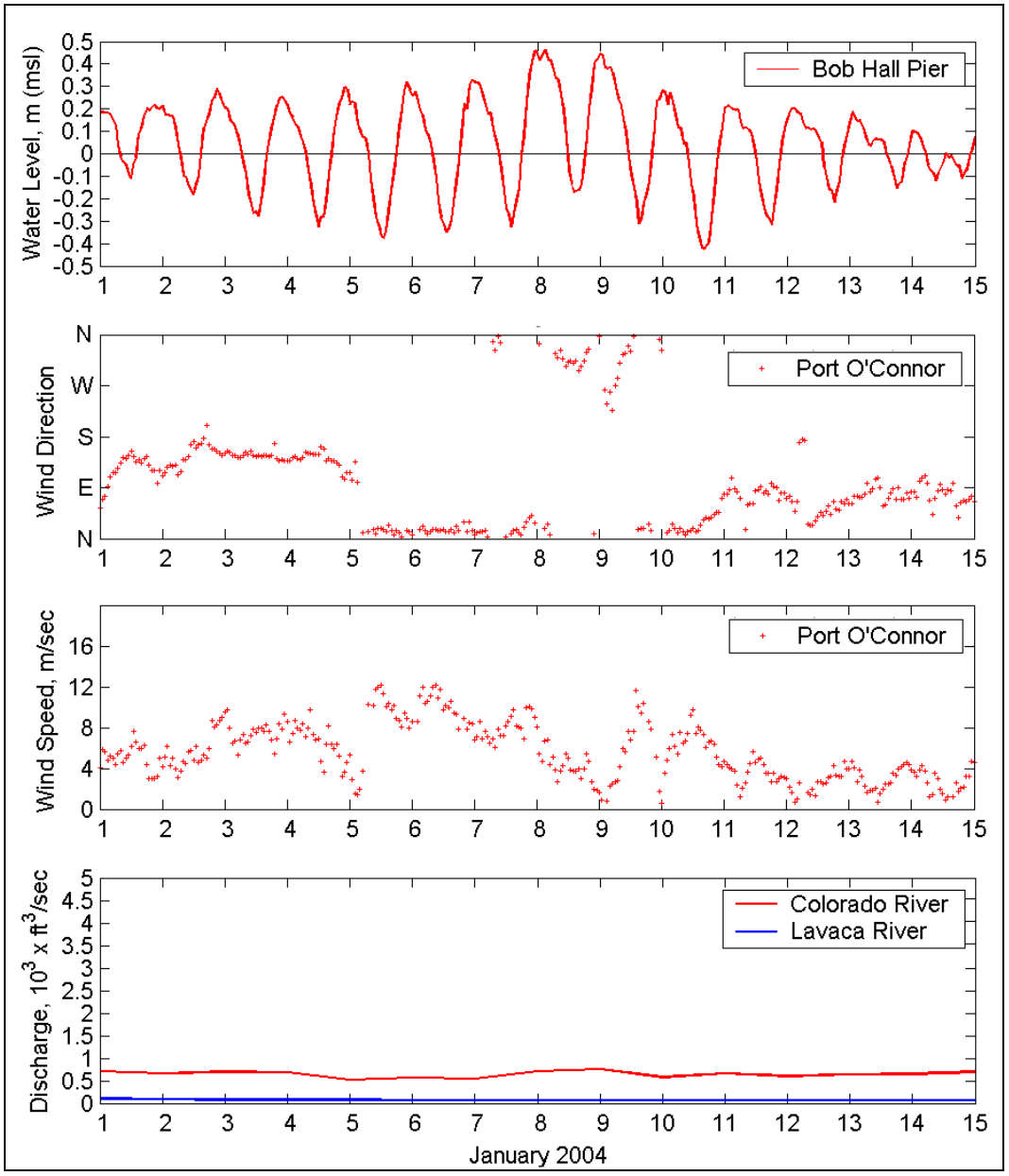

Figure 20. Measured water levels, wind speed and direction, and river discharge for 1-15 January 2004.

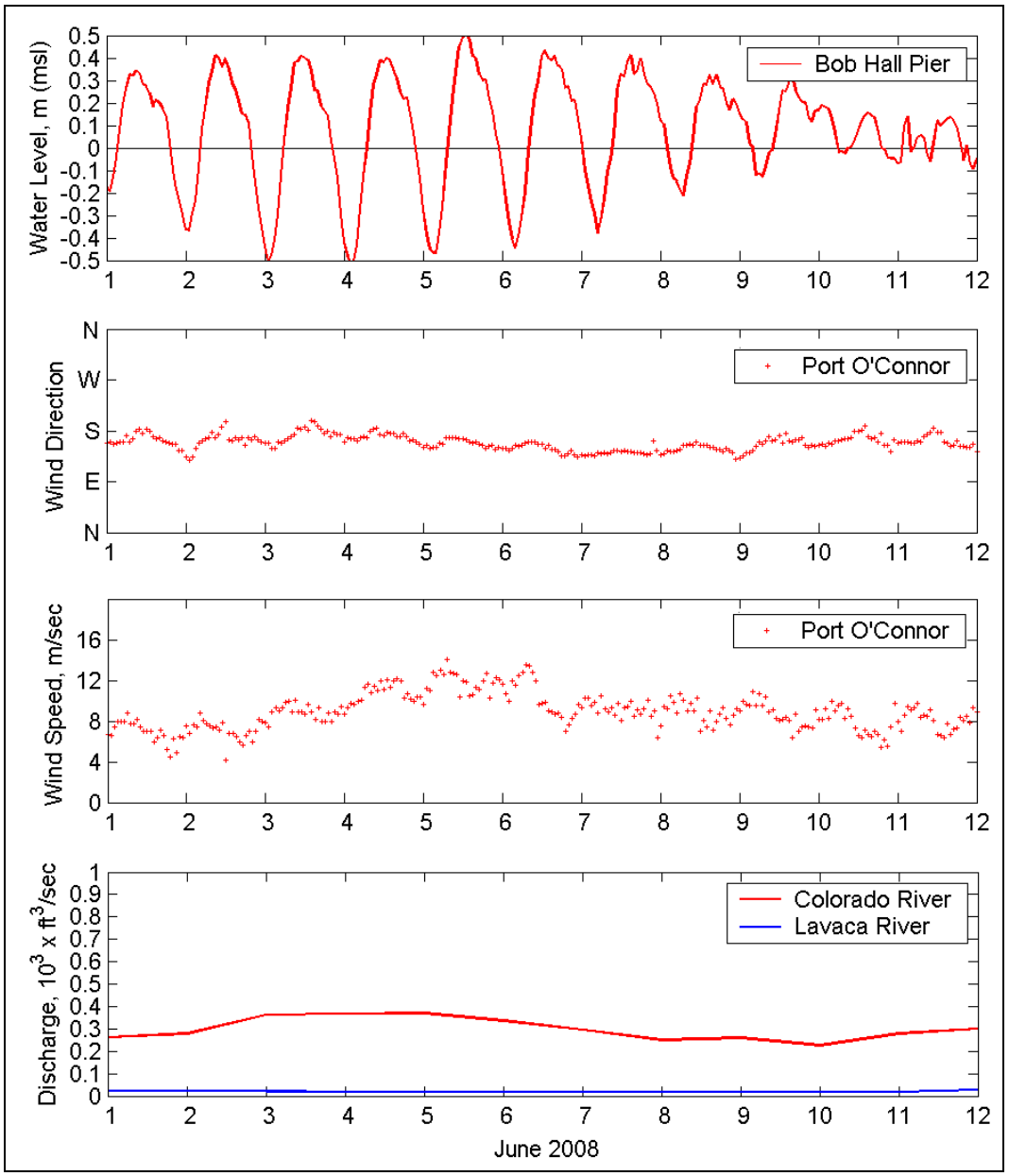

Figure 21. Measured water levels, wind speed and direction, and river discharge for 1-12 June 2008.

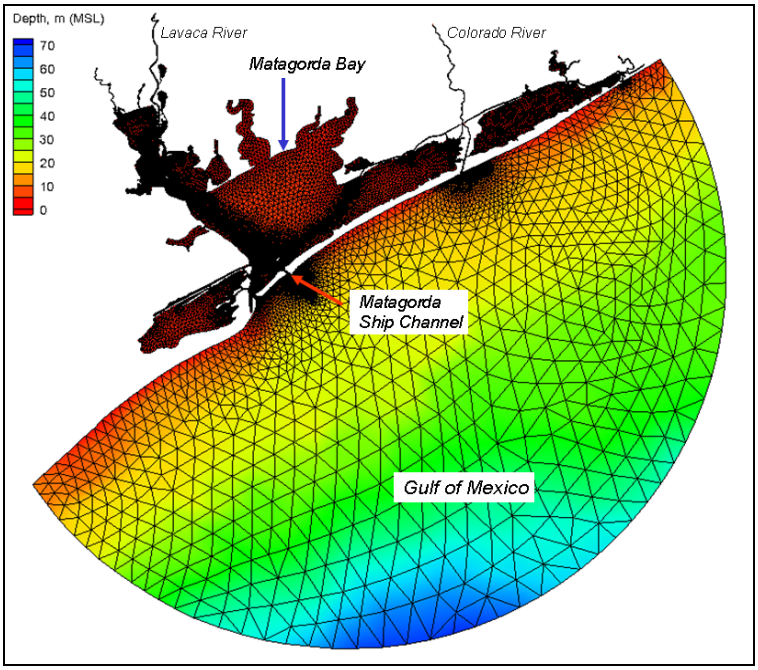

Figure 22. Regional grid model (from Kraus et al. 2008).

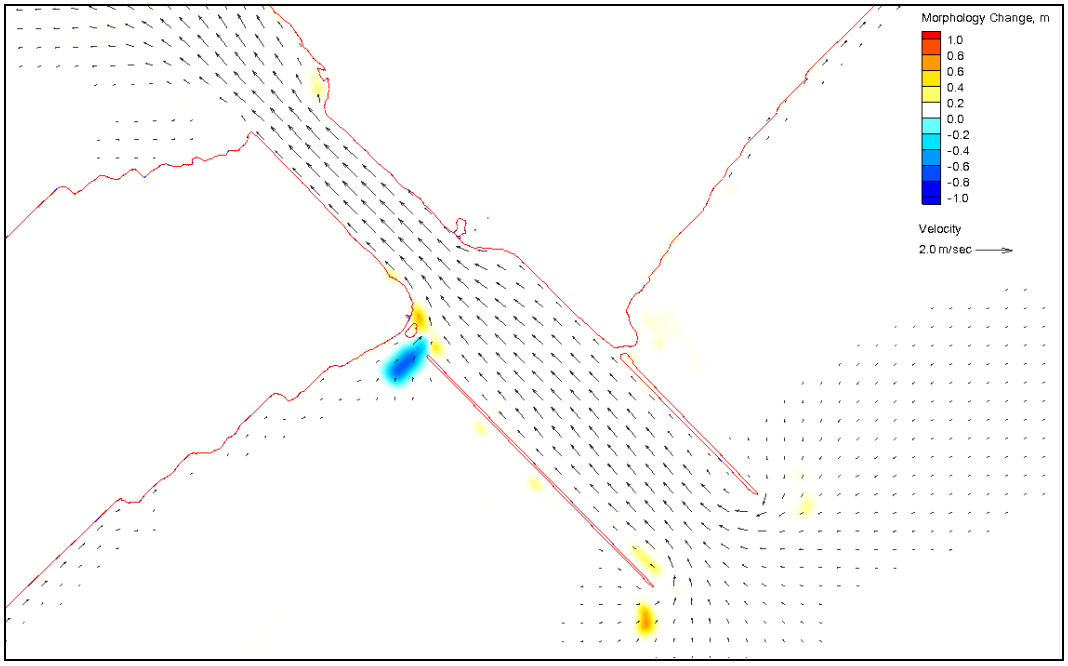

Figure 23. Post-storm morphology change with south jetty breach and waves from south, 1-14 January 2004.

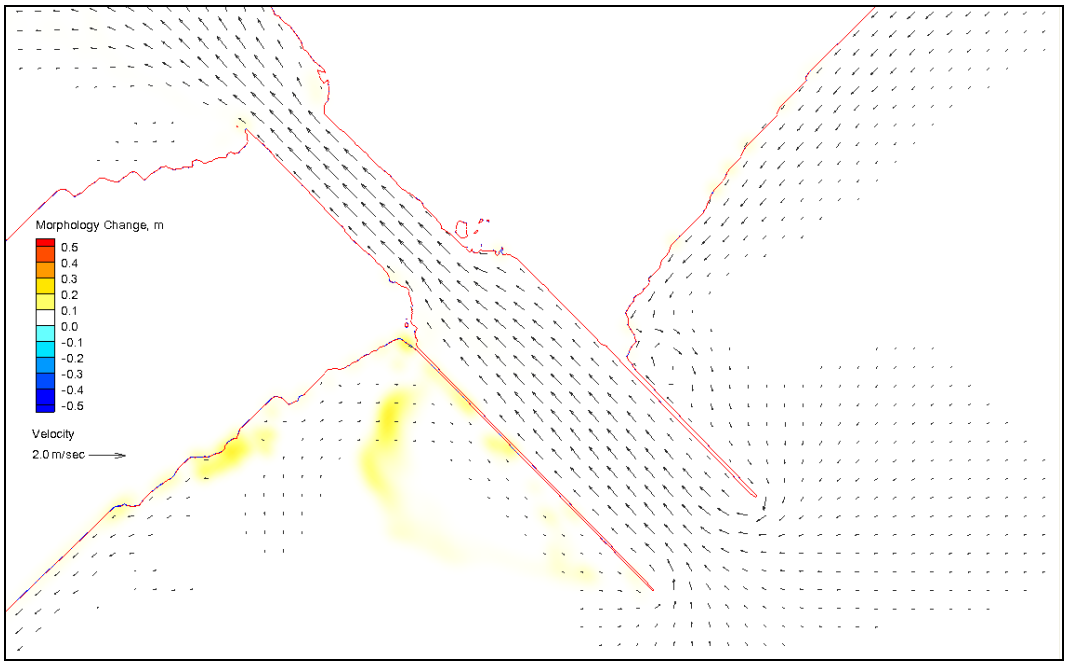

Figure 24. Post-storm morphology change for existing MSC with waves from east, 1-14 January 2004.

For the period of 1-10 June 2008, four CMS runs were conducted using the wave energy spectra measured by the National Buoy Data Center (NDBC) as the incident wave condition for the assumed morphology change of: (1) a large south jetty breach from the simulation of Category 3 hurricane waves from the south, (2) a large north jetty breach from the simulation of Category 3 hurricane waves from the east, (3) a moderate south jetty breach from the simulation of Category 3 hurricane waves from the south-east, and (4) the existing configuration (no breach). Figure 26 shows the time series of wind and wave data collected at NDBC 42019 and transformed to the local CMS grid seaward boundary offshore from the MSC entrance for 1-12 June 2008. Figures 27 and 28 show the calculated post-storm morphology change with the breach caused by hurricane waves from the south and east, respectively. The flow fields shown in Figures 27 and 28 are the maximum flood current condition in the simulations. Figure 29 compares the calculated current speeds at the bay entrance, gulf entrance, and in the middle of the bottleneck from the post-storm simulations for 1-10 June 2008. These simulations show that the impact of the jetty breach and flanking from a Category 3 hurricane is insignificant to sediment transport and current magnitude for the post-storm normal tide and wave condition in the MSC.

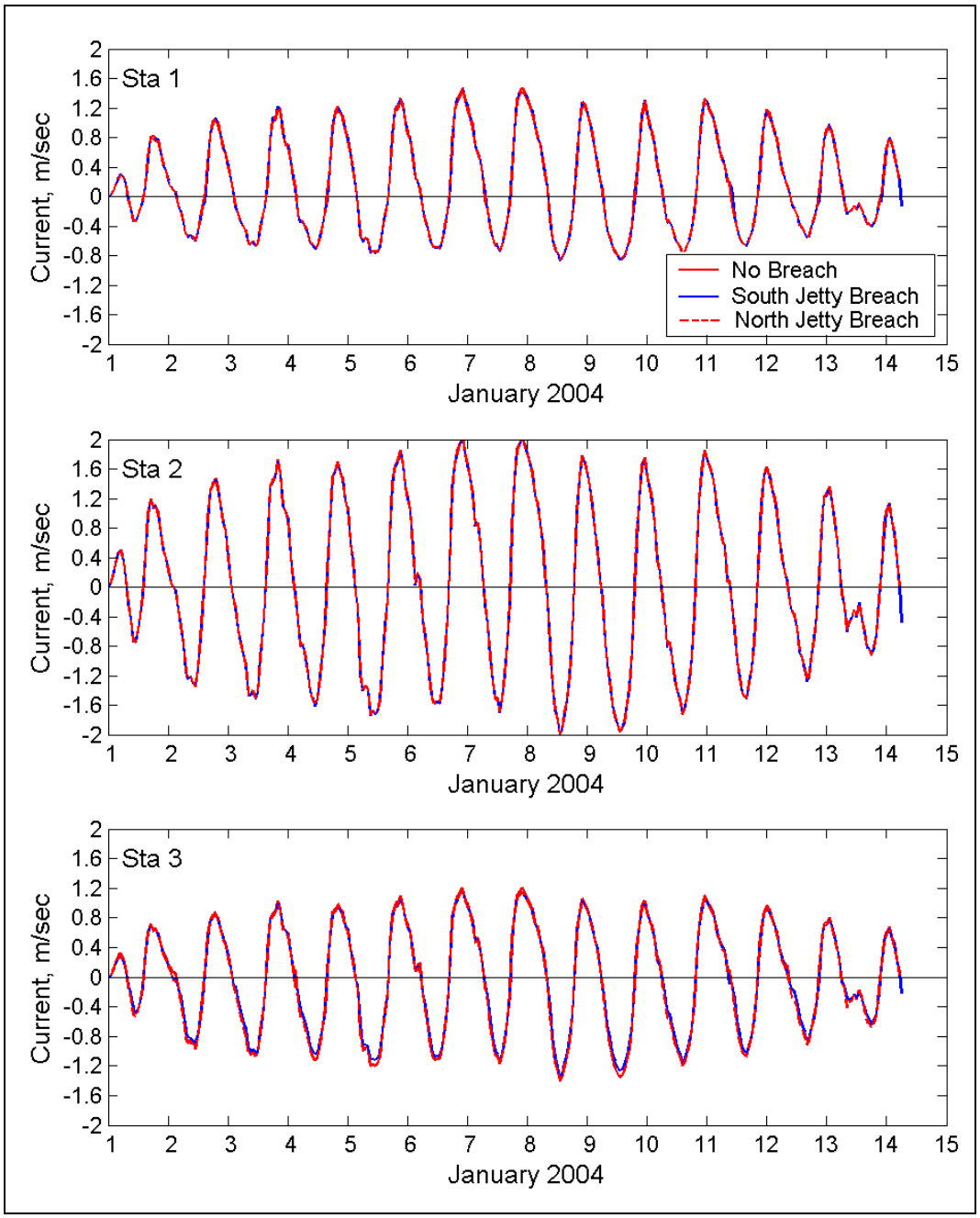

Figure 25. Calculated current speeds at MSC entrance (sta 1), middle of bottleneck (sta 2), and gulf entrance (sta 3) in the post-storm simulations for 1-14 January 2004.

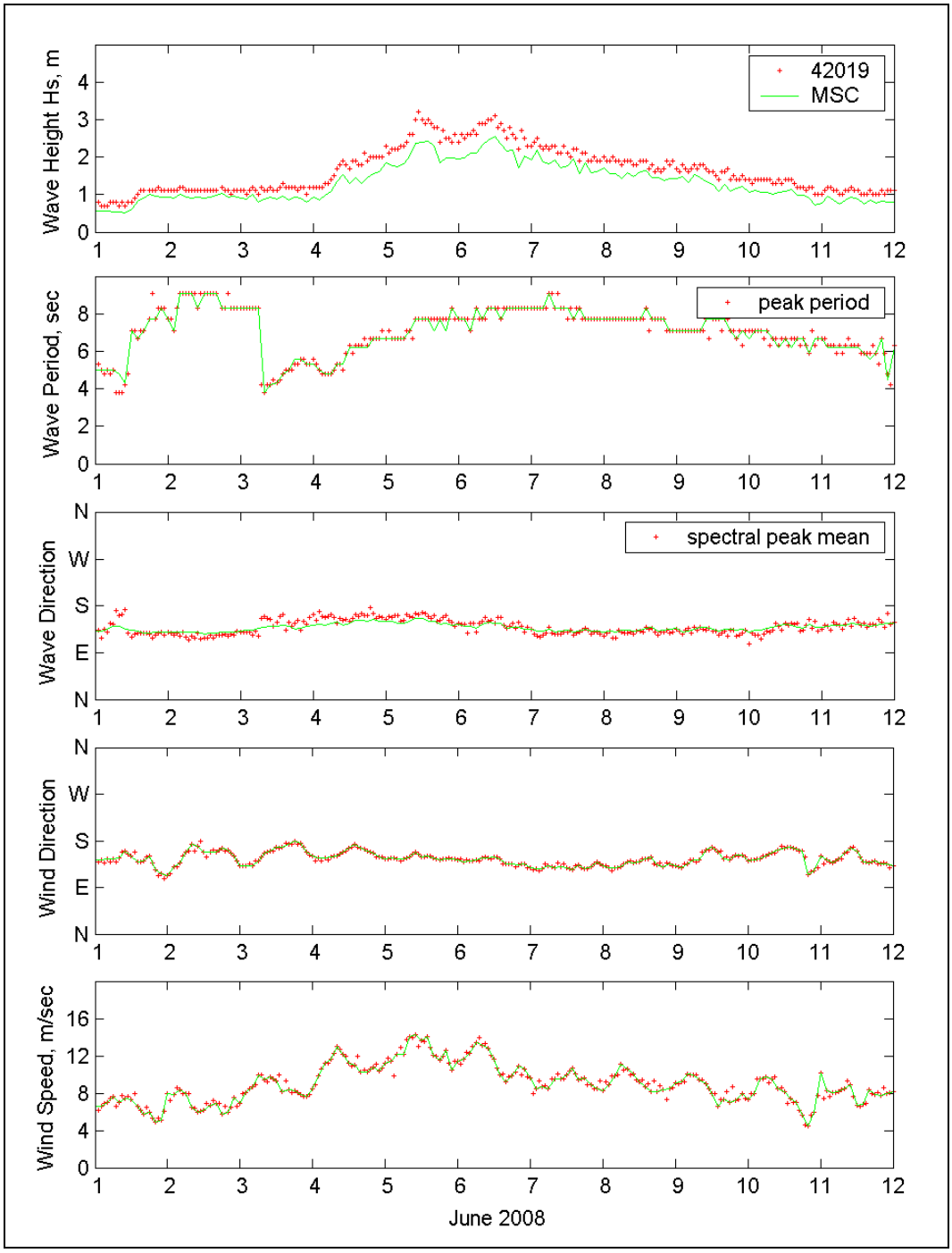

Figure 26. Wind and wave data at NDBC 42019 and offshore of MSC entrance, 1-12 June 2008.

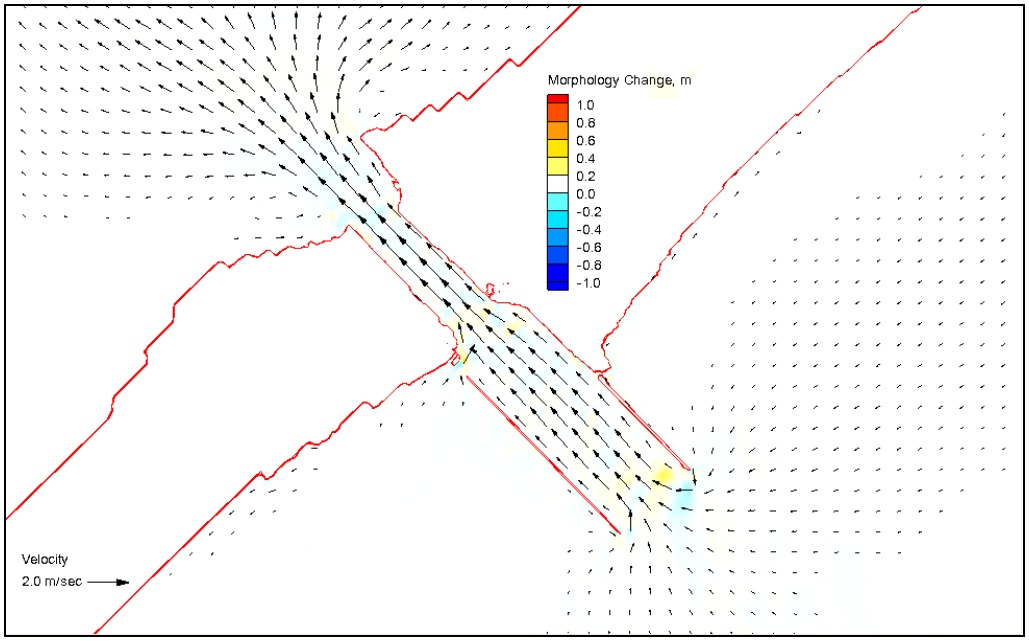

Figure 27. Post-storm morphology change with the south jetty breach and waves from south, 1-12 June 2008.

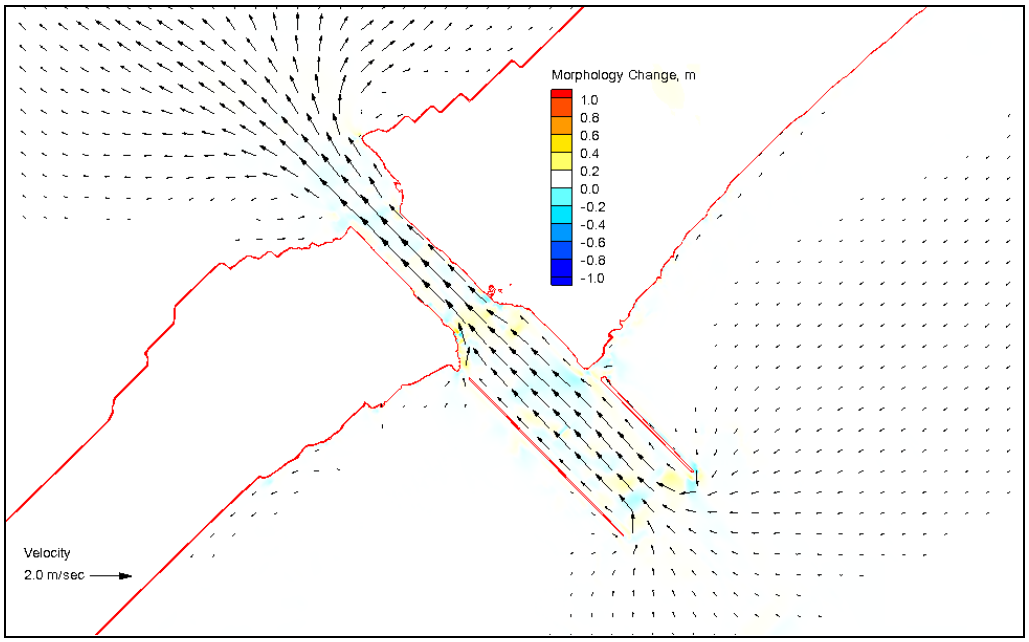

Figure 28. Post-storm morphology change with south jetty breach and waves from east, 1-12 June 2008.

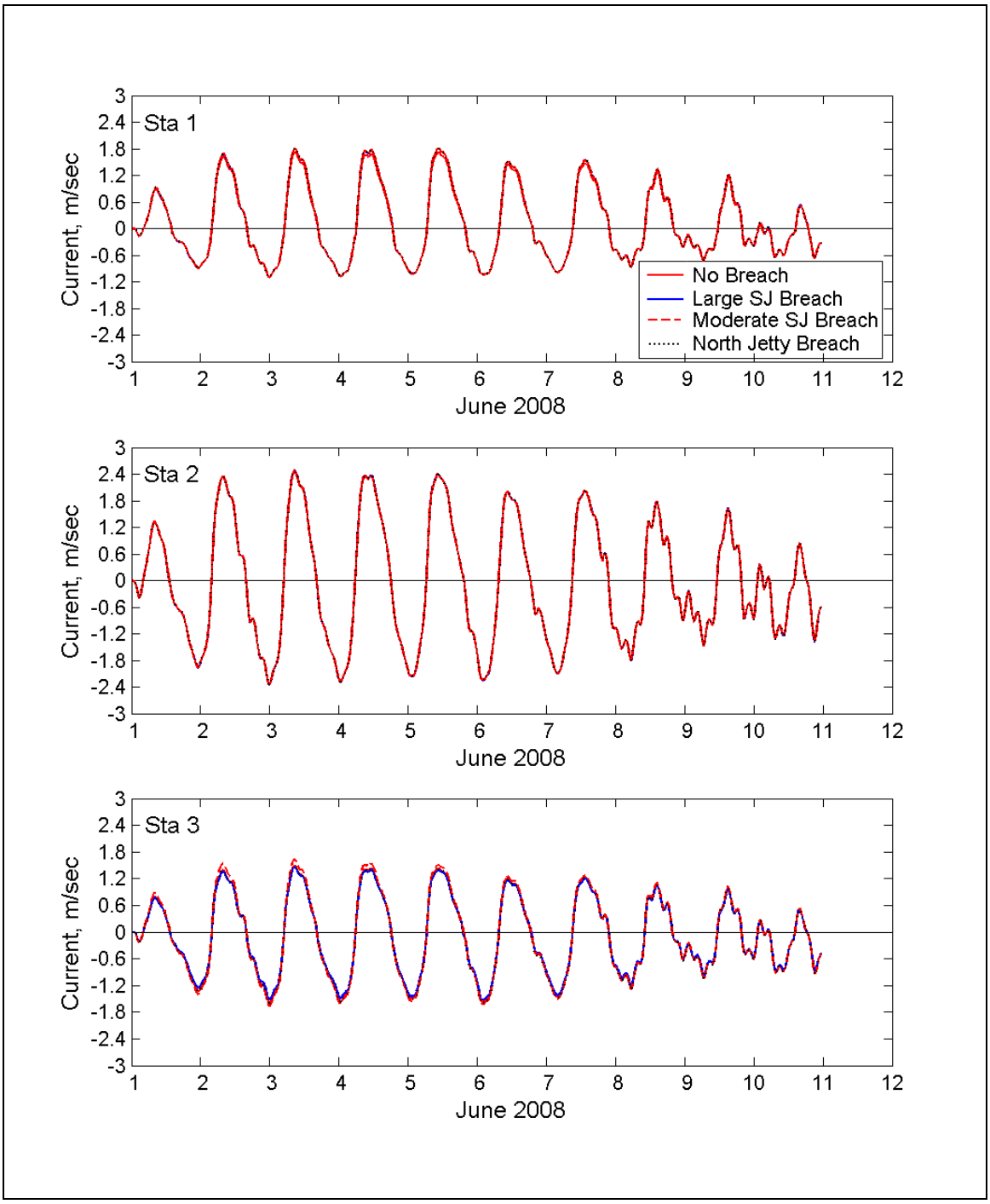

Figure 29. Calculated current speeds at bay entrance (sta 1), middle of bottleneck (sta 2), and gulf entrance (sta 3) in post-storm simulations for 1-12 June 2008.

3 Structural Risk to Navigation- Slope Failure

Purpose and approach

The purpose and scope of the material described in this chapter was to determine channel slope stability and the expected impact of slope failures on navigation for existing channel slope geometry and future deeper geometries as a result of scouring. This study was prompted by a previous study conducted by CHL (Maynord et al. 2007), which concluded that scour of channel bottom leading to slope failures is one of the significant factors that poses a risk of disrupting navigation and recommended additional study to quantify this risk. The recommendations further stated that this study should be based on site-specific data. Therefore, the feedback of these results will not only quantify risk, but include potential slope failure scenarios for input to numerical hydraulic channel simulations.

The approach was to conduct a geologic and geotechnical site exploration that included drilling, sampling, and laboratory testing to ascertain needed parameters to conduct a slope stability analyses. Then, slope stability analyses were conducted on specific cross sections developed for each of the eight boring locations, four on each side of the channel. After these deterministic slope stability analyses were completed, three critical sections were selected and simplified to use in the probabilistic slope stability analyses to provide information to quantify and assess risks to facilitate decision-making. Additionally, the likely magnitude (size) of the failure masses was estimated for input to hydraulic channel simulations to determine the impact, if any, on navigation.

Future scour of bottleneck

Inlet cross-sectional stability and tidal prism

In the Phase 1 study, inlet area stability was examined to understand whether the existing inlet channel is in an equilibrium state or whether the channel will tend to scour or to shoal. The equilibrium-area concept for a tidal inlet has been a useful approach to understand the adjustment of an entrance channel's minimum cross-sectional area to the basic hydraulic and sedimentation characteristics of the inlet it serves. The development

of the equations is presented in the Phase 1 study. The inlet stability curve concept was first developed analytically by Escoffier (1940, 1977). He proposed a diagram for inlet stability analysis in which two curves are initially plotted (Figure 30). One curve (thick, blue line) is the calculated maximum velocity through the inlet versus the inlet's cross-sectional flow area. A single curve represents changing inlet cross-section area conditions if ocean tide parameters and bay and inlet plan geometry remain relatively fixed. As the channel cross-sectional area approaches zero, velocity approaches zero because of increasing frictional stress, which is inversely proportional to channel area. As channel area increases, friction stress is reduced, but on the far right side of the curve, velocity decreases, because tidal prism has reached a maximum, and any channel area increase will decrease the current velocity, as determined by the continuity equation. This curve can be constructed by calculating the maximum velocity V, resulting by varying channel cross-sectional area A. The velocity in the inlet V can be determined by an analytical or numerical model. The second curve (thin, green line), the equilibrium velocity, is an empirical stability criterion curve as given by Jarrett (1976). The stability curve is based on sandy inlet material.

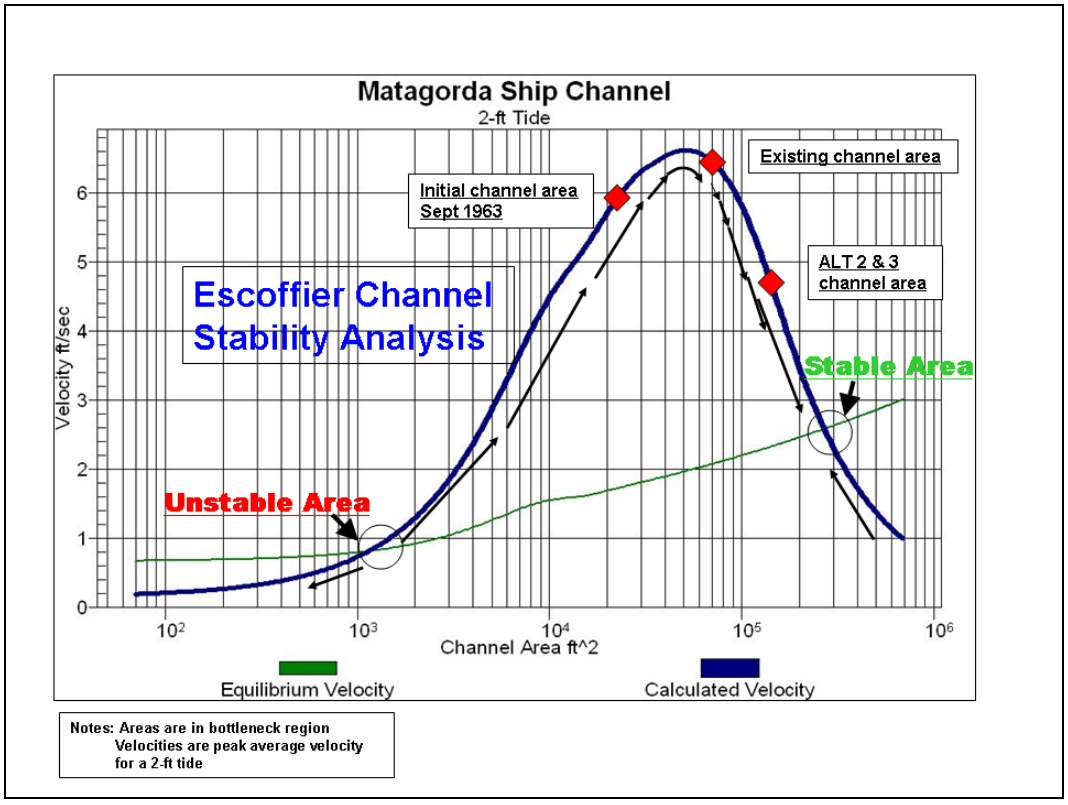

Figure 30. Escoffier plot for examining existing conditions in MSC entrance.

The Phase 1 Study describes the development of the Escoffier stability curve. To apply the calibrated Escoffier curve, a tide range of 2 ft was chosen, corresponding to the average diurnal range of tide at the Galveston Pleasure Pier water level gauge. Also plotted on Figure 30 are data points representing the channel area and current velocity through it for the initial 1963 channel, the existing channel area, and a data point for the proposed bottleneck removal from Kraus et al (2006). Also indicated are the unstable and stable areas. Based on the Escoffier analysis, the channel will continue to enlarge until it reaches the stable point. Figure 30 shows an important finding of this study. The velocity through the inlet has reached its peak value. Although future velocities will decline, the rate of reduction is extremely low.

The Galveston District (1963) reports that stiff Beaumont clay is present below an elevation of about -45 ft. Almost all of the bottom of the bottleneck is below an elevation of -45 ft. The stable area point in the Escoffier analysis could lie higher up the current velocity curve because this analysis is based on sandy inlets. Once a clay layer is reached during channel scour, the equilibrium velocity could be greater due to the greater resistance to erosion of the clay layer. In other words, the inlet's stable cross-section area might be less than the value of 250,000 ft^2 found in Figure 30. The stable area could possibly be in the 100,000-200,000 ft^2 range.

During this Phase 2 study, four borings on each side of the bottleneck were taken down to as much as 200-ft. The soil profiles shown in Appendix B indicate a complex layering of sands, silts, and clays and not the thick Beaumont clay below about -45 ft hypothesized in the Phase 1 study. The complexity of the profile makes it difficult to establish the stable inlet cross sectional area as well as the rate of erosion. To further complicate the determination of future scour, Figure 31 shows the bed material in the inlet based on sonar and grab samples. The bed of the inlet is almost completely covered with a layer of shell hash of unknown thickness.

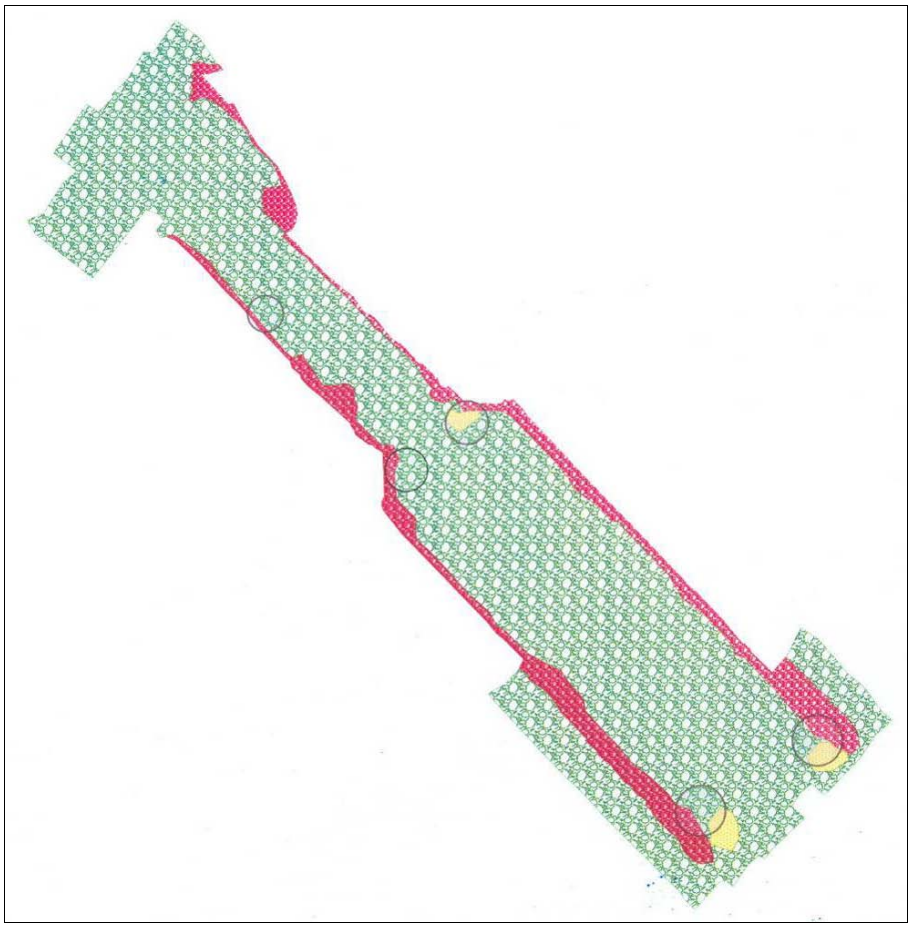

Figure 31. Results of side scan sonar showing shell hash (green) along bed of MSC, riprap and jetty stone (red), and sand with trace amounts of shell (yellow).

The complex soil profile and the presence of shell hash makes application of the Escoffier analysis only approximate. As hypothesized in the Phase 1 study, it is likely that the stable inlet cross sectional area is less than the stable point of the Escoffier stability analysis. An inlet area of about 120,000 ft^2, that is equal to the cross-section area of Alternatives 2 and 3 of Kraus et al. (2006), is considered to be the best estimate of stable inlet area. Using a 700-ft bottom width, the existing channel of about 70,000 ft^2 would have to scour the bottom about 70-ft before reaching the stable cross-sectional area of 120,000 ft^2.

Observed scour in bottleneck

Based on the complex sediment profile and presence of shell hash in the inlet, the estimate of future scour used herein is based on the analysis of historical bathymetry data presented in the Phase 1 study. The Phase 1 scour analysis is summarized herein.

Figure 32 shows stationing along the channel. All elevations in this scour evaluation are in feet relative to MLT.

Cross sections were evaluated at various locations along the channel. Figure 33 shows the 2000-2007 surveys at sta 1+100 where there is a bulge on the lower bank that may indicate one or more past slope failures. Figure 34 shows the as-built section from 1963 along with the 2000-2007 surveys at sta 2+600.

Over the bottleneck area from sta 0+000 to 3+500, the average depth over the erodable portion of the channel (excludes riprap side slopes) is about 80 ft in 2007. Since the channel opened 44 years ago in 1963, the bottom elevation has degraded from elevation -40 ft to the average bed elevation of about -80 ft. Channel area has about tripled since 1963. Some areas have degraded to an elevation of -105 ft MLT. Using the average bed elevation in 2007, the channel has degraded 40 ft/44 years = 0.9 ft/year. No other data points are available to determine how the rate of scour has varied over the 44 year period. The Escoffier analysis presented previously shows that the

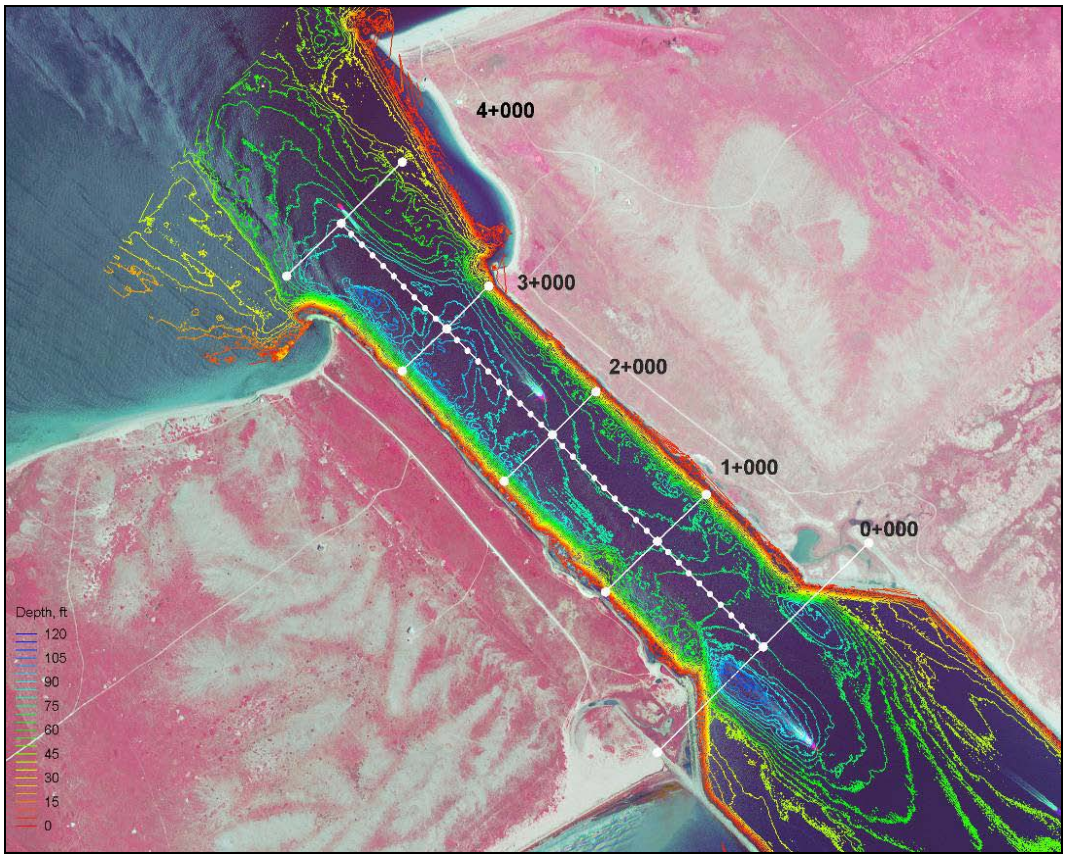

Figure 32. Channel stations and 2007 bathymetry plotted on 2004 aerial photograph.

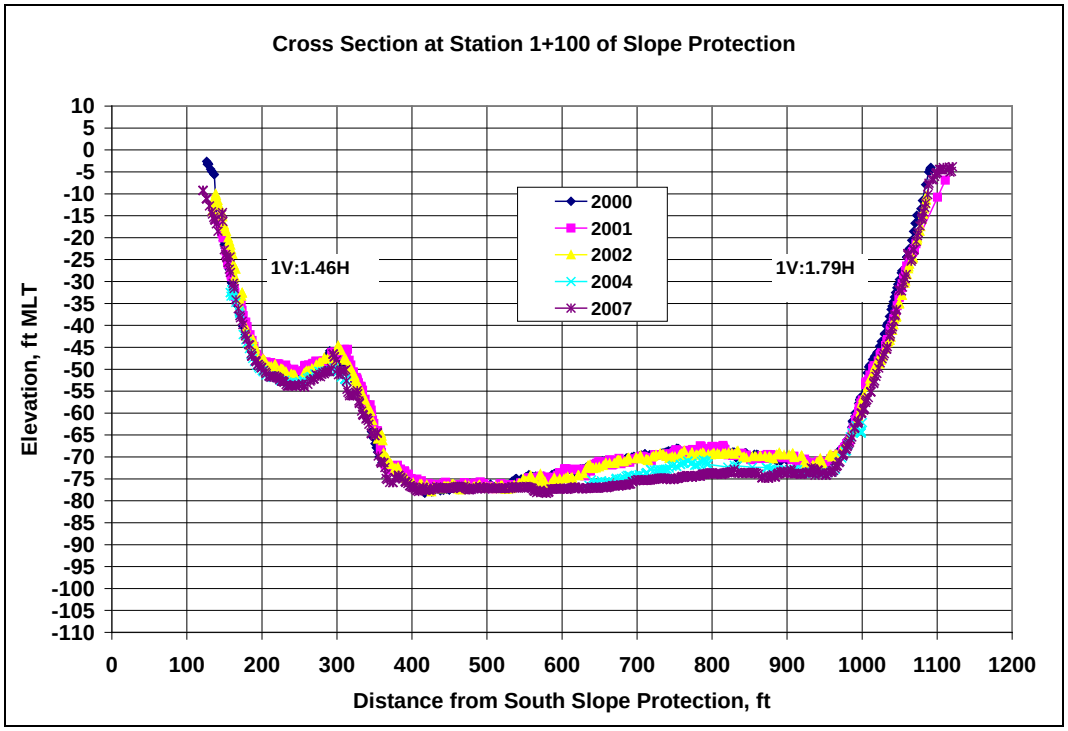

Figure 33. Cross section at sta 1+100. Bank slope based on average slope between elevation -20 and -50 ft MLT on north slope protection and -20 and -40 ft MLT on south slope protection. Cross section plotted looking inland.

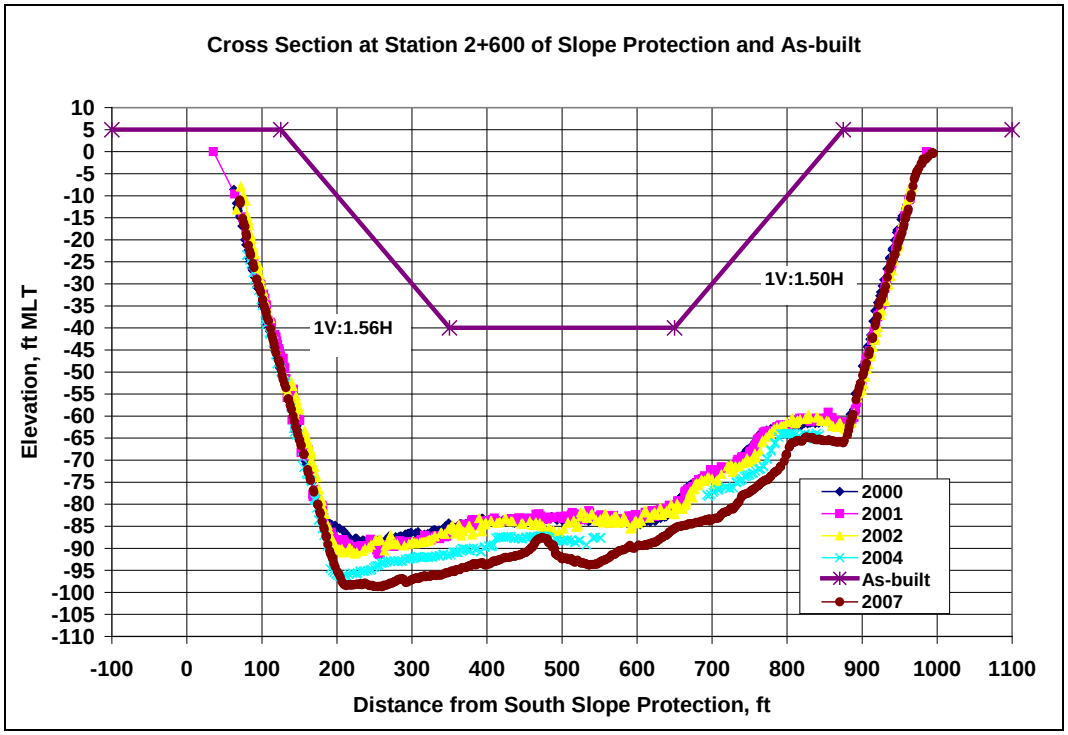

Figure 34. Cross section at sta 2+600 and as-built section. Bank slope based on average slope between elevation -20 and -50 ft MLT. Cross section plotted looking inland.

velocity in the MSC Entrance is presently at its peak value and present scour is likely equal to or greater than the average value of 0.9 ft/year. Based on the recent data and the Escoffier stability analysis, the channel bed has not reached an equilibrium condition with respect to scour. The damage to the slope protection that has occurred since the last repair in 1994 supports the conclusion that the inlet bed has not reached equilibrium.

Potential Triggering mechanisms for slope failures - ship induced drawdown and waves

As ships traverse a confined channel, rapid drawdown of the water level occurs followed by a return velocity moving from bow to stern as the ship displaces water. The ship-induced rapid drawdown could lead to slope failure of the steep side slopes in the channel. Using the cross section at sta 2+600 as representative, the cross section area and top width are 65,000 ft^2 and 950 ft, respectively. The drawdown and return velocity analysis will use a Panamax ship (beam = 106 ft) and draft of 36 ft. Based on conversation with MSC Pilot Larry Robinson, ship speed through the bottleneck will be 9 knots (15.2 ft/sec) relative to the water. He stated that speed applies to an inbound ship going against a 6-knot ebb current (speed over ground = 3 knots) or a ship transiting with no current (speed over ground = 9 knots). Based on water level drawdown data collected on the Savannah River compiled in Maynord (2007) where channel sizes are similar, and using those ships having similar beam and draft and similar speeds, maximum drawdown will be about 1 ft. Based on a one-dimensional ship effects analysis in Maynord (1996), return velocity for sta 2+600 will be about 1.5 ft/sec.

The width and depth present in the existing bottleneck is adequate for wider and deeper draft ships, and 0ne-way traffic. This statement does not address problems larger ships might experience with currents in the existing channel. If wider beam ships having deeper draft start using the bottleneck channel, drawdown and return velocity magnitude will increase. For example, if a 140-ft beam ship with draft of 40 ft transits the bottleneck section at 9 knots, maximum drawdown will be about 1.5 ft based on similar ship size and speed in the Savannah River. Return velocity will be about 2 ft/sec.

Numerical model simulations show that the bottleneck portion of the entrance channel can be subject to 3-5 ft waves having period of about 5 sec (transformed from 11-sec spectral waves in the offshore). The shorter

waves (5-sec) inside the entrance channel is a result of more dissipation of longer waves (11-sec) from greater wave breaking and stronger wind and current interactions with waves near the entrance channel. Depending on the material properties of the slope, these waves could cause enough pressure change over the slope to trigger a slope failure in the bottleneck. These potential mechanisms will be examined later in this chapter to see if they affect slope stability.

Geology

Geologic data were compiled for Matagorda Island to evaluate the Holocene and Pleistocene stratigraphy in the navigation channel to support the engineering analysis. Geologic maps important to this effort were the Beeville-Bay City Sheet (Bureau of Economic Geology 1975a and b) and the Port Lavaca Area, Environmental Geologic Atlas of the Texas Coastal Zone (McGowen et al. 1976). Matagorda Island is part of an extensive Holocene barrier beach complex that fringes the Texas Gulf Coast. This barrier beach system began developing in response to eustatic sea level rise, caused by glacial melting of the polar ice sheets, beginning about 12,000 years before the present. Sea level rise continues today because of warming global climates, and the rate is estimated at 2.75 cm/100 years (Watson 1990). Data compiled by McGowen et al. (1976) and the Bureau of Economic Geology (1975a and b) for the Port Lavaca bay area indicate that the shallow stratigraphy beneath Matagorda Island and the bay is composed of Holocene estuarine deposits, overlying Pleistocene sediments assigned to the Beaumont Formation.

General stratigraphy and chronology

The Beaumont clay is approximately 400 to 900 ft (120 to 275 m) thick along the Texas Gulf Coast and was produced from fine-grained fluvial-deltaic deposition of coastal plain river systems that were draining into the Gulf of Mexico during lower stands of sea water. These various river systems deposited a geographically widespread, thick sequence of mostly fine-grained sediments along the gulf coast. The Beaumont is not restricted to any one river system, but incorporates all of the various fluvial-deltaic systems that were draining the Texas hill country and the sediments that were deposited by these systems. Beaumont deposits include mainly stream channel, point bar, natural levee, and back swamp deposits, and to a lesser extent coastal marsh, mudflat, and lagoonal sediments (Sellards et al. 1990, p. 790; Bureau of Economic Geology 1968a and b, 1975a and b; 1976).

The present elevation surface of the Beaumont, combined with the nature of Holocene and Pleistocene gulfward subsidence rates along the Louisiana and Texas coastal zones, point to interglacial climatic conditions for the formation of the Beaumont and the presence of maximum high sea level stands. Deposition of the Beaumont Formation has been estimated to have occurred between 50,000 to 125,000 years before present, or the time period corresponding from Middle Wisconsin to Sangamon (McGowen et al. 1976).

During the most recent Pleistocene glacial maximum in the northern latitudes, about 15,000 years before present, the sea level was about 350 to 400 ft lower than present throughout the Gulf Coast region. Thus, the Beaumont surface beneath Matagorda Island would have been exposed to atmospheric weathering, and dissected by an ancestral drainage network. Because of this atmospheric exposure and weathering, the Beaumont surface is easily recognized in boring data because of distinct lithologic characteristics. These properties include diagnostic colors, calcareous nodules and concretions, stiff to very stiff consistency, high shear strengths, and low water contents in comparison to the overlying Holocene back barrier and barrier beach deposits.

Formation of the present day barrier island chain began developing as the sea level started rising 12,000 years before the present. The rapid rise in sea level, as shown by Figure 35, drowned the preexisting coastal drainage network, and created the modern day coastline with its fringing barrier islands and back barrier bays.

Boring data and geologic cross sections

Eight borings were drilled for this study, as shown by Figure 36, and detailed location and depth of holes are provided in Table 4. Four borings were drilled on either side of the navigation channel to determine the stratigraphy and material properties of the various geologic units beneath Matagorda Island for the engineering analysis. The complete boring logs are provided in the report by Rock Engineering and Testing Laboratory (2008), *Geotechnical Investigation at the Matagorda Ship Channel Matagorda Peninsula, TX*, and parts of this data are included in the geotechnical summary tables presented in Appendix B.

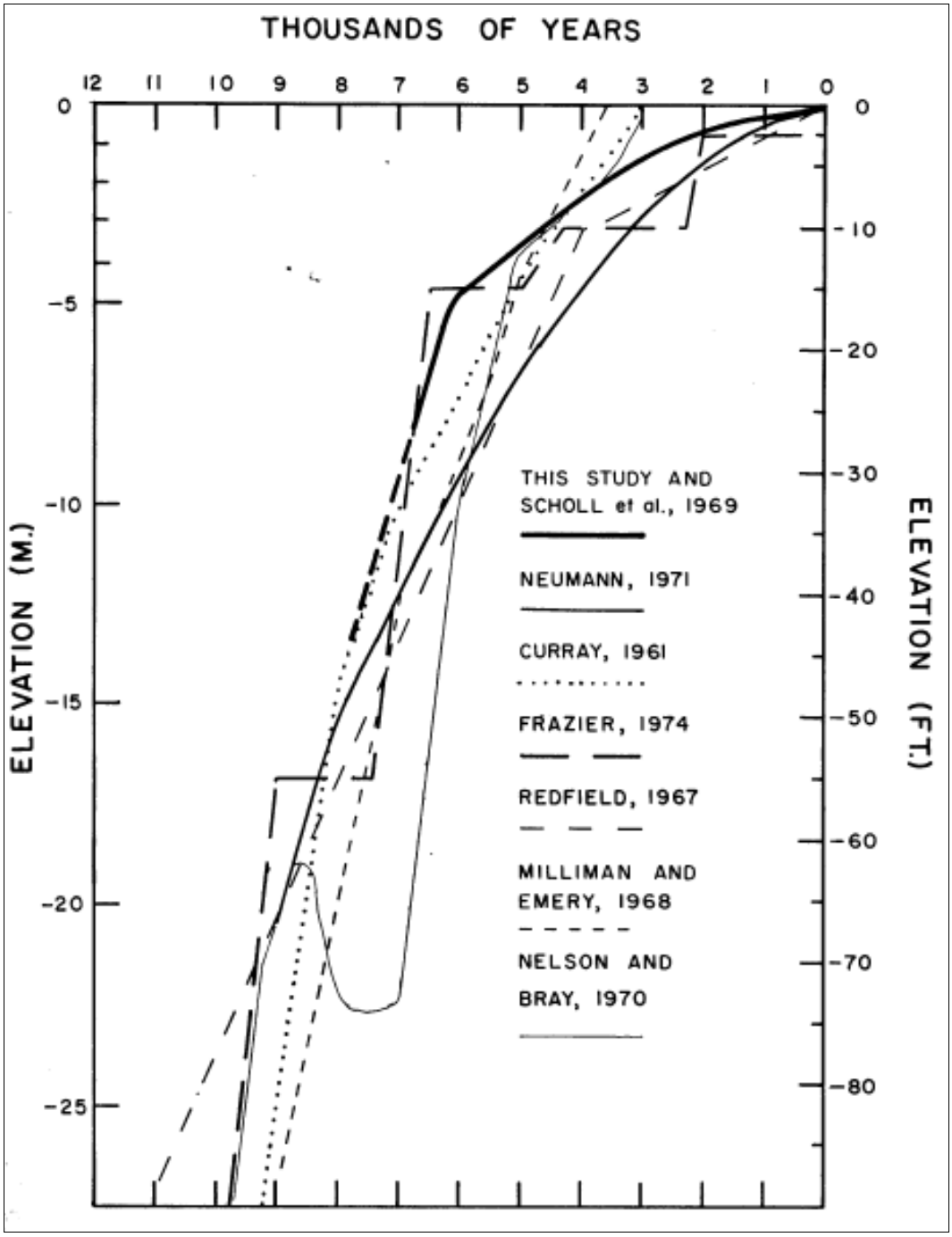

Figure 35. Holocene sea level curve of south Texas coast (Watson 1990). (Courtesy of Richard L. Watson, Ph.D., P.G., TexasCoastGeology.com).

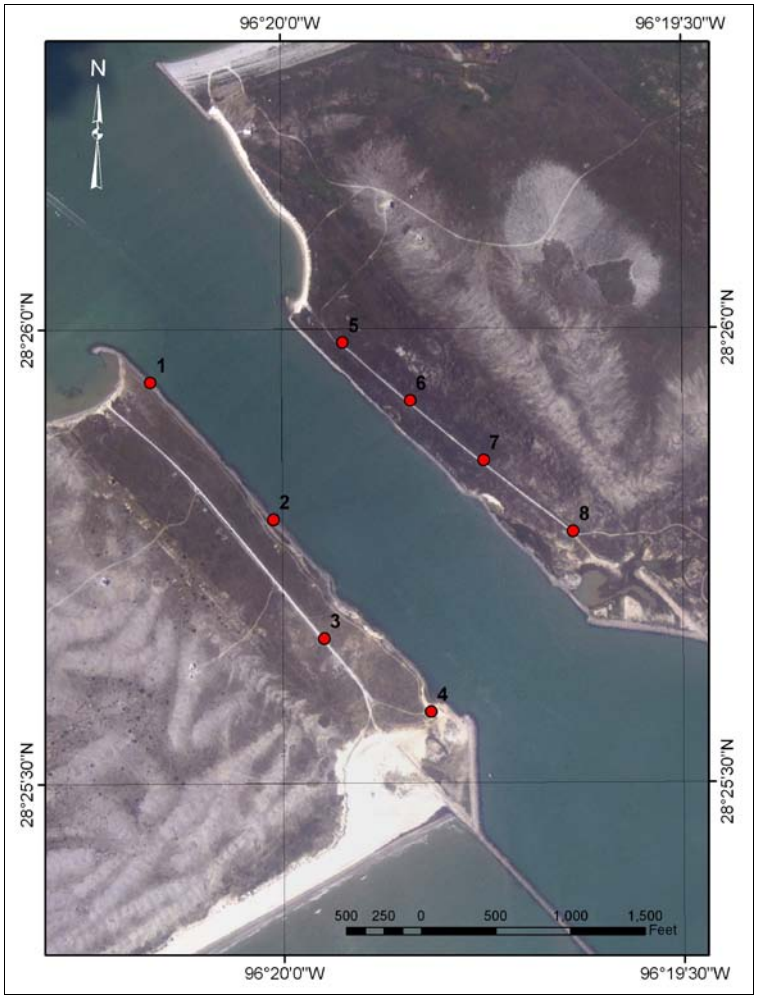

Figure 36. Location of borings drilled for this study.

Table 4. Borehole locations and depths drilled.

Boring	Northing	Easting	Elevation (top of hole (ft)	Depth (bottom of hole (ft)
B1	13,350,938.67	2,824,540.51	4.29	200
B2	13,349,907.43	2,825,248.57	6.81	170
B3	13,349,406.86	2,825,859.84	6.78	175
B4	13,348,741.57	2,826,452.95	7.41	195
B5	13,349,943.77	2,827,478.65	5.26	200
B6	13,350,423.79	2,826,825.70	6.20	175
B7	13,350,784.31	2,826,362.60	6.23	200
B8	13,351,183.80	2,825,865.70	3.91	175

Geologic cross sections were prepared from the available boring data to identify the soils and stratigraphic units both vertically and laterally along the reach of the navigation channel. Cross sections parallel with the south and north banks of the channel are presented in Figures 37 and 38, respectively. Sections extending across the navigation channel are presented in Figures 39 through 42, starting at the gulf side near sta 0+00 (see Figure 32 for stationing) and extending to the back barrier side at sta 3+100.

Bathymetry surveys

Elevation data from the navigation channel were obtained from a bathymetry survey by the Galveston District in 2007. The raw point data from this survey were imported into ESRI's ArcView software, and gridded to develop an elevation model of the navigation channel (Figure 43). This data was then incorporated into the geologic cross sections presented in Figures 39 through 42. The vertical exaggeration in these cross sections is ten times the horizontal scale. This vertical exaggeration causes the channel profile to show a near vertical slope, which is an artifact of these drawings. A topographic pseudo-3D view of the navigation channel from the back barrier side is presented in Figure 44 to show the bathymetry of the channel. This channel has downcut into the underlying Beaumont Formation to a depth of about -112 ft, National Geodetic Vertical Datum (NGVD), and has developed a deep pool along the south bank of the navigation channel. The Holocene section is approximately 50 to 55 ft thick. The project depth was originally dredged to -40 ft NGVD according to the design project documents.

Summary description of navigation channel sediments

Holocene sediments consist of fine barrier beach sands and nearshore gulf deposits, containing silty and clayey sands and back barrier estuarine muds. The Holocene section corresponds to the orange and brown elevation color range in Figures 43 and 44. Unified Soil Classification System (USCS) soil types are primarily coarse grained and are identified on the respective cross sections in Figures 37 through 44. Also, detailed USCS soils information is presented on the boring logs in the foundation investigation report (Rock Engineering and Testing Laboratory 2008) and included in geotechnical summary tables in Appendix B.

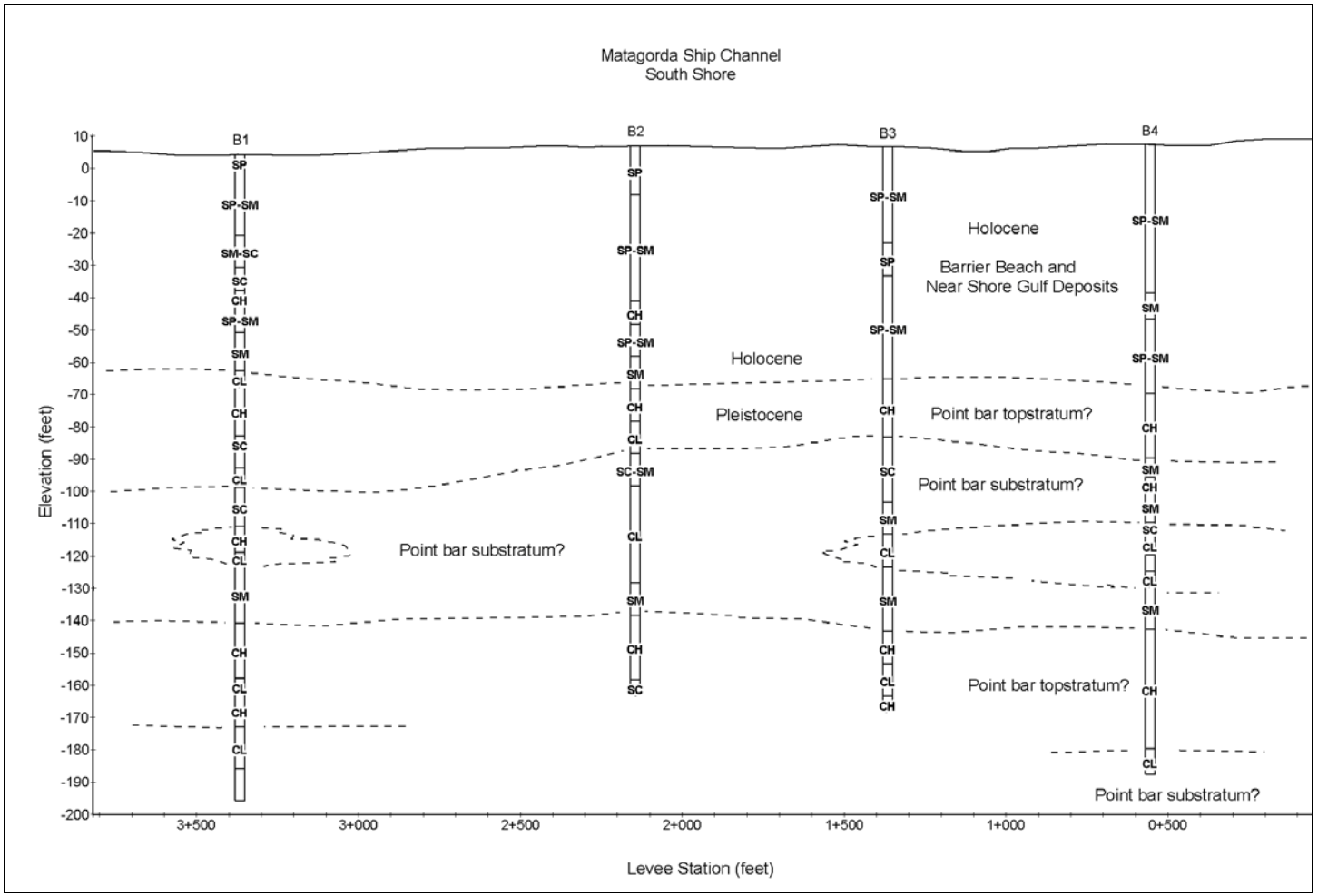

Figure 37. Cross section along south shore with view looking north. Vertical exaggeration of section is ten times horizontal. Individual boring logs are presented in Appendix B.

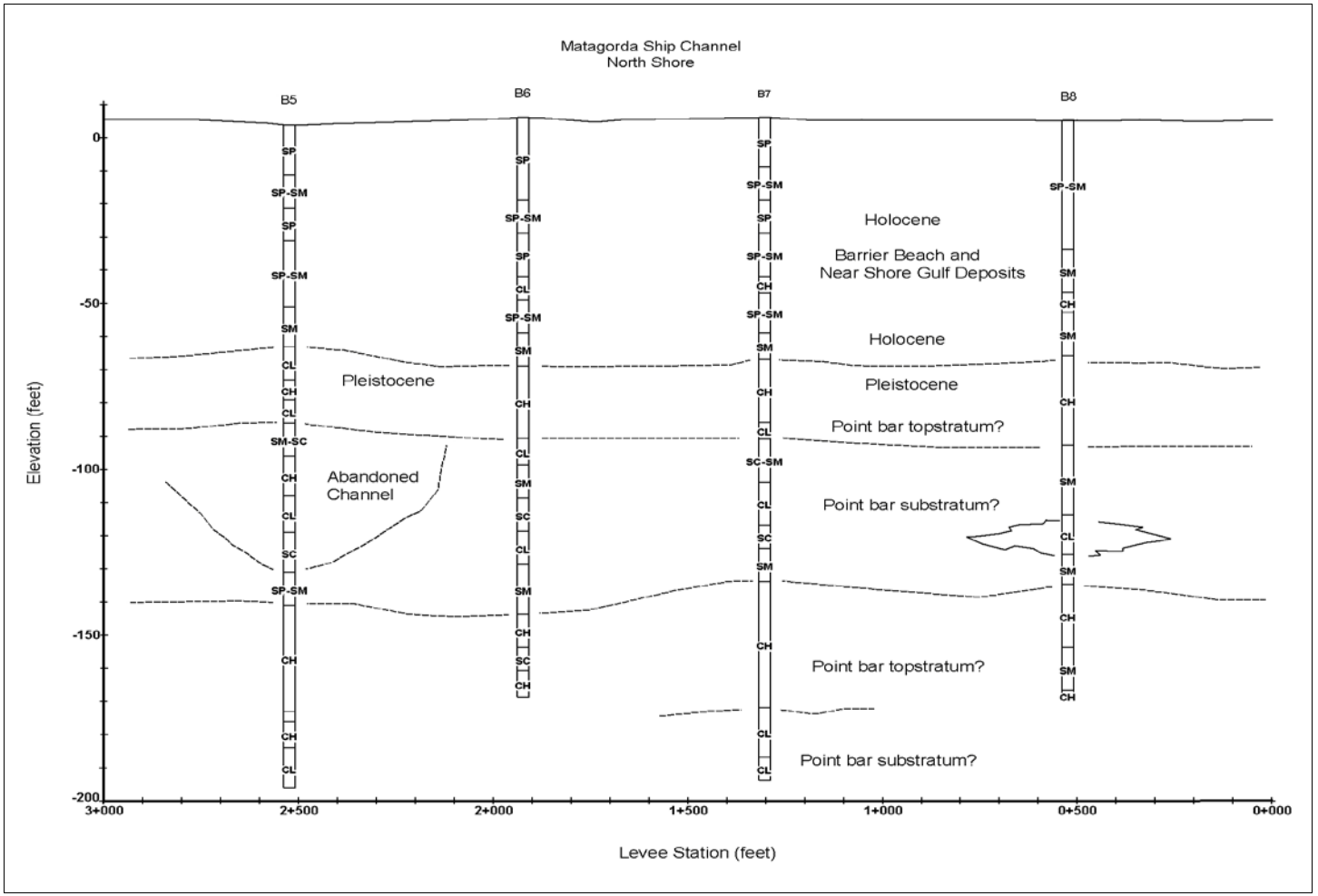

Figure 38. Cross section along north shore with view looking north. Vertical exaggeration of section is ten times horizontal. Individual boring logs are presented in Appendix B.

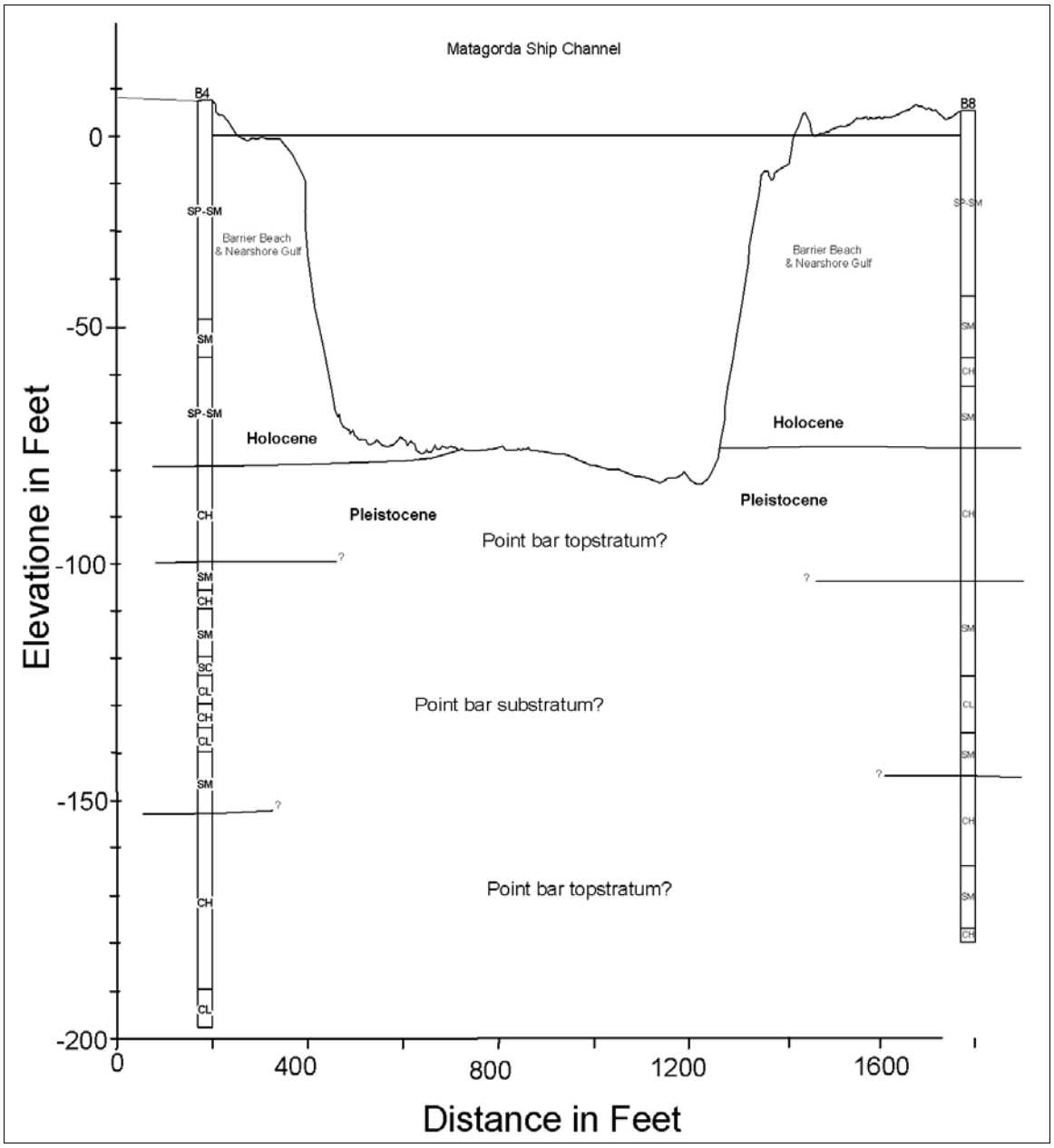

Figure 39. Cross section and channel profile between borings B4 and B8, corresponding to about sta 0+500. Channel profile data obtained from bathymetry survey data in Figure 43. Vertical exaggeration is ten times horizontal.

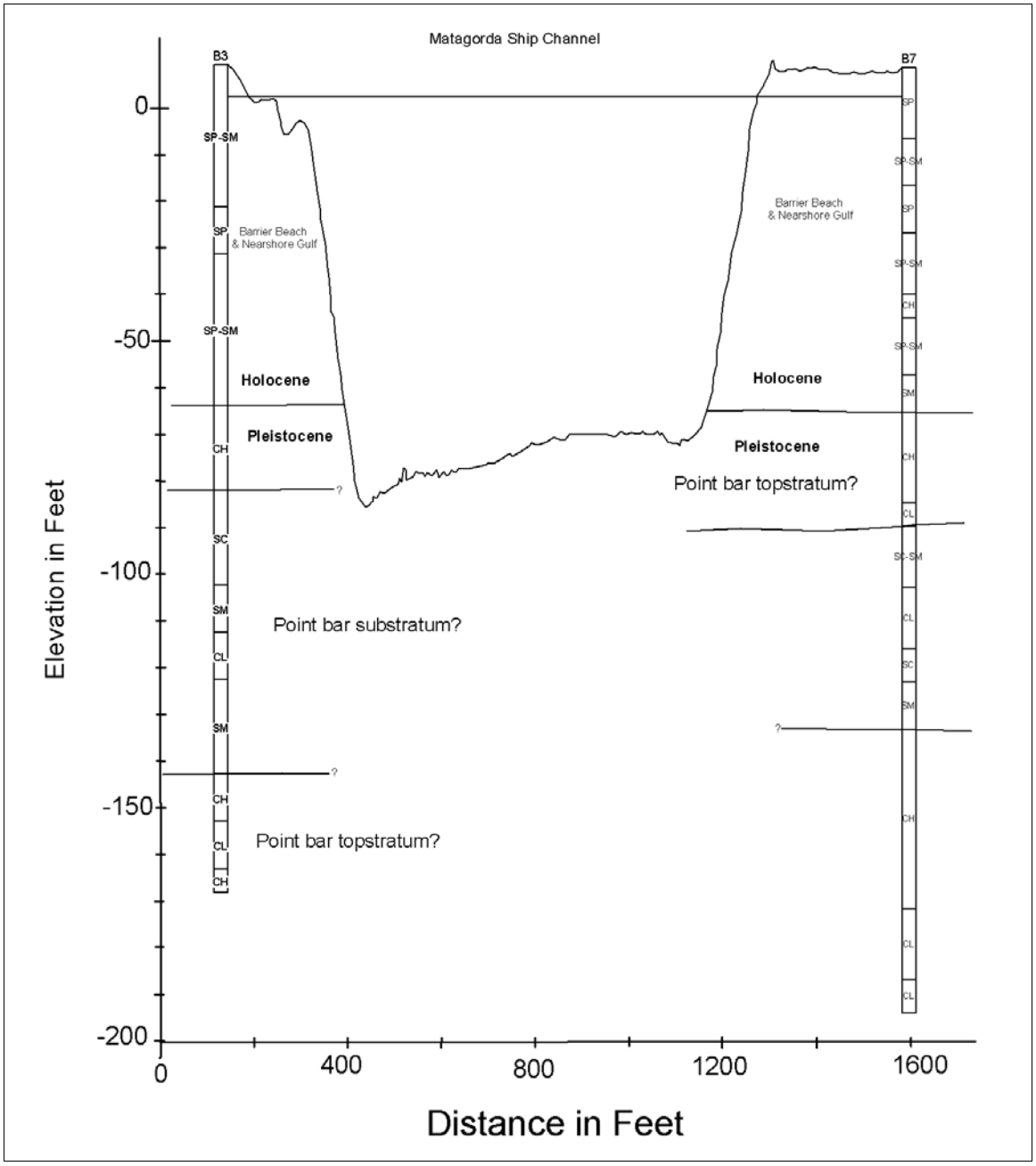

Figure 40. Cross section and channel profile between borings B3 and B7, corresponding to about sta 1+450. Channel profile data obtained from bathymetry survey data in Figure 43 Vertical exaggeration is ten times horizontal.

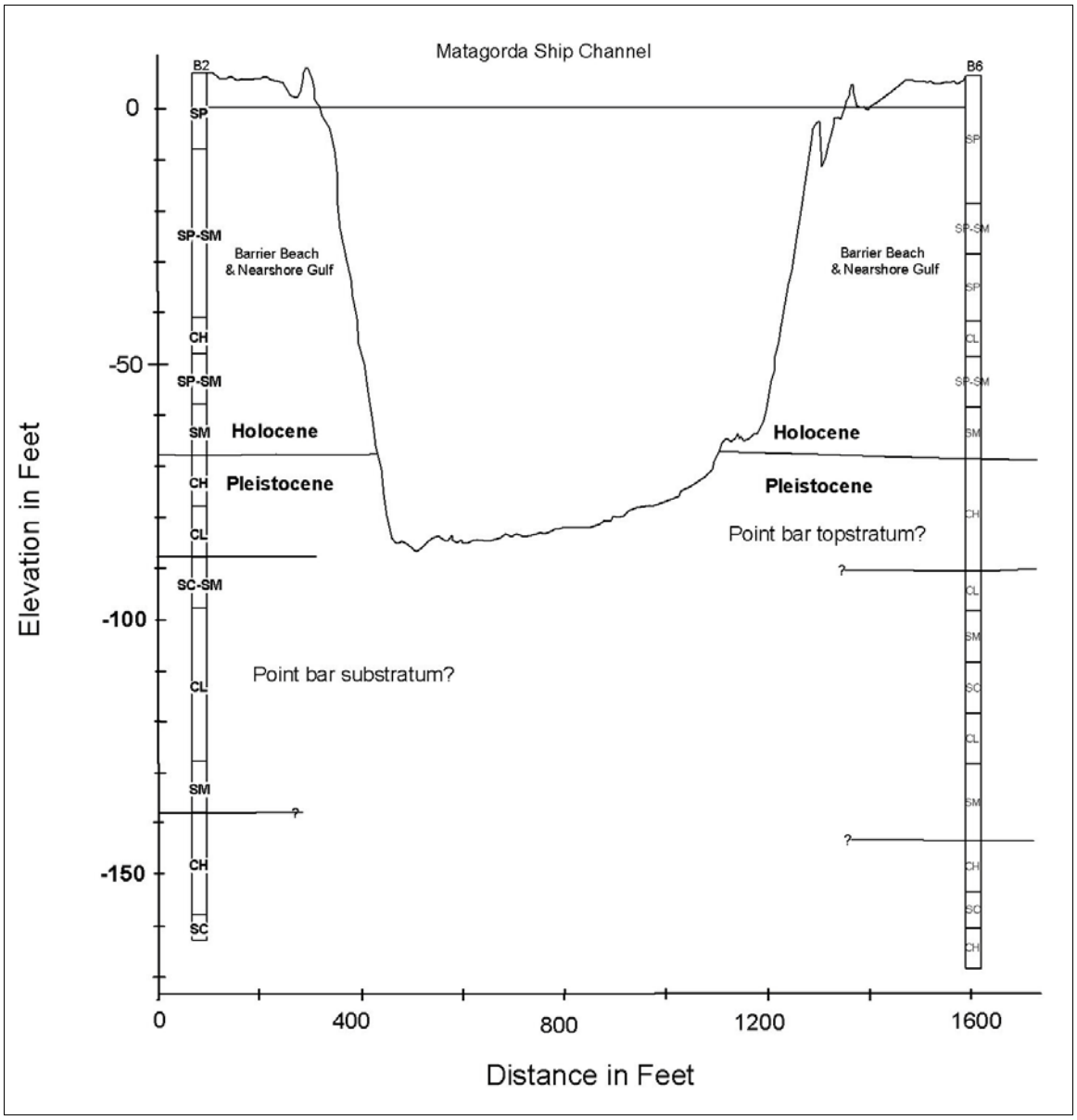

Figure 41. Cross section and channel profile between borings B2 and B6, corresponding to about sta 2+150. Channel profile data obtained from bathymetry survey data in Figure 43. Vertical exaggeration is ten times horizontal.

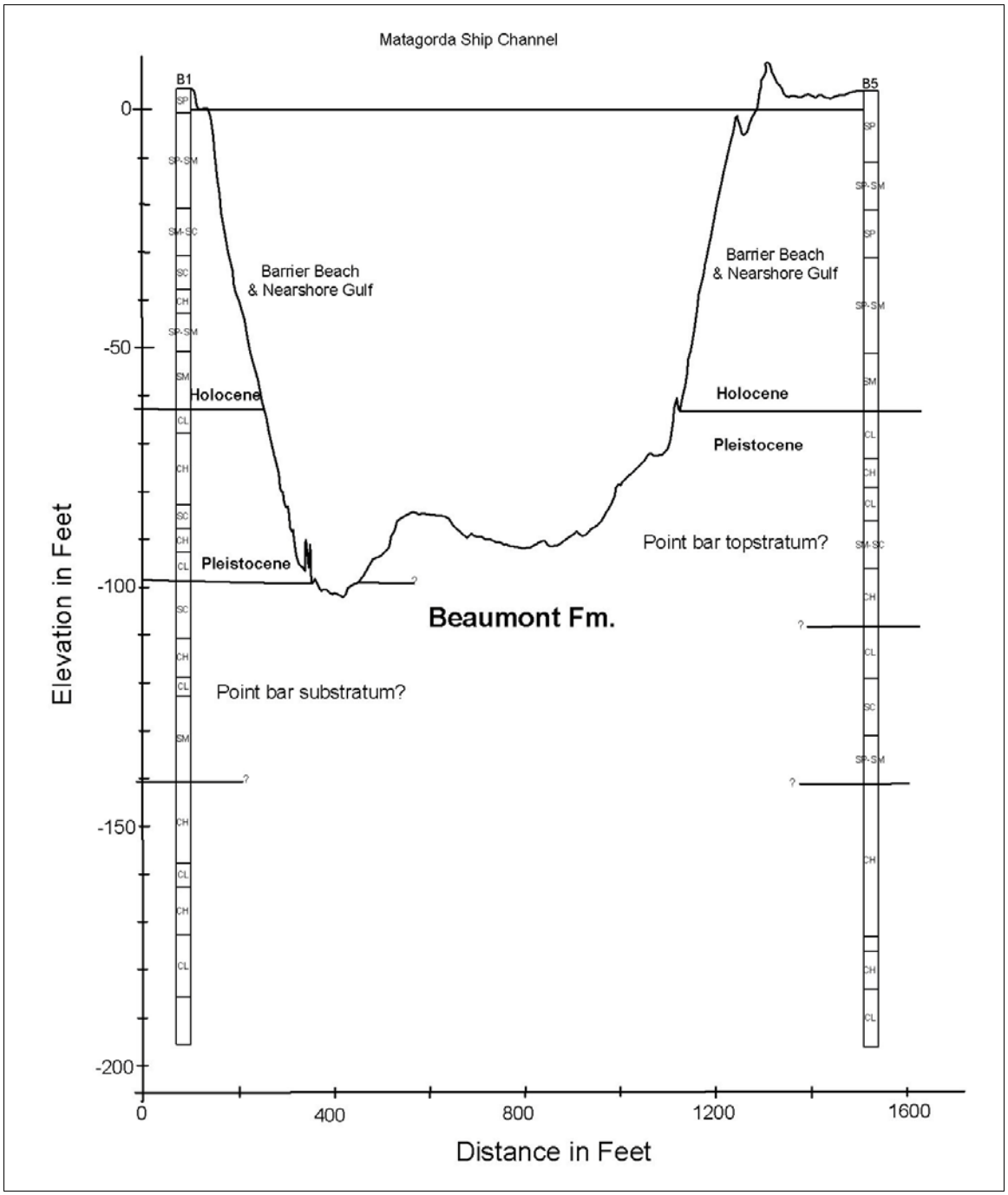

Figure 42. Cross section and channel profile between borings B1 and B5, corresponding to about sta 3+100. Channel profile data obtained from bathymetry survey data in Figure 43. Vertical exaggeration is ten times horizontal.

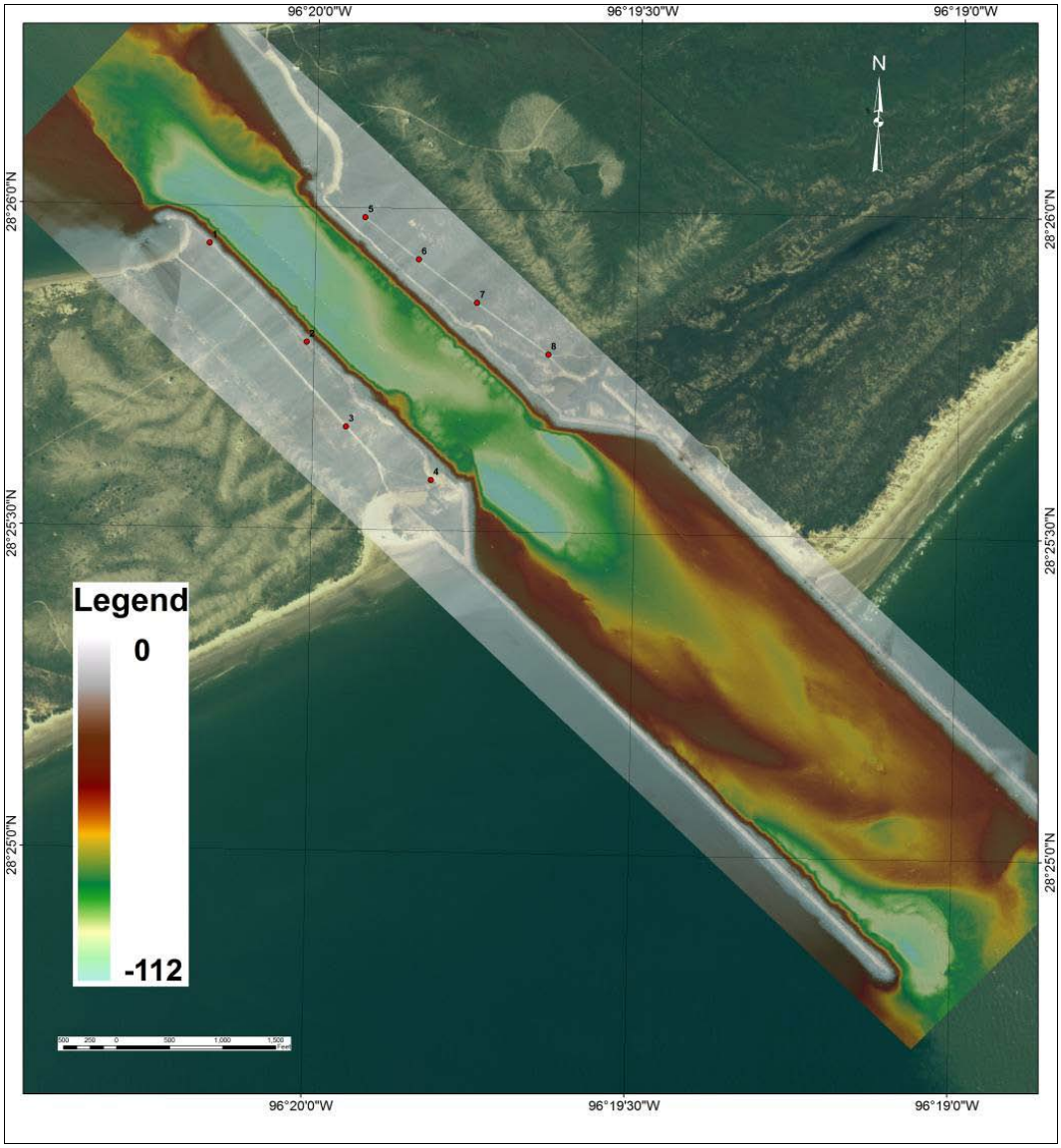

Figure 43. Bathymetry grid of Matagorda navigation channel developed from channel survey by Galveston District in 2007. Survey data were gridded with ArcView to produce a contour map of the channel and to develop topographic profiles across the channel in Figures 39 through 42.

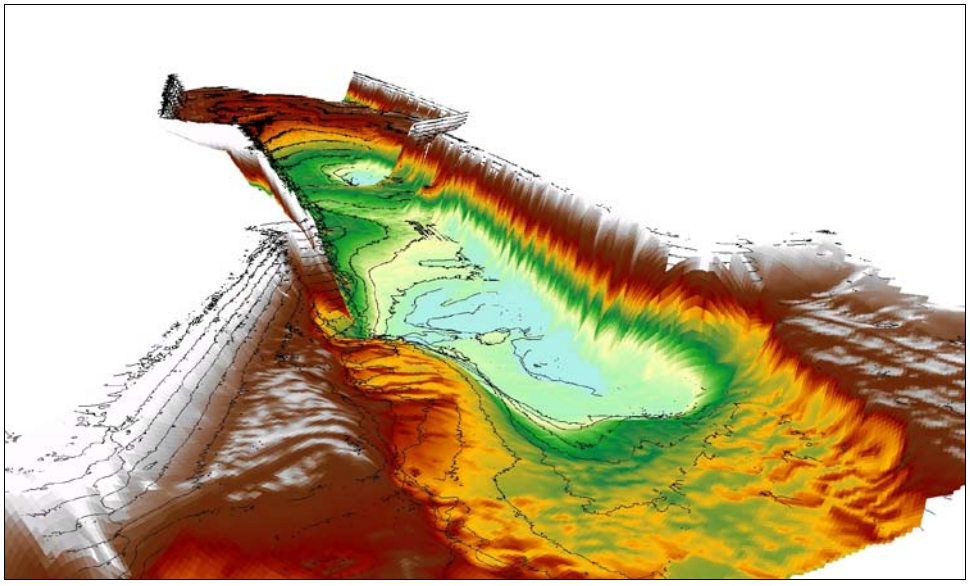

Figure 44. Pseudo-3D view of the Matagorda navigation channel looking toward the Gulf of Mexico from the back barrier bay side. This view shows a deep channel that has downcut into the Beaumont Formation. The top of the Beaumont surface is approximately shown by transition from orange to green in illustration.

Sediments belonging to the Beaumont Formation correspond to the green to cyan elevation color range in Figures 43 and 44. The Beaumont surface is characterized by a significant increase in soil stiffness, as compared to the Holocene sediments, because of sub-aerial exposure during glacial maximum conditions. The surface of the Beaumont is fine-grained (CL and CH). Boring and cross-section data in Figures 37 through 42 identify what appears to be a point bar depositional sequence, containing a fine-grained top stratum (CL and CH), underlain by a coarser-grained substratum (SM, SP). Boring data indicates that there are stacked point bar sequences beneath the navigation channel. This picture is consistent with the regional geology that has been developed for the Beaumont. The navigation channel has progressively down cut through the stiff top stratum of the Beaumont Formation.

Soils data and material properties

Drilling and sampling program

The drilling and sampling program was conducted along the north and south sides of the MSC entrance to collect site-specific geotechnical properties of the subsurface to aid in the stratigraphy development needed to conduct slope stability analyses. The exploration program consisted of eight borings, four on each side of the channel, B1 to B4 on the south side

and B5 to B8 on the north side. The borings ranged in depths from 175 to 200 ft. Sampling consisted of undisturbed samples and split spoon along with Standard Penetration Tests (SPT). The locations of the boreholes are shown in Figure 36 and tabulated in Table 4.

Standard Penetration Testing was performed in the Barrier Island Sands. Disturbed split spoon samples recovered from the SPT were used in the laboratory testing program for sieve analysis and specific gravity testing. Both Standard Penetration Testing and undisturbed sampling were employed in the Beaumont clay underlying the Barrier Island sands. Undisturbed samples were recovered using Shelby tubes at depths where the material was cohesive. Where the material was sandy, SPT were performed with recovery of samples using the split spoon sampler. The decision as to which sampling technique to use was made in the field by the drilling contractor, based on observations made from cuttings. The Beaumont clay was nominally sampled at 5 ft for the 200 ft depth holes (B-1, B-4, B-5, and B-7) and at 10 ft depth intervals for the 175 ft holes (B-2, B-3, B-6, and B-8) from the contact elevation between the Barrier Island Sand and Beaumont clay to the bottom of the borehole.

For the clay materials of the Beaumont Formation, undisturbed samples were recovered using 3 in diameter Shelby tubes having a length of 30 in. The drilling contractor extruded the samples from the Shelby tubes in the field. A detailed description of the sample, the hydraulic pressures to advance the Shelby tube, pocket penetrometer resistance values and depth interval for sample recovery were noted in the boring log. The complete boring logs are provided in the report by Rock Engineering and Testing Laboratory (2008), *Geotechnical Investigation at the Matagorda Ship Channel Matagorda Peninsula, TX*, and parts of this data are included in the geotechnical summary tables presented in Appendix B.

Standard Penetration Tests

SPT were conducted in the Barrier Island sands and at depths where sand lenses or gravel lenses were encountered in the Beaumont clay formation to provide strength information needed for slope stability analyses. The SPT is an in-situ soil test performed on the drill rig which measures the penetration resistance of the soil at various depths. The penetration resistance is measured in terms of the blow count or N-value. The N-value is the number of blows of a weight (hammer) of 140-lbs dropping a distance of 30-inches that advances the split-spoon sampler a distance of 1-ft. The hammer weight

and drop distance represents a standardized energy level for each blow. The N-value is an index value that can be correlated to soil properties such as near strength. Thus, generally, the higher the N-value the greater the strength. The ASTM Standard for the SPT is D1586-08a. A description of the SPT and the procedure needed to correlate SPT results to strength is provided in Appendix B. A plot of SPT N-values corrected to $(N_1)_{60}$ values from all the borings are presented in Figure 45. The SPT $(N_1)_{60}$ values show a fair amount of scatter throughout the site. There is a very diffuse trend in this data of N values which decreases with depth. This trend is interpreted as predominately attributed to the increased clay nature of the foundation with depth. The N-values range from a minimum of 5 to a maximum of 73 for the entire site with most values found between 5 and 40. The Barrier Island sands exhibit a wider range in N-values than those in the underlying Beaumont clay formation. The range of median N-values for each boring show that the Barrier Island sands range between 22 and 30, and that the Beaumont clays formation sands range between 12 and 23. Comparing the range of medians from individual borings provides a measure of spatial variability for this site based on the site characterization boring plan. This shows that although the Barrier Island sands have wider minimum to maximum variability, the most likely values are less variable across the site than the underlying Beaumont Clay formation sands. A nominal correlation of N-values to strength defined as friction angle is also provided on the figure. This strength correlation is based on Table 5 and is shown as a general comparison, as the actual assignment of strengths for analysis involved further evaluation, which resulted in the strengths discussed and documented in the “Stability analyses” section.

Laboratory test program

The laboratory test program included classification and strength testing to characterize the Barrier Island sands and the clay layers in the Beaumont Clay formation. These objectives were achieved by performing tests on undisturbed samples recovered from the drilling and sampling program. The tests were performed by the Rock Engineering, Corpus Christi, TX, and Tolunay–Wong Engineers, Inc., Houston, TX, laboratory soil testing firms; both laboratories are approved and certified by the USACE Material Testing Center. The types of tests performed on the soil samples were designated by ERDC’s Geotechnical and Structures Laboratory and performed in accordance to ASTM standards. The classification tests included sieve analysis, Atterberg limits, specific gravity, and water content. These tests allowed the soil composing each sample to be classified in accordance

with the USCS (ASTM D2487-00). These data for each of the eight borings are provided in the geotechnical summary tables in Appendix B.

The undrained soil strength of the clay samples was determined from Unconsoldidated Undrained (UU) shear tests, also known as Q-tests. A strength envelope was determined from specimens trimmed from each specified undisturbed sample. Additionally, four consolidation tests were performed on selected samples to determine the preconsolidation pressure (P_c) of the samples in question to evaluate the stress-history in the Beaumont clay. The interpreted strength values and their assignment to layers for use in developing a geotechnical cross section for each of the eight borings for analyses are provided in Appendix C.

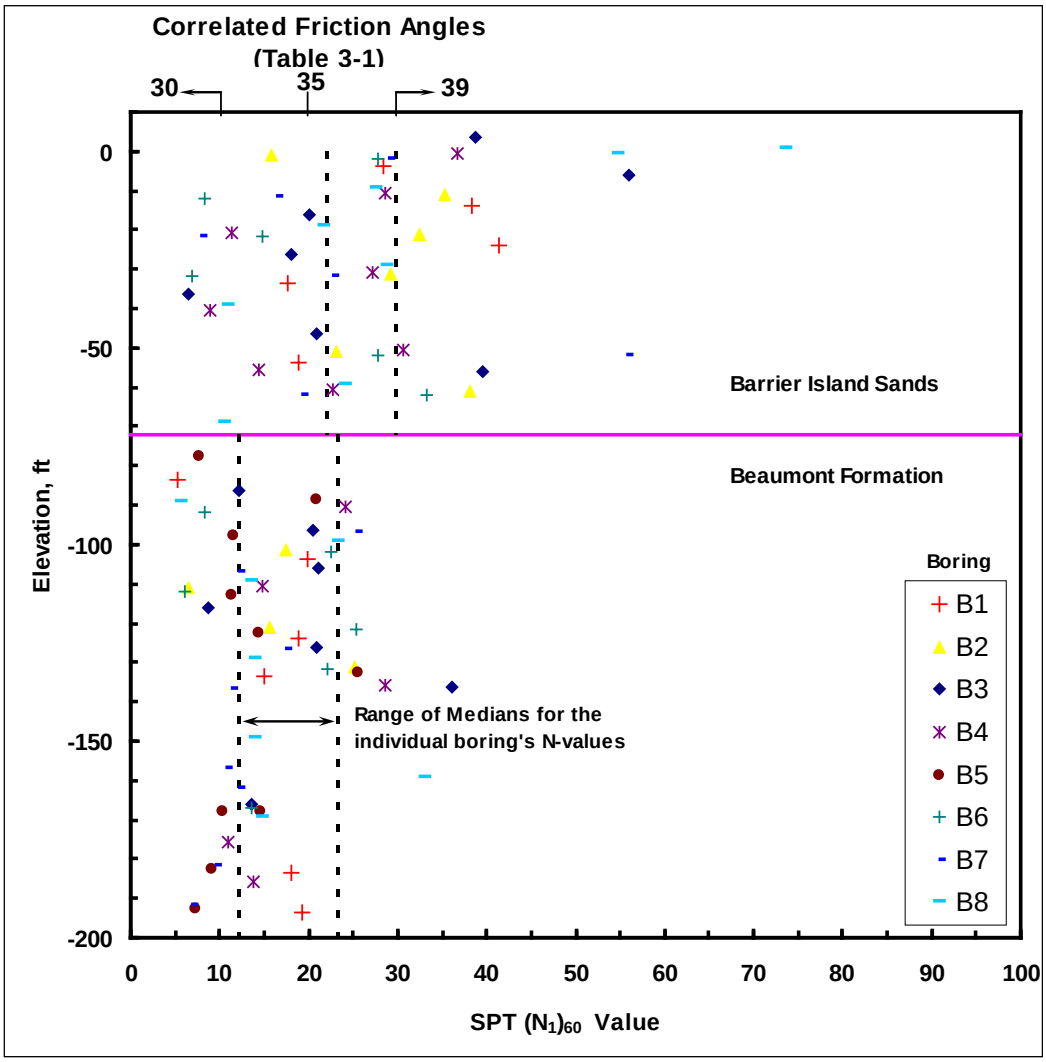

Figure 45. SPT $(N_1)_{60}$ values for all borings.

Table 5. $(N_1)_{60}$ correlations to friction angle and total unit weight (derived from Bowles 1977).

Blow Count	Friction Angle (deg)	Total Unit Weight (pound/cubic foot)
<10	30	125
10-11	31	
12-13	32	
14-16	33	130
17-20	34	
21-23	35	
24-26	36	135
27-28	37	
29-30	38	
>30	39	140

The number of each type of test performed is tabulated in Table 6.

Table 6. Type and number of tests performed in laboratory testing program.

Soil Tests	Number of Tests	ASTM standard
Sieve Analysis	175	D422-63 Reapproved (07)
Atterberg Limits (LL, PL, PI)	71	D4318
Specific Gravity	25	D854
Water Content	176	D2216-05
UU or Q-Tests	102	D2850-03a
Consolidation	4	D2435-04

Consolidation

The consolidation test results were performed to estimate the value of the P_c. The P_c and the current loading pressure allow the over-consolidation ratio (OCR) to be calculated. The OCR value indicates whether clay soils in the strata are normally (current overburden stress is the maximum) or over-consolidated (current overburden stress is less than a maximum past stress). An OCR value equal to 1.0 implies that a soil is normally-consolidated; values greater than 1.0 imply that the soil is over-consolidated. The OCR value is important when correlations are used to infer shear strength values because of its influence on strength. The OCR values were calculated for the four consolidation tests performed on the Beaumont clays found in the substrata of Matagorda Island. These values are presented in Table 7 and plotted in Figure 46. These data show that the

OCR generally decreases with depth from 1.8 to 1.2 for depths 79 to 149 ft, respectively, and are generally consistent among the borings. The P_c can be difficult to determine for highly disturbed samples and is a potential source of error. For example, the OCR for boring B-4, shown in Figure 46, could be attributed to sample disturbance. These data show that the clays are lightly over-consolidated.

Table 7. Calculated OCR values for soils in Beaumont Formation.

Boring	Depth (ft)	OCR
B-1t	79	1.8
B-4	89	1.2
B-5	89	1.65
B-6	149	1.2

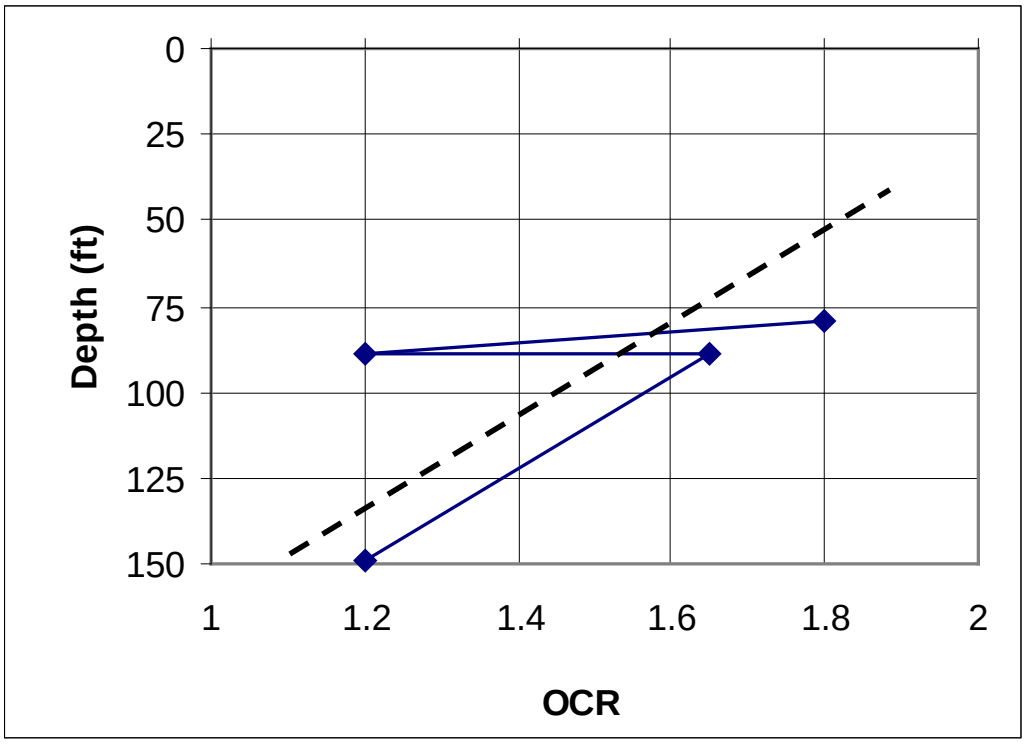

Figure 46. Calculated OCR values versus depth.

General geotechnical foundation assessment

Stratigraphy

The geotechnical evaluation of the boring and laboratory data show that the major geologic stratigraphy description of the adjacent Barrier Island sands consists of a composite of poorly sorted sands (classified as plastic SP) and dirty sands (classified as either SM or SC depending on the Atterberg limits of the fines content of the soil). Dirty sands have a fines content greater than 12% by weight and the fines content is defined as the material passing through the #200 sieve. These sands extend from the ground surface to an approximate depth of 65 ft. The fines content found in the barrier island sands are non-plastic silts and are generally less than 20 percent. The Barrier Island sands are fairly consistent with depth throughout the site, showing only a modest increase of fines with depth. This general stratigraphy of the Barrier Island sands, based on all of the boring data, is shown in Figure 47 in a plot of percent fines with depth for the eight borings.

The Beaumont unit was interpreted to extend from the bottom of the Barrier Island Sands, at a depth of 65 ft, to beyond the limit of the exploratory program (depth of 200 ft). The sands found within the Beaumont Clay deposits are more uniform in grain size and exhibit higher fines content and more variability, with fines contents nominally ranging from 10 to 40 percent. These fines are predominately non-plastic (SM). However, some samples had plastic fines that cause them to classify as clayey sands (SC). There are two main sand layers within the dominant clays found at depths of 95-115 ft and 130-145 ft. Also, there appears to be sand lenses located a depth of 160-170 ft.

As discussed in the “Geology” section, the Beaumont Formation is described as a series of point bar deposits composed of a clay top-stratum overlying a substratum of sand. The Beaumont Clay formation clays are a mixture of lean to fat clays (low plastic (CL) to high plastic (CH)). Inspection of Figure 47 show that clays at the upper point bar deposit of this unit, at depths 65 to 95 ft, range from CL to CH. Below this top-stratum, a distinct zone substratum of sand is evident, completing the point bar. The next point bar begins with a layer of clays starting at a depth of 120 ft and an associated sand layer extending to 140 ft. The clay in this layer is more diffuse and is classified as CL. Another point bar begins, which contains a diffuse-intermixed sand-clay layer, at a depth of about165 ft, with the clays containing much higher plastic fines, and is classified predominately as CH. The

clay characteristics are further presented in Figure 48, which plots plasticity index (PI) versus depth. Figure 48 is overlaid with classification and correlated drained strengths, which indicate their range and variability.

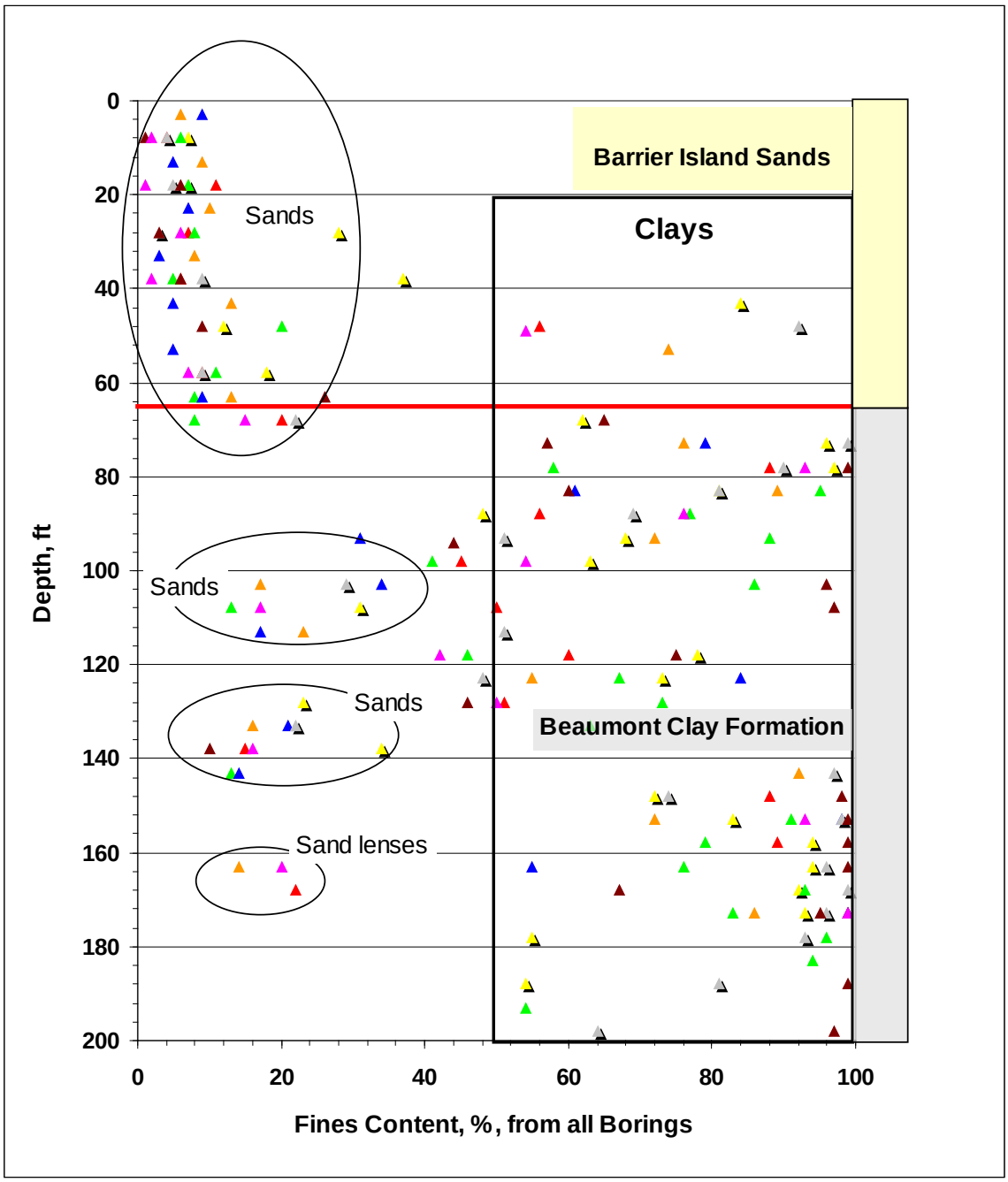

Figure 47. Relation of general soil stratigraphy to fines content.

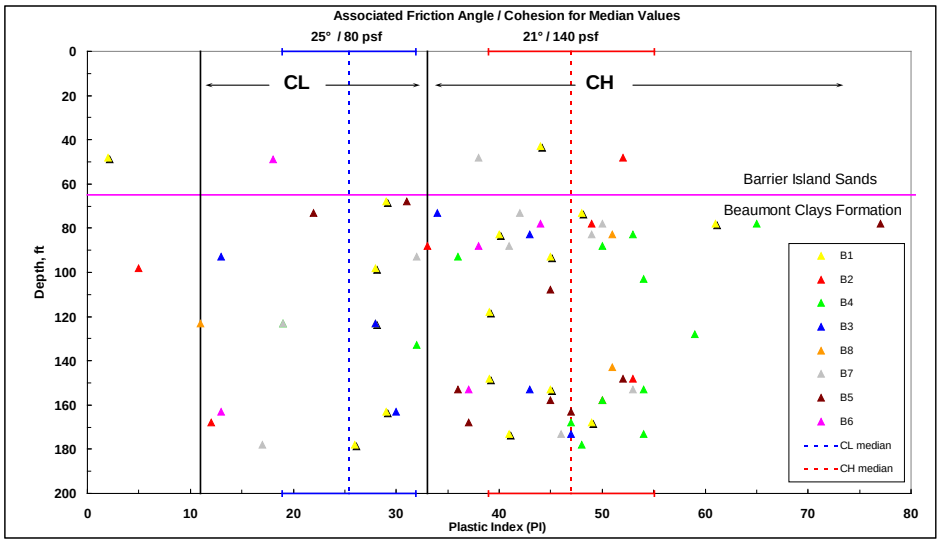

Figure 48. General clay properties for all borings.

Strength assignment methodology

The approach for developing strengths for use in the stability analyses was based on site-specific field and laboratory data and applicable published state-of-practice correlations. Strengths were developed for use in undrained analyses (short-term loading) and drained analyses (long-term loading).

Cohesionless soils

The field measurement of SPT N-values for the cohesionless materials (sands and silts) was the basis for assigning undrained shear strength as a friction angle (φ). The friction angle was assigned based on the correlation presented in Table 5. This table was derived from Bowles (1977) and modified to allow more refined interpolation of friction angles.

Cohesive soils

Laboratory shear tests provided the basis for developing undrained strengths, S_u, for the clay (cohesive) materials. The laboratory shear tests are documented in Rock Engineering and Testing Laboratory (2008). The drained strengths, effective cohesion (c') and effective friction angle (φ') were developed from correlations to plasticity index (PI) data. The correlation between effective cohesion (c') and PI for normally consolidated soils (Galveston District 1963), and the correlation between effective friction angle (φ') and PI for normally consolidated soils (Galveston District 1963) are shown in Figures 49 and 50, respectively.

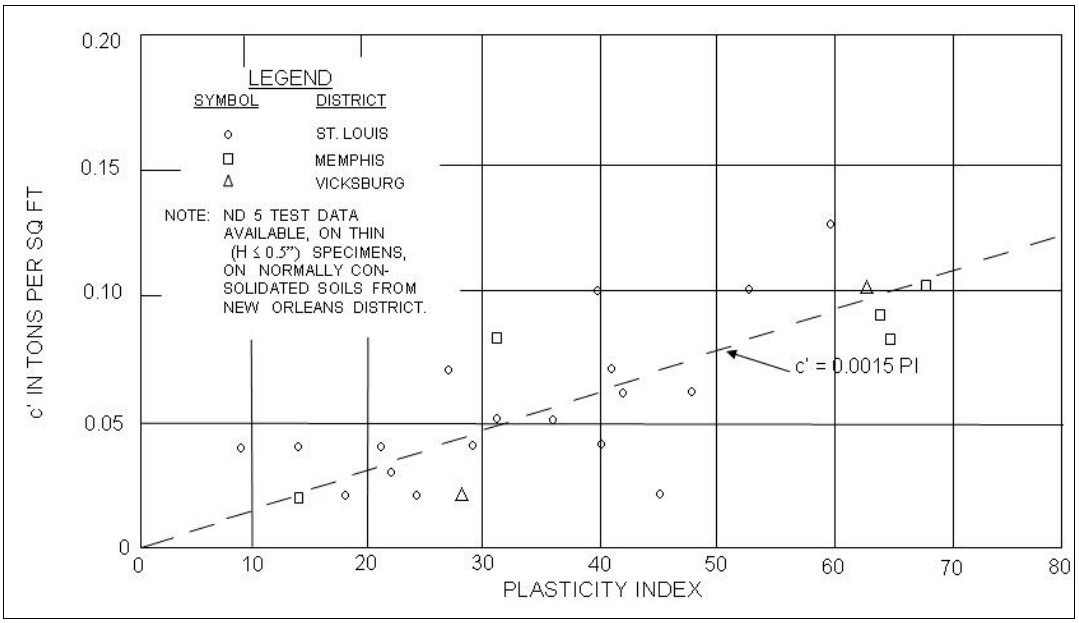

Figure 49. Correlation between effective cohesion (c') and PI for normally consolidated soils (Department of the Army, 1962).

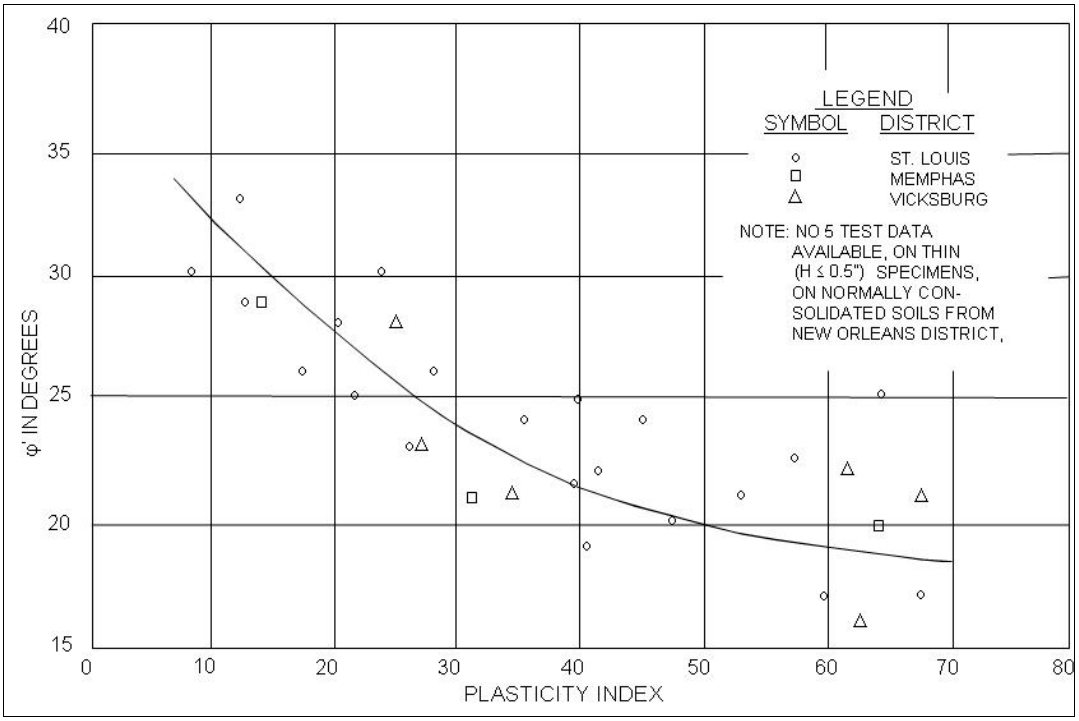

Figure 50. Correlation between effective cohesion (φ') and PI for normally consolidated soils (Department of the Army 1962).

A statistical analysis of SPT and PI correlation data was conducted to assist in assigning strength properties to cross sections developed for the stability analyses. These are shown in Tables 8 through 10. Table 8 is a summary of PI for Clays and correlated strength values for borings B-1 through B-8. This data is sorted into Barrier Island clays and two depth zones for the clays in the Beaumont Formation. Table 9 summarizes $(N_1)_{60}$ and correlated strength values for Borings B-1 through B-8. This data is sorted into Barrier Island sands and sands in the Beaumont Formation. Table 10 is a summary of PI for Clays and $(N_1)_{60}$ for Sands and correlated strength values sorted into CL and CH clays, all clays, and all sands.

Table 8. Summary of PI and correlated drained strength values of clays for borings B-1 through B-8.

Borings	B-1	B-2	B-3	B-4	B-5	B-6	B-7	B-8	ALL
Barrier Island Clays (0 - 65 ft)									
Number of Samples	1	1	0	0	0	1	1	0	4
Mean (PI)	44.0	52.0	na	na	na	18.0	38.0	na	38.0
Standard deviation	na	na	na	na	na	na	na	na	14.5
Correlated Strengths									
Friction angle	21	20	na	na	na	28	22	na	22
Cohesion (psf)	132	156	na	na	na	54	114	na	114
Beaumont Clays (65 - 140 ft)									
Number of Samples	8	2	2	8	4	2	6	1	33
Mean (PI)	39.8	41.0	38.5	46.0	43.8	41.0	38.8	51.0	42.0
Standard deviation	11.6	11.3	6.4	15.5	24.1	4.2	11.7	na	13.2
Correlated Strengths									
Friction angle	22	22	22	21	21	22	22	20	21
Cohesion (psf)	119	123	116	138	131	123	116	153	126
Beaumont Clays (> 140 ft)									
Number of Samples	6	2	4	5	5	1	3	2	28
Mean (PI)	48.2	51.5	37.0	50.6	43.4	37.0	38.7	31.0	41.6
Standard deviation	9.0	2.1	9.4	3.3	6.8	na	19.1	28.3	11.3
Correlated Strengths									
Friction angle	20	20	22	20	21	22	22	24	22
Cohesion (psf)	145	155	111	152	130	111	116	93	125

Table 9. Summary of $(N_1)_{60}$ and correlated strength values of sands for borings B-1 through B-8.

Borings	B-1	B-2	B-3	B-4	B-5	B-6	B-7	B-8	ALL
Barrier Island Sands (0 - 65 ft)									
Number of samples	5	6	6	7	5	4	5	6	44
Median $(N_1)_{60}$	28.5	30.8	29.8	27.3	22.1	27.8	22.8	28.3	27.8
Standard deviation	na	na	na	na	na	na	na	na	13.2
Correlated strengths									
Friction angle	37	39	38	37	35	37	35	37	37
Beaumont Formation Sands (> 65 ft)									
Number of Samples	6	4	5	5	2	4	5	4	35
Median $(N_1)_{60}$	18.5	16.6	20.9	14.8	23.3	22.3	12.2	18.7	18.9
Standard deviation	na	na	na	na	na	na	na	na	7.4
Correlated Strengths									
Friction angle	34	33	34	33	35	35	32	34	34

Table 10. Summary of (N1)60 for sands and PI for clays and correlated strength values.

Plasticity Index and Strength Values for all Clay		**$(N_1)_{60}$ and Strength Values for all Sands**	
Number of Samples	65	Number of Samples	79
Mean (PI)	41.6	Median $(N_1)_{60}$	22.1
Standard deviation	12.3	Standard deviation	12.2
Correlated Strengths		**Correlated Strengths**	
Friction angle	21	Friction angle	35
Cohesion (psf)	125		
Plasticity Index and Strength Values for all CL Clays		**Plasticity Index and Strength Values for all CH Clays**	
Number of Samples	17	Number of Samples	48
Mean (PI)	25.4	Mean (PI)	47.3
Standard deviation	6.5	Standard deviation	8.1
Correlated Strengths		**Correlated Strengths**	
Friction angle	26	Friction angle (deg)	20
Cohesion (psf)	76	Cohesion (psf)	142

Stability analyses

Limit equilibrium slope stability analyses were performed to calculate factors of safety against sliding. The factor of safety represents the ratio of mobilized shear stress to available shear stress (strength) along an assumed failure surface (Bishop 1955). These analyses required developing cross sections (geometry), assigning soil strengths to each layer in the cross section, applying water loads, and performing stability computations to determine the failure surface that has the minimum factor of safety for each cross section. The surface associated with the minimum factor of safety is called the critical failure surface and the minimum factor of safety is called the critical factor of safety. The critical failure surface and its factor of safety are determined using systematic search routines provided in the slope stability software that analyzes many different potential failure surfaces. Both drained and undrained analyses were performed to determine if either short- or long-term loading condition was the most critical for slope stability of the channel walls. Additionally, stability analyses were performed for each cross section at various depths in an effort to estimate the effects of channel erosion.

Cross sections for deterministic analysis

Site-specific cross sections were developed for each of the eight boring locations. The geotechnical cross sections were based on the geologic cross sections, as shown in Figures 37 and 42, and further refined using laboratory data. The summary tables of properties for each cross section are provided in Appendix C. After analysis of these site-specific cross sections, three critical profiles were selected for further analysis. These three critical cross sections were simplified to facilitate a probabilistic analysis.

Geometry

Two-dimensional cross sections or models were developed to represent existing geometric conditions. The geometry of these models included soil stratigraphy, channel slope, flowable rip-rap armoring the channel slopes, and water loads (water table and channel water level).

Material properties

The stability analyses require material density and shear strength parameters (friction angle and cohesion values) for each soil layer, for both drained and undrained conditions. The undrained shear strength for clay

materials was assigned using a linear Mohr-Coulomb strength envelope. The friction angle for sands was determined using correlations between $(N_1)_{60}$ values and friction angles (Table 5).

Clays were assigned both a friction angle and cohesion for drained analyses. The friction angle was determined using a correlation between friction angle and PI, and the cohesion value was determined using a correlation between cohesion and PI (Galveston District 1963). The correlations are derived from the engineering properties of fine-grained alluvial deposits of the Mississippi Valley test results from normally consolidated soils.

Consolidation tests on the Beaumont Clay indicated that these clays were slightly over-consolidated with an OCR ranging from 1.2 and 1.8 for 150 ft and 80 ft depths, respectively. The soil profiles (see Figures 37 and 38) indicate that some clay lenses were found in the barrier island sands at approximately 40 ft. These clay lenses, if encountered, were often thin (less than 5 ft). Other clay layers that may affect the stability analyses are located below 70 ft. The impact of using the correlations for normally consolidated clays when the lay is actually slightly over-consolidated will produce friction angle and cohesion values that are conservative. Therefore, the strength values used in the drained analyses could be lower than what exists in the field.

Slope stability calculations

Slope stability analyses were conducted using the UTexas4 version 4.1.0.4 (10/05/2008) computer program (Wright 1999a) and a graphics post processor TexGraf Version 4.1.0.4 (Wright 1999b). The procedure involves calculating the factor of safety against the sliding of a soil mass above a given trial failure surface. Circular failure surfaces were employed to facilitate this search. A non-circular failure surface was also checked to insure the adequacy of the circular failure surface to accurately represent the critical failure geometry. A systematic search procedure was employed to find the critical failure surface. A critical failure surface is the lowest factor of safety for an engineering significant failure, in this case a failure mass that begins at the top of the slope and exits near the toe. An example slope stability analysis is presented in Figure 51. This figure shows a typical cross section or model properties (soil layers and channel geometry), the table of soil properties, and the water loads included in the analyses. The critical failure surface is plotted in bold red and shows that the critical factor of safety is 1.039. In addition to the critical failure surface,

numerous other trial failure circles generated during the thorough search procedure were analyzed. This thorough evaluation was used to ensure that the critical failure surface agreed with overall slope behavior and provided insight into the sensitivity of results with respect to the factor of safety and failure geometry.

Description and comparison of analyses

The analyses were conducted for total stress (undrained) and effective stress (drained) representing short-term and long-term conditions, respectively.

Total stress analysis

The total stress analysis is based on short-term or undrained conditions. The UU laboratory test was used to determine the undrained properties as discussed in the "Strength assignment methodology" section. Pore pressures are not allowed to dissipate during the rapid shearing of the sample during the UU test, which is indicative of short-term field loading conditions. The factor of safety for the current channel depth ranges from 0.971 to 1.778 (Table 11 and Figure 52) and reduces in range to 0.867 through 1.583 for the 150 ft depths. The factor of safety for B-3 and B-4 does not change with depth, indicating that upper strata soil strengths control stability or that the cross-section geometry is unrealistic. In general, the factor of safety decreases with channel depth for each cross section as would be expected. The cross sections with their critical failure surfaces are presented in the "Undrained analyses" section in Appendix D.

Effective stress analysis

The effective stress analysis is based on long-term or drained conditions. The clay strengths were derived from PI based correlations as discussed in the "Strength assignment methodology" section. The factor of safety for the drained set of analyses ranges from 0.956 to 1.283 for the current channel depth, Table 12 and Figure 53, and reduces in range from 0.877 to 1.233 for the 150 ft depth. Only the cross section for boring B-4 had a

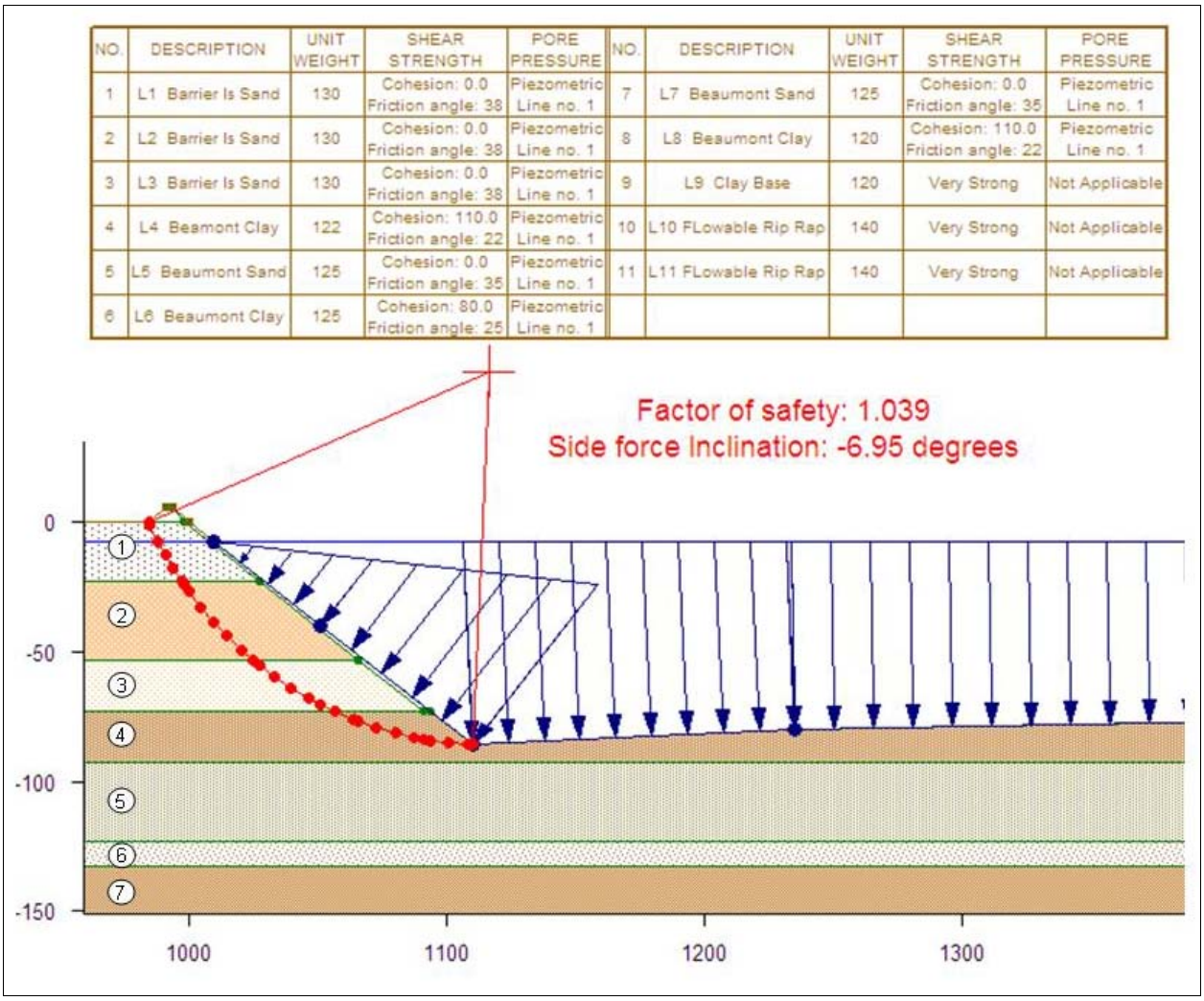

Figure 51. Example slope stability analysis.

constant factor of safety with depth. In general, the factor of safety decreases with increasing channel depth for each cross section as would be expected. The cross sections with their critical failure surface are presented in the "Drained analyses" section of Appendix D.

Critical sections

The undrained and drained analyses were compared to evaluate their criticality and determine which type of analysis should be used for a more detailed analysis. In general, the drained analyses tend to be more consistent with depth and group at a lower factor of safety. The lower factor of safety from these analyses appears to best represent the overall stability of the channel and is consistent with the instabilities that have occurred in the past, shown in Figure 54. Additionally, the borings that show a low

factor of safety correlate well with field evidence of past failures. A comparison of the drained versus undrained factor of safety are presented in Table 13. The data in this table are from Tables 11 and 12. These results show that for each cross section, the factors of safety for the drained condition are lower than the undrained condition. Hence, the drained condition is deemed the most critical and the remaining analyses will be based on drained conditions.

All cross sections were evaluated and boring B-4 did not appear to have a realistic representation of the upper portion of the cross section. The bathymetric survey near boring B-4 (Figure 39) indicated that the slope was 69 deg between the surface and a depth of 40 ft. An angle this high is unrealistic for the barrier island sands, which tend to have an angle of repose in the range of 28-38 deg. Therefore, the bathymetric data are considered inaccurate in this area and cross-section B-4 was not considered to represent actual geometry.

Three cross sections of the ship channel were selected from the remaining seven cross sections to represent the range of factors of safety from low to high, two with the low factor of safety and one with a high factor of safety, Table 13. Cross sections for borings B-3 and B-7 were determined to have the lowest factor of safety and considered the most critical. The cross section associated with boring B-1 had the lowest channel depth and highest factor of safety with depth. Based on the above criterion, cross-sections B 1, B 3, and B 7 were selected for probabilistic analysis and are shown in Figures 55, 56, and 57, respectively.

Table 11. Summary of factor of safety values for depths analyzed using undrained properties.

	Factor of Safety							
Boring Depth (ft)	B-1	B-2	B-3	B-4	B-5	B-6	B-7	B-8
Existing (depth)	1.778 (100)	1.690 (85)	1.265 (86)	0.971 (66)	1.413 (69)	1.499 (65)	1.469 (72)	1.625 (73)
130	1.617	1.424	1.265	0.971	1.376	1.283	1.042	1.347
150	1.583	1.363	1.265	0.867	1.318	1.283	1.042	1.347

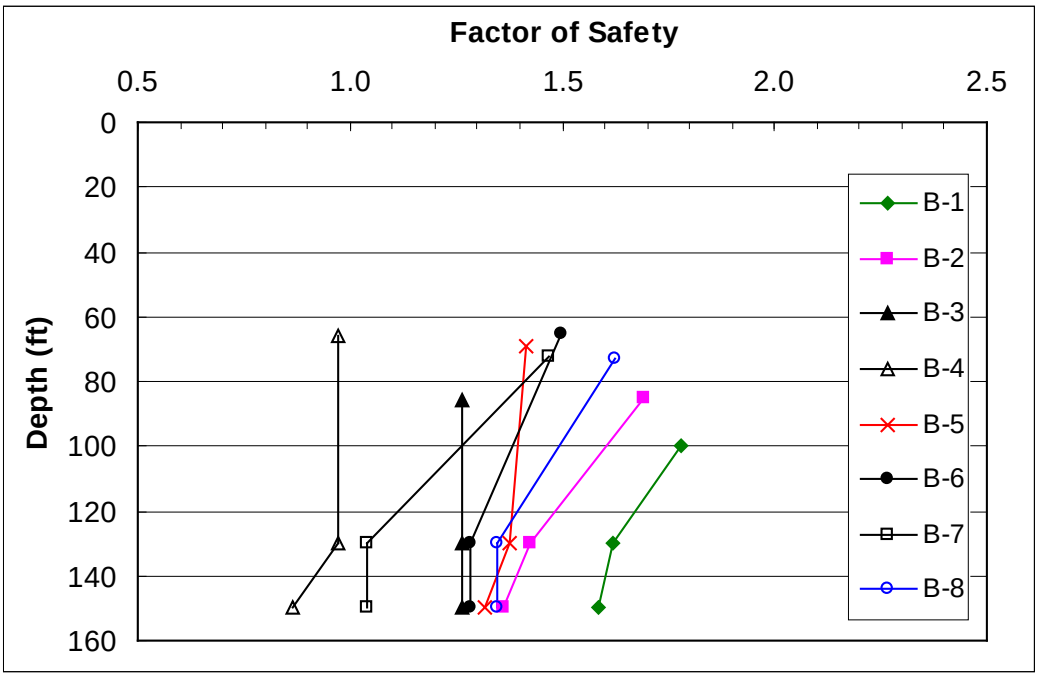

Figure 52. Factor of safety versus depth for undrained slope stability analyses.

Table 12. Summary of factor of safety values for depths analyzed using drained properties.

	Factor of Safety							
Boring Depth, ft	B-1	B-2	B-3	B-4	B-5	B-6	B-7	B-8
Existing (depth)	1.283 (100)	1.178 (85)	1.039 (86)	0.956 (66)	1.405 (69)	1.272 (65)	1.050 (72)	1.216 (73)
130	1.235	0.993	0.947	0.971	1.157	1.066	0.890	0.998
150	1.233	0.994	0.927	0.971	1.148	1.066	0.877	0.998

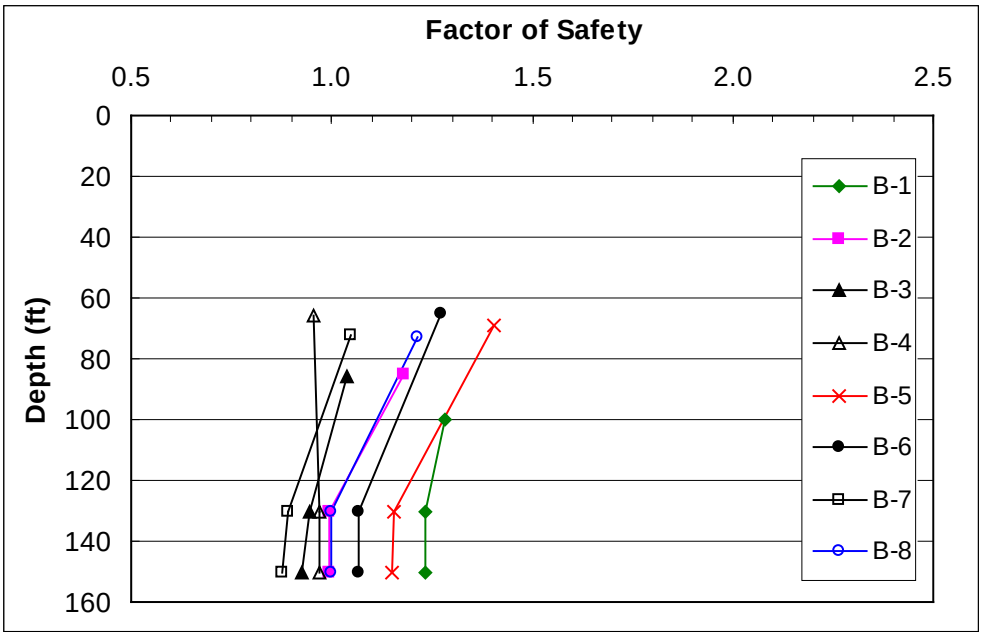

Figure 53. Factor of safety versus depth for drained slope stability analyses.

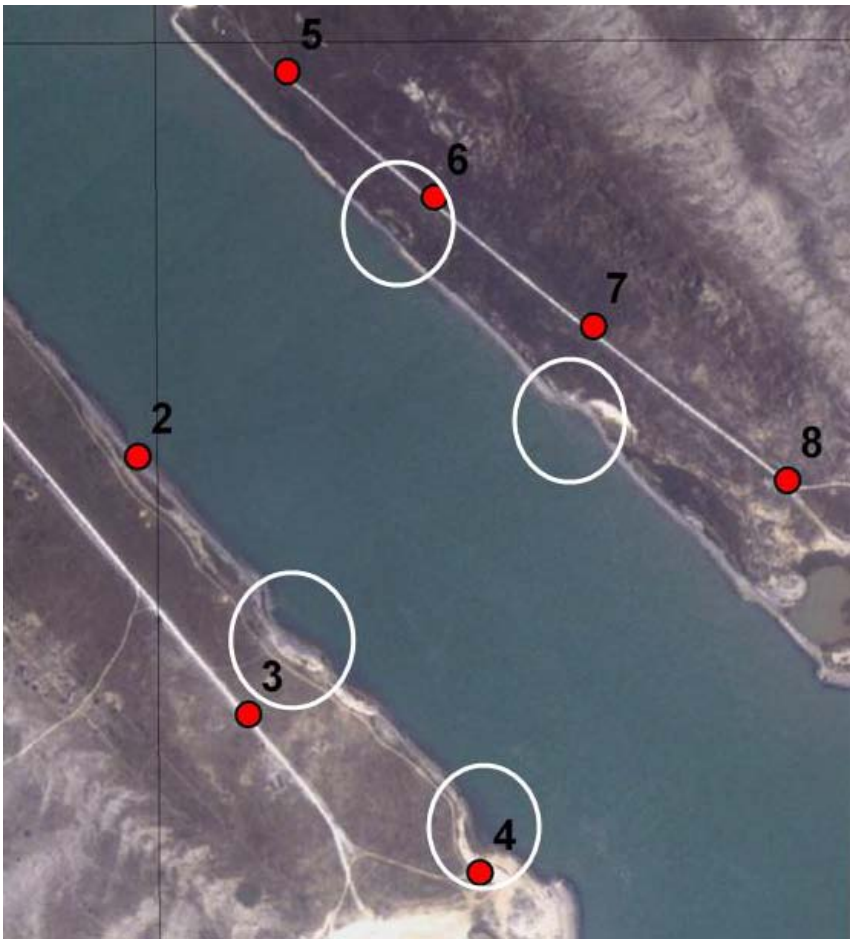

Figure 54. Field evidence of past slope failures (annotated with while circles) extracted from Figure 36.

Table 13. Comparison of drained and undrained factors of safety for each cross section.

Boring	B-1		B-2		B-3		B-4	
Depth (ft)	Drained	Undrained	Drained	Undrained	Drained	Undrained	Drained	Undrained
Current (depth)	1.283 (100)	1.778 (100)	1.178 (85)	1.690 (85)	1.039 (86)	1.265 (86)	0.956 (66)	0.971 (66)
130	1.235	1.617	0.993	1.424	0.947	1.265	0.971	0.971
150	1.233	1.583	0.994	1.363	0.927	1.265	0.971	0.867
Boring	B-5		B-6		B-7		B-8	
Depth (ft)	Drained	Undrained	Drained	Undrained	Drained	Undrained	Drained	Undrained
Current (depth)	1.405 (69)	1.413 (69)	1.272 (65)	1.499 (65)	1.050 (72)	1.469 (72)	1.216 (73)	1.625 (73)
130	1.157	1.376	1.066	1.283	0.890	1.042	0.998	1.347
150	1.148	1.318	1.066	1.283	0.877	1.042	0.998	1.347

Probabilistic slope stability analyses

Description of analysis

Probabilistic slope stability analyses were performed using the critical cross sections developed from borings B-1, B-3 and B-7 to determine the probability of failure at these locations. The probabilistic analysis is based on the idea of treating both the strength and factor of safety as random variables. The probabilities of failure were estimated using an approximate technique based on the Taylor Series Method and described by Duncan and Wright (2005) and Wolff (1996). For each of the three sections, the probability of failure was computed for five different canal bottom depths to determine the impact of continuing erosion (or deepening of the channel) on the stability of the side slopes of the channel. These five depths included the current depth and depths deeper by 5, 10, 25, and 50 ft. Thus, if an erosion rate of 1 ft/year is assumed to continue, the probabilities of failure computed for these levels would represent the current probability of failure and those in 5, 10, 25, and 50 years from now. The probability of failure for these sections was based on the variation in the long-term (drained) shear strength parameters.

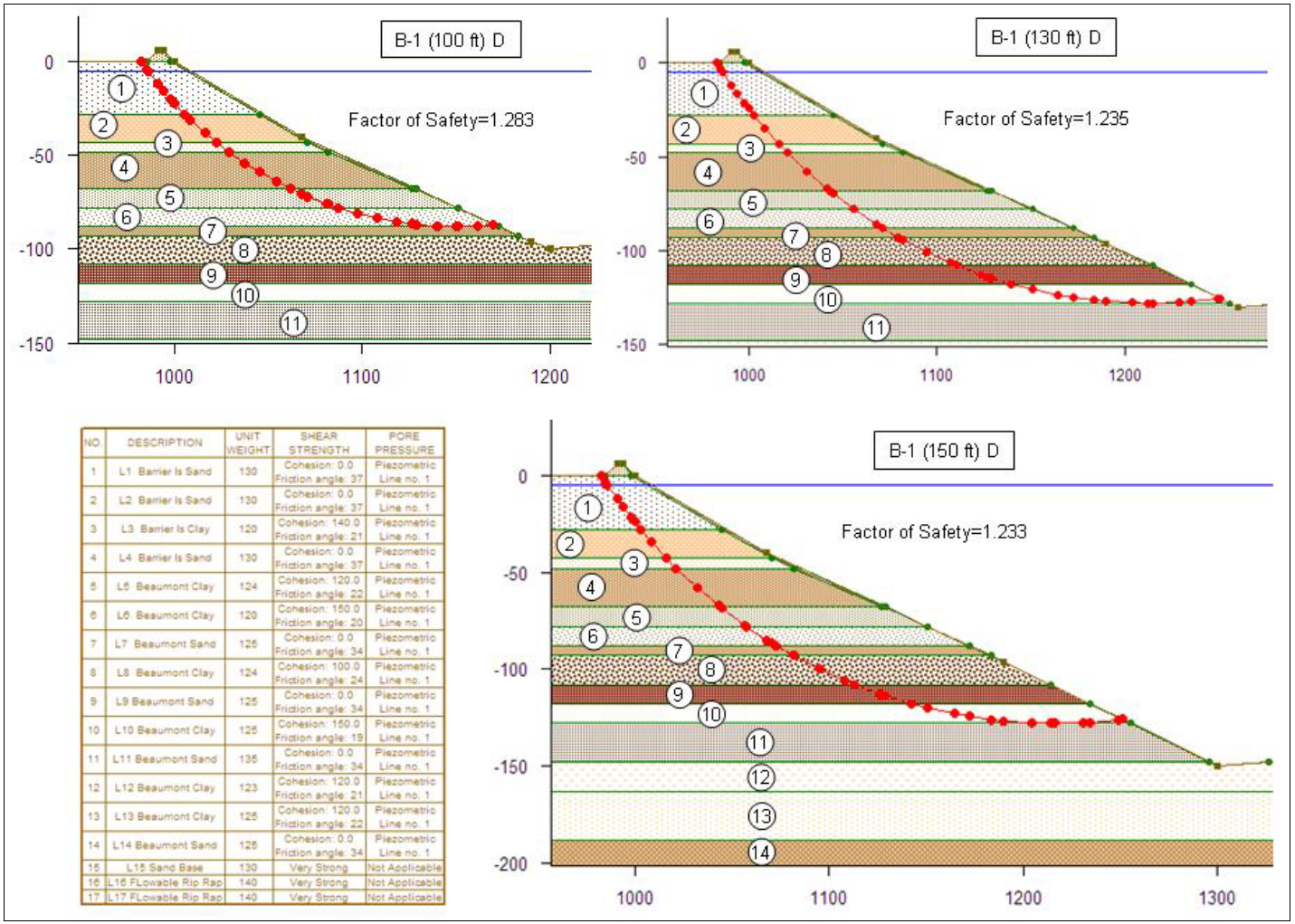

NO.	DESCRIPTION	UNIT WEIGHT	SHEAR STRENGTH	PORE PRESSURE
1	L1 Barrier Is Sand	130	Cohesion: 0.0 Friction angle: 37	Piezometric Line no. 1
2	L2 Barrier Is Sand	130	Cohesion: 0.0 Friction angle: 37	Piezometric Line no. 1
3	L3 Barrier Is Clay	120	Cohesion: 140.0 Friction angle: 21	Piezometric Line no. 1
4	L4 Barrier Is Sand	130	Cohesion: 0.0 Friction angle: 37	Piezometric Line no. 1
5	L5 Beaumont Clay	124	Cohesion: 120.0 Friction angle: 22	Piezometric Line no. 1
6	L6 Beaumont Clay	120	Cohesion: 150.0 Friction angle: 20	Piezometric Line no. 1
7	L7 Beaumont Sand	126	Cohesion: 0.0 Friction angle: 34	Piezometric Line no. 1
8	L8 Beaumont Clay	124	Cohesion: 100.0 Friction angle: 24	Piezometric Line no. 1
9	L9 Beaumont Sand	125	Cohesion: 0.0 Friction angle: 34	Piezometric Line no. 1
10	L10 Beaumont Clay	126	Cohesion: 150.0 Friction angle: 19	Piezometric Line no. 1
11	L11 Beaumont Sand	135	Cohesion: 0.0 Friction angle: 34	Piezometric Line no. 1
12	L12 Beaumont Clay	123	Cohesion: 120.0 Friction angle: 21	Piezometric Line no. 1
13	L13 Beaumont Clay	125	Cohesion: 120.0 Friction angle: 22	Piezometric Line no. 1
14	L14 Beaumont Sand	126	Cohesion: 0.0 Friction angle: 34	Piezometric Line no. 1
15	L15 Sand Base	130	Very Strong	Not Applicable
16	L16 FLowable Rip Rap	140	Very Strong	Not Applicable
17	L17 FLowable Rip Rap	140	Very Strong	Not Applicable

Figure 55. Critical failure surfaces with depth for cross section based on boring B-1 (drained condition).

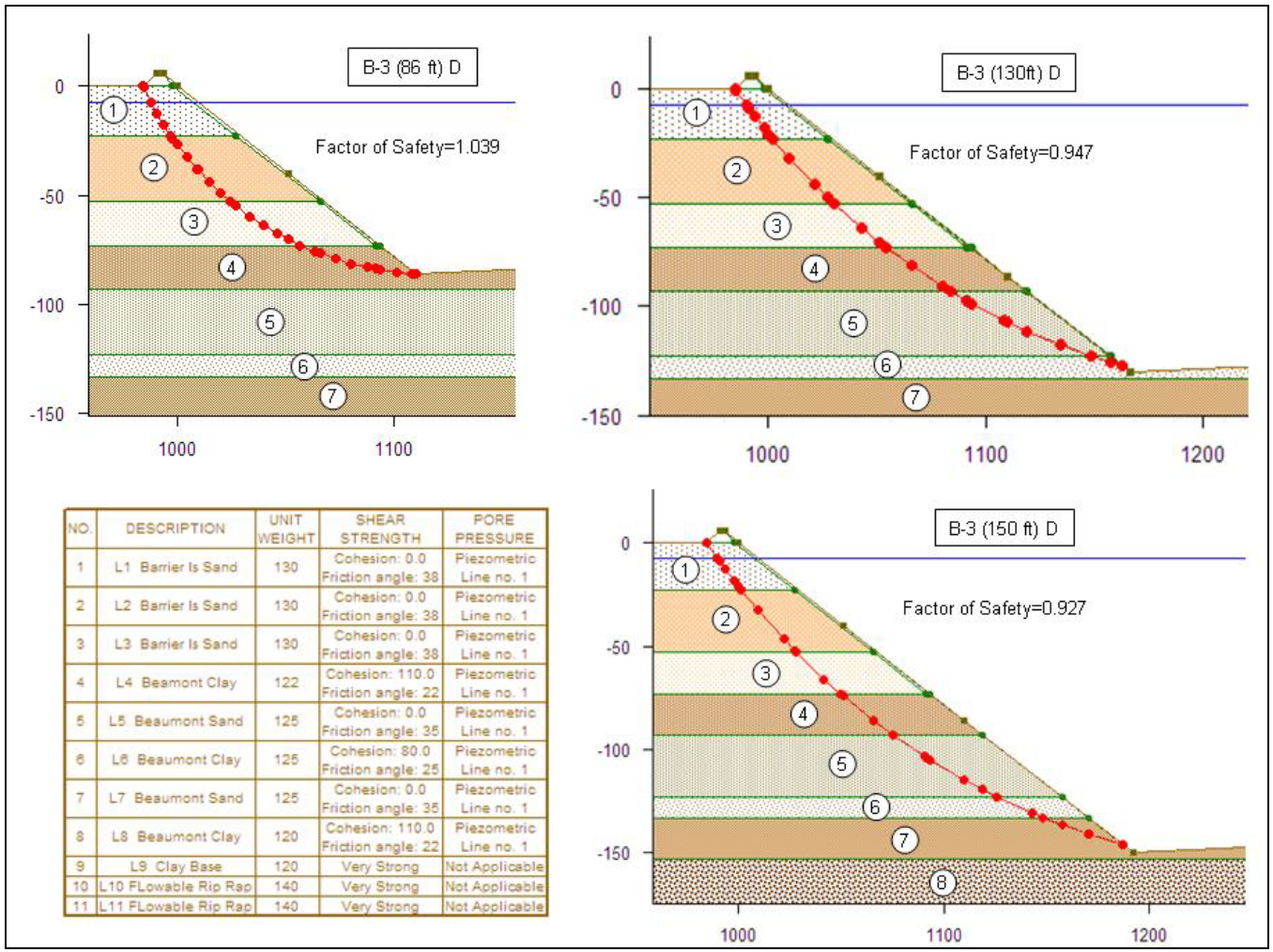

NO.	DESCRIPTION	UNIT WEIGHT	SHEAR STRENGTH	PORE PRESSURE
1	L1 Barrier Is Sand	130	Cohesion: 0.0 Friction angle: 38	Piezometric Line no. 1
2	L2 Barrier Is Sand	130	Cohesion: 0.0 Friction angle: 38	Piezometric Line no. 1
3	L3 Barrier Is Sand	130	Cohesion: 0.0 Friction angle: 38	Piezometric Line no. 1
4	L4 Beamont Clay	122	Cohesion: 110.0 Friction angle: 22	Piezometric Line no. 1
5	L5 Beaumont Sand	125	Cohesion: 0.0 Friction angle: 35	Piezometric Line no. 1
6	L6 Beaumont Clay	125	Cohesion: 80.0 Friction angle: 25	Piezometric Line no. 1
7	L7 Beaumont Sand	125	Cohesion: 0.0 Friction angle: 35	Piezometric Line no. 1
8	L8 Beaumont Clay	120	Cohesion: 110.0 Friction angle: 22	Piezometric Line no. 1
9	L9 Clay Base	120	Very Strong	Not Applicable
10	L10 FLowable Rip Rap	140	Very Strong	Not Applicable
11	L11 FLowable Rip Rap	140	Very Strong	Not Applicable

Figure 56. Critical failure surfaces with depth for cross section based on boring B-3 (drained condition).

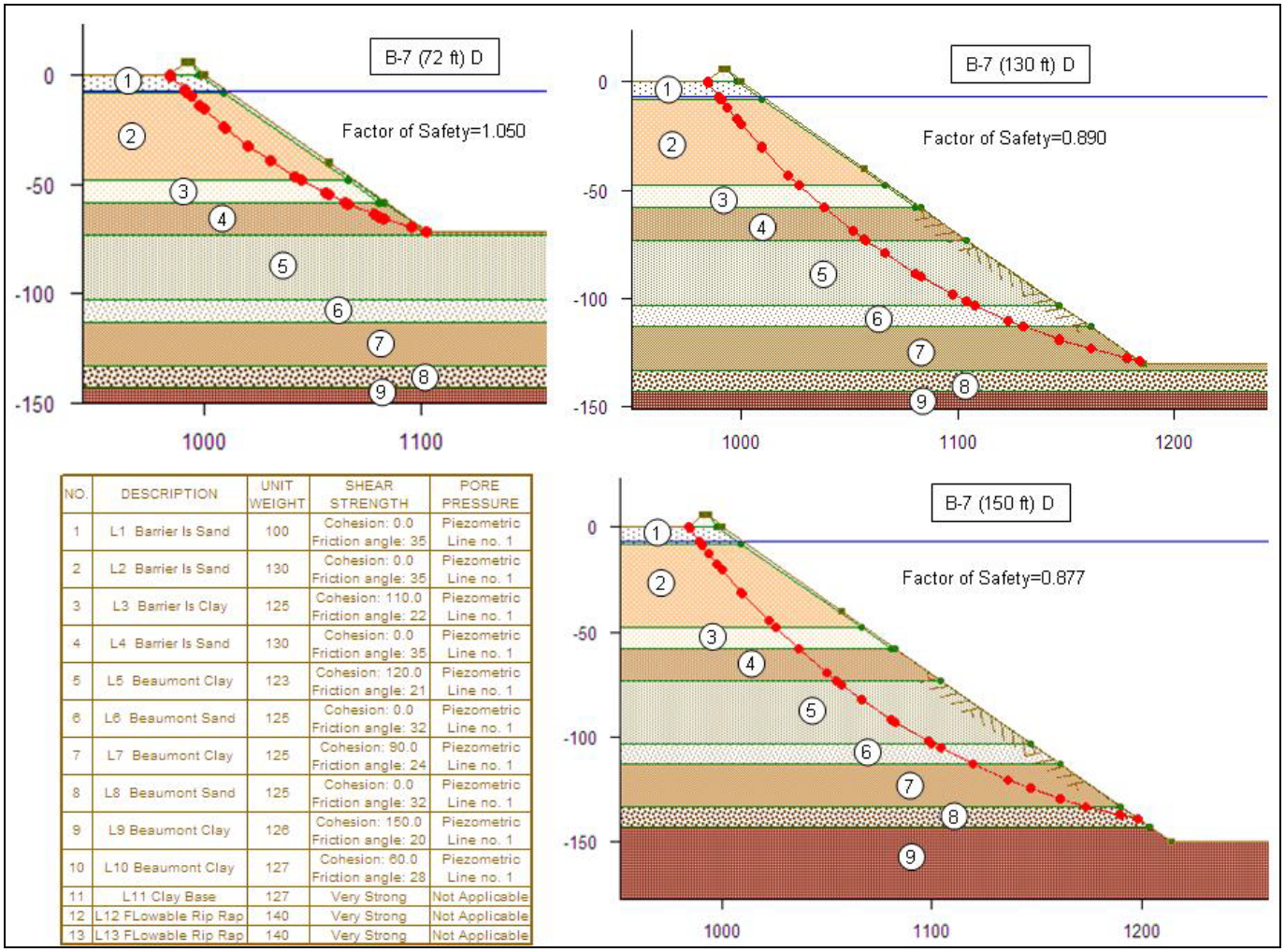

NO.	DESCRIPTION	UNIT WEIGHT	SHEAR STRENGTH	PORE PRESSURE
1	L1 Barrier Is Sand	100	Cohesion: 0.0 Friction angle: 35	Piezometric Line no. 1
2	L2 Barrier Is Sand	130	Cohesion: 0.0 Friction angle: 35	Piezometric Line no. 1
3	L3 Barrier Is Clay	125	Cohesion: 110.0 Friction angle: 22	Piezometric Line no. 1
4	L4 Barrier Is Sand	130	Cohesion: 0.0 Friction angle: 35	Piezometric Line no. 1
5	L5 Beaumont Clay	123	Cohesion: 120.0 Friction angle: 21	Piezometric Line no. 1
6	L6 Beaumont Sand	125	Cohesion: 0.0 Friction angle: 32	Piezometric Line no. 1
7	L7 Beaumont Clay	125	Cohesion: 90.0 Friction angle: 24	Piezometric Line no. 1
8	L8 Beaumont Sand	125	Cohesion: 0.0 Friction angle: 32	Piezometric Line no. 1
9	L9 Beaumont Clay	126	Cohesion: 150.0 Friction angle: 20	Piezometric Line no. 1
10	L10 Beaumont Clay	127	Cohesion: 60.0 Friction angle: 28	Piezometric Line no. 1
11	L11 Clay Base	127	Very Strong	Not Applicable
12	L12 FLowable Rip Rap	140	Very Strong	Not Applicable
13	L13 FLowable Rip Rap	140	Very Strong	Not Applicable

Figure 57. Critical failure surfaces with depth for cross section based on boring B-7 (drained condition).

Taylor Series Method

The Taylor Series Method as used for the three sections developed from borings B-1, B-2, and B-3 takes into account the uncertainty of the drained shear strength parameters of the soils in these cross sections to determine the reliability of the slope. If the shear strength parameters are treated as random variables, then the factor of safety will be a random variable assumed to have a log normal probability distribution as shown in Figure 58. The total area under the factor of safety probability distribution curve will be equal to one. The area of the portion of the curve where the factor of safety is less than one is equal to the probability of failure. These probabilities of failure are conditional given the variation of strength.

The Taylor Series Method can account for variation in any quantity used in analyzing the stability of a slope. These quantities could be the shear strengths of the soil, the unit weights, loads on the slope, and piezometric and water levels outside the slope. However, in the case of the three MSC cross sections, only the shear strength uncertainties were accounted for in each layer in each section. Thus, the first step in performing the probabilistic analysis of the slope was to estimate the standard deviation of the shear strength of the soils in the cross sections.

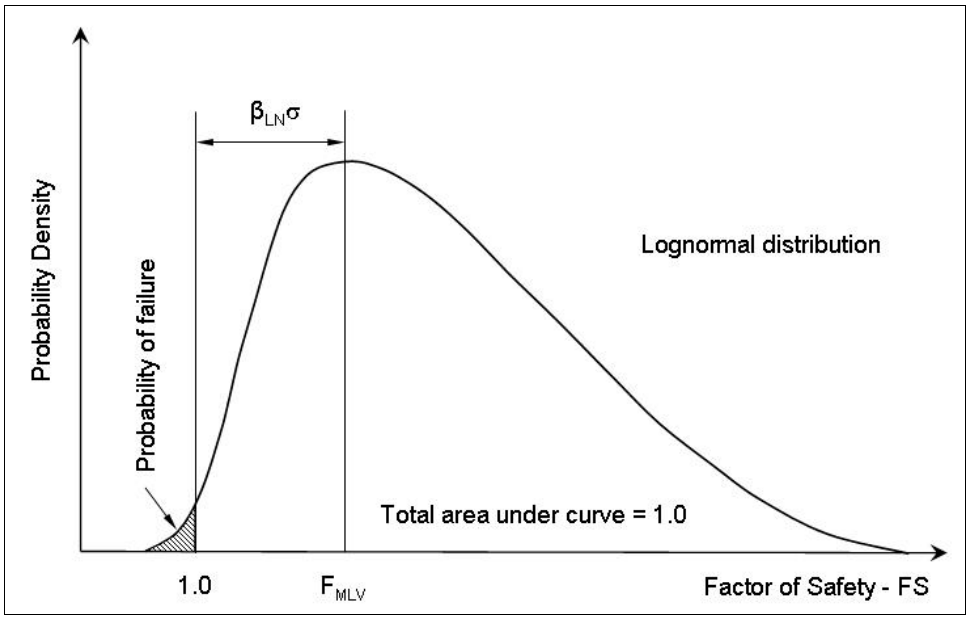

Figure 58. Relationship of B_{LN} to probability distribution (based on Duncan and Wright 2005).

The Taylor Series numerical method was used to estimate the standard deviation (σ_F) and the coefficient of variation of the factor of safety (COV_F) using these formulas:

$$\sigma_F = \sqrt{\left(\frac{\Delta F_1}{2}\right)^2 + \left(\frac{\Delta F_2}{2}\right)^2 + ... + \left(\frac{\Delta F_N}{2}\right)^2} \quad (1)$$

$$COV_F = \frac{\sigma_F}{F_{MLV}} \quad (2)$$

where:

ΔF_N = difference in values of the factor of safety calculated with the soil strength of layer N increased by one standard deviation and decreased by one standard deviation, and is given by

$$\Delta F_N = \left(F_N^+ - F_N^-\right)$$

where:

F_{MLV} = the "most likely value" for the factor of safety using the most likely values for shear strength parameters.

In calculating ΔF_N, separate stability analyses are performed to compute F_1^+ and F_1^- for the nth layer, with the values of all other variables (shear strengths) maintained at their most likely values. The ΔF values are inserted into Equation 1 to determine the standard deviation (σ_F) of the factor of safety. The coefficient of variation of the factor of safety (COV_F) is then determined using Equation 2 and the F_{MLV}. The probabilistic distribution of the factor of safety is assumed to be log-normal.

Spreadsheet calculations using EXCEL and based on Equations 1 and 2 were set up to compute the σ_F and COV_F. Once these were determined, the probability of failure was computed using the NORMSDIST function in EXCEL with β_{LN} where:

$$\beta_{LN} = \frac{\ln(F_{MLF} / \sqrt{1 + COV_F^2})}{\sqrt{\ln(1 + COV_F^2}} \quad (3)$$

Once β_{LN} is computed, the probability of failure can be determined in the spreadsheet from Equation 4:

$$p(f) = (1\text{-NORMSDIST}(\beta_{LN})) \quad (4)$$

Cross-section development for probabilistic analyses

The selected critical cross sections used for the deterministic analyses were further refined by combining adjoining similar sand and clay layers and averaging their respective properties to simplify the probabilistic analysis. Cross-sections B-1, B-3 and B-7 consist of 11, 6 and 8 soil layers, respectively. As a result of this refinement, the factors of safety cited in the deterministic analyses differ slightly from the F_{MLV} values cited in the Probabilistic analyses. Tables C.1, C.3, and C.7 show the most likely values for the drained shear strength parameters of each layer. The coefficients of variation were selected depending on the type of material representing a particular layer. If the layer was cohesionless sand, the coefficient of variation was selected to be 5 percent for the properties based on SPT blow counts. If the layer was clay, the coefficient of variation was chosen to be 30 percent. A higher coefficient of variation was assigned to the clay layers because the drained shear strength parameters were determined from correlations with the PI, which have a greater degree of uncertainty (Galveston District 1963). The refined cross-sections, B-1, B-3, and B-7, for the probabilistic analyses are tabulated in Appendix C, Tables C.1, C.3, and C.7, and are shown in Appendix E, Figures E.1, E.3, and E.5, respectively.

Results of probabilistic analysis for cross-section B-1

Probabilistic analyses were performed for five channel depths representing different levels of erosion (see Appendix E, Figures E.1 and E.3). The depths of the channel bottoms for these analyses were 100 ft (current depth), 105 ft, 110 ft, 125 ft, and 150 ft. Table 14 summarizes results from the calculations that make use of Equations 1 though 4 to arrive at the probability of failure for each of these five depth levels. The results in terms of the probability of failure versus depth are presented in Figure 59. Table 14 also includes the values for F_{MLV} for each depth level.

Results of probabilistic analysis for cross-section B-3

Probabilistic analyses were performed for channel canal depths representing different levels of erosion (see Appendix E, Figures E.3 and E.4).

The depths of the channel bottoms for these analyses were 86 ft (current depth), 91 ft, 96 ft, 111 ft, and 136 ft. A depth of 150 ft was added to the analysis so boring B-3 would extend to the maximum eroded depth of boring B-1. Table 15 summarizes results from the calculations that make use of Equations 1 though 4 to arrive at the probability of failure for each of the six depth levels. The results in terms of the probability of failure versus depth are presented in Figure 60. Table 15 also includes the values for F_{MLV} for each depth level.

Table 14. Probability of failure versus depth of shipping channel for B-1.

Case	Depth (ft)	F_{MLV}	Probability of Failure (%)
B1-100	100	1.327	0.07
B1-105	105	1.328	0.12
B1-110	110	1.329	0.11
B1-125	125	1.324	0.26
B1-150	150	1.321	0.28

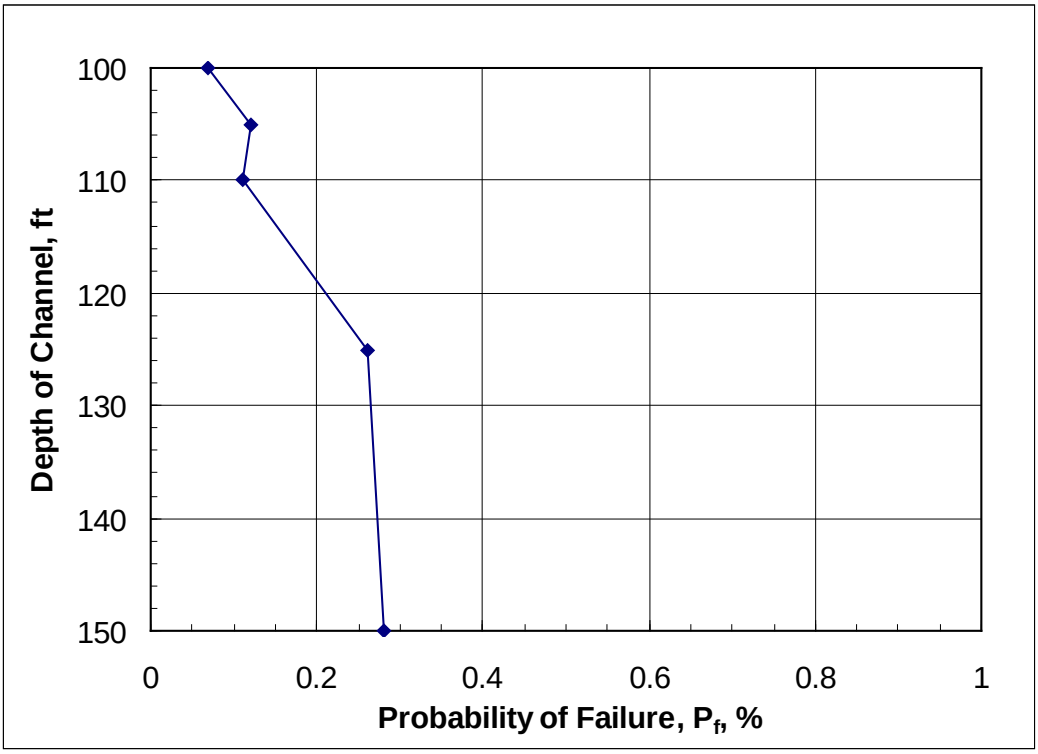

Figure 59. Probability of failure versus depth for B-1 cross section

Table 15. Probability of failure versus depth of shipping channel for B-3.

Case	Depth (ft)	F_{MLV}	Probability of Failure (%)
B3-86	86	1.044	33
B3-91	91	0.993	55
B3-96	96	0.975	62
B3-111	111	0.957	72
B3-136	136	0.941	82
B3-150	150	0.928	87

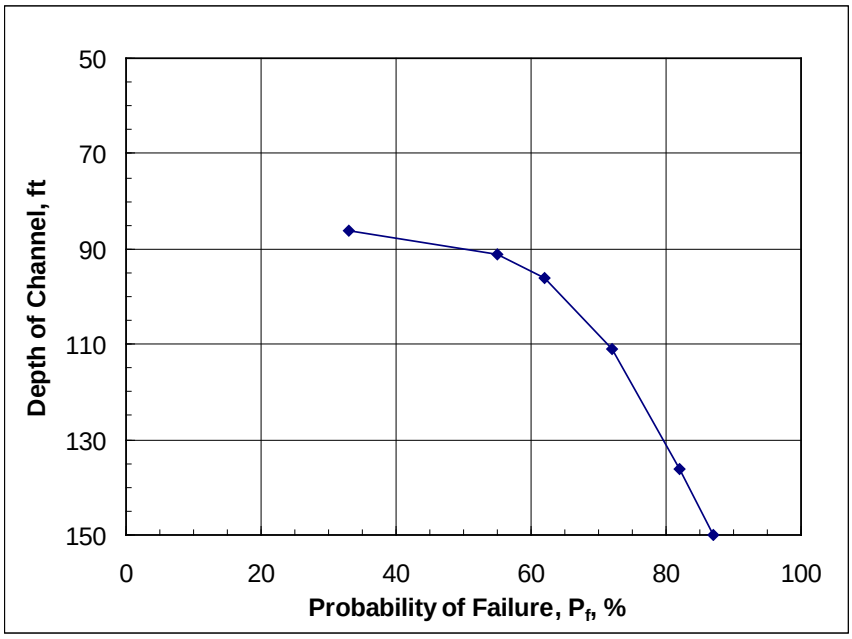

Figure 60. Probability of failure versus depth for B-3 cross section.

Results of probabilistic analysis for cross-section B-7

Probabilistic analyses were performed for five channel depths representing different levels of erosion (see Appendix E, Figures E.5 and E.6). The depths of the channel bottoms for these analyses were 72 ft (current depth), 77 ft, 82 ft, 97 ft, and 122 ft. A depth of 150 ft was added to the analysis so boring B-7 would extend to the maximum eroded depth of boring B-1. Table 16 summarizes results from the calculations that make use of Equations 1 though 4 to arrive at the probability of failure for each of the six depth levels. The results in terms of the probability of failure versus depth are presented in Figure 61. Table 16 also includes the values for F_{MLV} for each depth level.

Table 16. Probability of failure versus depth of shipping channel for B-7.

Case	Depth (ft)	F_{MLV}	Probability of Failure (%)
B7-72	72	1.012	42
B7-77	77	1.017	40
B7-82	82	1.016	41
B7-97	97	0.931	78
B7-122	122	0.897	92
B7-150	150	0.877	93

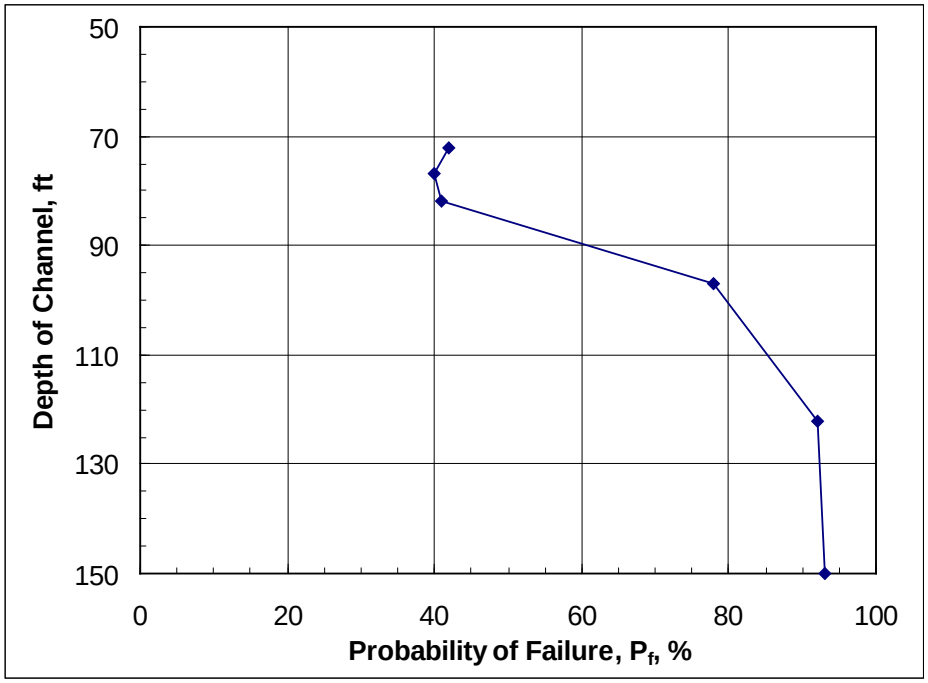

Figure 61. Probability of failure versus depth for B-7 cross section.

Failure mode assessments

Failure wedge mass characterization

All analyses were examined to determine the range of possible failure wedge masses that could flow into the ship channel as the result of slope instability. These masses were characterized into typical volumes that might be expected from ridge body block slides at 70, 75, 100, 125 and 150 ft channel depths. It was assumed that the failure mass, as shown by the dashed line in Figure 62, would move down and rotate outward into the channel. The amount of side block that protruded into the channel was characterized as a parallelogram having approximately the same volume as

the protruding block. The amount of movement was estimate by assuming that movement would not occur after the downward motion of the block's center of gravity stopped. Field observations suggest that the width of the failure mass would be about four times the depth into the slope of the scarp (D). Table 17 details the volume of material that would protrude into the channel for associated channel depths if all sections are assumed to be the same.

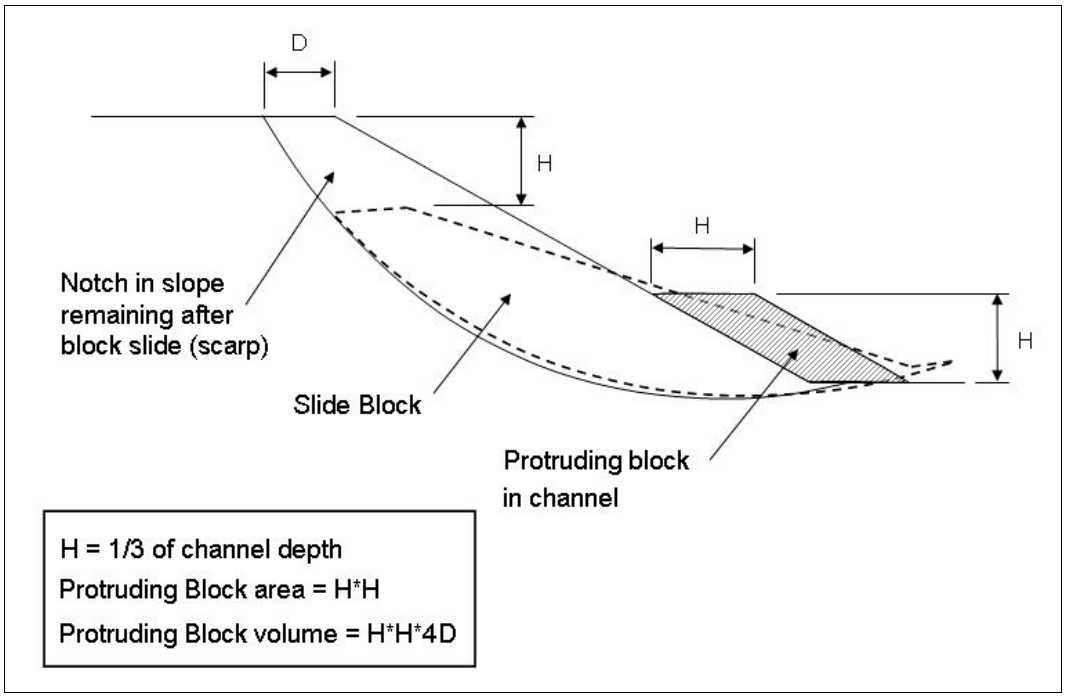

Figure 62. Failure mass characterization.

Table 17. Characterization of failure mass dimensions and associated volume.

Channel Depth, (ft)	H (ft)	D (ft)	W (ft)	Protruding Block Volume, (yd^3)
70	22	10	40	720
75	25	12	48	1,110
100	35	15	60	2,720
125	42	17	68	4,440
150	50	20	80	7,400

Wake and drawdown effects as cause for slope instabilities

The effect of a rapid change in water depth caused by boat passage was analyzed as a critical gradient piping-type failure. Given a soil with a buoyant unit weight of 60 lb/ft^3, the thickness of soil that would uplift (pluck) would be equal to the change in water depth caused by the ship passage. Any area of influence will be localized and, in light of a critical gradient analysis, near-toe scouring effects should not present a significant risk factor for slope failure initiation.

Further, to simulate the effect of a rapid change in water depth caused by boat passage, an analysis was performed where the channel water level was lowered by 2 ft. This change in water level was considered to happen in a short time period (minutes), therefore, an undrained analysis was used. The cross section used for this analysis was the same as those used in the undrained deterministic analyses. The analyses show that this change in water level affected the factor of safety by approximately 0.06, which is considered to be insignificant (Table 18).

Table 18. Undrained factor of safety versus drop in channel water level.

Boring	Existing Water Level	Drop in Water Level by 2 ft
B-1	1.778	1.734
B-3	1.265	1.222
B-7	1.469	0.428

Summary of results

The probabilities of failure for boring B-1 increase with depth, are low, and range from 0.07 percent at 100 ft (existing depth) to 0.28 percent at the 150-ft depth.

The probabilities of failure for borings B-3 and B-7 increase with depth and are high. The probability of failure for boring B-3 ranges from 33 percent at 86 ft (current depth) to 87 percent at the 150 ft depth. The probability of failure for boring B-7 ranges from 42 percent at 72 ft (current depth) to 93 percent at the 150-ft depth.

The high probabilities of failure for B-3 and B-7 are consistent with field observations that provide evidence of past instabilities in the slopes of the shipping channel. The aerial photographs show locations where instabilities have occurred (Figure 54). The slope stability analyses indicate that the volume of the critical failure circles is comparable to field observations and bathymetric data that indicate past instabilities in the MSC entrance.

The analyses show that if the factor of safety is much greater than one (e.g., F_{MLV} for B-1 = 1.33), the probability of failure is less than 1.0 percent. Conversely, if the factor of safety is near one (e.g., F_{MLV} for B-3 = 1.04) then the probability of failure is much higher, ranging from 33 to 93 percent. The fact that the probability of failure increases with depth, as shown in Figure 63, is an indicator that slides may possibly show up more frequently as the scour in the MSC entrance progresses.

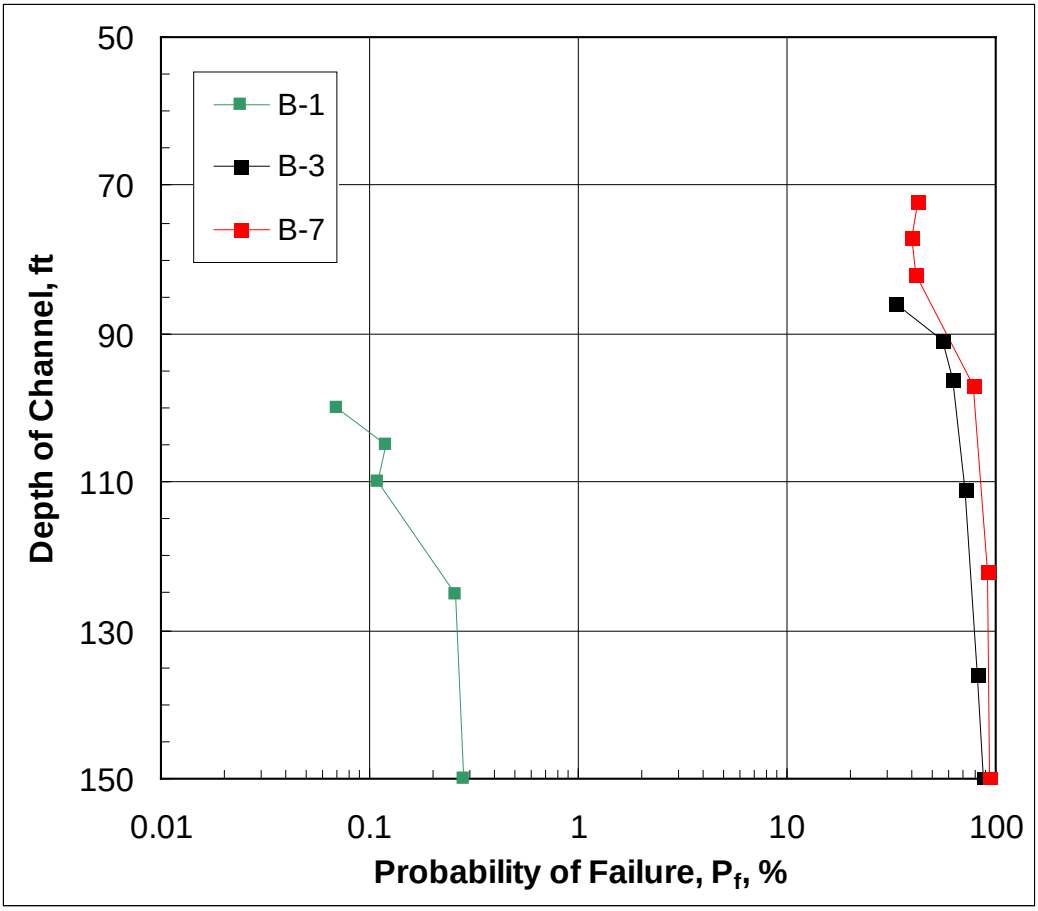

Figure 63. Summary of probability of failure versus depth for borings B-1, B-3 and B-7.

Effect of slope failures on navigation

The existing channel has a bulge on the south bankline, as shown in Figures 32 and 33. It is not known whether this bulge is a past slope failure or failures or whether it is an erosion resistant material. The volume of the existing bulge is about 150 ft (alongshore) × 100 ft (out from bank) × 30 ft (height)/27 = 16,670 yd^3. Based on both velocity patterns from CMS and the absence of comments from the pilots about adverse currents, this bulge does not cause adverse currents. The slope failures shown in Table 17 are all less than half the volume of the existing bulge and should not cause adverse currents. In addition, none of the calculated heights of the failed slope material, when subtracted from the depth, result in channel depths that are close to the draft of the ships.

Another concern about slope failures is the potential for the channel to rapidly scour the bankline after a slope failure leaves the bank uprotected. The best information about this potential problem is the existing channel. Past slope failures and loss of riprap on the upper bank because of channel bottom scour have left the upper bank exposed to high currents. While some bank recession has occurred, the bankline has not receded rapidly, and the stability of the bottleneck is not threatened. Should a slope failure occur at the ends of the bottleneck protection, unraveling from the end will likely occur but should not lead to rapid loss of the bottleneck.

4 Operational Risk to Navigation-Adverse Currents

Purpose and Approach

The purpose of the material described in this chapter is to determine the operational risks to navigation because of the adverse currents that are frequently present in the MSC Entrance. The approach in this chapter starts with a description of navigation conditions in the existing MSC Entrance. Next, previous studies are examined concerning the likelihood of a powered grounding in the MSC Entrance. This chapter then characterizes the fleet using the MSC and the environmental conditions present at the MSC. Expert elicitation of the pilots is then used to determine the relative likelihood of a powered grounding in the MSC for the various traffic and environmental conditions. Next, a ship event model (SEM) is developed to combine traffic distributions and environmental distributions to evaluate relative likelihood of grounding in the existing channel and for 3 risk reduction alternatives. Ship simulation is used to evaluate the effects of removal of the bottleneck. Finally, an evaluation is made of the bathymetric change near Sundown Island and the effects of Sundown Island on navigation.

Navigation in the Existing Channel

Navigation along the existing channel can be shut down because environmental (meteorological or oceanographic) conditions are too hazardous for deep-draft navigation. These environmental conditions are fog, strong longitudinal current in the bottleneck, and strong cross current at the jetty entrance. This type of disruption occasionally happens now and is only temporary until the adverse environmental conditions subside. Pilot Larry Robinson stated in January 2008: “We are currently experiencing the strongest currents on the Gulf Coast through the Matagorda Ship Channel Jetties. The reason for the extreme currents is due to the shape of our jetties, wide at the approach and narrowing to a small bottleneck. This configuration produces a normal current of about 3 knots with 6 to 7 knots not being uncommon and extreme currents in the winter of up to 10 knots. Due to these strong currents we have had to occasionally hold ships outside until the current subsides.”

Another risk factor in the existing channel is a grounding. A grounding could be a powered grounding due to adverse environmental conditions or a drift grounding due to loss of propulsion or steerage. Groundings present a range of consequences from virtually no effect if the grounding is minor in a soft bottom or soft side slope portion of the channel to the extreme case of a grounding resulting in sinkage, blockage of the channel, and/or loss of life or release of hazardous material into the bay and gulf.

Collision with other ships is not addressed herein because the study reach is one-way traffic and is south of the congestion present in the reach at and north of the GIWW. Other risk factors such as fire, explosion, or hull failure are not addressed in this study.

The existing navigation channel entrance at the MSC is subject to adverse currents at several locations along the entrance. The adverse currents are present in three areas as follows:

a. **Cross Current at Jetties**. One of the existing risks to navigation at the MSC is the cross current at the gulf entrance to the jetties. Wind at the MSC is primarily from the southeast and generates a cross current directed toward the southwest at the gulf entrance to the jetties. A cross current at the gulf entrance is only a significant problem for inbound ships. Once the bow of the inbound ship is inside the jetties, cross currents (either toward the southwest or toward the northeast) on the stern region of the ship start rotating the ship. In the case of a cross current toward the southwest, the ship is rotated clockwise. In anticipation of this rotation, the pilot applies a significant amount of port rudder. For a strong cross current, the ship will have a significant starboard drift angle even after it is completely inside the jetties. The pilot must realign the ship with the channel before reaching the bottleneck. The pilots have stated that when they begin their approach, they try to maintain a maximum of 12 deg of drift angle, which is the angle between the ship axis and the channel axis. If they are unable to maintain this angle or less, they abort the entry and turn around and either try again with sea speed (the maximum power of the ship) or wait for the current to subside.

   Figure 64 displays bathymetry data from January 2008 that shows variability in depth across the MSC entrance. Near the gulf end of

the southwest jetty, depth is great and decreases across the inlet toward the northeast jetty. About halfway along the jetty, the trend in depth reverses. Greater depths are found near the northeast jetty and smaller depths near the southwest jetty. The trend in depth is similar to a meander and must be indicative of the currents between the jetties. This variability in current could be responsible for some of the navigation problems in this reach.

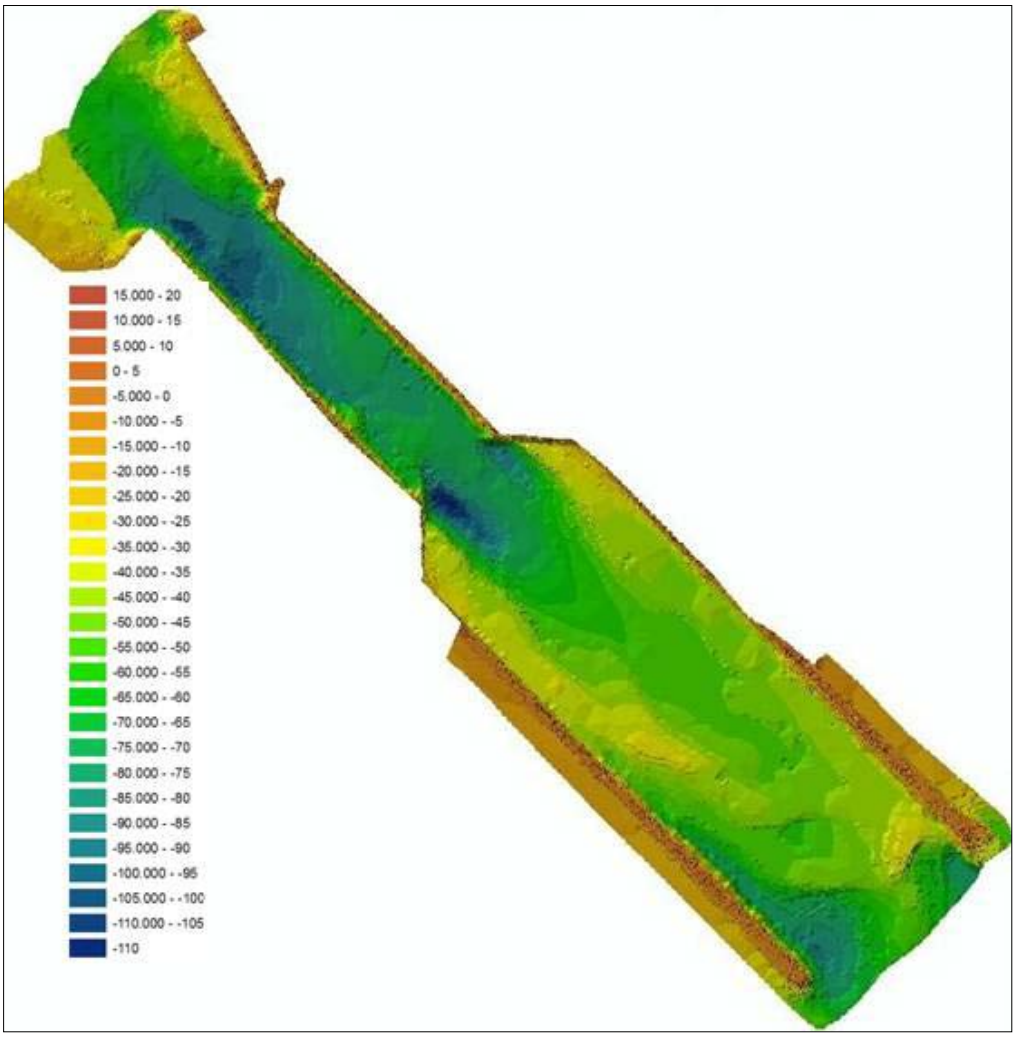

Figure 64. 2008 bathymetry of MSC entrance.

b. **Strong Current Velocity in Bottleneck**. Another existing risk to navigation is the strong current velocity through the bottleneck. The Kraus et al. (2006) report documents depth-averaged velocities in the center of the channel in the bottleneck as great as 5.2 knots based on numerical modeling of two significant tide conditions. The pilots use their pilot boat as a float along with a Global Positioning

System (GPS) and report measured current velocities of up to 9.2 knots (Pilot Larry Robinson reported this value and stated that it was a one-time rare event). A velocity from the boat measurement method would tend to be larger than the computed velocity from Kraus et al. (2006) because the boat method represents a surface velocity as opposed to depth-averaged velocity from the numerical model. Also, the boat measurement technique could have been affected by waves and wind. As a general rule, strong current velocities tend to pose a larger problem for ships traveling in the same direction as the current because the ship must maintain sufficient power to push enough water past its rudder for steerage control. Ships moving with the current have a large speed over the ground and a reduced level of maneuverability. For ships heading into a strong current, the speed over the ground is low and the speed through the water is great. The primary problem reported by the pilots when going against a strong current is the sensitivity of a ship to steerage. Small ship angles relative to the current tend to become larger because of the lateral forces acting on the bow of the ship and must be quickly counteracted to keep the ship under control. The MSC pilots have reported that the most likely condition for grounding at the MSC is when the ship is moving against the current, which is opposite to the situation reported for most channels.

c. **Sundown (also known as Bird) Island Reach**. Another risk factor faced by ships in the existing MSC entrance results from a cross current entering the channel from the northeast during an ebb tide or a cross current from flow leaving the channel toward the northeast during flood tide. These cross currents are further complicated by Sundown Island creating an area of variable horizontal current velocity in the channel for a ship as it travels southwest of the island. This problem is most significant on ebb tide. A major portion of the ebb tide approaches Sundown Island from the northeast. Sundown Island blocks the flow over a significant area southwest of the island that extends to the ship channel. Shadowing by the island creates an area of variable cross currents that is a problem for both inbound and outbound ships. Pilot Larry Robinson reported that the area on the northeast side of the ship channel between Sundown Island and Matagorda Peninsula has enlarged and deepened significantly in recent years, allowing more flow to approach the inlet through that opening on ebb tide.

On flood tide, water leaves the channel through this same area between the peninsula and Sundown Island in a northeast direction and sets the ship to the northeast. The Sundown Island reach is also the location of a channel course change and a rapid change in depth from the deep bottleneck to the dredged channel of the bay. This course change and depth change are most problematic for inbound ships. Sundown Island serves as a detriment to navigation in the MSC entrance because it reduces flow area and concentrates the ebb tide in the area between the island and the peninsula, making cross currents variable and stronger. Relocation of Sundown Island far from the entrance would likely improve navigation conditions at the MSC Entrance.

These three adverse current locations affect navigation in different ways depending on ship direction and stage of tide. The four combinations of tidal current direction and ship direction are discussed in the following paragraphs. These descriptions are based on an alongshore current in a southwest direction that produces a cross current at the jetty entrance and a large tide range creating a large water level difference between the gulf and the bay.

a. **Inbound Ship, Ebb Tide (low speed over ground, large speed through water)**. For an inbound ship on an ebb tide at the gulf entrance, the starboard drift angle of the ship from the alongshore current toward the southwest at the jetty entrance and the opposing tide causes forces on the bow of the ship that tend to increase the clockwise rotation of the ship (i.e., increase the starboard drift angle). The rotation makes it more difficult for port rudder to counteract the starboard drift of the ship. Upon reaching the bottleneck, the ship must maintain control in the strong current velocity through the bottleneck. Any residual drift angle from a cross current at the jetties becomes harder to correct in the bottleneck. After leaving the bottleneck at a low speed relative to ground, the ship experiences varying cross currents in the Sundown Island reach. At first, the ship experiences forces on the bow from flow between Sundown Island and the peninsula that causes a drift angle and translation to port. When the bow arrives in the lee of Sundown Island, only the stern is subjected to the cross flow, and the ship will tend to a starboard drift angle, but still be subjected to forces tending to translate it to port. Once the bow passes the lee of Sundown Island and the

stern is still in the lee of Sundown Island, the ship again experiences a drift angle and translation forces to port.

b. **Inbound Ship, Flood Tide (large speed over ground, low speed through water)**. For an inbound ship on a flood tide at the gulf entrance, the starboard drift angle of the ship must be overcome by enough power and thus rudder force. This situation causes the ship to have a large speed over the ground that causes it to reach the bottleneck portion of the channel quickly. For example, a ship traveling at 8 knots relative to water with a 4 knot current traverses the 6,000-ft-long jetty in about 5 min. Upon reaching the bottleneck, the ship speed over ground increases even more due to the stronger current in the bottleneck and the need to maintain steerage. The unusually large ship speed continues through the bottleneck and into the Sundown Island reach. The channel bottom rises from the deep scour of the bottleneck up to project depth of about 38 ft at sta 7+400, that is about halfway between the northwest side of the peninsula (about sta 5+000) and Sundown Island (about sta 10+500). The 200-ft bottom width channel at this point is not a well-defined trench channel and gradually slopes up and decreases in depth away from the channel to typical depths in the bay of about 9-11 ft. The ship reaches the shallower authorized channel depth of about 36 ft at sta 7+400 at a high rate of speed, and pilots report problems with control and large bow squat that continues past Sundown Island. Some problems are related to the flow leaving the channel in a northeast direction and resulting in cross currents that set the ship to the northeast.

c. **Outbound Ship, Ebb Tide (large speed over ground, low speed through water)**. The ship reaches the Sundown Island area and is exposed to a varying cross current because of blockage of the current by Sundown Island and the flow between Sundown Island and the peninsula. Once past the bottleneck, an outbound ship on ebb tide experiences few problems.

d. **Outbound Ship, Flood Tide (low speed over ground, large speed through water)**. The ship experiences cross currents with flow leaving the channel between Sundown Island and the peninsula. The ship must make headway against a strong longitudinal current in the bottleneck that makes steerage sensitive to small drift angles.

Once past the bottleneck, an outbound ship on flood tide experiences few problems.

Previous studies on probability of grounding

The primary risk to navigation addressed in this study is a powered grounding of a ship. Studies performed for other navigation channels were examined to determine the probability of a powered grounding.

Solem (1980) evaluated probability models for grounding and developed the probability of a powered grounding as $10^{-5}L/W$, where L is the length of the waterway, and W is the width of the navigation lane. Inserting a length of 3.5 miles for the reach studied herein and an average width of 400 ft based on the variation of width in the dredged channel and the bottleneck, the probability of grounding becomes 0.00046.

De Vries (1990) examined the use of simulators in port design and noted that simulators have two advantages. First, simulators assist in evaluating the behavior of humans in charge of maneuvering procedures. De Vries notes that this behavior is normally challenging to simulate in mathematical or other descriptive models. The second reason is that results from simulator experiments can be incorporated into probabilistic design.

Dand and Lyon (1993) determined a grounding rate of 0.03 per 1,000 ship movements. They stated that this value was consistent throughout the data and that the inference can be drawn that this level is acceptable to port and ship operators. This results in a probability of grounding of 0.00003.

Briggs et al. (1994) conducted physical model tests of the Barbers Point Harbor, HI, using a remotely controlled ship to assess the probability of unacceptable navigation conditions or groundings. They divided the environmental domains into A, B, and C. Domain (A) was the state of extreme or rare environmental conditions having low frequency of occurrence that might be expected to occur 3 to 5 percent of the time. The upper boundary to this domain is the limiting condition where ships would not attempt to enter, such as during a storm. The second domain (B) is characterized by frequently occurring environmental conditions which would influence navigation. They are the normal conditions ships encounter on a weekly basis. The last domain (C) is the no-problem domain that has a negligible influence on navigation. Domain (C) has the highest frequency of occurrence.

In Domain (A), waves were the dominant navigation consideration. For the existing plan, the fraction of unacceptable navigation or grounding in Domain (A) for average conditions was 0.53 for an inbound ship and 0.17 for an outbound ship. In Domain (B), both waves and currents were considered to influence navigation risk. For the existing plan, the fraction of unacceptable navigation or grounding in Domain (B) for average conditions was 0.18 for an inbound ship and 0.06 for an outbound ship. Combining the probability of environmental domain, the probability of a ship being present, and the fraction of unacceptable navigation or grounding, results in the probability of unacceptable navigation for each domain. Using the existing harbor and average test conditions with 100 ships per year resulted in the probability of unacceptable navigation in Domain (A) of 0.000042. Domain (B) results in the probability of unacceptable navigation of 0.000132. For Domain (C), waves and currents are not considered hazardous, and the probability of grounding was assigned a value of $6(10)^{-5}$, as being an international standard for the probability of a ship accident per ship call.

Total probability of unacceptable navigation is the sum of the three domains, 0.000234. For the existing harbor and worst conditions with 200 ships per year, the total probability of unacceptable navigation was 0.00072. The recommended plan at the lowest level of traffic and the best conditions resulted in a probability of grounding or unacceptable navigation of 0.00007.

Knott (1996) presented an equation for the probability of a ship colliding with a bridge pier. Although different from a grounding, there are some similarities in a ship running aground and a ship colliding with a fixed object, because both occur on the edge of the navigation channel. Knott quotes the base rate for collisions has a probability of 0.00006 that is modified upward if the bridge is in a bend, if a current runs parallel to the ship, if a cross current is present, and depending on traffic density.

Brown and Amrozowicz (1996) evaluate risk from oil tankers, but much of their work is applicable to the MSC. The authors refer to “top = down” statistics that provide only limited insight. They state, “We must work fundamentally from the bottom-up so that systemic causes and effects can be filtered from the apparent randomness and properly addressed.” The bottom-up approach they use deals with the details of the response of the ship’s crew and the probabilities of their actions. The authors consider

four primary causes of accidental oil spill as (1) grounding, (2) collision, (3) fire or explosion, and (4) structural failure. They present a chart showing that 65 percent of all oil spill volume is the result of groundings. The authors develop a fault tree analysis to arrive at a comprehensive understanding of the navigation system. They note that major disasters are rarely caused by one factor. They also note that the human element in maritime accidents is the major contributor to grounding accidents.

Lin et al. (1998) reported on risk factors for ship groundings. They examined data from five U.S. ports: Boston, MA, New York/New Jersey, Tampa, FL; Houston/Galveston, TX; and San Francisco, CA. Data from 1981 to 1995 were analyzed. They report on risks due to errors in tide prediction and daytime versus nighttime navigation. They found that tide forecast error was not a significant risk factor, but that nighttime navigation was far more risky than daytime navigation. Based on the five port areas evaluated, 15 percent of groundings occurred during daytime, 43 percent during nighttime, 36 percent during transition (dawn or dusk), and 6 percent during unknown times. At the Houston/Galveston port area, 7 percent of groundings occurred during daytime, 44 percent during nighttime, 45 percent during transition (dawn or dusk), and 5 percent during unknown times. Although the largest ships on the MSC are daylight restricted, the non-daylight restricted smaller ships at night would have a significantly greater risk of grounding than the non-daylight restricted ships passing during the daytime.

Kite-Powell et al. (1998) note that groundings of commercial ships account for about one-third of all commercial maritime accidents, including some of the most expensive such as the Exxon Valdez incident in Alaska. The authors make a clear distinction between the association between circumstances surrounding a transit and the occurrence of a grounding and avoid reference to the cause of grounding. They state that proving cause is difficult to accomplish and list the following attributes that can reasonably be expected to contribute to likelihood of a grounding:

a. Vessel characteristics (draft, beam, maneuverability).

b. Topography of the waterway (water depth, channel width, channel length, complexity of turns, traffic density).

c. Environmental condition (wind, visibility, currents, waves).

d. Operator (experience, training, local knowledge).

e. Information available to operators (quality of charts, quality of information about tide levels and currents, VTS guidance, navigation aids).

Under visibility, they distinguish good and poor visibility by a distance of 2 km. For small ships defined as draft < 30 ft, poor visibility had a probability of grounding of 7-9 times greater than good visibility. For large ships having draft > 30 ft, poor visibility had a probability of grounding of 5 to 8 times greater than good visibility. For barge trains at the Houston/Galveston ship channel, poor visibility produced a probability of grounding seven times greater than good visibility. Wind was found to be a lesser factor than visibility, and the paper notes that strong wind conditions along the gulf coast are rare. The MSC pilots state that while wind can be a problem, strong current is the major concern.

Kite-Powell et al. (1998) examined data from 1981 to 1995. They considered only accidental groundings and ignored those identified as intentional or due to mechanical failure or other non-navigational causes. They define ship transits whereby one port call is two ship transits, one inbound transit and one outbound transit. All five ports average around 0.75 groundings per 1,000 ship transits. Houston/Galveston, the only gulf coast port, had 0.89 ship groundings per 1,000 transits or a probability of 0.00089. The authors also found that low visibility produces an order of magnitude increase in the probability of grounding. Strong wind (speed > 10 m/sec) appears to have a less significant effect, which is consistent with the statements by the Matagorda Bay Pilots. Large ships (draft > = 30 ft) and barge trains were found to have the highest probability of grounding.

Harrald et al. (1998) reports on human error in a maritime system and state that it is the primary cause of most transportation-related accidents. They state that prevention programs must reduce human errors. The authors define an incident as a triggering event, such as human error or mechanical failure creating an unsafe condition that may result in an accident. They developed a six-stage causal chain reproduced in Figure 65.

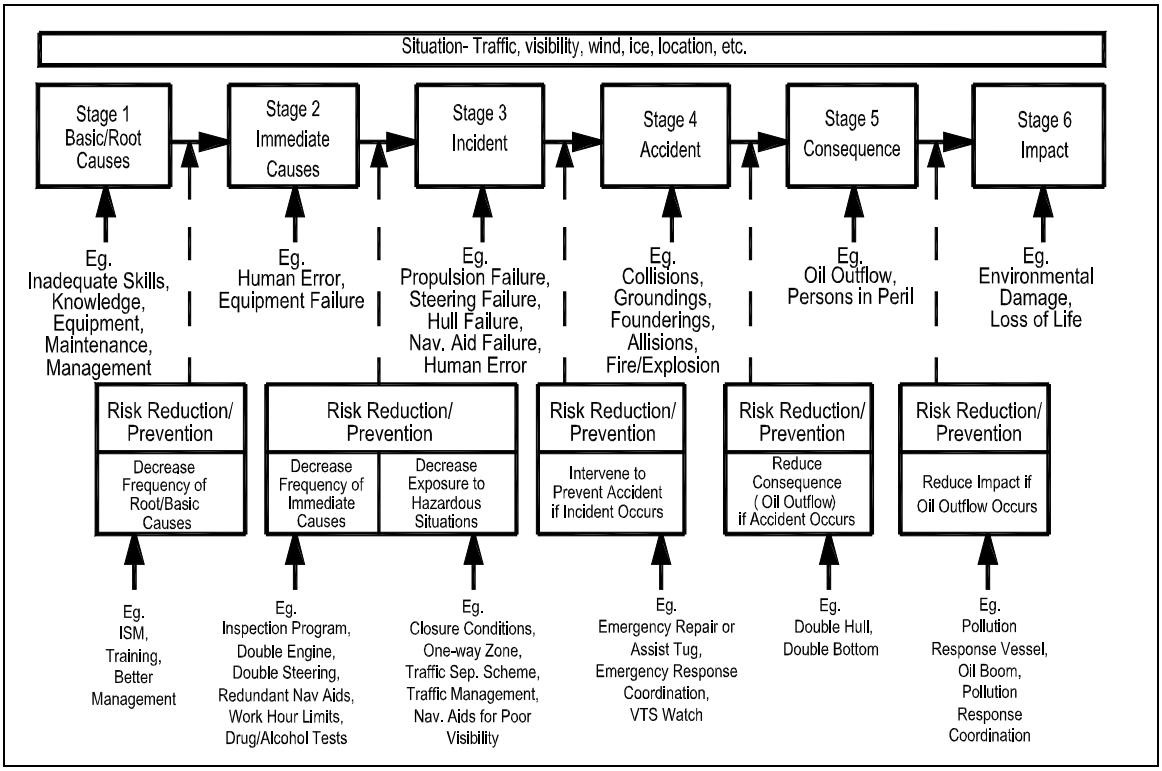

Figure 65. Framework for maritime risk assessment and risk reduction intervention, replotted from Harrald et al. (1998).

Brown and Haugene (1998) examine the impact of organizational and management factors on the risk of tanker grounding. They separate groundings into powered and drift. They break down the grounding into the details of what happened leading up to the grounding by examining the individual human actions that led to or could have prevented the grounding. Similar to other risk approaches reported herein, they applied the Analytical Hierarchy Process (AHP) to quantify subjective influences. They note that AHP was developed by Saaty (1980) for solving multi-attribute decision problems. AHP is a way of measuring the relative value of quantitative and qualitative information.

The U.S. Coast Guard (USCG) conducted a risk-based decision-making process to evaluate the need for and plan future vessel traffic management projects. Ports and Waterways Safety Assessment (PAWSA) workshops were completed in 28 ports around the United States between 1999 and 2001. Port Lavaca was one of the 28 ports. The port risk model includes 20 risk factors as shown in Table 19. The typical workshop panel was composed of pilots, port authorities, environmental interest groups, recreational and commercial fisherman, USCG, Corps of Engineers, tug and towboat operators, local and state officials, etc. Note that this evalu-

ation is based on the entire MSC channel whereas the study conducted herein only evaluates the gulf entrance to just south of the old GIWW. Based on information from all 28 ports, Port Lavaca ranked high in the following of the 20 categories considered:

1. 3rd in percent of high-risk shallow draft.
2. 7th in volume of shallow draft vessels.
3. 7th in volume of fishing and pleasure craft.
4. 3rd in tide and river currents. (Behind: (a) Berwick Bay that has 5-6 knot river currents during floods with primarily barge traffic and (b) Port Everglades that has variable and strong cross currents and larger number of ships).
5. 1st in waterway complexity.
6. 4th in volume of hazardous chemical cargoes.

Table 19. Final PAWSA model (USCG 2001) of 20 risk factors in six categories and weighting factors. Numbers in parentheses are weighting factors.

Maximize Safety in a Port or Waterway					
Decrease Frequency of Accidents (0.70)				Decrease Consequences of Accidents (0.30)	
Fleet Composition (0.29)	Traffic Conditions (0.25)	Environmental Conditions (0.21)	Waterway Configuration (0.25)	Short-term Consequences (0.52)	Subsequent Consequences (0.48)
% of high risk deep draft (0.35)	Volume of deep draft vessels (0.24)	Wind conditions (0.26)	Visibility obstructions (0.26)	Volume of passengers (0.38)	Economic Impacts (0.43)
% of high risk shallow draft (0.65)	Volume of shallow draft vessels (0.32)	Visibility conditions (0.12)	Passing Situations (0.24)	Volume of petroleum cargoes (0.38)	Environmental impacts (0.34)
	Volume of fishing and pleasure craft (0.29)	Tide and river currents (0.27)	Channels and Bottoms (0.29)	Volume of hazardous chemical cargoes (0.24)	Health and safety impacts (0.23)
	Traffic density (0.14)	Ice conditions (0.35)	Waterway complexity (0.21)		

One statement in the PAWSA report (USCG 2001) about Port Lavaca was that the risks to deep-draft navigation are “partially offset by the low volume of such traffic, currently in the order of two to three ships per day, and by a process of vetting, implemented by the major shippers as a means

of ensuring the quality of ships used." Quality of ships implies that ships not having good maneuvering characteristics were not allowed in the MSC. The pilots were asked about this concept of vetting and stated emphatically that it does not happen.

Linke and Huesig (2000) evaluated the effects of cross currents on barge operation. They provide equations for allowable cross flow for a given lateral translation for barge trains on canals. No information on ships was presented.

The risk assessment for Prince William Sound (Merrick et al. 2002) was conducted as a result of the oil spill from the grounding of the Exxon *Valdez* on 24 March 1989. Following the accident, various risk-reduction measures were implemented including weather-based closures during strong wind, designation of a portion to one-way traffic, and assistance by escort tugs. Subsequently, questions arose about the effectiveness of these measures and the need for additional measures. All parties agreed on conducting a risk assessment to evaluate the risks of oil transport in the Prince William Sound and to identify and rank proposed future risk reduction measures. The authors applied a discrete event simulation of the system to deal with the complex dynamic nature of the system and to model the interactions between the vessels and their environment.

Roy and Maes (2006) report on a risk assessment of ships in the Belgian waters of the North Sea. For these ships, they specified a probability of powered grounding for ships with a pilot and good visibility of 0.000247 for all ship types. Powered grounding with a pilot and poor visibility had a probability of 0.000687. Although not specifically stated, these values appear to be probability per ship movement. Drift groundings were expressed in a different manner as ship frequency per hour. For ship types at the MSC entrance, drift groundings due to ship breakdown per hour had a probability of about 0.00034.

Hart (2007) presents the expert witness statement of Captain Frank Hart in opposition to the deepening of the Port of Melboune due to concerns about navigation safety. The primary concern was grounding at the entrance due to a strong cross current that sometimes exceeds 4 knots. The witness states that the full experiences of the pilots have not been taken into account in assessing the risks associated with the deeper draft ships in

the same width channel. This study simply serves as a reminder to consider all stakeholders in the risk-evaluation process.

Uluscu et al. (2008) conducted a risk analysis of vessel traffic in the Strait of Istanbul. Their objective was to determine operational policies that mitigate the risk of having an accident that will endanger the environment, the residents of Istanbul, and impact the economy, while maintaining an acceptable level of vessel throughput. They define the events that may trigger an accident as instigators. Their five instigators are human error, rudder failure, propulsion failure, communication and/or navigation equipment failure, and mechanical and/or electrical failure. Accidents are two types; the first tier is the initial accident, and the second tier is the accidents that could happen as a consequence of a first tier accident. First tier accidents are collision, grounding, ramming, and fire and/or explosion. Second tier accidents that may follow a first tier accident are grounding, ramming, fire and/or explosion, and sinking. Note that in some cases, there may not be a second-tier accident. An example at the MSC entrance would be if a ship grounds on a soft portion of the channel, but no other accident follows.

Uluscu et al. (2008) state that the occurrence of an instigator depends on the situation. At the MSC entrance, the situation of most concern is the presence of an adverse current. They describe the situation with vessel attributes and environmental attributes. Vessel attributes are vessel type and length, reliability, pilot request, and tugboat request. At the MSC entrance, tugs are not called, and pilots are always present, so these attributes can be eliminated. Uluscu et al. (2008) consider environmental attributes as vessel proximity, visibility, current, geographic location, local traffic density, and time of day. For the one-way traffic on the MSC, vessel proximity and local traffic density are not issues. Visibility is broken down by Uluscu et al. (2008) as < 0.5 mile, 0.5 to 1.0 mile, and > 1.0 mile. They phrase the risk question as: (1) how often do the various situations occur?; (2) for a particular situation, how often do instigators occur?; (3) if an instigator occurs, how likely is an accident?; and (4) if an accident occurs, what would be the damage to human life, property, environment, and infrastructure?

Uluscu et al. (2008) quantify risks based on historical data, expert judgment, and a simulation model of traffic. Based on historical accident data, they found the probability of the four first tier accident types for each of

the five instigators shown in Table 20. Based on historical accident data, they found the probability of the four second tier accident types plus the probability of no second tier accident for each of the four first tier accidents shown in Table 21.

Table 20. Probability of four accident types as result of five different instigators based on historical accident data at Strait of Istanbul.

1st Tier Accident	Instigator				
	Human Error	Steering Failure	Propulsion Failure	Comm/Nav Equip Failure	Mech/ Electrical Failure
Collision	0.0002936	0.0000087	0	0	NA
Ramming	0.0001526	0.0000262	0.0000238	0	NA
Grounding	0.0001670	0.0000384	0.0000192	0	NA
Fire/Explosion	0.0000638	NA	NA	NA	0.0000798
NOTE: NA = Does not cause first-tier accident, but may cause second-tier accident. For example, a steering failure does not cause a first-tier fire/explosion, but a steering failure could cause a grounding that could result in a second-tier accident of a fire or explosion.					

Table 21. Probability of second-tier accident after first tier accident based on historical accident data at Strait of Istanbul.

1st Tier Accident	Second Tier Accident				
	No 2nd Tier Accident	Grounding	Ramming	Fire/Explosion	Sinking
Collision	0.8737	0.0289	0.0000	0.0158	0.0816
Grounding	0.9794	NA	NA	0.0041	0.0165
Ramming	0.8325	0.1218	NA	0.0102	0.0355
Fire/explosion	0.9355	0.0081	0.0000	NA	0.0565

Grounding probability in MSC entrance

Based on the Merrick et al. (2002) risk assessment of PWS, the preferred method of estimating probabilities is through data. The probability of grounding in a waterway is best determined by a large volume of historical data. Historical ship grounding data for the MSC could not be found. Data was requested from the pilots, the port, and the USCG, but none was available. USCG databases did not contain information to define the historical rate of grounding.

Another methodology for defining the probability of grounding is the approach taken by Briggs et al. (1994), in which a remotely controlled ship model was operated to evaluate various channel and environmental conditions. The track of the model ship was recorded, and the probability of exceeding the channel limits was determined. The physical model approach was not considered herein because of the difficulty of replicating the complex current in the bay and in the bottleneck.

Another approach for defining the probability of grounding is to use a simulator similar to the approach described above for the physical model. The present study conducted a ship simulator exercise (discussed subsequently) to provide a relative comparison of the risks to navigation in the existing channel and the channel with the bottleneck removed as presented in Kraus et al. (2006). A complete ship simulator to establish the probability of grounding in the MSC entrance would have been a large challenge because of the complexity of the current and the relatively few pilots (four) available to make the numerous simulations required to establish the probability of grounding.

The remaining method for establishing the probability of grounding is to adopt data from another similar channel. The available data are summarized in the previous section of this report and shown in Table 22. No waterway was found in which a large longitudinal current is the primary problem in the channel. The data set represents various levels of adverse navigation conditions and various lengths of channels. Channel length is central because the results are often expressed as probability per ship movement. The range of probabilities in the table is 0.00003 to 0.00089. The closest port for which we have data is the Houston/Galveston data from Kite-Powell (1998). The Houston/Galveston channel has great length and a large amount of traffic sometimes leading to congestion. Kite-Powell (1998) states that the method of data gathering may have resulted in high rates. Roy and Maes' (2006) data on the North Sea for ships with pilots and poor visibility had a probability of grounding of 0.00069. The Roy and Maes (2006) value is consistent with the worst conditions in the Briggs et al. (1994) tests, having a probability of 0.00072.

Table 22. Summary of ship grounding information.

Source	Location	Type of Grounding	Probability per Transit
Briggs et al. (1994)	Barbers Point model	Powered	0.00007-0.00072
Uluscu et al. (2008)	Strait of Istanbul	Powered	0.000167
Uluscu et al. (2008)	Strait of Istanbul	Drift = steering + propulsion	0.0000576
Kite-Powell et al. (1998)	Five US ports	Powered	0.00075
Kite-Powell et al. (1998)	Houston-Galveston	Powered	0.00089
Dand and Lyon (1993)	universal	Powered	0.00003
Knott (1996)	Bridge locations	Powered and drift	Min of 0.00006
Roy and Maes (2006)	North Sea	Powered, good (poor) visibility with pilot	0.000247 (0.000687)
Roy and Maes (2006)	North Sea	Drift	0.00034/ hr
Solem (1980)	General	Powered	0.00046

Because the Permanent International Association of Navigation Congress (PIANC) guidelines classify longitudinal currents of greater than 3 knots as strong and the MSC entrance has a longitudinal current exceeding 3 knots over 60 percent of the time, an argument can be made for adopting a high probability of grounding. It is likely that a grounding that does not cause damage to the ship or waterway often goes unreported, which would reduce all published reports of groundings. Because the existing channel has one-way traffic, and the largest vessels are daylight restricted, an argument can be made for adopting a low probability of grounding. The grounding data from other sources can only be consulted to estimate a baseline probability to use for comparing to other risks to navigation. A probability of grounding of 0.0007 per ship transit will be specified for the MSC entrance based on the larger values from Houston/Galveston, Roy and Maes (2006), and Briggs et al. (1994). This value does not reflect the strong longitudinal current velocity, particular channel condition, or fleet characteristics at the MSC entrance, and only represents a navigation channel with a relatively high probability of grounding. At 732 ships transits per year, this rate gives an expected value of 0.5 powered groundings per year.

Analysis of existing traffic and environmental conditions

Based on interviews with MSC pilots, the breakdown of the system into attributes that contribute to likelihood of grounding are: (a) reach or where a ship is located in the MSC entrance, (b) ship direction, (c) direction of tidal current, (d) ship class, (e) tidal current magnitude in the bottleneck, (f) visibility, and (g) magnitude of cross current at the gulf entrance for entering ships only. A tree diagram in Figure 66 shows the breakdown of the navigation system into attributes. Every attempt is made to completely describe the system while maintaining the minimum number of attributes. Each of the attributes is discussed in the following paragraphs.

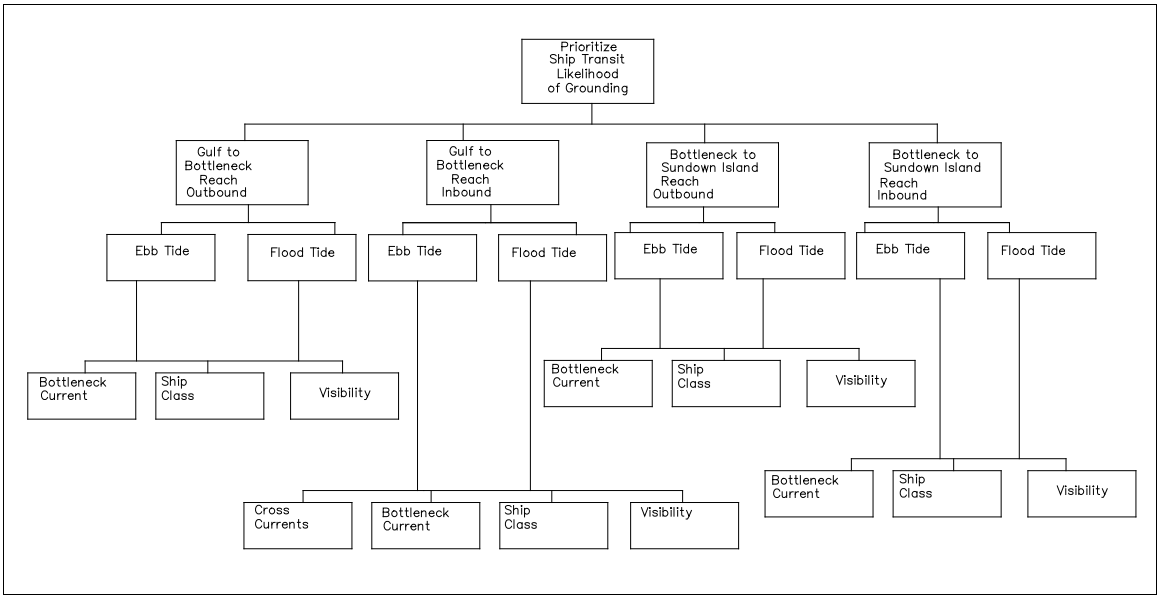

Figure 66. Tree showing attributes of MSC entrance navigation.

Reach. The study area is broken into the reach from the gulf to the bottleneck and the reach from the bottleneck to just north of Sundown Island. The two reaches have two separate navigation problems that have different underlying attributes. For example, the gulf to the bottleneck is affected by the cross current at the gulf entrance to the jetties, whereas a cross current at the gulf entrance would have no affect on the bottleneck to Sundown Island Reach.

Ship Direction. Based on interviews with MSC pilots and experience with other navigation channels, inbound ships have a much greater difficulty navigating the channel than outbound ships, generally as a result of the cross current at the inlet and/or having to reduce speed just north of

the peninsula because of the course change and steep decrease in depth of the channel.

Tidal Current Direction. The direction of the tidal current enters a degree of navigation difficulty because, according to most reports, ships traveling with a current have far less maneuverability than ships traveling against a current. At the MSC entrance, the pilots report that the opposite is true, with travel against the current being more difficult to navigate. There was not complete agreement from the pilots on this issue. This diversity of opinion demonstrates the complexity of navigation at the MSC entrance. At the MSC, the ebb tide lasts longer than flood tide. Based on tide records, ebb tide occurs about 60 percent of the time versus 40 percent for flood tide.

Ship Classes on MSC and Ship Frequency. The Port of Port Lavaca/Point Comfort and Aluminum Company of America (ALCOA) provided data on annual ship berthings on their MSC docks, as shown in Table 23. The average number of berthings since 2001 is 366 ships per year. Because each berthing represents one inbound and one outbound transit, the MSC has an average of 732 transits per year or 2.0 ship transits per day. Of the total ships, 71 percent call at the port docks, and 29 percent call at the ALCOA docks, based on data since 2001.

Table 23. Annual ship berthings at MSC.

Year	Point Comfort Dock	ALCOA Dock	Total Ships
1997	121		
1998	136		
1999	188		
2000	239		
2001	238	98	336
2002	289	73	362
2003	248	106	354
2004	274	130	404
2005	250	138	388
2006	237	101	338
2007	282	101	383
Average 2001-2007	259.7 (71%)	106.7 (29%)	366

In addition to the annual data, the port and ALCOA provided data on individual ship transits for 5 months, from 1 August to 31 December 2007. During this 5-month (153 days) period, 315 ship transits occurred or an average of 2.06 ship transits/day for the port and ALCOA docking ships. Table 24 shows the observed breakdown of ship transits per day that occurred during the 5 months. The Poisson distribution information will be discussed subsequently.

At the Point Comfort Dock, ship length averages 500 ft, beam averages 80 ft, and draft averages 27 ft, based on inbound and outbound ships. At the ALCOA dock, ship length averages 596 ft, beam averages 105 ft, and draft averages 28 ft. Based on both docks over the 5-month data period, ship length is a maximum of 673 ft, beam is a maximum of 106 ft, and draft is a maximum of 38 ft.

Table 24. Distribution of ship transits per day from 1 August - 31 December 2007.

Ship Transits Per Day	Number of Days, Actual	Number of days, Poisson Distribution for Mean of 2.06 Ships Per Day
0	12	19.5
1	47	40.2
2	43	41.4
3	33	28.4
4	10	14.6
5	6	6.0
6	1	2.1
7	1	0.6

Because of the types of cargo carried on MSC ships and the adverse current conditions, some ship sizes are restricted to daylight transit only. Daylight restrictions are based on either:

a. All ships having draft within 1 ft of the “current maximum draft” will be restricted to daylight only transits, under normal conditions. (Current maximum draft varies but is generally 36 ft except when channel shoaling is present and the current maximum draft is reduced to 35 ft.)

b. All vessels with a beam of 102 ft or greater or a length of 725 ft or greater and whose draft is within 4 ft of the current maximum draft shall be restricted to daylight only transits, under normal conditions.

Daylight transit is defined as: (a) enter or depart 30 min after sunrise, and (b) enter 3 ½ hr prior to sunset or depart 3 hr prior to sunset. Figures 67 and 68 show the variation of allowable daylight entry and departure times throughout the year.

The daylight restriction rules define the ships that the port, ALCOA, and the pilots believe to be the most likely to experience navigation difficulty. Those rules will be incorporated in the risk evaluation to differentiate ships. Based on discussions with pilots, the daylight-restricted ships should be further divided into draft less than 32 ft and draft greater than or equal to 32 ft. In evaluating the ship data from August to December, few ships were daylight restricted and draft less than 32 ft. The draft was changed to less than 34 ft and greater than or equal 34 ft and a few more ships were added to the lower draft category. The daylight-restricted ships with draft less than 34 ft were DRLT34 and those with draft greater than 34 ft were DRGT34. In addition, any study evaluating grounding probability during daytime versus nighttime shows a considerably higher rate during the night. For that reason, the not daylight restricted (NDR) ships are sub-classified into daytime (NDRD) and nighttime (NDRN) passage. MSC ships were classified into four categories as shown in Table 25. Each category has ships at one or both of the docks.

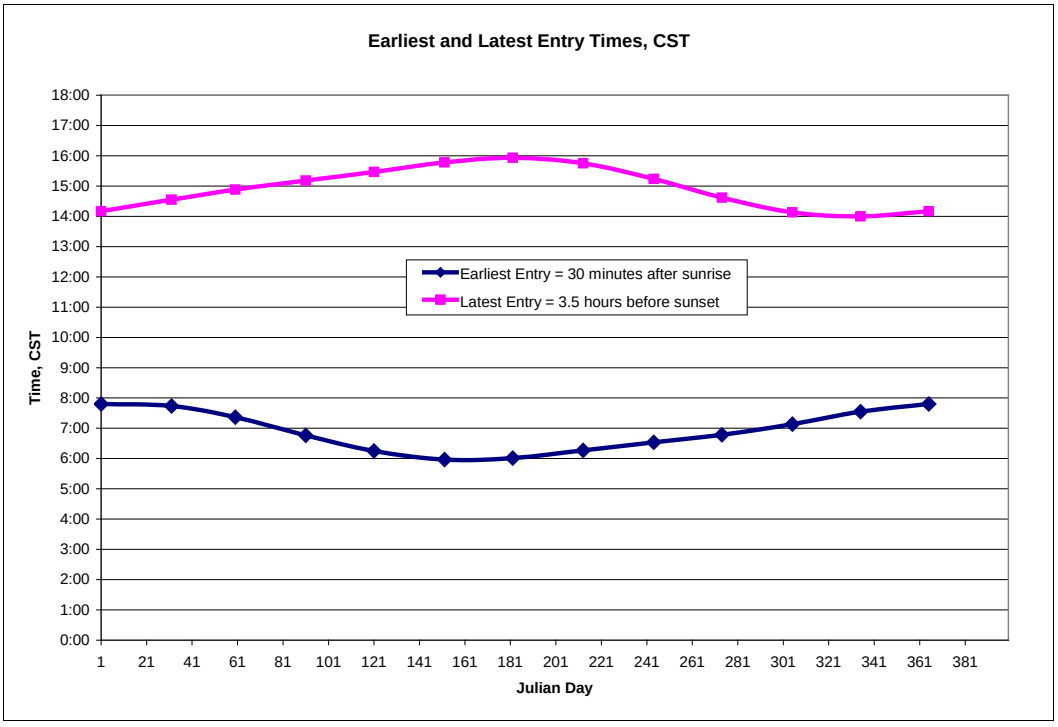

Figure 67. Earliest and latest entry times at MSC (note: times are in central standard time and must be adjusted for daylight savings time).

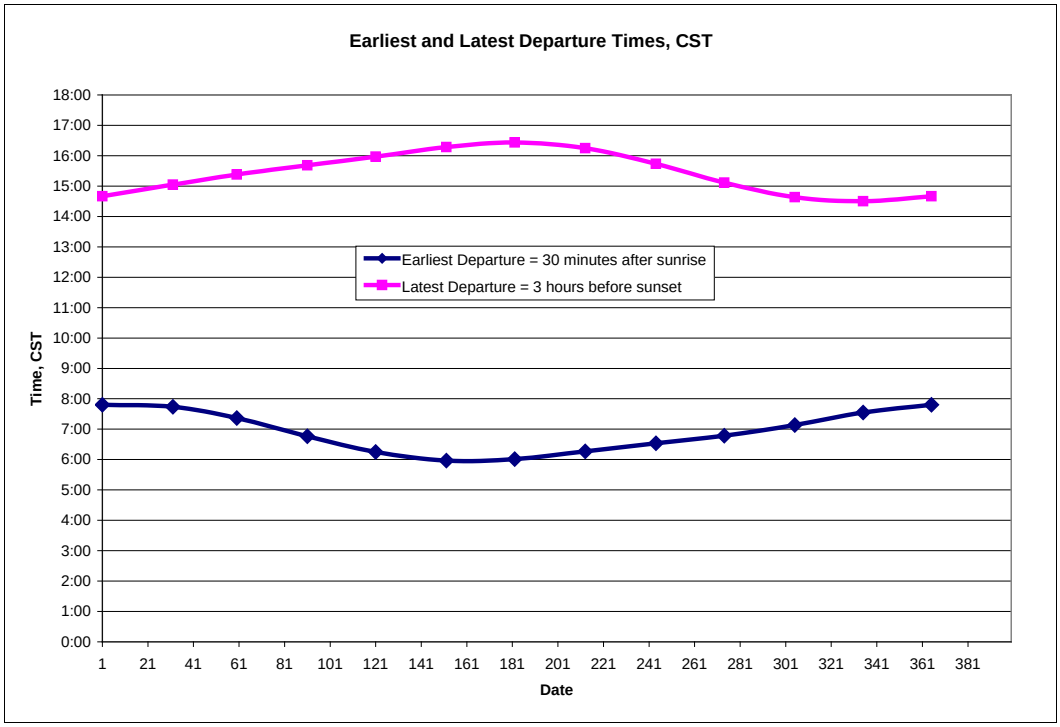

Figure 68. Earliest and latest departure times at MSC (note: times are in central standard time and must be adjusted for daylight savings time).

Table 25. Ship categories based on daylight restriction rules, pilot input, and difficulty of nighttime navigation.

Ship Category	% of Ships at Port	% of Ships at ALCOA	% of all ships using 71%/29% at Port/ALCOA
NDR Day (NDRD)	In = 14.61 Out = 15.73	In = 8.25 Out = 49.48	In = 12.76 Out = 25.52
NDR Night (NDRN)	In = 29.78 Out = 30.9	In = 0 Out = 0	In = 21.14 Out = 21.94
DRLT34	In = 0.56 Out = 1.69	In = 4.12 Out = 1.03	In = 1.59 Out = 1.50
DRGT34	In = 5.62 Out = 1.12	In = 37.11 Out = 0	In = 14.75 Out = 0.80

Based on contact with the pilots, 99 percent of ALCOA ships are daylight restricted because of either the daylight restriction rules, gear (cranes and booms) on deck that restrict visibility, or company policy. Because the goal herein is to differentiate ships based on difficulty of ship transit, and because it is almost impossible to sort out which ships are daylight restricted based on cranes/boom or company policy, the published daylight restriction rules were applied to differentiate the ALCOA docking

ships just as was done for the port docking ships, but none of the ALCOA ships transited at night.

Table 25 shows the four categories of ships classified as port ships or as ALCOA ships and inbound versus outbound. The last column adjusts the percentage from each dock to represent the long-term average of 71 percent ships at the port dock and 29 percent at the ALCOA dock, and expresses the result as the percentage of all ship transits. For example, 12.76 percent of all ship transits on the MSC enter in a category NDRD ship on an inbound transit. These four ship categories and the inbound and outbound division incorporate the fact that the largest inbound ships are generally loaded, and these same ships when outbound are unloaded. The ship comes in as category DRGT34 or DRLT34 and departs as either category NDRD or NDRN.

Tidal Current Magnitude in Bottleneck and Safe Current Guidelines. The primary concern of the pilots and the port is the strong longitudinal current present in the MSC entrance. The literature was examined for safe levels of longitudinal currents for ship navigation. PIANC guidance classifies longitudinal currents of 3 knots or greater as "strong," and that category is PIANC's highest category. Spanish ship channel guidance from the *Recommendation for Maritime Works* shows 4 knots to be a recommended upper limit. The USACE (2006) provides channel width design guidance for deep draft navigation as a function of three categories of maximum current. The maximum category in the USACE guidance is 1.5 to 3 knots. The MSC has longitudinal currents of 3 knots or greater about 65 percent of the time. For this evaluation of risk, the velocity in the bottleneck will be the parameter that defines the magnitude of adverse longitudinal current. Long-term measurement of velocity in the bottleneck is not available. Numerical simulations can provide detailed information about specific time periods, but long-term data are needed to define the probability of occurrence. Although there is a lag between velocity and tide difference, velocity through the bottleneck is a function of the water level difference between the gulf and the bay. Long-term records at Bob Hall Pier in Corpus Christ are taken as representative of the gulf at the MSC entrance. The Port O'Connor gage is the gage in the bay closest to the MSC entrance and is taken as representative of the bay for purposes of determining water level difference and velocity in the bottleneck. Hourly water level data from both locations were obtained for 2005-2007 from the Texas A&M University Division of Nearshore

Research website and the distribution of difference between the two gages is plotted in Figure 69. Also shown is a uniform distribution with mean of -0.14 ft and standard deviation of 0.55 ft.

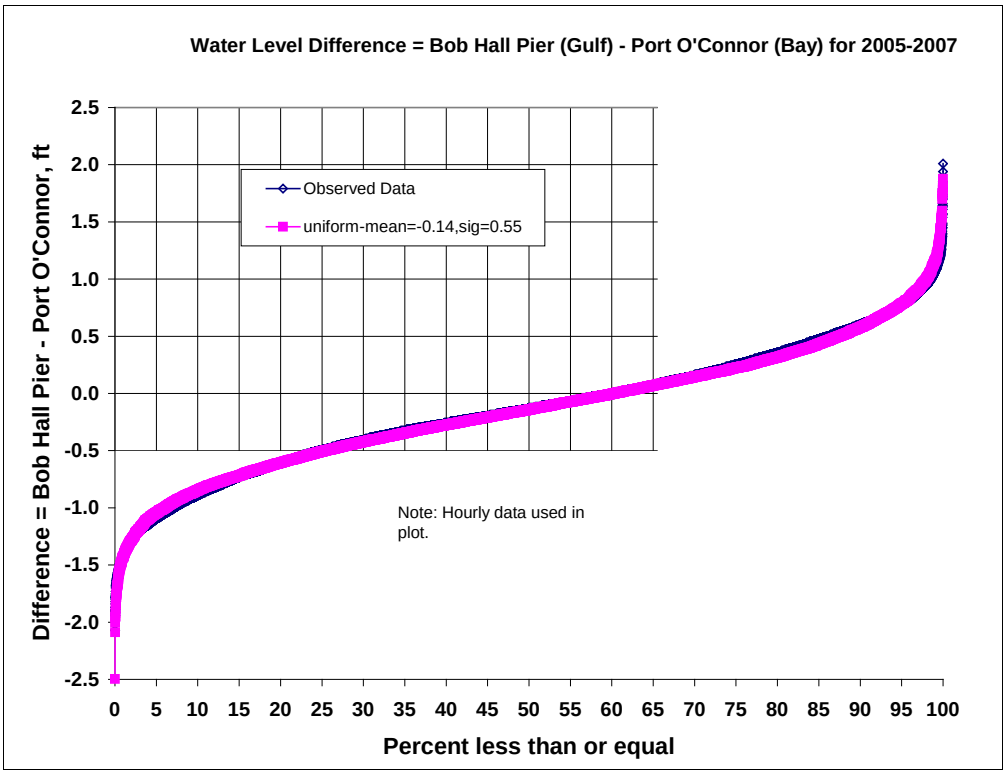

Figure 69. Distribution of water level difference between Bob Hall Pier and Port O'Connor, observed and normal distribution.

An approximate average channel velocity through the MSC entrance can be calculated using the water level difference in Figure 69 in the equation

$$V = C_v\sqrt{2g\Delta h} \tag{5}$$

where:

V = velocity through the inlet entrance
C_v = empirical velocity coefficient
G = acceleration due to gravity
Δh = water level difference

C_v depends on entrance conditions and other losses through the inlet. C_v is generally close to, but less than 1.0 and is specified herein as 0.9. (An alternate approach, the Manning equation, was evaluated and yielded

essentially the same results.) Equation 5 gives the average channel velocity. Depth-averaged velocity at the center of the channel will be greater than the average channel velocity. Surface velocity will be greater than depth averaged velocity. The pilots report making water velocity measurements in the bottleneck with their pilot boat as a float and using GPS to measure the speed. This technique would give a centerline surface velocity. Pilot Larry Robinson reports that on one rare occasion, a centerline surface velocity of 9.2 knots was measured. He said velocities of 6-7 knots are present and not rare. Any velocity greater than 5 knots is considered "strong" by the MSC pilots. Velocities between 3 and 5 knots are considered "medium." The pilots generally report no significant difficulties with bottleneck currents when currents are less than 3 knots that are classified as "light."

PIANC classifies a longitudinal current of 3 knots or greater as strong. To be comparable to the pilots' measurements and observations of current-related navigation problems, the Equation 5 average channel velocity is multiplied by 1.20 to obtain depth-averaged velocity near the channel center and then multiplied by 1.15 to convert depth-averaged velocity to surface velocity. This computed centerline surface velocity is intended to be comparable to the centerline surface velocity measured by the pilots and thus comparable to their description of currents being "light," "medium," and "strong." Figure 70 shows the distribution of this centerline surface velocity through the MSC entrance and is based on Equation 5, the water level difference data for 2005-2007, and the adjustments for centerline surface velocity that is $C_v = 0.9 \times 1.2 \times 1.15 = 1.24$. Table 26 shows the ranges of currents based on pilot input and percentage of occurrence from Figure 70. Note that a light current, which is not a problem according to the pilots, occurs about 36 percent of the time. Strong currents occur 22 percent of the time. This means that about one out of every five ships experiences a current equal to or exceeding 5 knots. A current exceeding 6 knots occurs 8 percent of the time. Table 27 shows the comparisons of currents observed by the pilots, the current calculated with Equation 5, and the observed water level difference for the date and time of the pilots' measurement of current in the channel.

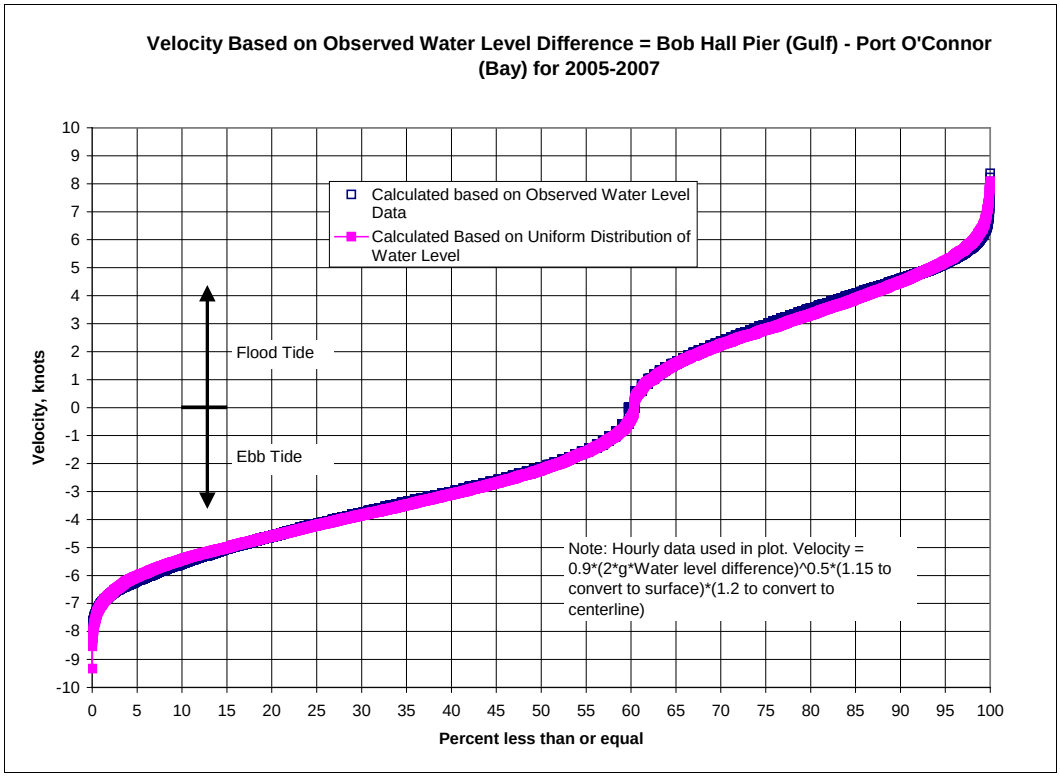

Figure 70. Centerline surface velocity computed based upon water level difference between Bob Hall Pier (representing the Gulf of Mexico) and Port O'Connor (representing Matagorda Bay).

Table 26. Ranges of bottleneck currents, pilots description, and percent of occurrence based on currents computed using observed water level difference.

Current category	Direction	Magnitude (knots)	% Occurrence	Pilots Description
EG5	Ebb	> = 5	15.5	Strong
E35	Ebb	> = 3 to < 5	25.0	Medium
EL3	Ebb	< 3	19.5	Light
FL3	Flood	< 3	15.3	Light
F35	Flood	> = 3 to < 5	18.4	Medium
FG5	Flood	> = 5	6.3	Strong

Table 27. Comparison of observed current by pilots and computed current by equation based upon observed water level difference between Bob Hall Pier and Port O'Connor.

Date	Pilot	Inbound/ Outbound Ship	Flood or Ebb Tide	Observed Current, knots	Current Description	Bob Hall Pier Water Level, ft MSL	Port O'Connor Water Level, ft MSL	Difference, ft	Computed Current, knots
1/9/05 17:30	Robinson	Out	Flood	4.7	Strong	1.02	0.12	0.9	5.6
4/25/08 15:30	Robinson	In	Flood	2.0	Light	1	1.13	-0.13	-2.1
4/26/08 10:00	Robinson	Out	Flood	6.0	Strong	1.7	0.25	1.45	7.1
4/26/08 15:00	Robinson	In	Flood	2.0	Light	1.23	0.86	0.37	3.6
4/27/08 8:00	Robinson	In	Flood	4.0	Medium	0.79	0.29	0.5	4.2
4/28/08 7:00	Robinson	In	Flood	4.0	Medium	0.46	-0.25	0.71	5.0
4/28/08 18:00	Robinson	Out	Slack	0.0	Light	0.54	0.57	-0.03	-1.0
4/29/08 18:00	Robinson	Out	Flood	2.0	Light	0.37	0.46	-0.09	-1.8
5/3/08 15:00	Robinson	In	Flood	4.0	Medium	0.23	0.6	-0.37	-3.6
5/6/08 2:15	Robinson	Out	Flood	5.0	Strong	0.75	0.12	0.63	4.7
5/6/08 2:45	Robinson	In	Flood	6.0	Strong	1	0.17	0.83	5.4
6/4/08 12:00	Robinson	In	Flood	3.5	Medium	0.86	0.91	-0.05	-1.3
6/5/08 11:00	Robinson	In	Flood	4.5	Medium	1.24	1.11	0.13	2.1
6/5/08 21:00	Robinson	Out	Ebb	-3.0	Medium	-1.05	0.59	-1.64	-7.6
6/8/08 14:00	Robinson	In	Flood	3.0	Medium	0.8	0.96	-0.16	-2.4
6/9/08 16:30	Robinson	Out	Ebb	-1.0	Light	0.47	0.78	-0.31	-3.3
6/9/08 19:30	Robinson	In	Ebb	-3.0	Medium	0.58	0.7	-0.12	-2.0
6/10/08 2:20	Robinson	Out	Ebb	-4.0	Medium	-0.06	0.38	-0.44	-3.9
6/11/08 9:30	Robinson	Out	Flood	1.0	Light	0.39	0.37	0.02	0.8
6/11/08 11:45	Robinson	In	Flood	2.0	Light	0.38	0.39	-0.01	-0.6
6/16/08 11:45	Robinson	Out	Flood	1.0	Light	0.94	0.69	0.25	3.0
6/18/08 18:45	Robinson	Out	Ebb	-3.0	Medium	-0.8	-0.02	-0.78	-5.2
6/18/08 20:00	Robinson	In	Ebb	-4.8	Medium	-0.96	-0.13	-0.83	-5.4
6/21/08 20:30	Robinson	Out	Ebb	-3.1	Medium	-0.66	0.19	-0.85	-5.4
6/22/08 10:30	Robinson	In	Flood	3.4	Medium	0.67	0.35	0.32	3.3
6/22/08 18:30	Robinson	Out	Slack	0.0	None	0.17	0.43	-0.26	-3.0
6/23/08 7:15	Robinson	In	Flood	3.3	Medium	0.46	0.02	0.44	3.9
6/24/08 11:35	Robinson	Out	Flood	3.5	Medium	0.37	0.33	0.04	1.2
6/25/08 22:40	Robinson	Out	Ebb	-1.0	Light	0.2	0.25	-0.05	-1.3
6/26/08 17:25	Robinson	Out	Ebb	-1.0	Light	-0.04	0.37	-0.41	-3.8
7/1/08 18:40	Robinson	Out	Ebb	-4.0	Medium	-1.2	0.12	-1.32	-6.8
7/2/08 10:10	Robinson	Out	Flood	3.8	Medium	1.24	0.89	0.35	3.5
8/6/08 8:00	Adrian	In	Slack	0.0	None	-0.01	0.09	-0.1	-1.9
8/6/08 18:00	Adrian	Out	Slack	0.0	None	-0.22	-0.25	0.03	1.0
8/7/08 0:30	Adrian	In	Flood	2.0	Light	0.19	0.21	-0.02	-0.8
8/29/08 11:00	Adrian	Out	Flood	3.5	Medium	0.44	0.45	-0.01	-0.6
9/2/08 19:15	Adrian	In	Flood	4.0	Strong	0.59	0.12	0.47	4.0
9/3/08 9:00	Adrian	In	Ebb	-4.0	Medium	0.14	0.85	-0.71	-5.0
9/4/08 15:40	Adrian	Out	Ebb	-2.0	Light	0.49	0.23	0.26	3.0
9/4/08 16:30	Adrian	In	Ebb	-2.0	Light	0.6	0.23	0.37	3.6
9/5/08 10:15	Adrian	In	Ebb	-2.5	Medium	-0.07	0.63	-0.7	-4.9
9/5/08 18:00	Adrian	Out	Flood	2.0	Light	0.45	0.16	0.29	3.2
9/6/08 8:00	Adrian	Out	Ebb	-2.0	Light	0.7	1.03	-0.33	-3.4
9/26/08 8:30	Adrian	In	Flood	2.0	Light	1.48	1.47	0.01	0.6
9/26/08 18:00	Adrian	Out	Ebb	-4.0	Medium	0.57	1.03	-0.46	-4.0
9/27/08 9:00	Adrian	Out	Slack	0.0	None	0.67	0.96	-0.29	-3.2
9/27/08 9:30	Adrian	In	Slack	0.0	None	0.67	0.9	-0.23	-2.8
9/28/08 13:00	Adrian	Out	Flood	2.0	Light	0.77	0.45	0.32	3.3
9/29/08 8:00	Adrian	In	Ebb	-3.0	Medium	0.21	0.53	-0.32	-3.3

Visibility. Visibility is also a factor in many navigation studies. Visibility data were obtained from the National Oceanic and Atmospheric Administration (NOAA) National Climatic Data Center. The evaluation of visibility was based on 2005-2007 for Port Lavaca, Corpus Christi Naval Air Station (NAS), and Rockport Aransas County. An attempt was made to find visibility information on the coast and close to the MSC, but no data were available at Port O'Connor. The Port Lavaca station is well inland of the MSC and may not be representative. The Corpus Christi NAS station is closer to the coastline, but relatively far from the MSC. The Rockport

Aransas County data was considered to be most representative of conditions at the MSC entrance.

A previous navigation study (Uluscu et al. 2008) broke down visibility into < 0.5 mile, 0.5 to < 1 mile, and 1 mile and greater. Another study used 2 km (= 1.25 miles) as the dividing line between poor and good visibility. Pilot Larry Robinson stated that on outbound ships, the pilots want 1 mile of visibility for good conditions. For inbound ships meeting an adverse current, they want 3 miles for good conditions, but sometime have to enter with less. Table 28 provides a breakdown of the visibility data based on the 1 and 3 mile limits. The percentages are based on the number of hours during the year.

Table 28. Distribution of visibility for 2005 through 2007.

Visibility (miles)	% Port Lavaca 722209	% Corpus Christi NAS 722515	% Rockport Aransas Co. 722524
< = 1	0.9	0.9	2.0
< = 3	4.0	4.3	5.7

The pilots state that the visibility problems vary throughout the year and are worse in January through March, a time period when weather fronts out of the north are common. The hourly data for 2005 to 2007 were broken down into monthly percentages, as shown in Table 29. The data show a trend consistent with the pilots' observations. December through February are months with the lowest visibility, with May through October being months with relatively high visibility.

The pilots also state that when visibility is low, the transit is often delayed until conditions improve. They state that the most significant visibility problems occur if visibility deteriorates after a transit has begun. Under this circumstance, the pilot generally has no choice but to continue the transit. A transit on the MSC requires about 3 hr. The database was searched for the number of hours that had good visibility followed by low visibility within the next 3 hr to represent a ship beginning a transit in good visibility and then experiencing unacceptable visibility. The monthly breakdown of declining visibility cases is shown in Table 30. As in the visibility data, December through February are months with the greatest percentage of declining visibility during a ship transit.

Table 29. Visibility data broken down by month.

Month	Total Hourly Observations During Month	Number of Observation (< = 1 mile)	% of Monthly Hourly Observations (< = 1 mile)	Number of Observations (< = 3 mile)	% of Monthly Hourly Observations (< = 3 mile)
1	2268	111	4.89	322	14.20
2	2058	140	6.80	322	15.65
3	2231	25	1.12	108	4.84
4	2098	12	0.57	78	3.72
5	2228	3	0.13	36	1.62
6	2191	7	0.32	27	1.23
7	2192	26	1.19	89	4.06
8	2236	17	0.76	41	1.83
9	2123	8	0.38	41	1.93
10	2229	14	0.63	57	2.56
11	2156	66	3.06	143	6.63
12	2284	107	4.68	231	10.11

Table 30. Decline of visibility data broken down by month. Conditions where visibility is adequate but declines to inadequate sometime during the following 3 hr that represents transit time of ship.

Month	Total Hourly Observations During Month	Number of Observation (< = 1 mile)	% of Monthly Hourly Observations (< = 1 mile)	Number of Observations (< = 3 mile)	% of Monthly Hourly Observations (< = 3 mile)
1	2268	105	4.63	214	9.44
2	2058	94	4.57	152	7.39
3	2231	43	1.93	115	5.15
4	2098	21	1.00	84	4.00
5	2228	9	0.40	51	2.29
6	2191	18	0.82	36	1.64
7	2192	51	2.33	103	4.70
8	2236	10	0.45	53	2.37
9	2123	15	0.71	57	2.68
10	2229	24	1.08	61	2.74
11	2156	61	2.83	114	5.29
12	2284	102	4.47	140	6.13
Average	-	-	2.1	-	4.5

Cross current at gulf entrance to jetties. A cross current at the gulf entrance to the jetties has been reported by the pilots as being significant on a frequent basis. The PIANC navigation guidance states that a cross current of < 0.2 knots is negligible, 0.2-0.5 knots low, 0.5-1.5 knots moderate, and 1.5-2.0 knots strong. No category is given for a cross current velocity exceeding 2 knots. It may also be significant that the PIANC guidance is for a cross current over the entire length of the ship, whereas the problems with a cross current at the MSC entrance is because the bow of the entering ship is not exposed to such a current whereas the stern of the ship is exposed. The cross current at the MSC entrance is caused by wind stress that generates a current in the same direction as the wind and the longshore current from waves breaking at an angle to the shoreline. The wind stress current is dependent on the local winds. A rule of thumb is that the wind stress current speed is 3 percent of the wind speed for a fully developed flow on a large water of body.

An analysis was done to determine which of these two mechanisms (wind or waves) was responsible for the cross current at the entrance to the MSC as calculated from simulations with the CMS. Table 31 summarizes the results for three locations just gulfward of the ends of the jetties. Based on the chosen wind and wave conditions, the cross current at the MSC entrance is primarily caused by the wind stress. The waves only added at most about 10 percent to the wind stress speed. The peak current of 0.58 knots is just barely in the PIANC category of moderate. Because local wind is responsible for the wind stress current and wind stress current is the dominant factor at the MSC entrance, the wind data at Port O'Connor were analyzed to define the probability of the cross current at the MSC. The 3 percent rule was applied together with the component of the wind that was parallel to the shoreline. The values for down-shore current (toward the southwest) were adjusted by a factor of 1.2 to agree with the CMS runs. The values for up-shore currents (toward the northeast) were adjusted by a factor of 0.97 to agree with the CMS runs. Both down-shore and up-shore velocities were increased by 10 percent to account for the small addition from longshore current by obliquely incident breaking waves. Based on the Port O'Connor winds for 2007, the distribution of cross current was determined as shown in Figure 71. Note that only about 8 percent of all currents are greater than the PIANC threshold for moderate. Also note that two-thirds of all cross-shore currents are directed toward the southwest and that only 0.1 percent of all currents exceed 0.5 knots and are toward the northeast.

The pilots have stated that strong currents toward the northeast are infrequent. Pilot Larry Robinson was asked to estimate the percent of time that the cross current was light, medium, and strong. He estimated that the light category corresponds to a crab angle of less than 3 deg and occurs 40 percent of the time. Moderate cross currents correspond to crab angles of 3 deg to less than 8 deg and occur 35 percent of the time. Strong cross currents correspond to crab angles of 8 to 12 deg and occur 20 percent of the time. For 5 percent of the time, the cross current is so severe that a crab angle of 12 deg cannot be maintained, and the ship is held outside until the cross current strength subsides. It is difficult to reconcile the published guidelines for cross currents, the computed cross currents, and the pilots' observations. One possibility is that the flow in and out of the inlet is not uniform across the width of the inlet and this contributes to the cross current effect. The bathymetry shown in Figure 64 suggests a non-uniform current. Non-uniformity of the current on an ebb tide can result

Table 31. Cross currents at MSC (note that shoreline is at an azimuth of about 60 deg).

Condition	Wind and/or Wave	Current (knots)		
		sta 1	sta 2	sta 3
Waves only	2-m, 8 sec from east (90 deg)	0.19	0.18	0.08
	1-m, 6 sec from east (90 deg)	0.02	0.0	0.0
	1-m, 6 sec from south (180 deg)	0.06	0.02	0.0
Wind only	10 knot from 60 deg	0.23	0.21	0.21
	10 knot from 105 deg	0.18	0.18	0.19
	10 knot from 195 deg	0.18	0.16	0.16
	10 knot from 240 deg	0.16	0.14	0.16
	20 knot from 60 deg	0.54	0.45	0.47
	20 knot from 105 deg	0.51	0.45	0.45
	20 knot from 195 deg	0.41	0.37	0.29
	20 knot from 240 deg	0.43	0.39	0.35
Wind and waves	20 knot from 60 deg and 2-m, 8 sec from east (90 deg)	0.58	0.45	0.49
	20 knot from 105 deg and 2 m, 8 sec from east (90 deg)	0.53	0.45	0.47
	20 knot from 195 deg and 1 m, 6 sec from south (180 deg)	0.43	0.37	0.29
	20 knot from 240 deg and 1 m, 6 sec from south (180 deg)	0.43	0.39	0.35

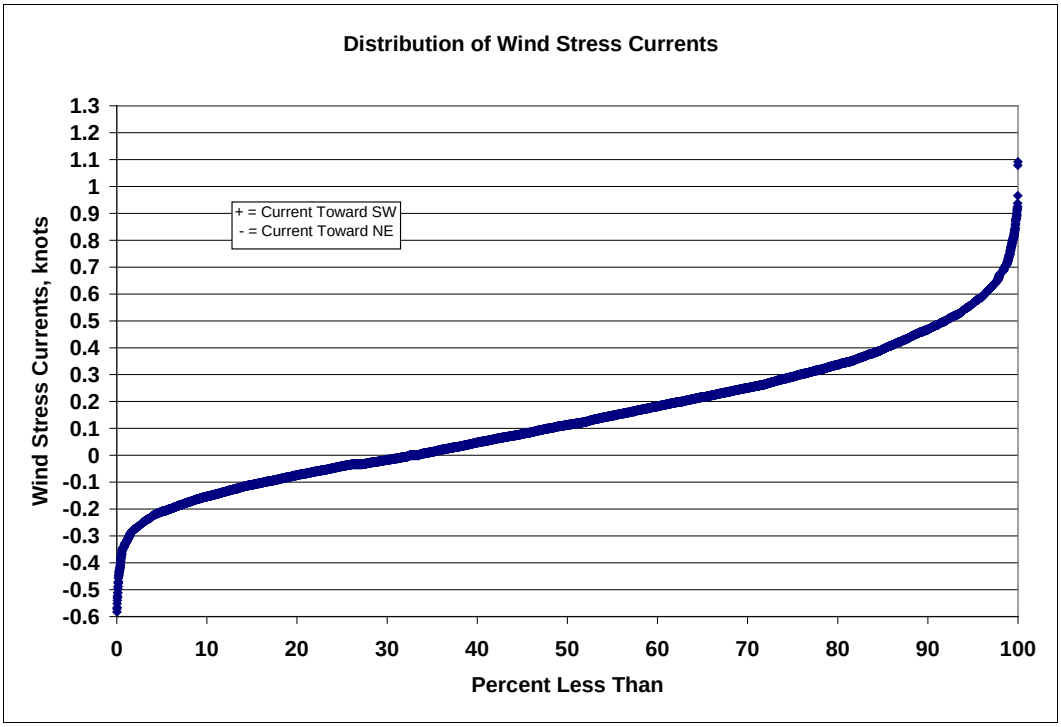

Figure 71. Cross currents.

from the expansion of the bottleneck to the jetties. As a general rule, any abrupt expansion will result in currents favoring one side of the channel or the other. A current concentrated on one side of the jetty entrance would have an effect similar to a cross current driven by wind along the shore. For this evaluation, cross currents will be characterized using the pilots' observations and the percent of time that each category is estimated to occur by the pilots.

Expert elicitation of pilots

The selected probability of 0.0007 groundings per ship transit represents all ship classes, ship directions, and environmental conditions. The probability of grounding of specific ship transits in the MSC varies widely based on the primary attributes of magnitude of bottleneck currents, ship class, day or night, visibility, ship direction, tide direction, location along the MSC entrance channel, and for inbound ships, magnitude of the cross current at the jetty entrance. These attributes result in hundreds of combinations of ship transits. It is infeasible to sort out the differences in grounding probability between the various combinations of these primary attributes by using a ship simulator, a physical ship model, or historical data.

Two studies (Merrick et al. 2002, Uluscu 2008) are the most notable examples of determining the probability of a large number of combinations of attributes. Both studies used expert elicitation to develop relative conditional probabilities. An example of a relative conditional probability is that a ship in a 4-knot longitudinal current is 3 times as likely to ground as the same ship in a 1.5-knot current. Nothing is stated about the absolute likelihood of grounding. The Merrick et al. (2002) risk assessment of the PWS did not have local historical accident data delineating all of the attributes that could affect risk. They used expert elicitation to assess relative conditional probabilities of the numerous combinations of attributes.

The study by Uluscu et al. (2008) also used expert elicitation to define relative conditional probabilities and historical data to convert the relative values to absolute values of a powered grounding. In both studies, the experts were asked about the likelihood of grounding in various magnitudes of currents, winds, visibility, presence of other ships, reach characteristics, ship characteristics, etc. The questions were presented to the experts as pairwise comparisons where only one attribute is changed and the expert compares one situation or circumstances (scenario) to the same situation with one change. The expert answers that scenario 1 is "X" times as likely to experience a grounding as scenario 2. For example, scenario 1 could be a loaded ship in 3 knot current in 1 mile visibility in reach A. Scenario 2 would be a loaded ship in 3 knot current in 1 mile visibility in reach B. Only one thing was changed in the comparison, the reach. The experts are asked $n(n\text{-}1)/2$ pairwise comparisons to determine relative conditional probability, where n is the number of attributes. Results of the pairwise comparisons can be compiled using the AHP methodology (Saaty 1980) or a regression analysis as discussed in Uluscu et al. (2008).

In the absence of historical data on absolute probabilities to calibrate the relative conditional probabilities, the relative probabilities can be used to rank the various combinations of attributes and assess the importance of various attributes.

Expert elicitation of the available MSC pilots was used to determine relative conditional probabilities of grounding. This study also uses a simulator to assess the effects of removal of the bottleneck as a means of reducing the risks to navigation.

The navigation system at the MSC was described by breaking it down into various attributes. In previous risk assessments, accidents have included groundings, collisions, fire/explosion, and structural hull failure. Because the study reach used herein is one-way and is south of the congestion north of the GIWW, collisions are not considered. Fire/explosions and structural hull failure are not caused by the focus of this study that are adverse currents in the bottleneck. Only powered groundings, the accident most controlled by an adverse current at the MSC, are considered in this study.

Based on the breakdown of attributes described above, the pilots were asked to compare different attributes to prioritize the likelihood of grounding in the existing MSC entrance. Three of the four MSC pilots were able to participate in the questionnaire. Each pilot was asked 48 pairwise comparison questions. The questions are compiled in Appendix F.

The pilots' pairwise comparisons of grounding likelihood were analyzed using the AHP by Jongbum Kim, contractor to the ERDC Environmental Laboratory. In assessing relative probability, it is difficult for the expert to give precise values. The AHP is useful guideline for making pairwise comparison judgments.

An example matrix of relative probability is shown in Table 32. For example, Attribute A is 3 times more likely than C, and C is 1/3 of Attribute A. These likelihoods may not be completely consistent. For example, if B is 3 times more likely than Attribute A, and B is 7 times more likely than C, then in theory, A should be 7/3 times more likely than C, rather than 3 times more likely, which is elicited from the example. Such inconsistencies are to be expected because the experts; values or their quantitative expressions are often inconsistent, contradictory, or not sufficiently considered amid many complexities.

Table 32. Simple example of likelihood matrix.

Attribute	A	B	C
A	1	1/3	3
B	3	1	7
C	1/3	1/7	1

The AHP solves for the probabilities set that is most consistent with these relative probabilities by a mathematical procedure called eigenvector analysis. Although the AHP has been the subject of many research papers and the technique has been found to be both technically valid and practically useful, there are critics of the method because the process has no sound underlying statistical theory. The AHP is described in Saaty (1980).

The results of the AHP analysis of the pilots' responses is shown in the tree diagram in Figure 72. The breakdown of navigation attributes shown in Figure 72 is based on there being no dependence between attributes. This assumption of independence is an approximation because there were not enough experts to try to elicit any dependencies. The values shown are the average of the three pilots' responses. The probabilities of each level of the tree are normalized to sum = 1.0 that is standard AHP procedure. Results show that the probability of grounding in the bottleneck to Sundown Island (B-SI) reach in an inbound ship is 0.36/0.26 = 1.4 times as likely as the probability of grounding in the B-SI reach in an outbound ship. Another example is that an inbound ship in the B-SI reach transiting against an ebb current is 0.69/0.31 = 2.2 times as likely as the probability of grounding in the B-SI reach in an inbound ship transiting on a flood tide.

Note that for outbound ships, a daylight-restricted ship with draft greater than 34 ft is 0.36/0.13 = 2.8 times as likely to ground as a not-daylight restricted ship transiting during the daytime. For inbound ships, a daylight-restricted ship with draft greater than 34 ft is 0.38/0.09 = 4.2 times as likely to ground as a not-daylight restricted ship transiting during the daytime.

Based on the pilots' responses, the following paragraphs summarize their expert opinions. The pilots clearly stated that many exceptions exist as to how they answered the questions. In a few cases, two of the pilots responded one way and the other pilot responded the other way. The large majority of cases had similar responses from all three pilots.

a. The reach and ship direction most likely to experience a grounding was an inbound ship in the B-SI reach. The next most likely was an outbound ship in the B-SI reach. The next most likely was an inbound ship in the gulf to bottleneck (G-B) reach. The least likely was an outbound ship in the G-B reach. The worst case inbound B-SI ship is twice as likely to ground as the best case outbound G-B ship, with all other factors being equal.

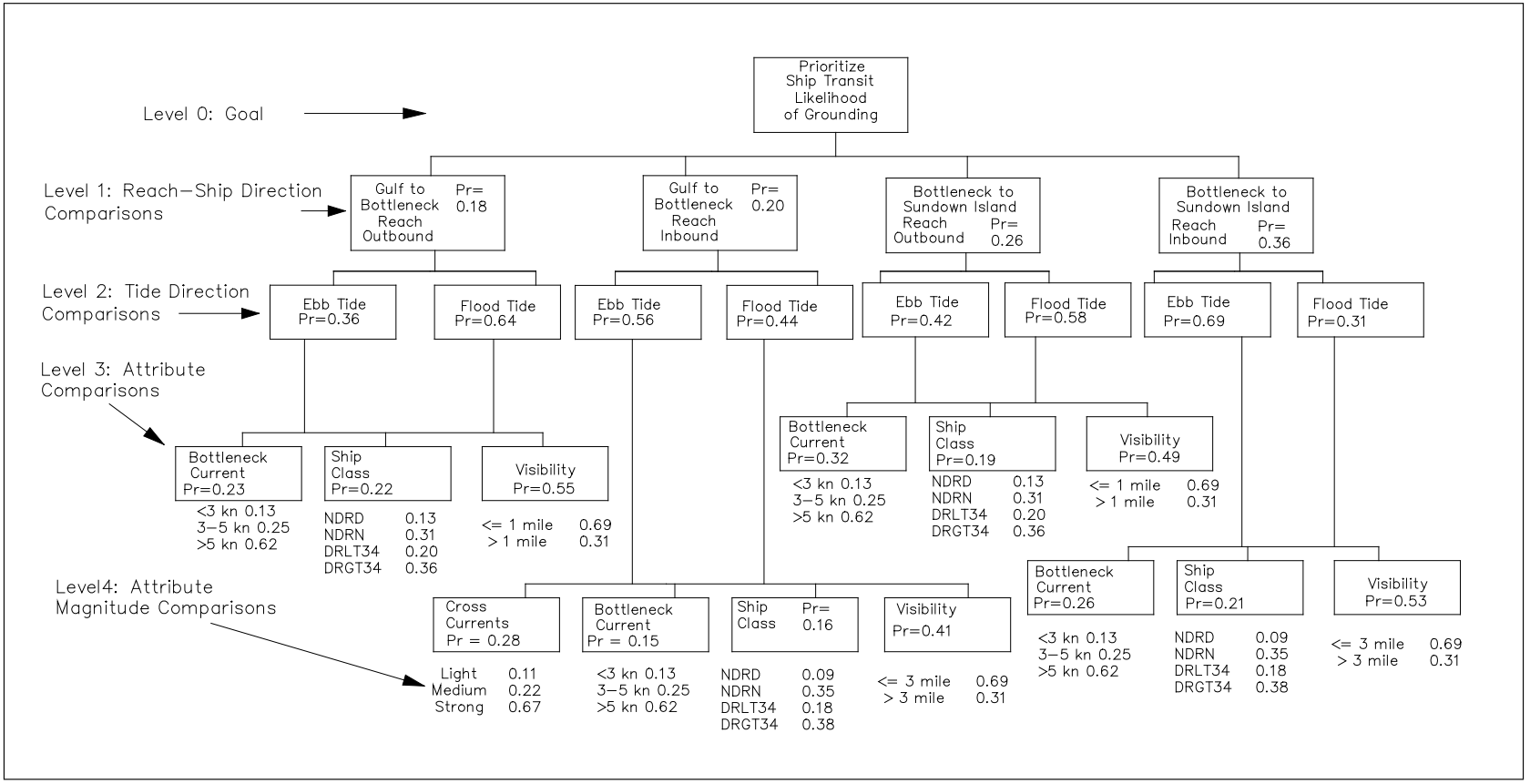

Figure 72. Schematic of attributes that define risks to navigation at MSC and result of expert elicitation of pilots (based on normalization to sum = 1.0).

b. In all four reach and ship direction combinations, a ship moving against the tidal current was more likely to ground than a ship going with the tide. This finding was the one part of the survey that generally differs from other navigation channels and the area where some differences in pilot opinion was expressed.

c. In all four reach and ship direction combinations, visibility was the factor most likely to contribute to a grounding. The pilots pointed out that if visibility is low; they wait for improvement before transit. The problem arises when they begin a transit and visibility becomes low while underway. Under these conditions, all other factors become secondary, and that is why visibility received such a high ranking.

d. In the only reach and ship direction where cross currents at the jetty entrance are a problem, G-B inbound, cross-current magnitude was the second most important factor after visibility. In the other three combinations (G-B out, B-SI in, and B-SI out), tidal current magnitude in the bottleneck was the second most important factor after visibility.

e. For tidal currents in the bottleneck of greater than 5 knots, grounding likelihood was about 5 times as likely to occur than with 0-3 knots current in the bottleneck.

f. Ship class was the least important attribute compared to visibility or tidal current magnitude, but definite differences exist between ship types. For example, inbound ships that are daylight restricted and draft greater than 34 ft are more than 4 times as likely to ground as inbound ships that are not daylight restricted that travel during daytime. For both inbound and outbound ships, the daylight-restricted ship with draft greater than 34 ft is only slightly more likely to ground than the not-daylight restricted ships traveling at night.

The pilots' responses to the questions rarely indicated strong differences in the pairwise comparisons. They almost always stated attribute 1 was 2 to 3 times more significant than attribute 2 rather than saying ratios like 5 times more significant.

Two factors from the expert elicitation of the pilots were adjusted and differ from those shown in Figure 72. First, the pilots rated visibility as the most important attribute. However, the pilots rated poor visibility as being only 2.2 times more likely to ground as good visibility. Based on the study by Kite-Powell et al. (1998), the Houston/Galveston ship channel had a probability of grounding of 7 to 9 times greater in poor visibility for ships with draft < 30 ft. For ship draft > = 30 ft, probability of grounding was 0.5-8 times greater with poor visibility. Based on Fowler and Sorgard (2000), powered grounding probability in poor visibility is 3 to 6 times higher than in good visibility. Therefore, in the present study, probability of grounding for poor visibility was set at 5 times that of good visibility.

The second adjustment of the expert elicitation is in the bottleneck current (BC). The pilots were provided questions in the expert elicitation that compared bottleneck currents of 0-3 knots, 3-5 knots, and > 5 knots. These ranges were based on the pilots' input. The results of their responses showed relative probabilities of grounding of 0-3 of 0.13, 3-5 of 0.25, and > 5 of 0.62. There are problems with this approach because bottleneck currents are the primary focus of this study. The main problem is that current magnitude must be reduced sufficiently to move from one category to another before a change in probability occurs. Therefore, for example, a bottleneck current of 4.9 knots is no worse than a current of 3.1 knots. The same problem is that once above 5 knots, all current magnitudes produce the same result, whereas we know that an 8 knot-current would be far more difficult than a current of 5 knots.

Figure 73 shows the three ranges along with an exponential equation that provides an estimate of grounding probability that is continuous and avoids the problems with the step function. The exponential equation is:

$$RP(BC) = 0.057 \exp(0.39BC) \tag{6}$$

Based on the relative probability in Figure 72 for the individual attributes, the total relative probability of grounding for each of the 288 combinations of attributes in each reach is computed using

$$\begin{aligned} RP(\text{reach}) = {} & RP(\text{reach and ship direction}) * RP(\text{tide direction}) * \\ & [Weight(BC) * RP(BC) + Weight(SC) * RP(SC) + Weight(Vis) * \\ & RP(Vis) + Weight(CC) * RP(CC)] \end{aligned} \tag{7}$$

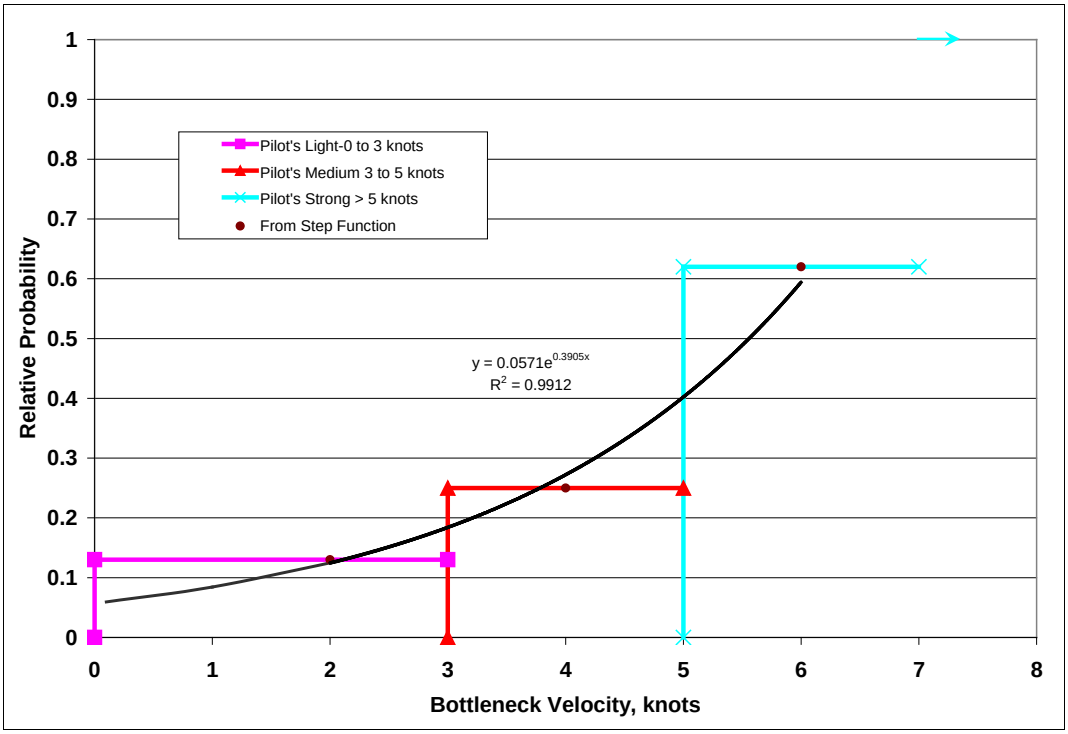

Figure 73. Exponential function used for relative probability of grounding in bottleneck.

In Equation 7, *RP* = relative probability, *BC* = bottleneck current, *SC* = ship class, *Vis* = visibility, and *CC* = cross currents. Equation 7 enters in the ship-event model discussed subsequently.

Ship event model

To evaluate risk for the various combinations of ship traffic, bottleneck velocity, daylight restriction, and other attributes, a ship-event model (SEM) was used to evaluate the MSC entrance. The SEM is not intended to be a ship traffic model intended to examine individual ship times or delays. The model combines the relative probabilities of grounding from the expert elicitation of the pilots, in Figure 72, with various statistical distributions of longitudinal current, cross current, ship category, ship direction, tide direction and magnitude, visibility, etc. Figure 74 shows the percentage of occurrence of the various attributes describing the MSC. The various steps in the SEM process are described next.

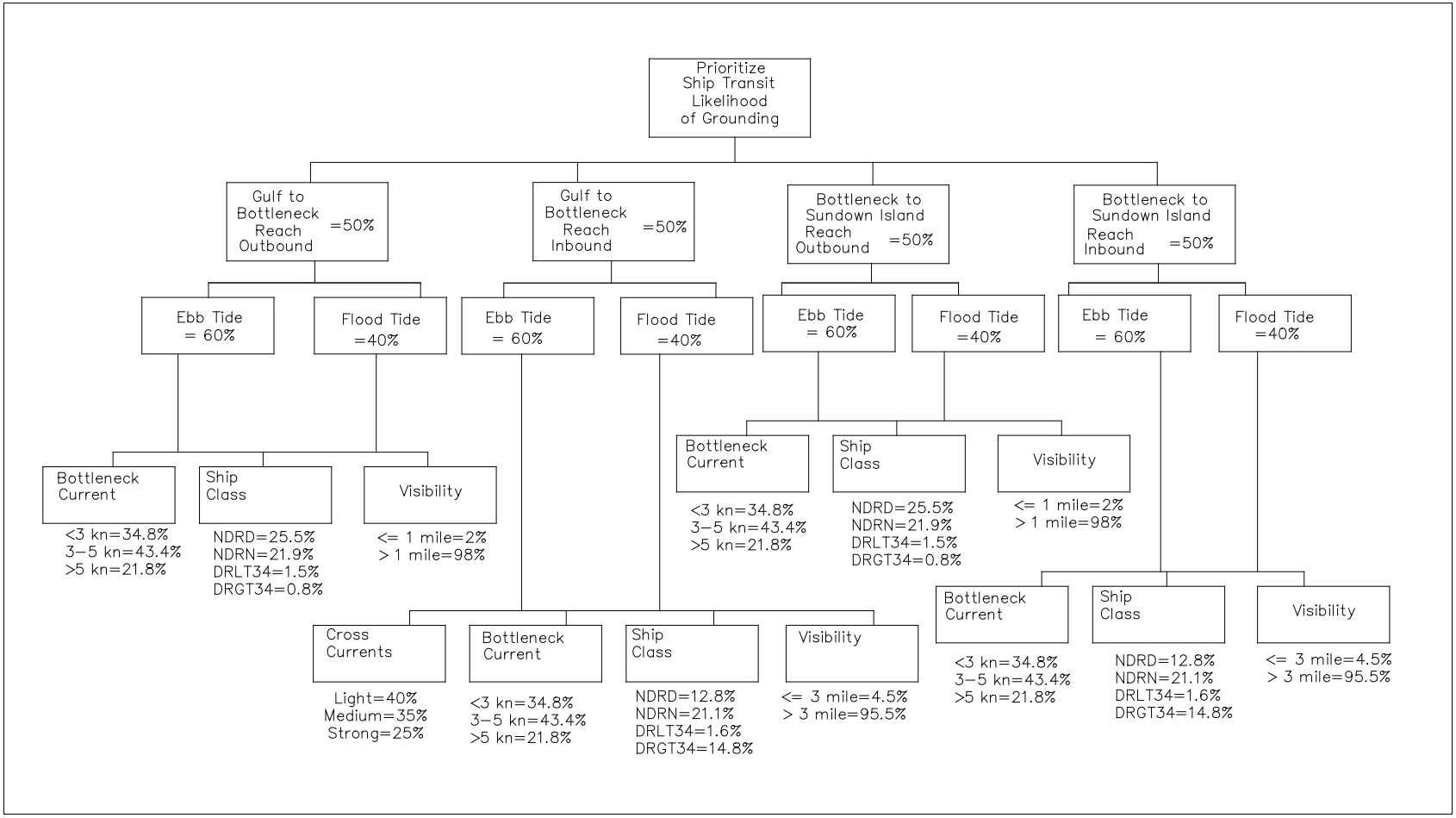

Figure 74. Percent of ships for each attribute.

The first step is to determine how many ship transits occur each day. To model the number of ships per day, a Poisson distribution was evaluated. A Poisson distribution is a discrete distribution that is often applied to systems with a large number of possible events, each of which is rare. It has probability defined by:

$$P_K = \frac{e^{-\lambda}\lambda^K}{K!} \tag{8}$$

where:

K = integer number of ships per day (0, 1, 2, 3,...)
λ = mean value
P_0 = $e^{-\lambda}$

Based on probabilities from Equation 8 and the duration of observed data during August-December 2007 (153 days), the computed number of days having K ships per day based on the Poisson distribution is shown in Table 24 together with the observed number of days having K ships. The Poisson distribution provides a fair approximation of the ships per day. Table 33 shows the number of days during a 365 day year having none to seven ships per day based on an average of two ships per day. The number of ship transits per day was limited to seven because Pilot Larry Robinson said he had only seen eight ship transits in 1 day once in his career. If the program selected a number of ships per day greater than seven, the value was set equal to seven as opposed to sampling again.

Table 33. Distribution of ship transits per day from Poisson distribution for MSC average of two ships per day based on 2001-2007 ship data.

Ship Transits Per Day	Number of Days During 1 year, Poisson Distribution for Mean of Two Ships Per Day
0	49.4
1	98.8
2	98.8
3	65.9
4	32.9
5	13.2
6	4.4
7	1.3

After determining that a Poisson distribution provides a reasonable description of the number of ships per day, the following routine from Rubinstein (1981) was used to randomly sample the Poisson distribution for each day of the year.

```
        C = exp(-1*λ)
        B = C
        K = 0
        rannum = rand(0)
100     if (rannum.le.B) go to 200
        C = C * (λ/(K + 1))
        B = B + C
        K = K + 1
        go to 100
200     continue

        output K
```

The above code outputs the number of ships per day for each day of the simulation period into file named “shipsperday.”

The next step is to determine the ship category for each of the *K* ships arriving during each day. The four ship categories are shown in Table 25. Each category is broken into percentage of inbound and outbound ships. Sampling the fleet according to the percentages shown in the last column of Table 25 was used in the SEM. This sampling provides the ship category and ship direction. The number of inbound or outbound during any single day is limited to four. For example, on a day with seven ship transits, four will be one direction and three will be the other direction. On a day with four ship transits, all four could be in one direction, or three and one, or two and two.

At this point, a “shipcatdir” file is generated with an entry for the Julian day, ship category, and ship direction for each of the *K* ships for each day. A few days are not present in the file because no ships transited on those days. Each entry represents either an inbound or outbound transit of the channel and is not a ship call representing both transits. The random selection was set such that each run of the program resulted in a different combination of ships per day and a different number of total ships during the selected time period.

For each ship represented in the "shipcatdir" file, the next step is to randomly sample a uniform distribution having a mean of -0.14 ft and standard deviation of 0.55 ft to determine the water level difference between the gulf and the bay. If the sampled value is negative, the tide is an ebb tide. Positive values denote flood tide. Through the absolute value of this water level difference, a current velocity in the bottleneck is determined from Equation 5.

The next step is to randomly sample for the strength of the cross current at the jetty entrance based on the pilots' estimate of the percent of light, medium, and strong cross currents at the entrance. A cross current was only entered for ships in the G-B reach for inbound ships.

The next step is to randomly sample for visibility of high or low based on the percentages presented previously. The SEM represented the probabilities of visibility declining during a transit and varied the percentage on a monthly basis.

At this point, ship category, ship direction, tidal current direction, bottleneck velocity magnitude, category of cross current, and category of visibility are known. The next step is to determine the probabilities from the expert elicitation of the pilots.

The relative probability values from Figure 72 are assigned for both the G-B reach and the B-SI reach. The probability for bottleneck current RP(BC) is determined from Equation 6. The relative probability for each reach is determined using Equation 7. For example, consider a NDRD ship that is inbound. The sampled water level difference is 0.293 ft (flood tide because of positive sign) and results in a bottleneck velocity of 3.2 knots. The relative probability of grounding in a 3.2 knot bottleneck current is 0.20. For this example, the cross current is medium and visibility is good. For the G-B reach, the relative probability = $0.20 \times 0.44 \times (0.15 \times 0.20 + 0.16 \times 0.0.09 + 0.41 \times 0.17 + 0.28 \times 0.22) = 0.015$. For the B-SI reach that does not have a cross current effect at the jetty entrance, the relative probability is $0.36 \times 0.31 \times (0.26 \times 0.20 + 0.21 \times 0.09 + 0.53 \times 0.17) = 0.018$. Because the ship must go through both reaches, the total relative probability for this ship is the sum of the G-B and B-SI reaches = 0.015 + 0.018 = 0.033. Table 34 shows a portion of the output file from the simulation.

Table 34. Output from ship event model (output shown is the first part of a 30-year simulation).

Julian	Ship	Direct	Tide	WLdif	Veloc	Vel RP	Cross	Visib	GB RP	BSI RP	Total RP
1.	NDRN	Out	Flood	1.5013	7.2360	0.9582	Light	High	0.044	0.068	0.112
1.	NDRD	In	Flood	0.3517	3.5024	0.2234	Strong	High	0.027	0.019	0.046
2.	DRGT34	In	Ebb	-0.0913	1.7840	0.1143	Light	High	0.020	0.050	0.070
2.	NDRD	Out	Ebb	-0.7310	5.0494	0.4084	Medium	High	0.014	0.026	0.040
2.	DRGT34	In	Flood	0.2375	2.8782	0.1751	Light	High	0.017	0.024	0.041
3.	NDRN	In	Flood	0.4170	3.8136	0.2522	Light	Low	0.041	0.065	0.106
3.	NDRD	In	Ebb	-1.4034	6.9960	0.8726	Medium	High	0.031	0.083	0.114
5.	NDRN	Out	Flood	0.3755	3.6191	0.2338	Strong	High	0.025	0.033	0.058
5.	NDRN	Out	Flood	0.5375	4.3298	0.3085	Medium	High	0.027	0.036	0.063
5.	NDRN	Out	Ebb	-0.4739	4.0657	0.2783	Strong	High	0.015	0.025	0.040
6.	NDRN	In	Ebb	-0.4502	3.9627	0.2673	Strong	High	0.040	0.058	0.097
6.	NDRN	In	Ebb	-0.9149	5.6489	0.5160	Strong	High	0.044	0.074	0.118
7.	NDRD	In	Ebb	-0.3345	3.4154	0.2159	Light	High	0.016	0.041	0.058
8.	DRLT34	In	Ebb	-0.5393	4.3370	0.3093	Strong	High	0.037	0.052	0.089
8.	NDRN	In	Ebb	-0.8329	5.3896	0.4664	Light	Low	0.056	0.158	0.213
8.	NDRN	In	Flood	0.8297	5.3795	0.4645	Medium	High	0.023	0.032	0.054
9.	NDRD	Out	Ebb	-0.0124	0.6586	0.0737	Light	High	0.009	0.014	0.023
9.	DRGT34	In	Ebb	-0.4641	4.0232	0.2737	Light	High	0.023	0.060	0.083
9.	NDRN	Out	Flood	0.1882	2.5621	0.1548	Strong	High	0.023	0.029	0.052
10.	NDRN	In	Ebb	-0.6367	4.7123	0.3581	Light	Low	0.054	0.151	0.205
10.	DRGT34	In	Flood	0.0750	1.6170	0.1071	Medium	High	0.018	0.022	0.040
10.	NDRN	Out	Ebb	-0.5665	4.4449	0.3226	Medium	High	0.015	0.027	0.042
12.	DRGT34	Out	Flood	0.6002	4.5753	0.3395	Medium	High	0.029	0.039	0.068
12.	DRGT34	In	Ebb	-0.4334	3.8877	0.2596	Light	High	0.022	0.059	0.081
13.	NDRD	In	Ebb	-0.5271	4.2875	0.3034	Strong	High	0.036	0.047	0.082
13.	NDRD	Out	Ebb	-0.7045	4.9567	0.3939	Strong	High	0.014	0.026	0.039
14.	NDRN	Out	Ebb	-0.3604	3.5455	0.2272	Medium	High	0.014	0.023	0.037
14.	NDRN	Out	Ebb	-0.0227	0.8899	0.0806	Medium	High	0.012	0.018	0.030
15.	DRGT34	In	Flood	0.2519	2.9641	0.1811	Light	High	0.017	0.024	0.041
15.	NDRD	In	Ebb	-1.0690	6.1061	0.6167	Strong	High	0.041	0.067	0.108
15.	DRGT34	In	Flood	0.3301	3.3929	0.2141	Light	High	0.017	0.025	0.042
15.	NDRN	In	Flood	0.3954	3.7136	0.2426	Strong	High	0.031	0.025	0.056
15.	NDRN	Out	Ebb	-0.1228	2.0692	0.1277	Medium	High	0.012	0.020	0.032
15.	NDRN	Out	Ebb	-0.2121	2.7199	0.1646	Medium	High	0.013	0.021	0.034
17.	NDRD	Out	Ebb	-0.3657	3.5714	0.2295	Strong	High	0.011	0.020	0.031
19.	NDRN	In	Flood	0.1059	1.9218	0.1206	Medium	Low	0.042	0.061	0.103
19.	NDRN	In	Ebb	-0.9777	5.8395	0.5558	Light	High	0.027	0.077	0.103
19.	NDRN	In	Ebb	-0.1430	2.2332	0.1362	Light	High	0.020	0.049	0.069
20.	NDRD	Out	Flood	0.0620	1.4707	0.1012	Light	Low	0.059	0.070	0.129
20.	DRLT34	In	Ebb	-0.4559	3.9875	0.2699	Strong	High	0.037	0.049	0.086
21.	NDRD	Out	Flood	0.5735	4.4723	0.3261	Medium	High	0.023	0.032	0.055
21.	NDRN	In	Ebb	-0.5372	4.3283	0.3083	Medium	High	0.026	0.061	0.087
22.	NDRD	In	Flood	0.5190	4.2544	0.2995	Strong	High	0.028	0.021	0.049
22.	NDRD	Out	Ebb	-0.0695	1.5565	0.1046	Medium	High	0.009	0.015	0.025
22.	NDRD	Out	Ebb	-0.0032	0.3344	0.0649	Strong	High	0.009	0.014	0.023
24.	NDRN	In	Ebb	-0.4064	3.7649	0.2475	Strong	High	0.039	0.057	0.096
25.	NDRN	In	Ebb	-0.9101	5.6338	0.5130	Medium	High	0.030	0.074	0.103
25.	NDRD	Out	Flood	0.0216	0.8680	0.0800	Strong	High	0.016	0.020	0.036
26.	NDRN	In	Ebb	-0.9245	5.6782	0.5219	Strong	Low	0.074	0.161	0.235
27.	DRLT34	Out	Ebb	-1.8363	8.0027	1.2922	Light	High	0.028	0.058	0.087
27.	NDRN	In	Ebb	-0.9286	5.6908	0.5245	Medium	High	0.030	0.075	0.104
27.	NDRD	In	Flood	0.0616	1.4661	0.1010	Strong	High	0.025	0.015	0.040
28.	DRGT34	In	Flood	1.1186	6.2461	0.6513	Light	High	0.023	0.038	0.061
28.	NDRD	Out	Flood	0.3966	3.7190	0.2431	Strong	High	0.021	0.028	0.049
29.	NDRD	Out	Ebb	-0.3897	3.6864	0.2400	Medium	High	0.011	0.020	0.032
29.	NDRN	In	Ebb	-0.6473	4.7512	0.3636	Medium	High	0.027	0.064	0.091
31.	NDRN	Out	Flood	1.1160	6.2388	0.6495	Light	High	0.036	0.053	0.089
31.	NDRN	In	Ebb	-0.5105	4.2196	0.2955	Light	Low	0.053	0.147	0.199

The calculations were run for 30 years to examine a sufficiently long period to reduce sample size effects. During the 30-year simulation period, approximately 21,960 ships transited the channel. The total relative probability from all ships was summed to determine the relative probability of grounding. It must be emphasized that the SEM provides a relative probability value that is more valid to rank risk reduction alternatives

rather than to determine how much risk has been reduced. The existing channel resulted in a total relative probability of 1,330 for the 30 year period based on the average of seven runs. This value has no physical significance and only represents a base condition against which all risk reduction alternatives can be compared. These risk reduction alternatives are presented subsequently.

The SEM was run for the 30 year simulation period using the lowest risk combination of all attributes, as shown in Figure 72. The simulation includes outbound ships, ebb tide, all NDRD ships, with velocity = 0 in the bottleneck, light cross current, and high visibility. The pilots state that these conditions lead to almost zero chance of a powered grounding. The resulting total relative probability was 494 for the 30 year period. This relatively high number for almost no probability of grounding reflects the pilots' reluctance to assign large differences in the pairwise comparisons. Consequently, as risk reduction alternatives are examined subsequently, one must consider that the range of possible relative probabilities is 494 to 1,330 and not 0 to 1,330. For ease of comparison, results from the SEM are normalized to the existing condition equal to one after removing the near-zero probability of grounding value of 494. The normalized relative probability will be computed from (total relative probability - 494)/(total relative probability for existing condition - 494).

Evaluation of risk reduction alternatives using SEM

Non-structural risk reduction techniques

The first non-structural risk-reduction alternative was to restrict all ships to daylight navigation. This alternative was simulated in the SEM by setting the probability of grounding for the nighttime ships (NDRN) equal to the probability of NDRD ships. Nighttime traffic comprises 43 percent of all ships. It is recognized that this approximation does not consider the effects of how this would change operation of the port and only addresses the higher probability of grounding during nighttime navigation. The resulting total relative probability for day only navigation was 1218 compared to 1,330 for existing navigation for the 30-year simulation. Based on normalizing the existing condition to 1.0, daylight navigation only has a normalized value of (1218-494)/(1330-494) = 0.87.

The next non-structural change would be to limit ship transits to times when currents are less than or equals 5 knots. Note that the current being

referenced is the surface centerline currents as considered by the pilots. Currents greater than 5 knots occur about 22 percent of the time. This could be implemented by the installation of a current meter in the bottleneck. The pilots have expressed interest in such a current meter. The resulting total relative probability of grounding is 1,279 for the 30-year simulation that is less effective than all daytime navigation. Based on normalizing the existing condition to 1.0, limiting navigation to times when currents are less than 5 knots has a normalized value of (1279-494)/(1330-494) = 0.94.

Structural risk reduction techniques

Background. The only structural alternatives evaluated were to widen the bottleneck channel to the width of the jetties or partially widen the channel by removing only one side of the bottleneck. Kraus et al. (2006) found that current magnitude was reduced and the horizontal current distribution was more uniform across the width of the channel with the bottleneck removed. Alternative 3 in Kraus et al. (2006) is the alternative considered herein with the SEM and has the bottleneck removed on both sides of the channel, with the bay entrance rounded on both sides of the channel. Without the bottleneck, the current magnitude is 70 percent of the bottleneck currents for ebb tide and 80 percent of bottleneck currents for flood tide, based on results from Kraus et al. (2006) (sta C in Figures 66 and 68 was used in determining these percentages.) The ship simulator was operated by a pilot to evaluate the complete removal of the bottleneck as well as partial removal on each side of the channel. The SEM and ship simulator evaluations of bottleneck removal are discussed next.

SEM Evaluation of Bottleneck Removal. The only way to simulate removal of the bottleneck in the SEM is to reduce the magnitude of the current. This is a simplification of the effects of removing the bottleneck, and it is likely that the effect of removal of the bottleneck is defined by more than a reduction in current magnitude. The increase in width is a significant advantage to navigation of the bottleneck removal that is not captured by only considering a reduction of the current in the SEM. Bottleneck current velocities were reduced by the 70 and 80 percent amounts discussed above. The total relative probability of grounding was 1,181 compared to 1,330 for the existing condition with the bottleneck. Based on normalizing the existing condition to 1.0, removal of the bottleneck has a normalized value of (1181-494)/(1330-494) = 0.82.

Evaluation of bottleneck removal using ship simulations

General. As stated previously, the SEM can only evaluate the effects of reduction of the magnitude of the current in the bottleneck. If the reduction in current in the bottleneck due to the removal of the bottleneck was the only effect on navigation, the need for a ship simulator study would be significantly decreased. However, two other effects are present that result from the fact that the discharge through the entrance will increase once the bottleneck is removed and may adversely affect navigation. Based on Alternative 3 (removal of the bottleneck to the width of the jetties and rounding the bay entrance) in Kraus et al. (2006) using their Tables 21 and 22, mean that discharge will increase by 11-16 percent on ebb tide and 21-25 percent on flood tide.

The first of the two potential adverse effects is in the jettied portion of the channel. For an ebb tide, the increase in discharge is offset by channel scour and velocity is not largely affected by removal of the bottleneck. For a flood tide, velocity in the jettied portion of the channel increases 11-14 percent, assuming the channel undergoes scour, and increases 17-28 percent, assuming no scour of the channel between the jetties. It is likely that removal of the bottleneck will make the increase in flood tide velocity less significant because the pilot has greater distance in the 2,000-ft-wide channel to realign the ship compared to the existing condition.

The second factor that could be adverse to navigation as a result of increased discharge accompanying removal of the bottleneck is the reach just north of the peninsula where the pilots reported a significant cross current in the existing channel (and also state that the cross current is becoming stronger or worse). Although there are some problems with a cross current on flood tide, the primary cross current problem occurs on inbound ships facing an ebb tide. This area also has a course change and significant depth and width changes. Based on expert elicitation of the pilots, this reach for an inbound ship and an ebb tide has the highest likelihood of grounding compared to all other reach, ship direction and tide direction combinations. One of the three pilots felt the flood tide in this reach for an inbound ship was the most problematic. Although some scour may occur and reduce the effects of increased discharge, it is likely that the increased discharge through the inlet will result in increased cross current magnitude in the reach just north of the peninsula. This increase in cross current with the proposed risk-reduction alternative of bottleneck

removal must be evaluated to make certain one problem is not being traded for another. The decision was made at the beginning of this study to make this evaluation with a ship simulator.

Currents were run using the 2D depth-averaged velocity version of the CMS to develop the velocity field for input to the ship simulator. The ship simulator is normally run with a 2D depth-averaged velocity. Pilot David Adrian came in November 2008 to operate the ship simulator. He ran only the existing condition. For an inbound ship on an ebb tide, Pilot Adrian felt that the ship simulator was realistic at the gulf entrance and in the bottleneck. Once the inbound ship arrived just north of the peninsula, he stated that the cross current action on the ship was not present or certainly not strong enough at this location.

Our first concern was that the bathymetry was not correct in this area. The pilot's boat was out and the crew was asked by Pilot Adrian to check the depth at several locations and provide the GPS coordinates of each location. At least one of these areas showed the depth to be considerably greater than that represented in the CMS numerical model. This was consistent with the pilots' stating that this area was experiencing more flow in recent years. Computed velocity vectors were plotted in this area, and Pilot Adrian examined the velocities, concluding that the angle of the current was not what they were experiencing in the ship channel. The recommendation was made that the Galveston District should obtain new bathymetry in this area. A 2-mile-wide by 2-mile-long rectangle was mapped where data was needed. The rectangle extended 2 miles northeast of the ship channel and covered 2 miles northwest of the peninsula. The northwest limit was just above the old GIWW. These data were received from the Galveston District in the middle of January 2009, and the new CMS simulations were completed toward the end of January. Although the new bathymetry data had some significant changes from the previous data, the newly calculated depth-averaged current was not significantly different from the original current.

The ERDC study team re-examined aerial images of this area. Figure 75 is one of the images, taken on 26 September 2002, and shows a trend in horizontal surface current that is consistent with the observations of the pilots and is not consistent with the calculated depth-averaged current.

Figure 75. Surface currents on north side of peninsula from 26 September 2002 image.

Based on the shadows in the picture, it was taken during the morning when there was a moderate ebb tide. Figure 76 is another image showing surface current trends consistent with the pilots' experience. It was taken on 7 August 2003, and the absence of shadows suggests that the photo was taken sometime during the middle of the day, during which there was a significant ebb tide.

Figure 76. Aerial taken on 7 August 2003 showing cross currents.

The study team proceeded with calculations of the current 3D mode of the CMS. Figure 77 shows a schematic of 2D velocities versus 3D velocities. The 2D velocities do not represent the stronger velocities acting on the side of the ship. ERDC concluded that the 2D current simulations cannot address the complex environment that exists in the MSC on the north side of the peninsula for the purposes of ship simulation. Therefore, a complete 3D numerical current simulation of the study area was conducted.

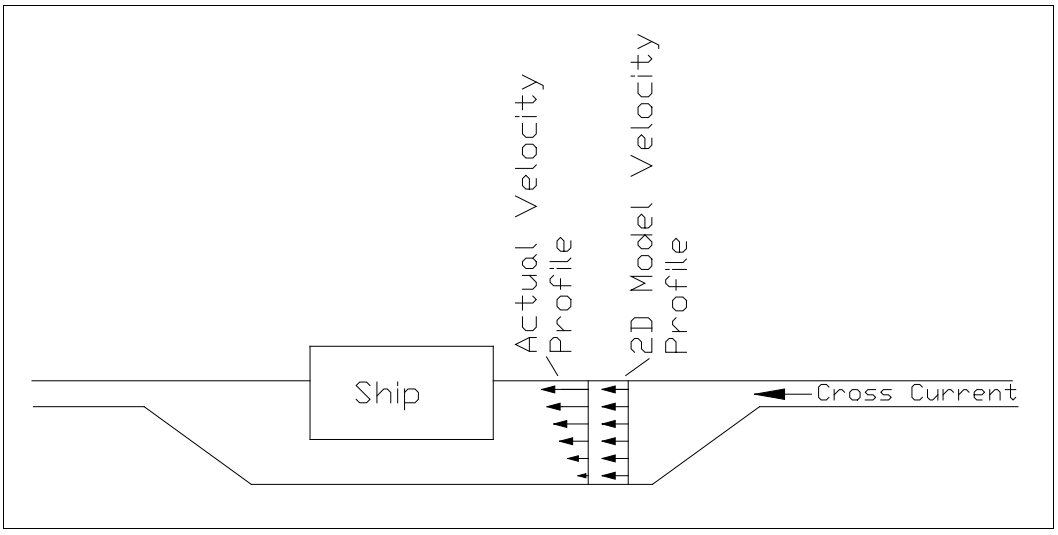

Figure 77. Schematic of 2D and 3D velocities in channel cross section with cross current.

3D current modeling

The CMS-Flow 3D is an extension to the vertical in the water column of the CMS 2D calculation. It solves the horizontal and vertical components of motion based on a numerical solution to the Reynolds-Averaged Navier-Stokes equations (RANS) with the shallow-water assumption (i.e., hydrostatic pressure) and the Boussinesq approximation. Both non-cohesive and cohesive sediment transport can be represented. The model can be driven by a larger-domain circulation model through the boundary input specification for the water-surface elevation or a combination of water-surface elevation and velocity.

The circulation and transport components of the model are expressed in a finite-volume numerical representation of the continuity and momentum equations for water, and transport equations for salinity, and sediment concentration. It contains an integrated representation of sediment transport and morphology change through transport rate formulations, the advection-diffusion equation, and the sediment continuity equation for updating change in the bathymetry. Bottom or morphology change is simulated by means of the Exner equation expressing conservation of sediment volume. Coupling between the hydrodynamics and sediment transport occurs in the suppression of turbulence generation by vertical density gradients due to suspended sediment gradients.

The governing equations are solved numerically by means of a semi-implicit time-marching method with explicit differencing in the horizontal

plane and implicit differencing in the vertical direction. A combination of finite-volume and finite-difference approximations is used to represent the spatial gradients. Discretization of the model domain is accomplished by a combination of a rectilinear grid in plan view and a sigma grid in the vertical. Special differencing methods for the pressure and diffusion terms are applied to reduce the truncation error and dissipation that have been shown to be problematic in sigma-grid approaches (Stelling and van Kester 1994; Slordal 1997).

The model presently supports two options for setting the lateral and vertical mixing coefficients. The first option consists of prescribed spatially and temporally constant values consisting of one value for the horizontal direction and an independent value for the vertical direction. The second option is based on the solution to a one and one-half equation turbulence closure scheme based on a differential equation for the turbulent kinetic energy and an algebraic description of the turbulent length scale for the vertical mixing.

In the applications to the MSC entrance, spatially constant vertical and lateral mixing coefficients were specified. The vertical mixing was set to 0.0001 m^3/sec, which is in the lower end of vertical mixing coefficient range of values typically used in 3D modeling. For lateral mixing, the value of 2 m^3/sec was specified. This value is representative of the lateral length scales associated with an inlet. These values were determined by a qualitative model calibration. They were systematically increased and decreased until a maximum cross-channel flow occurred in the simulation.

Figure 78 is a plot of the 3D velocities at a point in the center of the navigation channel and just north of the peninsula for the existing channel.

Standard ERDC practice in numerical modeling is to validate the numerical model derived currents using observed data to show that the model is capable of addressing the problem. The 3D numerical circulation model used herein to generate currents for the ship simulator study was not validated with observed MSC data. The numerical model currents were only compared to current patterns indicated by MSC aerial images and to observations of the ship pilot while piloting the ship simulator.

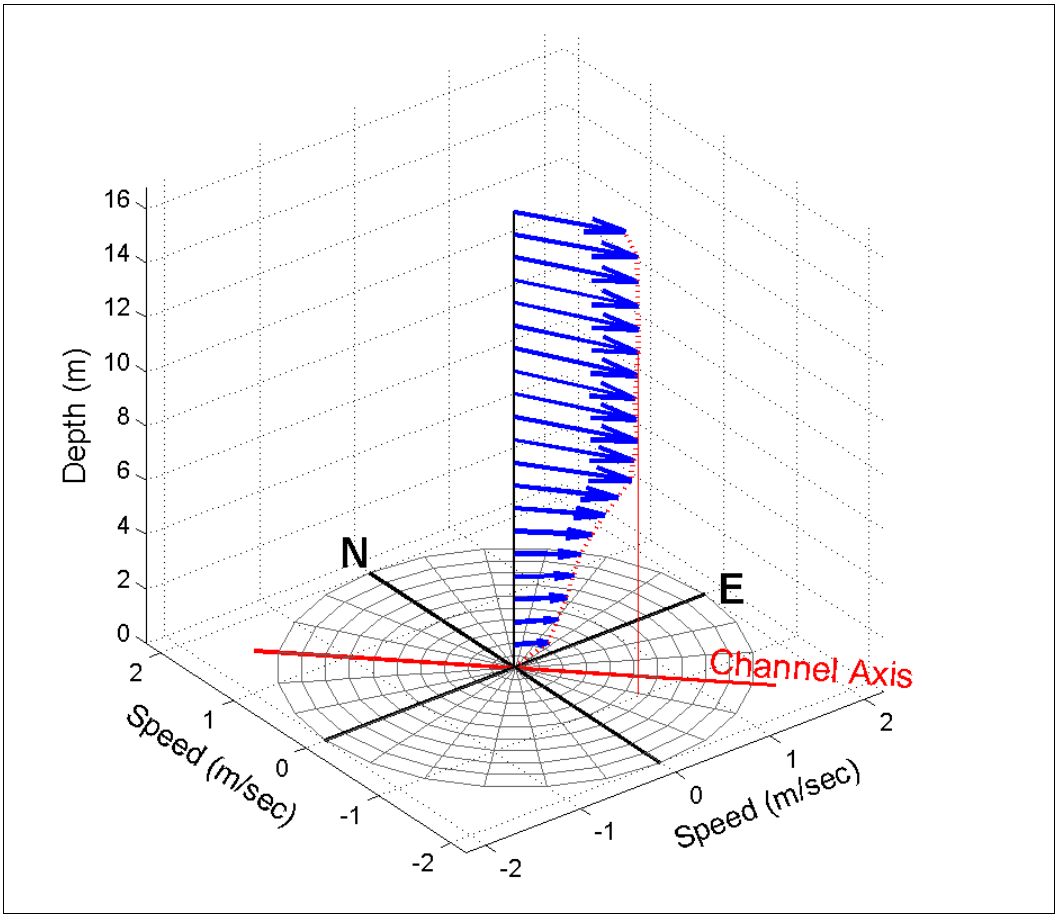

Figure 78. Output of 3D velocities from CMS for existing channel.

Conversion of 3D current to 2D current used in ship simulation

The 3D currents were calculated in 10 layers over the total depth at all locations in the computational grid. Each layer had a thickness of one-tenth of the total depth. The current was calculated without the presence of a ship. The currents that have the greatest effect on the ship are those in the layers above the keel of the ship. The drafts of the ships used in the simulator study were 34 ft. The 3D currents were averaged over all layers in the upper 32.8 ft (10 m) of the depth to determine the effective current to specify in the simulator. If the depth was less than 32.8 ft, all 10 layers were used to determine the average.

Results of ship simulation

The ERDC Ship/Tow Simulator was used to assess whether or not the partial or complete removal of the bottleneck at the MSC entrance would have any navigational effects upon the handling of vessels transiting the entrance channel. The Matagorda Bay Pilots Association participated in

the assessment. Pilot Joe Bokorney ran the ship simulator on 20-21 April 2009. Time constraints allowed only one pilot representative to participate in the tests. The pilot made comments about each run and a final write-up was completed.

Three ships were made available at the beginning of the tests for possible inclusion in the study. After initial practice runs with the pilot, only one ship was found to be typical of those that transit Matagorda Bay, a tanker with dimensions of length between perpendiculars = 584 ft, beam = 86 ft, and draft = 36 ft. Once the vessel was decided upon by the pilot and ERDC personnel, all tests were conducted with the tanker.

The pilot completed the scenarios shown in Table 35 in random order.

Table 35. Test matrix for Matagorda Bay.

Run Number	Ship	Condition
1	Tanker	Existing Ebb
2	Tanker	Existing Flood
3	Tanker	North Bottleneck Removed Ebb
4	Tanker	North Bottleneck Removed Flood
5	Tanker	South Bottleneck Removed Ebb
6	Tanker	South Bottleneck Removed Flood
7	Tanker	Bottleneck Removed Ebb
8	Tanker	Bottleneck Removed Flood

These tests are shown in Figures 79-86 as trackplots (processed from vessel transit data recorded by the simulator during testing) and pilot comments (written by the pilot after each run). The trackplots are a static representation of the position, heading, and indirectly (by the spacing of the icons from the regular time interval used) the relative speed of the vessel during the run. It can be noted from the trackplots that the tanker encroached the limits of the Federally defined channel, usually in the area just southeast of Sundown Island. The ship encroachment is not indicative of grounding, but reveals one of the sites where naturally deep water expands the area that pilots can utilize during their transit.

Figures 79 and 80 have the existing bay geometry with ebb and flood tide current magnitudes and direction respectively. Comments by the pilot about “13 and 14” on Figures 79-86 are in reference to the red and green

navigational aids on the bay side of Matagorda Peninsula. Although the pilot indicated that the cross current magnitudes were "slightly off," the overall feel was typical of current in the bay.

Figures 81 and 82 show runs with the northern side of the bottleneck removed. The comments made by the pilot state that the northern bottleneck removal was the "worst yet." In the words of the pilot, the partial bottleneck removal scenarios, Runs 3–6 shown in Table 35, all had "strange" and "unpredictable" current patterns that had adverse effects on handling the ship.

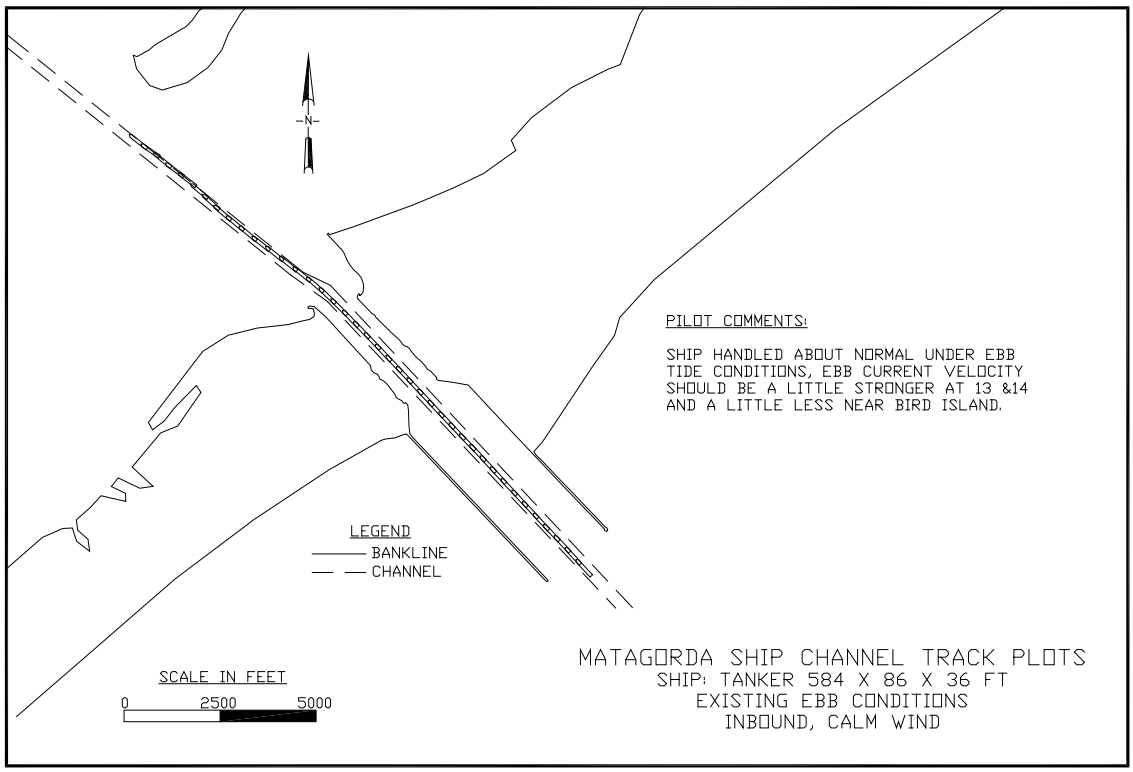

Figure 79. Run Number 1, existing ebb condition.

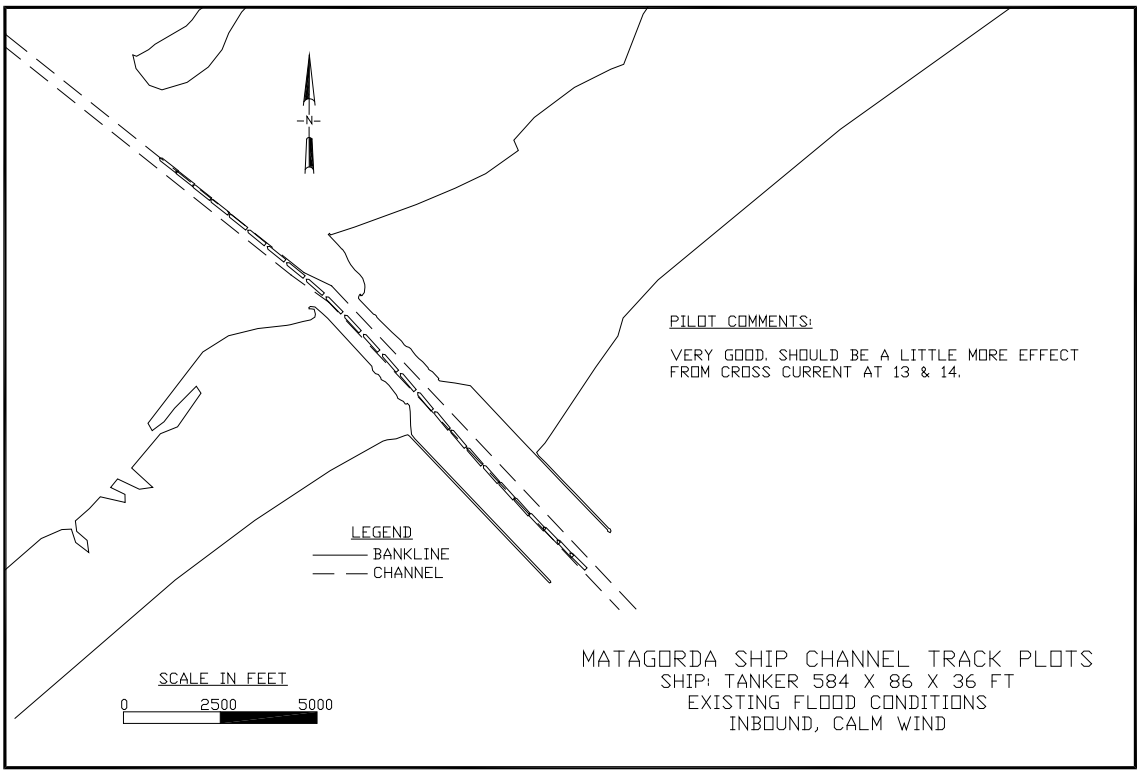

Figure 80. Run Number 2, existing flood condition.

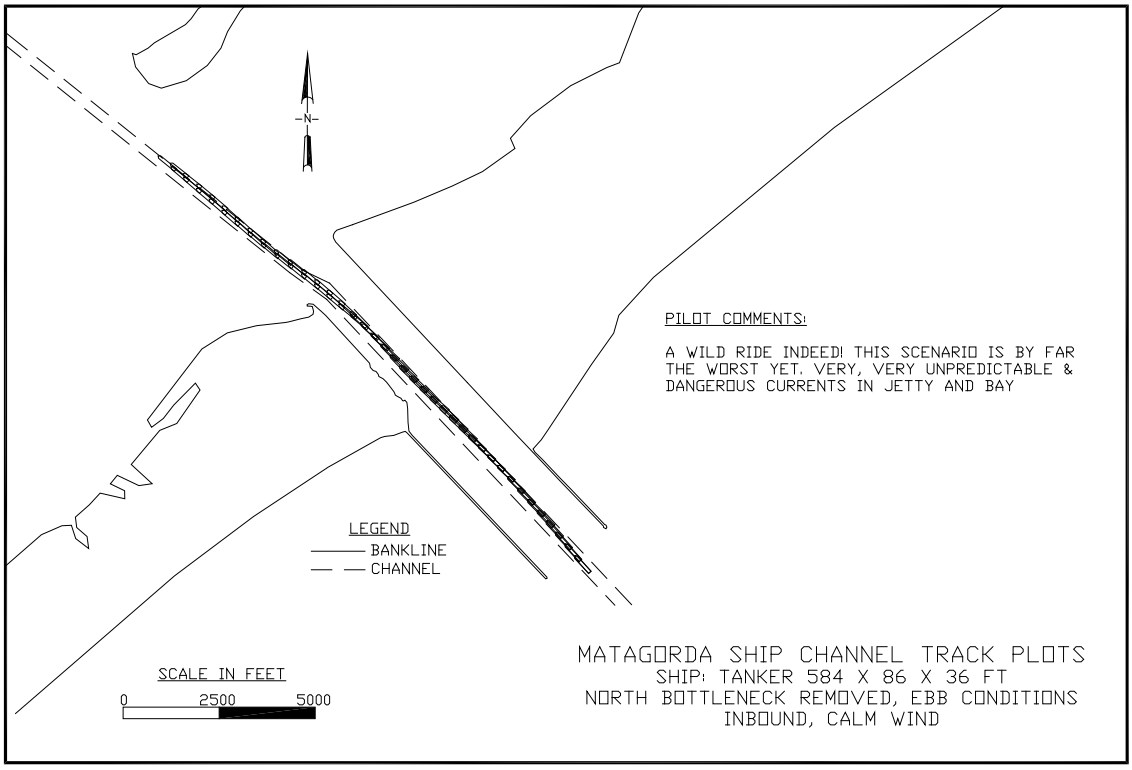

Figure 81. Run Number 3, north bottleneck removed condition, ebb tide.

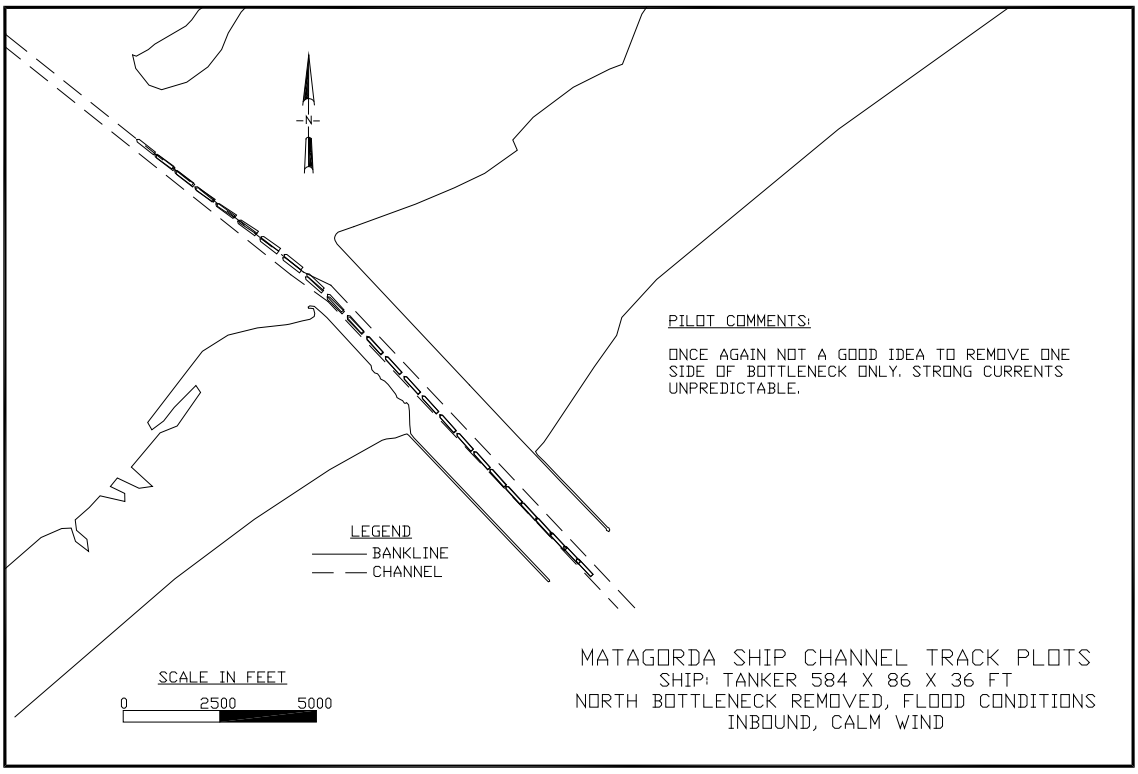

Figure 82. Run Number 4, north bottleneck removed condition, flood tide.

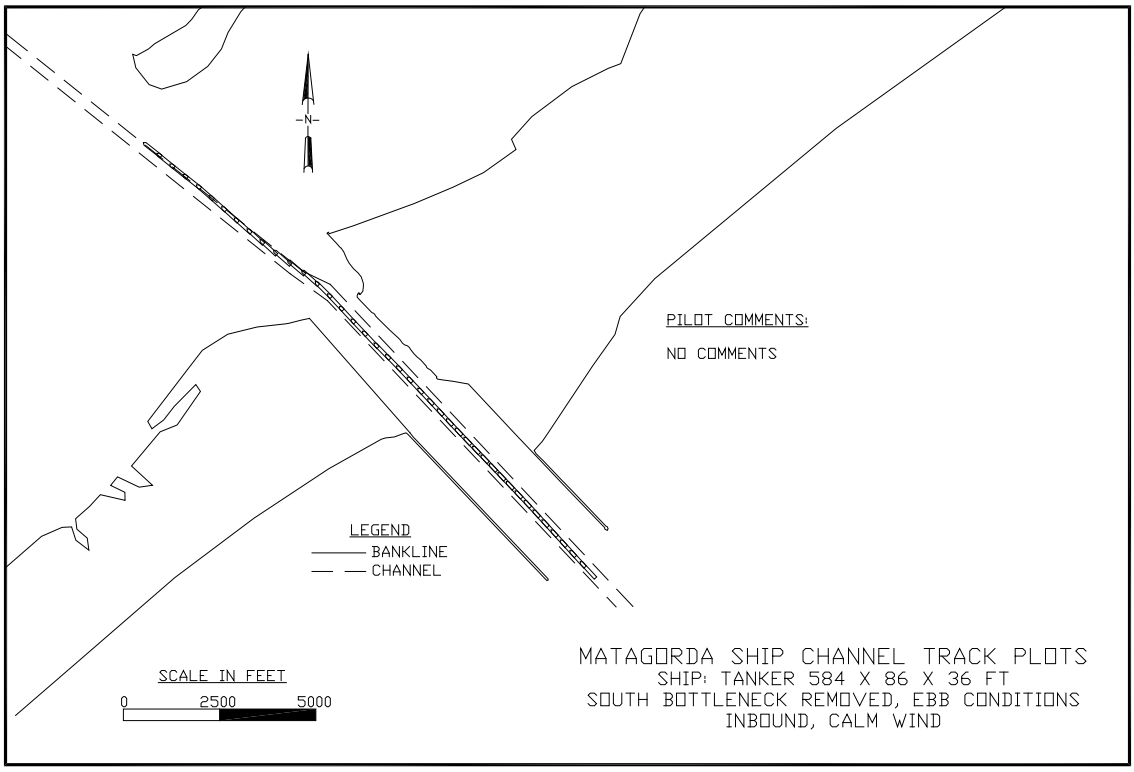

Figure 83. Run Number 5, south bottleneck removed condition, ebb tide.

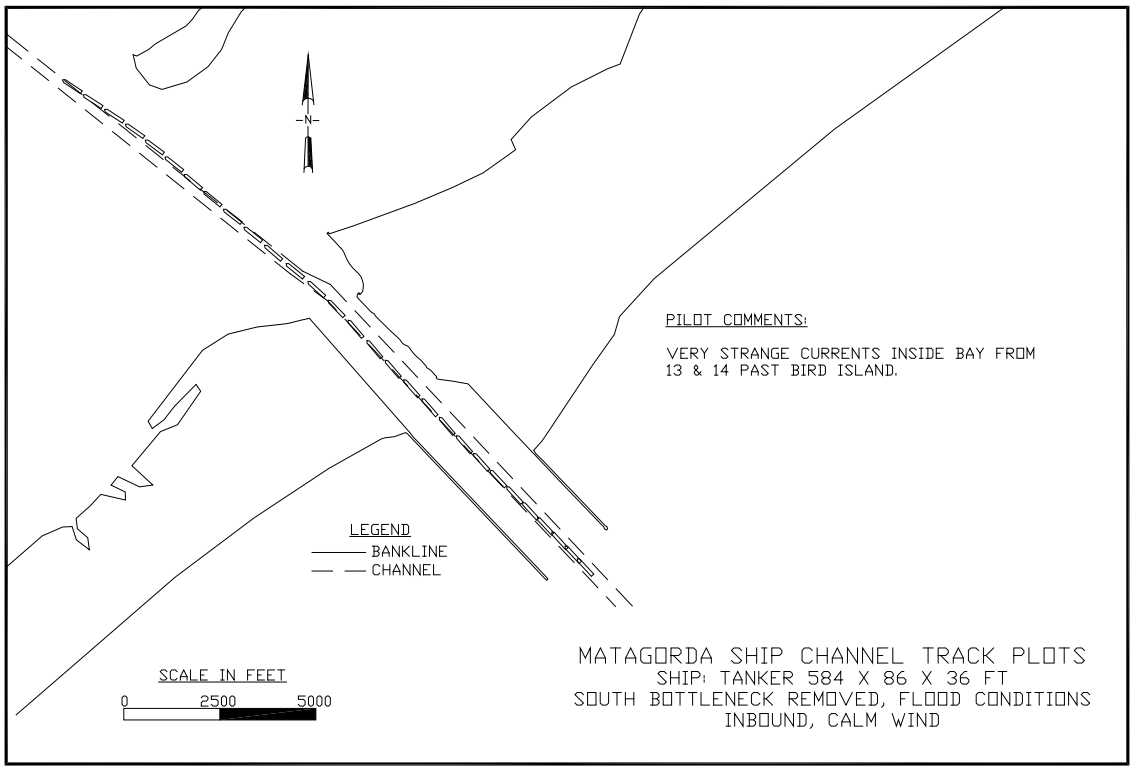

Figure 84. Run Number 6, south bottleneck removed condition, flood tide.

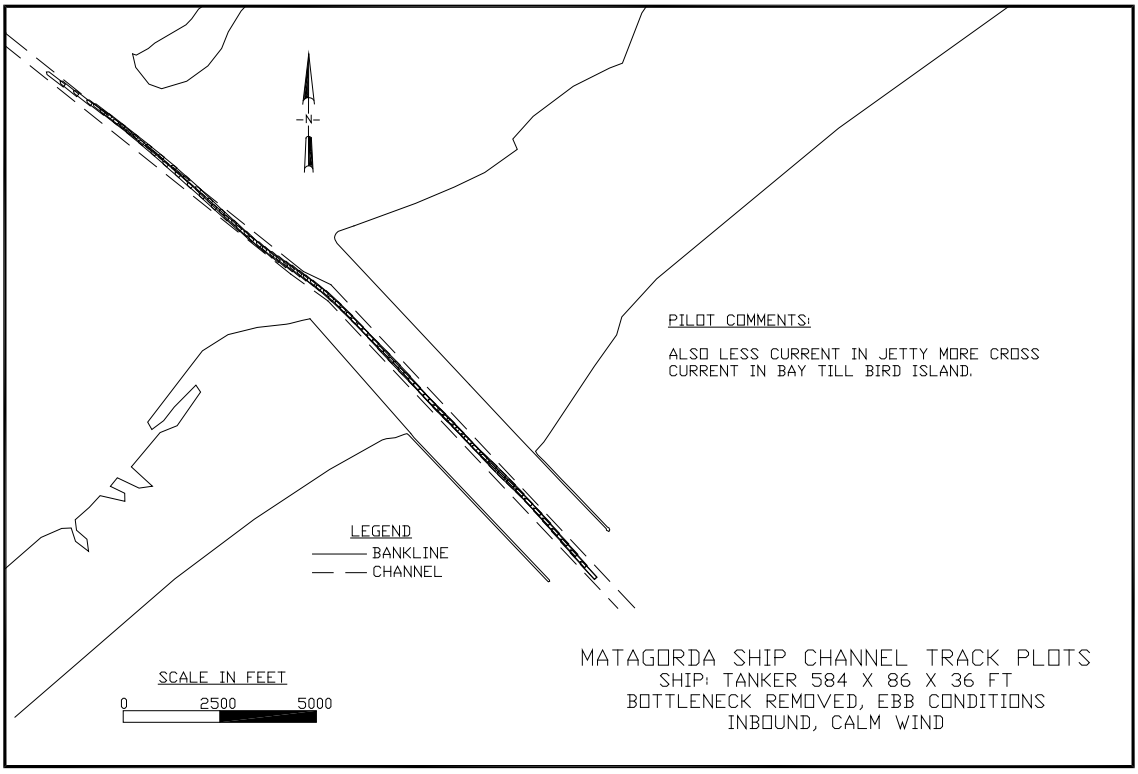

Figure 85. Run Number 7, bottleneck removed condition, ebb tide.

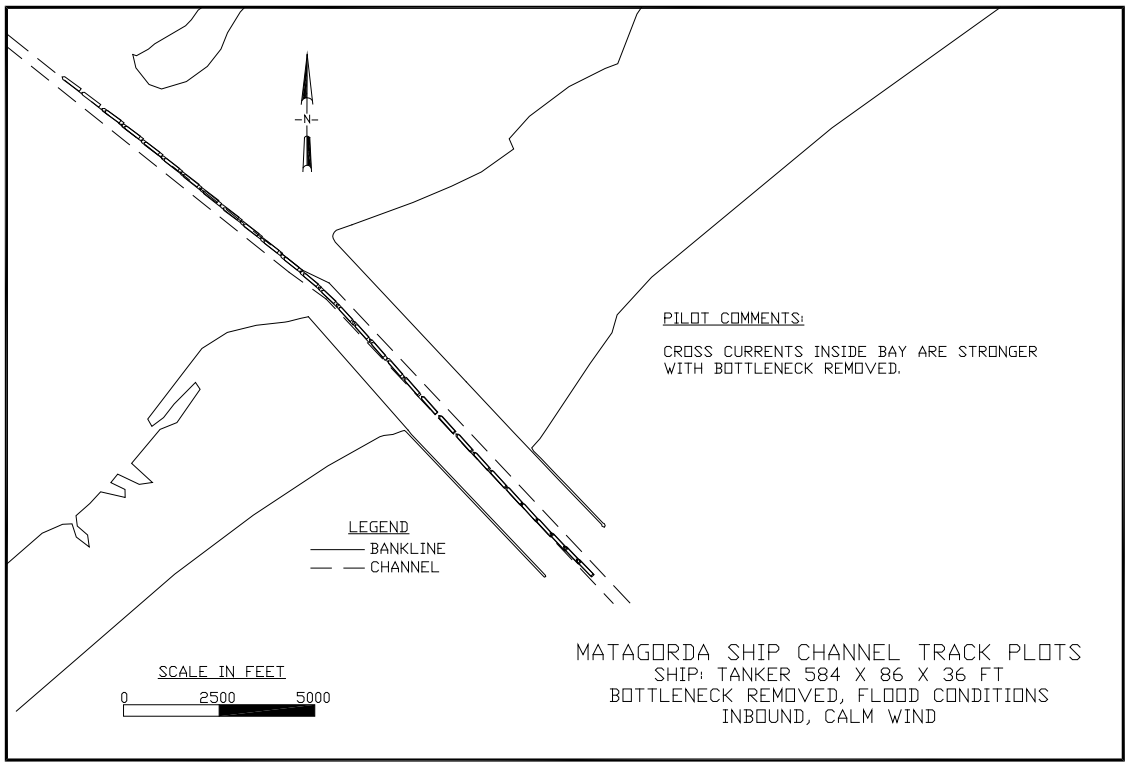

Figure 86. Run Number 8, bottleneck removed condition, flood tide.

The cross current in the area of Sundown Island increased with the full removal of the bottleneck, Figures 85 and 86; however, the longitudinal current in the bottleneck and jetties decreased. The reduction of the current in the jetties lessened the impact of the cross current upon the handling of the vessel during the entrance to the bay. The effect of increasing the cross current in the bay by the removal of the bottleneck did not make the passage at Sundown Island impractical for the pilot. The pilot's closing comments to sum up the simulations are shown in the following paragraph.

Pilot Statement: "The magnitude of the currents in and around the Matagorda Bay ship channel jetties have been increasing each year." The PIANC scale of horizontal currents only goes to 3 knots. It is common to encounter 3 to 5 knot currents in the MSC jetties; current velocity magnitude in excess of 7 knots has been calculated and observed. Studies indicate that removing the bottleneck will reduce the velocity of the longitudinal current. Ship traffic is presently being affected on occasion in the MSC due to a strong current, creating safety concerns.

"Several scenarios were run on the simulator. Removing the bottleneck decreased the current between the jetties. The vessel was easy to control

using small amounts of rudder. Removing the bottleneck did increase the cross current inside the bay from buoys 13 and 14 to Sundown Island. As a pilot, I would prefer to have less current in the jetty and bottleneck where it is now deep enough across the entire width of the channel for a ship to make contact with the rock jetty. The simulator did not change the ship channel dimensions in the bay with the removal of the bottleneck. It should be assumed that the channel would be wider from buoys 13 and 14 to Sundown Island, which would make it easier to navigate the increased cross current.

The worst-case scenario was to remove only one side of the bottleneck. This created extremely unpredictable currents in the bottleneck and an extreme cross current in the bay. A strong current was encountered for the south bottleneck, pushing the vessel to the south side as the current wrapped around the existing bottleneck on the north side. The vessel was difficult to steer and requiring extreme rudder. This must be taken into account during construction of new jetty project.

In conclusion, my opinion as a pilot is to eliminate the bottleneck in the MSC jetties, thus reducing the magnitude of the current. This would reduce delays and increase the safety of vessels transiting the channel."

Bathymetric change near Sundown Island and effects of Sundown Island on navigation

A comparison was made of bathymetry measured in 2004 and 2009 in the bay on the northeast side of the ship channel. The difference between the two surveys in Figure 87 shows that the area has increased in depth. This increase in depth is consistent with the pilots' statements that cross flow in this area has increased. Should the trend of increasing depth and increasing cross current continue, navigation in the existing channel of the MSC will become more hazardous. This could happen in conjunction with the bottleneck currents that presently are at their peak value with only a slow rate of decline expected in the future.

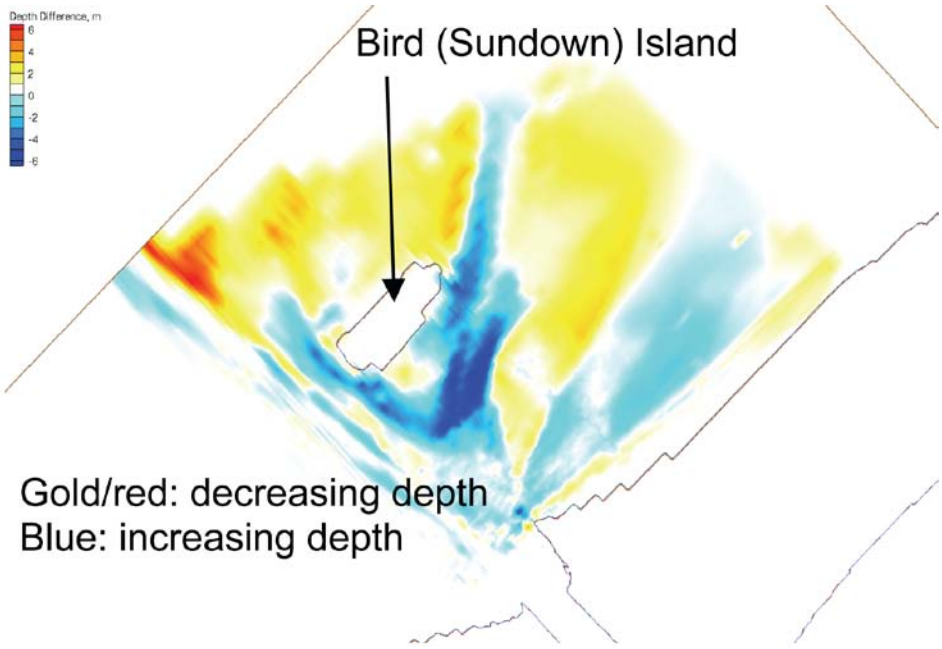

Figure 87. Change in depth in bay near Sundown Island.

As stated previously, Sundown Island causes a variable current pattern where one part of the ship is exposed to cross currents and the other part of the ship is in the lee of the island and is not subjected to cross currents. The varying lateral forces on the ship create difficulty for navigation. Relocation of Sundown Island to a location away from the inlet would eliminate the variable current and likely reduce the magnitude of cross currents.

5 Summary and Recommendations

Three factors were identified and evaluated that pose a potentially great risk of disrupting deep-draft navigation in the MSC entrance. A summary and recommendations are provided for each of the three factors.

Flanking of jetties and slope protection

Flanking of the jetties and slope protection from overwash from hurricanes, high tide, or strong wind conditions pose a risk to the entrance and navigation. The flanking at the MSC Gulf entrance jetties and adjacent beaches during tropical storms and the consequences to the post-storm navigation were simulated by the CMS for a 50-year return period hurricane. Based on the EST and extreme value analysis, three incident wave heights of 7.5, 8.1, and 9.3 m from the south, east, and southeast directions, respectively, were determined as input to drive the CMS in the local navigation channel and nearshore grid. The numerical simulation was conducted for a 12-hr storm surge during which the water level increased from 0 to 3.5 m (MSL) in the first 4 hr and remained at the peak level of 3.5 m for 4 hr before receding gradually to 0 m in the last 4 hr of the simulation.

The bathymetry calculated at the end of a storm surge simulation served as the initial condition in the post-storm simulation. Post-storm simulations include a north jetty breach, a south jetty breach, and both a north and a south jetty breach for two different weather conditions, one in a winter weather month and the other in a summer weather month that covered one complete spring tidal cycle. The calculated morphology change and the current magnitude from the post-storm simulations were compared for the navigation channel conditions. The following results were obtained:

1. The EST and extreme value analysis, based upon the historical data, shows that the 50-year return period hurricane at the MSC corresponds to a 3.5-m storm surge (Category 3) and a maximum wind speed of 151 mph (Category 4). The corresponding significant wave height and direction generated offshore MSC are 12.9 m and 13.8 sec. The hurricane wind field has a shoreward component of 61 mph that is effective at dissipating energy (through white-capping) in the wave propagation from deep water

to the MSC. The calculated significant heights for input to the CMS in the local grid seaward boundary at the 20-m depth contour are 7.5, 8.1, and 9.3 m from the south, east, and southeast directions, respectively.

2. The CMS shows channel bank erosion and overwash on the beaches and shores adjacent to the jetties as a result of inundation from the higher water level and breaching at the landward end of the jetties during the Category 3 storm surge. For hurricane waves from the south, a 150-m-wide and 3.5-m-deep breach occurred at the landward end of the south jetty. For storm waves from the east, a 110-m-wide and 2.5-m-deep breach occurred at the north jetty. Sediment (mainly sand) can enter the MSC through the breach under combined storm wave and current action. Because of the strong current in the navigation channel, the sediment that enters the MSC through the breach tends to either deposit near the breach or be deposited in the bayside and the gulf entrance channel areas.
3. Post-storm simulations show only local and minor sediment erosion and accumulation at the south jetty or north jetty breach area. Because the flow rate through the jetty breach is minor as compared to the discharge in the MSC, the influence of a jetty breach to the flow current magnitude in the navigation channel is not of significance to deep-draft navigation.

Scour leading to slope failures

Another factor that poses a risk to navigation is the on-going bottom scour in the bottleneck and adjacent to the jetty spur sections, together with steep side slopes that increase the potential for slope failure. The side slopes of the bottleneck are armored with riprap of sufficient size, and the channel has not experienced significant widening. The channel bottom of the bottleneck is scouring and will continue to do so. Historical data show that the channel bottom is degrading at about 1 ft/year. Scour in the near future will continue at this rate because current velocity through the inlet is near its maximum velocity and will remain close to the maximum for many years.

The general site stratigraphy consists of barrier island sands overlying a series of point bar deposits of the Beaumont Formation. Characteristics of the barrier island sands were similar for all borings. The barrier island sands extend to a depth of between 60 and 70 ft. These sands are primarily clean with less than 10 percent passing through the #200 sieve in most cases. Clay lenses less than 10 ft thick are located about mid-depth in the barrier island. The Beaumont Formation is predominately clays that are mostly CH below a depth of 140 ft.

Most existing channel slopes have a factor of safety slightly greater than 1.0. A factor of safety equal to 1.0 implies that a slope is near instability. The factor of safety for most channel slopes will decrease to values less than 1.0 as the channel increases in depth. Slope failures that may generate large earth movements are judged to be unlikely. Site observations indicate that the width of a slope failure is about 3 to 4 times the horizontal distance the top of the failure surface is from the head of the slope. The analyses show that the critical failure surfaces extend approximately 25 ft into the slope.

The slope of the bottleneck bank ranges in value from about 28 to 37 deg. Also, the friction angle of the sand is estimated to range between 32 and 39 deg. The equality of the bank slope and the friction angle indicates that the friction angle for sand tends to control the angle of the bank slope. The periodic sloughing of the slope material maintains the slope of the channel face at or slightly below the angle of repose. The analyses show the drained strength is more critical than the undrained because drained conditions give a lower factor of safety.

The analyses show that if the most likely values of the factor of safety (F_{MLV}) is much greater than 1.0 (e.g., F_{MLV} for boring B-1 = 1.33) the probability of failure is less than 1 percent. Conversely, if the factor of safety is near unity (e.g., F_{MLV} for boring B-3 = 1.04) then the probability of failure is much higher, ranging from 33 to 93 percent. The probability of failure for each of the critical sections increases with depth, which is consistent with field evidence. Therefore, this study concludes that the frequency of slope failure should increase as the channel deepens.

Slope failures that may generate large earth movements are judged to be unlikely. However, analyses show a slide from slope instability could result in a slide block protruding out from the existing side slope with an estimated volume of approximately 720 to 7,400 yd^3.

The existing channel has a bulge on the south bankline having a volume of about 16,700 yd^3. Based on both velocity patterns as calculated from the CMS and the absence of comments from the pilots about adverse currents, this bulge does not cause an adverse current. The calculated slope failure volumes are all less than half the volume of the existing bulge and should not cause an adverse current. In addition, none of the calculated heights of

the failed slope material, when subtracted from the depth, result in channel depths that approach the draft of commercial ships.

Another concern about slope failures is the potential for the channel to rapidly scour the bankline after a slope failure leaves the bank unprotected. The best information about this potential problem is the existing channel. Past slope failures and loss of riprap on the upper bank because of channel bottom scour have left the bank exposed to high currents. Although some bank recession has occurred, the bankline has not receded rapidly, and the stability of the bottleneck is not threatened. Should a slope failure occur at the ends of the bottleneck protection, unraveling from the end will likely occur, but should not lead to rapid loss of the bottleneck.

Adverse current

The port and pilots have expressed serious concern about the strong and asymmetric current on the bay side of the peninsula and in the bottleneck. Since construction of the inlet in 1963, current velocity through the inlet has increased as the inlet has enlarged. Based on the bay volume and configuration, tide range, and the cross sectional area of the MSC entrance channel, the velocity through the present inlet is at or near maximum velocity for this inlet. Future scour will result in a slight decrease in the current velocity through the entrance. At the rate of scour of 1 ft/year in the existing channel, a 5 percent reduction in current velocity will require about 25 years based on inlet stability analysis. Consequently, no improvement in adverse currents in the existing channel can be expected in the near future.

The strong longitudinal current in the MSC bottleneck is at or near the top of the list for approach channels for deep draft navigation. While cross current at the gulf and bay sides of the MSC is not extreme, the strong longitudinal current makes it difficult to overcome the effects of the MSC cross current. The USCG (2001) conducted a Port and Waterway Safety Assessment, evaluated more than 28 ports in the United States, and ranked the ports for various characteristics including “tide and river currents” and “waterway complexity.” Port Lavaca, connected to the Gulf of Mexico by the MSC, was rated first in waterway complexity and third in tide and river currents. The two ports rated higher than Port Lavaca for tide and river currents had either strong cross current from tides or strong longitudinal current during river flooding only whereas the MSC has

strong longitudinal current with cross current on a frequent basis. Ship channel design guidance by PIANC classifies longitudinal currents of greater than 3 knots as “Strong” and does not have a higher class. Spanish ship channel guidance from *Recommendation for Maritime Works* shows 4 knots to be a recommended upper limit. The USACE (2006) provides channel width design guidance for deep draft navigation as a function of three categories of maximum current. The maximum category in the USACE guidance is 1.5 to 3 knots. The longitudinal current in the bottleneck of the MSC entrance exceeds 3 knots more than 60 percent of the time and exceeds 5 knots more than 20 percent of the time.

Data could not be found on the probability of a powered grounding in the MSC entrance. An evaluation of the literature showed that other navigation channels having difficult navigation conditions have a powered grounding rate of about 0.0007 per ship transit but this value does not account for the specific conditions at the MSC, particularly the strong longitudinal current.

Navigation in the MSC entrance was classified into two reaches, two ship directions, two tide directions, visibility (as poor or good), four ship classes, three levels of cross currents at the jetties, and varying bottleneck current magnitudes. Probability of occurrence distributions were developed for each of these variables based on observed data and input from the ports and pilots. Expert elicitation of three of the four MSC pilots was used to determine the relative likelihood of a powered grounding for the various combinations of reach, ship direction, tide direction, etc. A Ship Event Model (SEM) was developed that incorporated the probability of occurrence distributions along with the relative grounding probability from the expert elicitation of the pilots. Because of the lack of powered grounding data at the MSC entrance, the SEM could only function as a relative comparison of various risk reduction alternatives. Two non-structural and one structural risk reduction alternatives were evaluated and compared to the existing condition. The first non-structural alternative was that of eliminating nighttime navigation for all ships and resulted in reduced probability of grounding compared to the existing day and night navigation. The SEM did not quantify delays and resulting costs associated with restricting navigation to daytime only.

The second non-structural risk reduction alternative was that of having ships wait until the bottleneck longitudinal current was less than 5 knots.

The probability of grounding was reduced, but not as much as for eliminating nighttime navigation. The one structural risk reduction evaluated with the SEM was the removal of the bottleneck to the same width and alignment as the jetties and rounding of the bay side entrance on each side of the channel. Based on results compiled by Kraus et al. (2006), removal of the bottleneck reduced the ebb tide longitudinal current to 70 percent of existing velocity and the flood tide current to 80 percent of existing velocity. These current reductions were the only way to simulate bottleneck removal in the SEM. The probability of grounding with the bottleneck removed was reduced more than either non-structural alternative. The SEM does not address some of the other navigation benefits of bottleneck removal such as the increased width available to pilots to recover from cross currents at both the gulf and bay entrances.

In addition to the SEM evaluation of bottleneck removal, a ship simulation was also conducted with one of the four MSC pilots. After significant challenge in obtaining the appropriate current for input to the simulator, output from a 3D numerical model of circulation was found to be necessary for determining current patterns described by the pilots and observed in aerial images. Removal of the bottleneck results in increased discharge through the MSC entrance. One of the primary concerns addressed in the simulator was whether the increased discharge would result in increased cross current north of the peninsula between Sundown Island and the peninsula. Based on input from the pilot on the simulator, the cross current effects were increased north of the peninsula with the bottleneck removed. Increased cross current with the bottleneck removed was also seen in the computed velocity patterns. The pilot stated that the reduced probability of grounding in the rock lined channel through the peninsula was much more important than the increased probability of grounding in the soft bottom and side portion of the channel northwest of the peninsula due to increased cross currents.

Recommendations

Based on the findings of this study, flanking of the jetties and slope protection from hurricanes or high tides has a minimal risk of disrupting navigation in the MSC because the cross current through the breach is weak compared to the longitudinal current in the navigation channel. This finding assumes that any damage from storms and high tides is repaired in a reasonable time frame. Slope failures from the continuing scour of the channel bottom will increase in frequency and severity, but cause minimal

disruption to navigation because the size of the slope failures are not large enough to greatly alter the current in the channel or cause shoaling problems. This finding also assumes that damage from slope failures is repaired in a reasonable time frame. The increased frequency and increased severity of slope failures will result in increasing frequency of repairs and increased cost to maintain the MSC entrance.

The primary risk to disrupting navigation is ship grounding as a result of human error in the strong longitudinal currents in the rock-lined bottleneck cut through the peninsula. The strong longitudinal current, along with cross current on the bay side of the peninsula, is the combination identified by the pilots as posing the greatest risk of a powered grounding. Based on observations by the pilots, the amount of flow entering the channel and the strength of the cross current on ebb tide between Sundown Island and the peninsula has increased over the years. Recent bathymetry data show that depths are increasing in this area, consistent with the pilots' observations of increased cross current. If this trend continues, navigation in the existing MSC from this factor will become more hazardous.

Non-structural changes of daytime-only navigation and limiting navigation to current speed of 5 knots or less can reduce this risk. A current meter installed in the bottleneck that can be read in real-time by the pilots and port would be required to implement the 5 knot limitation.

The structural change of complete removal of the bottleneck provides the greatest reduction of risk to navigation at the MSC entrance from strong longitudinal currents. Because removal of the bottleneck results in a cross-sectional area that was found to be the stable inlet area, future scour of the bottom should be minimal and current velocity should remain constant at about 70-80 percent of existing velocity. If the bottleneck is removed, construction should proceed on both sides simultaneously because ship simulation showed that removal of one side only resulted in a cross current worse than in the existing channel.

Relocation of Sundown Island should reduce adverse cross current effects in the bay.

References

Bishop, A. W. 1955. The use of the slip circle in the stability analysis of slopes. *Geotechnique* 5(1):7-17. Great Britain, March.

Bowles. J. E. 1977. *Foundation analysis and design*. 2nd Edition. McGraw-Hill Book Company.

Briggs, M. J., L. S. Lillycrop, G. S. Haskins, E. F. Thompson, and D. R. Green. 1994. *Physical and numerical model studies of Barbers Point Harbor, Oahu, Hawaii*. Technical Report TR-CERC-94-14. Vicksburg, MS: Coastal and Hydraulics Laboratory, U. S. Army Engineer Waterways Experiment Station.

Brown, A. J., and M. Amrozowicz. 1996. Tanker environmental risk - putting the pieces together. *Joint SNAME/SNAJ International Conference on Designs and Methodologies for Collisions and Grounding Protection of Ships*. San Francisco, CA.

Brown, A. J., and B. Haugene. 1998. Assessing the impact of management and organizational factors on the risk of tanker grounding. *8th International Offshore and Polar Engineering Conference*, ISOPE-98-HKP-03.

Bureau of Economic Geology. 1968a. Geologic Atlas of Texas, Beaumont Sheet. Scale 1:250,000. Austin, TX: University of Texas.

Bureau of Economic Geology. 1968b. Geologic Atlas of Texas, Houston Sheet. Scale 1:250,000. Austin, TX: University of Texas.

Bureau of Economic Geology. 1975a. Geologic Atlas of Texas, Beeville-Bay City Sheet. Scale 1:250,000. Austin, TX: University of Texas.

Bureau of Economic Geology 1975b. Geologic Atlas of Texas, Corpus Christi Sheet. Scale 1:250,000. Austin, TX: University of Texas.

Bureau of Economic Geology. 1976. Geologic Atlas of Texas, McAllen-Brownsville Sheet. Scale 1:250,000. Austin, TX: University of Texas.

Buttolph, A. M., C. W. Reed, N. C. Kraus, N. Ono, M. Larson, B. Camenen, H. Hanson, T. Wamsley, and A. Zundel. 2006. *Two-dimensional depth-averaged circulation model CMS-M2D: Version 3.0, Report 2: Sediment transport and morphology change*. Technical Report ERDC/CHL TR-06-9. Vicksburg, MS: U.S. Army Engineer Research and Development Center.

Camenen, B., and M. Larson. 2005. A bedload sediment transport formula for the nearshore. *Estuarine, Coastal and Shelf Science* 63:249-260.

Camenen, B., and M. Larson. 2007. *A unified sediment transport formulation for coastal inlet application*. Coastal Inlets Research Program Contract Report, ERDC/CHL CR-07-1. Vicksburg, MS: U.S. Army Engineer Research and Development Center.

Dand, I. W., and P. R. Lyon. 1993. The element of risk in approach channel design. *International Conference on Maritime technology: Challenges in Safety and Environment Protection*. Singapore.

De Vries, W. A. 1990. *Nautical risk analysis in port and fairway design*. Publication No. 443. The Netherlands: Delft Hydraulics Laboratory.

Duncan, J. M., and S. G. Wright. 2005. *Soil Strength and Slope Stability*. Hoboken, NJ: John Wiley and Sons.

Escoffier, F. F. 1940. *The stability of tidal inlets*. Shore and Beach 8(4):114-115.

Escoffier, F. F. 1977. *Hydraulics and stability of tidal inlets. General Investigation of Tidal Inlets* GITI Report 13. Vicksburg, MS: U.S. Army Engineer Waterways Experiment Station.

Fowler, T. G., and E. Sorgard. 2000. Modeling ship transportation risk. *Risk Analysis* 20(2):225-244.

Graf, W. H. 1971. *Hydraulics of sediment transport*. New York, NY: McGraw-Hill.

Harrald, J. R., T. A. Mazzuchi, J. Spahn, R. Van Dorp, J. Merrick, S. Shrestha, and Martha Grabowski. 1998. Using system simulation to model the impact of human error in a maritime system. *Safety Science* 30:235-247.

Hart, F. 2007. Expert witness statement to the Independent Panel relating to Port of Melbourne Corporation proposed channel deepening. http://www.dse.vic.gov.au/CA256F310024B628/0/CC0DD209F8B2EA41CA2572F900805E83/$File/Frank+Hart+expert+witness+statement12.6.07.pdf.

Headquarters, U.S. Army Corps of Engineers. 2002. *Coastal Engineering Manual*. EM 1110-2-1100. Washington, DC.

Jarrett, J. T. 1976. Tidal prism-inlet area relationships. General Investigation of Tidal Inlets GITI Report 3. Vicksburg, MS: U.S. Army Engineer Waterways Experiment Station.

Kite-Powell, H. L., D. Jin, J. Jebsen, V. Papkonstantinou, and N. Partikalakis. 1998. Investigation of potential risk factors for groundings of commercial vessels in U.S. ports. MIT Sea Grant Program. Cambridge, MA: Massachusetts Institute of Technology.

Knott, M. A.1996. Risk analysis of ship and barge collision loads on bridges. *Proceeding Seventh Specialty Conference: Probabilistic Mechanics & Structural Reliability*. Worcester, MA 7-9 August.

Kraus, N. C., L. Lin, B. K. Batten, and G. L. Brown. 2006. Matagorda ship channel, Texas: Jetty stability study. Coastal and Hydraulics Laboratory Technical Report ERDC/CHL TR-06-7, Vicksburg, MS: U.S. Army Engineer Research and Development Center.

Kumar, V. S., S. Mandal, and K. A. Kumar. 2003. Estimation of wind speed and wave height during cyclones. *Ocean Engineering* 30: 2,239-2,253.

Lin, L., Z. Demirbilek, H. Mase, F. Yamada, and J. Zheng. 2008. A nearshore spectral wave processes model for coastal inlets and navigation projects. Coastal and Hydraulics Laboratory Technical Report ERDC/CHL TR-08-13. Vicksburg, MS: U. S. Army Engineer Research and Development Center.

Lin, S., H. L. Kite-Powell, and N. M. Patrikalakis. 1998. Physical risk analysis of ship grounding. MIT Sea Grant Program. *In proceedings of 55th Annual Meeting of the Institute of Navigation*. 69-77. Cambridge, MA: Massachusetts Institute of Technology.

Linke, T., and A. Huesig. 2000. Effects of cross currents induced by lateral water introductions on ship operation on inland waterways. *In proceedings Water Resources 2000*, Section 16, Chapter 3, ASCE.

Mase, H., Oki, K., Hedges, T. S. and Li, H. J. 2005. Extended energy-balance-equation wave model for multidirectional random wave transformation. *Ocean Engineering* 32:961-985.

Maynord, S. T. 1996. *Return velocity and drawdown in navigable waterways*. Hydraulics Laboratory Technical Report HL-96-7. Vicksburg, MS: U.S. Army Engineer Waterways Experiment Station.

Maynord, S. T. 2007. *Ship forces on the shoreline of the Savannah Harbor project*. Coastal and Hydraulics Laboratory Technical Report ERDC/CHL TR-07-7. Vicksburg, MS: U.S. Army Engineer Research and Development Center.

Maynord, S. T., Seabergh, W. C., L. Lihwa, N. C. Kraus, D. W. Webb. 2007. *Evaluation of risks to navigation for the Matagorda Ship Channel Entrance*. Draft Technical Report, 16 October 2007. Vicksburg, MS: U.S. Army Engineer Research and Development Center.

McGowen, J. H., C. V. Proctor, L. F. Brown, T. J. Evans, W. L. Fisher, and C. G. Groat. 1976. *Environmental Geologic Atlas of the Texas Coastal Zone* – Port Lavaca Area. Austin, TX: Bureau of Economic Geology, The University of Texas.

Merrick, J. R. W., J. R. van Dorp, T. Mazzuchi, J. R. Harrald, J. E. Spahn, and M Grabowski. 2002. The Prince William Sound risk assessment. Interfaces 32(6):25-40.

Militello, A., C. W. Reed, A. K. Zundel, and N. C. Kraus. 2004. *Two-dimensional depth-averaged circulation model M2D: Version 2.0*, Report 1: Documentation and user's guide. ERDC/CHL TR-04-2. Vicksburg, MS: U.S. Army Engineer Research and Development Center.

Myers, V. A. 1954. Surface friction in a hurricane. *Monthly Weather Review* 82:307–311.

Natarajan, R., and K. M. Ramamurthy. 1995. Estimation of central pressure of cyclonic storms in the Indian seas. *Indian Journal of Meteorology, Hydrology and Geophysics* 26:65–66.

Neumann, C. J. 1987. The national hurricane risk analysis program (HURISK). NOAA Technical Memorandum NWS NHC 38. Coral Gables, FL: National Hurricane Center.

Ochi, M. K. 1990. *Applied probability and stochastic processes in engineering and physical sciences*. Wiley series in probability and statistics. John Wiley & Sons, Inc.

Rock Engineering and Testing Laboratory. 2008. Geotechnical investigation at the Matagorda Ship Channel Matagorda Peninsula, TX.

Roy, D. L., and F. Maes. 2006. *Risk analysis of marine activities in the Belgium part of the North sea*. Belgium, Europe: Belgium Science Policy, Brussels.

Rubinstein, R. Y. 1981. Simulation and the Monte Carlo method. New York, NY: John Wiley and Sons.

Saaty T. L. 1980. *The Analytic Hierarchy Process*. New York: McGraw-Hill.

Scheffner, N. W., J. E. Clausner, A. Militello, L. E. Borgman, B. L. Edge, and P. J. Grace. 1999. *Use and application of the Empirical Simulation Technique: User's guide*. Coastal and Hydraulics Laboratory Technical Report CHL-99-21. Vicksburg, MS: U.S. Army Engineer Research and Development Center.

Scheffner, N.W., D.J. Mark, C.A. Blain, J.J. Westerink, and R.A. Luettich, Jr. 1994. ADCIRC: *An Advanced Three-Dimensional Circulation Model for Shelves, Coasts, and Estuaries. Report 5 – A tropical Storm Database for the East and Gulf of Mexico Coasts of the Unites States*. Dredging Research Program Technical Report DRP-92-6. Vicksburg, MS: U.S. Army Engineer Waterways Experiment Station.

Sellards, E. H., W. S. Akdins, and F. B. Plummer. 1990. The geology of Texas, Volume I, Stratigraphy. *The University of Texas Bulletin* No. 3232. Austin, TX: Bureau of Economic Geology, University of Texas.

Shore protection manual. 1984. 4th ed., 2 Vol, U.S. Army Engineer Waterways Experiment Station, U.S. Government Printing Office, Washington, DC.

Slordal, L. H. 1997. The pressure gradient force in sigma co-ordinate ocean models. *International Journal for the Numerical Methods in Fluids* 24:987-1,017.

Solem, R. R. 1980. Probability models of groundings and collisions. *Automation for Safety in Shipping and Offshore Petroleum Operations Conference*. Amsterdam, The Netherlands: North-Holland Publishing Company.

Stelling, G. S., and J. A. Th.M. van Kester. 1994. On the approximation of the horizontal gradients in sigma co-ordinates for bathymetry with steep bottom slopes. *International Journal for the Numerical Methods in Fluids* 18:915-935.

Uluscu, O. S., O. Birur, T. Altiok, I. Or. 2008. Risk analysis of transit vessel traffic in the Strait of Istanbul. Piscataway, NJ: Laboratory for Port Security, Rutgers University.

U.S. Army Corps of Engineers .2006. Hydraulic design guidance for deep draft navigation projects. Engineer Manaual EM 1110-2-1613. Washington, DC.

U.S. Army Engineer District, Galveston. 1963. General design memorandum and supplement No. 3 (dated 1963). Galveston, TX.

U.S. Coast Guard. 2001. Port and waterway safety assessment. http://www.navcen.uscg.gov/mwv/projects/pawsa/PAWSA_home.htm.

U.S. Department of the Army, U.S. Army Corps of Engineers, Waterways Experiment Station. 1962. Engineering Properties of Fine-grained Mississippi Valley Alluvial Soils Meander Belt and Backswamp Deposits, TR No. 3-604, Vicksburg, Ms.

Watanabe, A. 1987. 3-Dimensional Numerical Model of Beach Evolution. *In proceedings Coastal Sediments '87*, ASCE, 802-817.

Watson, R. L. 1990. Postglacial submergence south Texas coast. www.TexasCoastGeology.com, 11 p.

Wolf, T. F. 1996. Probabilistic slope stability theory and practice. ASCE *Proceedings of the Special Conference Uncertainty in the Geologic Environment*. Madison, WI, pp 419-433, Also, ASCE *Geotechnical Special Publication* 58.

Wright, Stephen, G. 1999a. UTEXAS4 A computer program for slope stability calculations. Department of the Army, U.S. Army Corps of Engineers. Contract Report.

Wright, Stephen, G. 1999b. TexGraf4 A graphics program for UTEXAS4. Department of the Army, U.S. Army Corps of Engineers. Contract Report.

Young, I. R. 1988. Parametric hurricane wave prediction model. *Journal of Waterways Port Coastal and Ocean Engineering* 114(5):637–652.

Zundel, A. 2006. *Surface-water modeling system reference manual - Version 9.2*. Provo, UT: Brigham Young University Environmental Modeling Research Laboratory.

Appendix A: Life-Cycle Analysis for Hurricane Data

The maximum wind speed and minimum atmospheric pressure of a hurricane are considered as extreme values and expected to occur in a certain number of observations or in a certain period. The statistical method to evaluate these extreme values for the finite length data is known as the extreme value analysis (Ochi 1990). The reliability of the analysis and computed frequency of occurrence depends on the data fitting to the asymptotic distribution function. A more reliable approach is to generate a larger database from the finite length data using the resampling method known as the Empirical Simulation Technique (EST).

Distribution of extreme values

Four asymptotic distribution functions of a random variable x are applied in the present study for the extreme value analysis:

1. Fisher-Tippett Type I (Gumbel distribution):
   $F(x) = \exp\left[-e^{-a(x-b)}\right],\ a > 0,\ |x| < \infty$.

2. Weibull Distribution: $F(x) = 1 - \exp[-(\lambda x)^c],\ \lambda > 0,\ c > 0,\ x \geq 0$.

3. Fisher-Tippet (F.T.) Type III: $F(x) = \exp\left[-\left(\frac{w-x}{v}\right)^{\gamma}\right]$,
   $v > 0,\ \gamma > 0,\ x \leq w$

4. Tanh-power: $F(x) = \tanh^{\alpha}(\beta x),\ \alpha > 0,\ \beta > 0,\ x \geq 0$

where a, b, c, α, β, γ, λ, ν, and w are constants. According to the Order Statistics, if a total of N observations of a random variable x is made and arranged in the ascending order as $x_1 \leq x_2 \leq x_3 \leq \cdots \leq x_i \leq \cdots \leq x_N$, the unbiased estimate of the probability of x_i is $\tilde{F}(x_i) = \frac{i}{1+N}$.

The acceptance of an asymptotic distribution function is based on a data fitting method such as the least-square or moment-generating functions applied on the calculated extreme value probabilities.

Storm surge data-fitting and EST analysis

Figure A1 shows the ascending-order sample probabilities and least-square-fit curves of 35 storm surge data (Table A1) for the Fisher-Tippett Type I, Weibull, and Tanh-power functions. The best-fit function is the Tanh-power and, therefore, it is used as the base distribution for the EST. Figure A2 shows the EST results with a 60-percent confidence interval (C.I.) and the extrapolation of Fisher-Tippett Type I and Tanh-power functions for the return periods between 50 and 1,000 years. Table A2 presents the calculated return periods for the storm surge between 50 and 1,000 years.

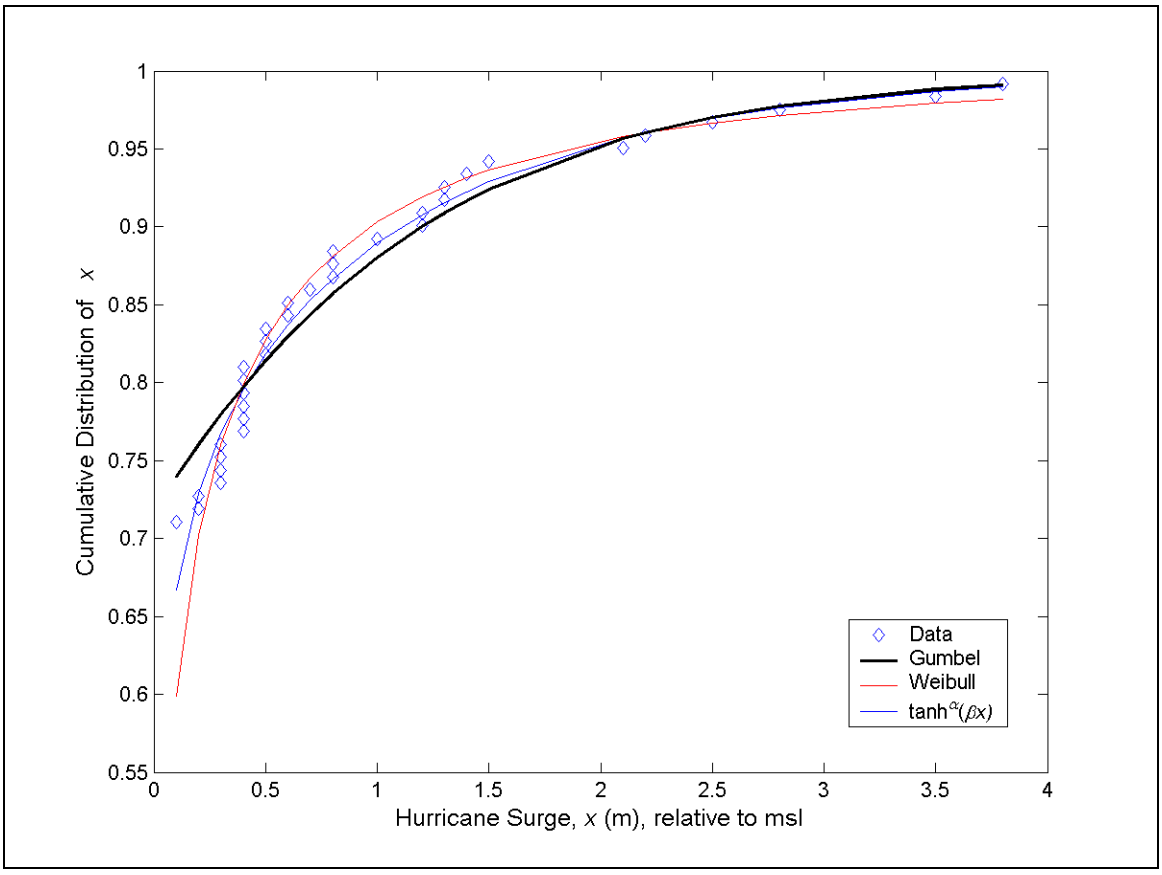

Figure A1. Storm surge data and Gumbell, Weibull, tanh-power functions.

Table A1. Tropical storm surge (m).

Return Period (year)	50	100	200	300	400	500	600	700	800	900	1000
Gumbel	2.9	3.7	4.4	4.8	5.1	5.3	5.5	5.7	5.8	5.9	6.0
$\tanh^{\alpha}(\beta x)$	3.0	3.8	4.6	5.1	5.4	5.7	5.9	6.1	6.3	6.4	6.5
EST	3.5	4.2	5.0	5.4	5.7	6.0	6.1	6.3	6.5	6.6	6.7

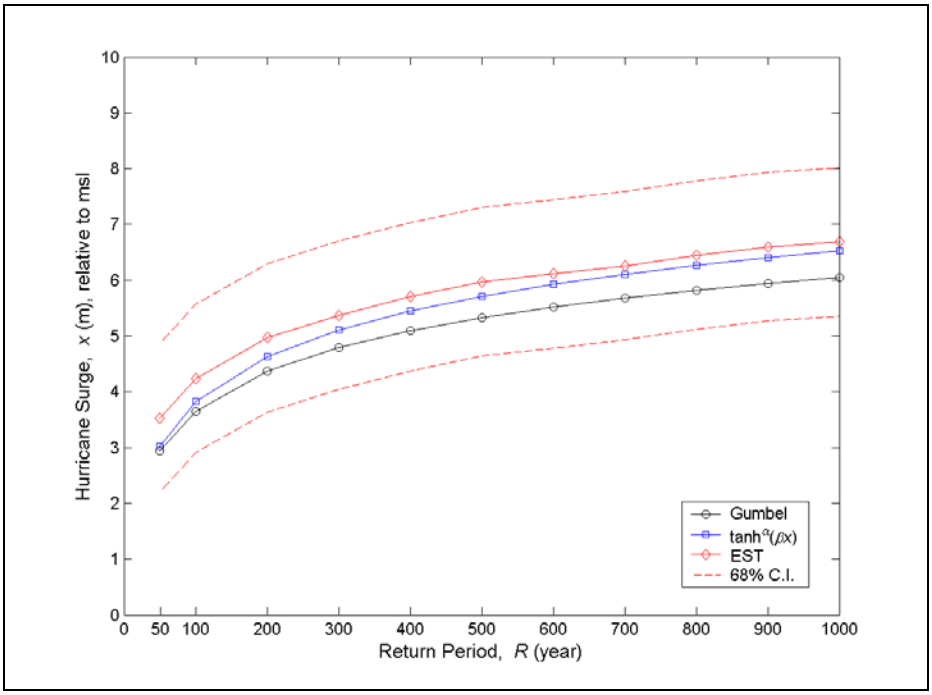

Figure A2. Storm surge frequencies by Gumbel, tanh power, and EST with 60 percent C.I.

Table A2. Comparison of measured and calculated hurricane waves.

Hurricane	Buoy	Depth (m)	Max Wind Speed (knot)	Meas. H_s (m)	Meas. T_p (sec)	Comp. H_s (m)	Comp. T_p (sec)
Lili (2002)	42001	3246	125	11.2	12.9	11.8	13.1
	42041	400		12.2	13.8		
Claudette (2003)	42019	28	75	5.6	10.0	4.2	7.9
Ivan (2004)	42003	3164	120	10.9	12.9	10.8	12.6
	42039	29		12.1	14.3		
	42040	29		16.0	16.7		
Katrina (2005)	42003	3164	125	10.6	12.9	11.8	13.1
	42040	29	150	16.9	14.3	16.9	15.8
Rita (2005)	42001	3246	125	11.6	13.8	11.8	13.1

Effective storm surge duration

A simple tropical storm pressure field model (Myers 1954) is:

$$p_r = p_o + (p_n - p_o)\exp(-R / r)$$

where:

p_o = the central pressure
p_n = the ambient pressure
p_r = the pressure at a distance r from the storm center
R = the radius of maximum wind speed $U_{\max}$

From the long wave theory, the storm surge x_r is proportional to the central pressure deficit $|p_n - p_o|$, therefore,

$$x_r = x \cdot \left[1 - \exp(-R / r)\right]$$

where x is the maximum surge elevation.

The effective surge duration for a storm moving with speed V_F is defined as:

$$D_{\text{eff}}\left(x_r / x \geq 0.95\right) = \frac{2R}{3V_F}$$

where $r \leq R/3$ as $x_r / x \geq 0.95$. Figures A.3 and A.4 show the storm surge data versus the calculated effective durations and cyclone moving speeds, respectively.

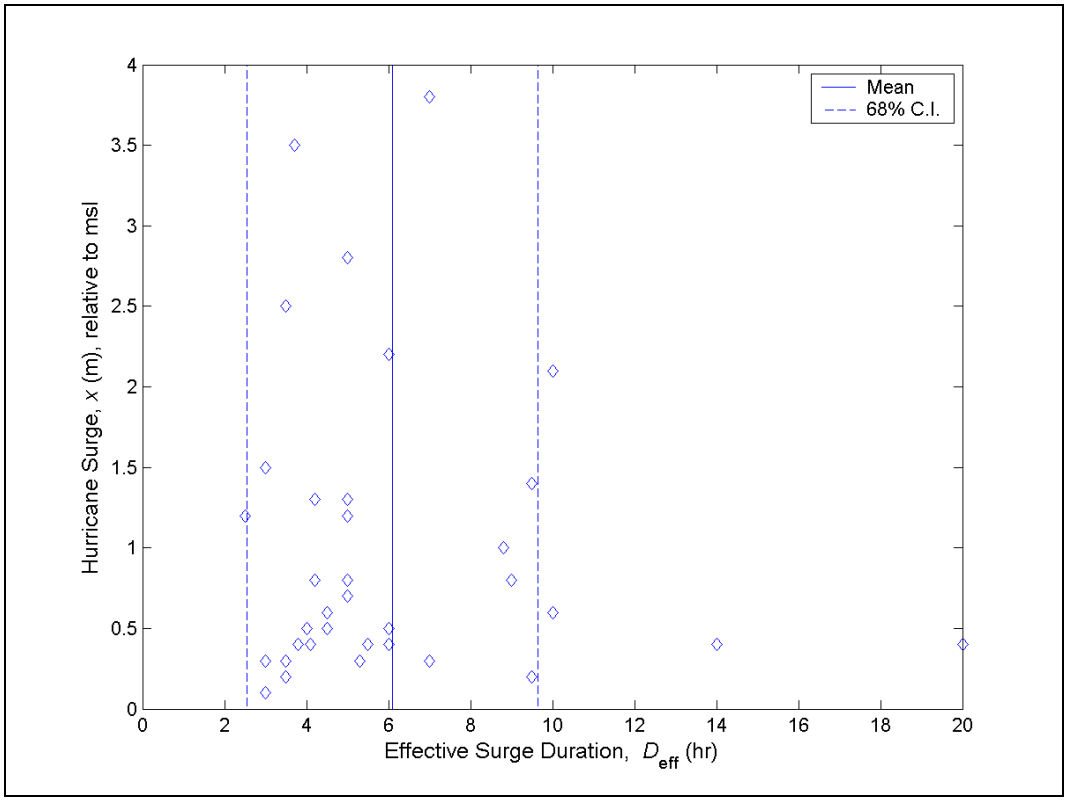

Figure A3. Storm surge data and calculated effective storm surge duration.

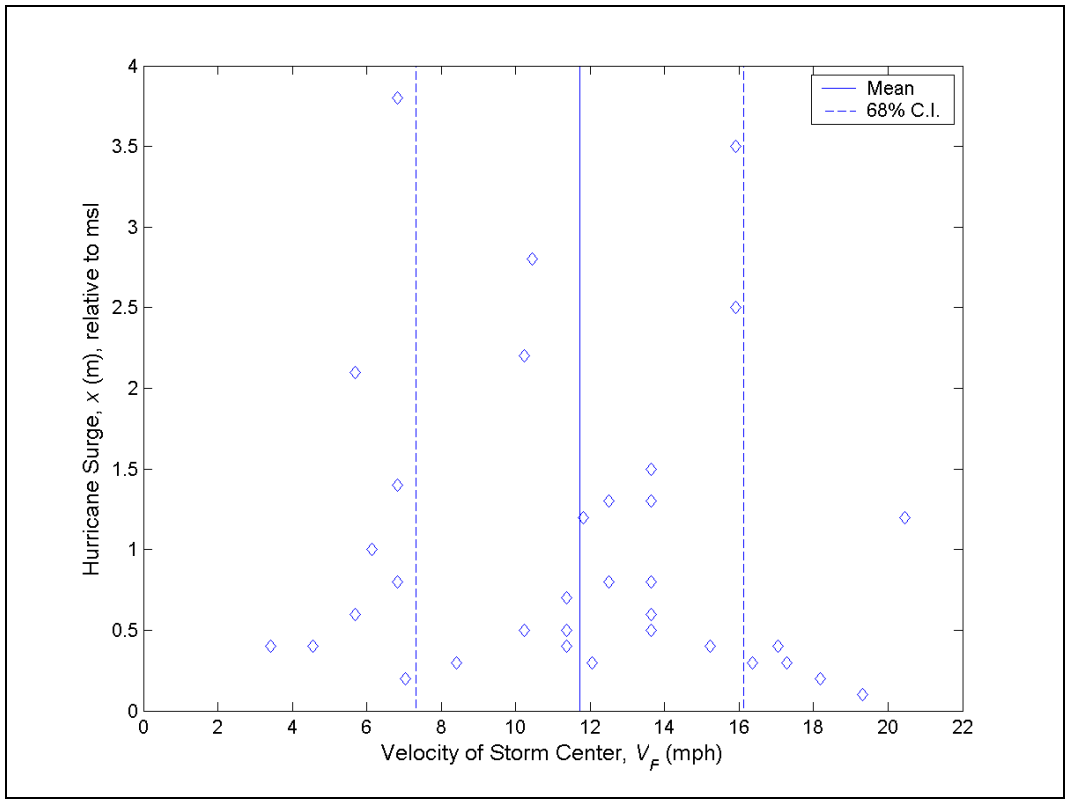

Figure A4. Storm surge data and cyclone moving speed.

Radius of maximum wind speed

The relation of the radius of maximum wind speed to latitude in the Gulf of Mexico (Neumann 1987) developed by the National Hurricane Center is:

$$R(\text{nm}) = 11.571 + 0.014487 \cdot Z^2 - 0.00000166035 \cdot U_{\max}^3$$

where Z is the latitude (deg), and $U_{\max}$ is the maximum wind speed (knots). Figures A5 and A6 show the storm surge data versus the radius of maximum wind speed and maximum wind speeds, respectively.

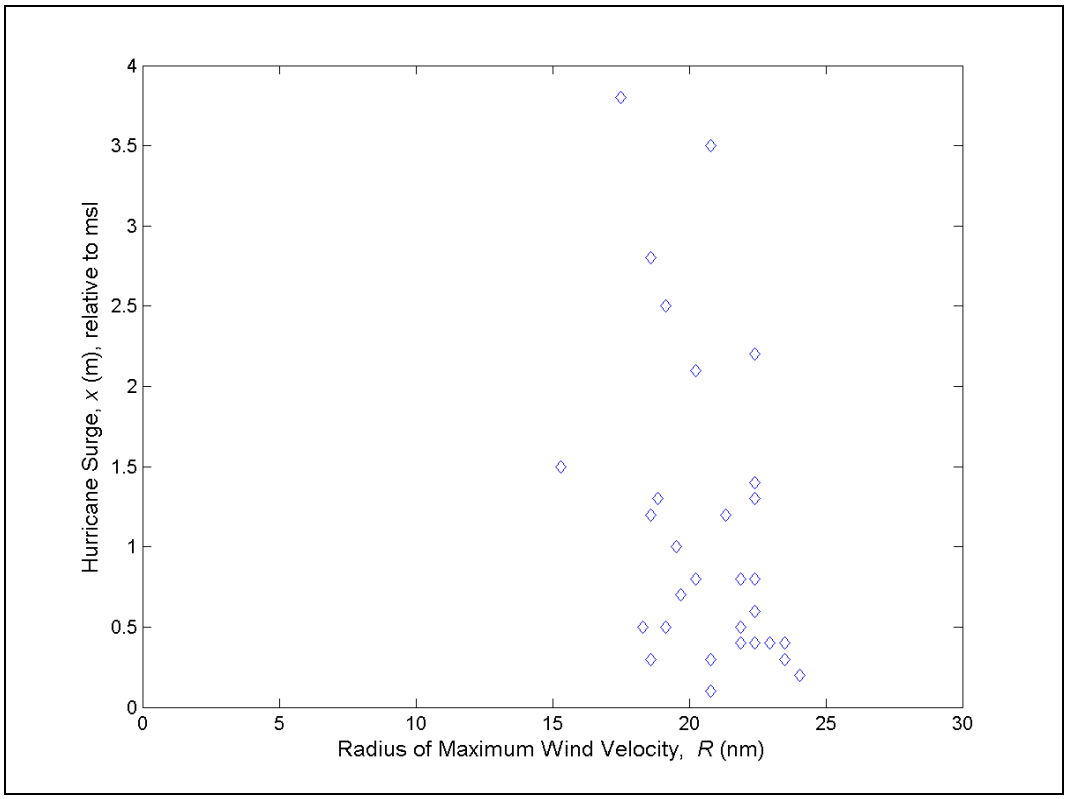

Figure A5. Storm surge data and radius of maximum wind speed.

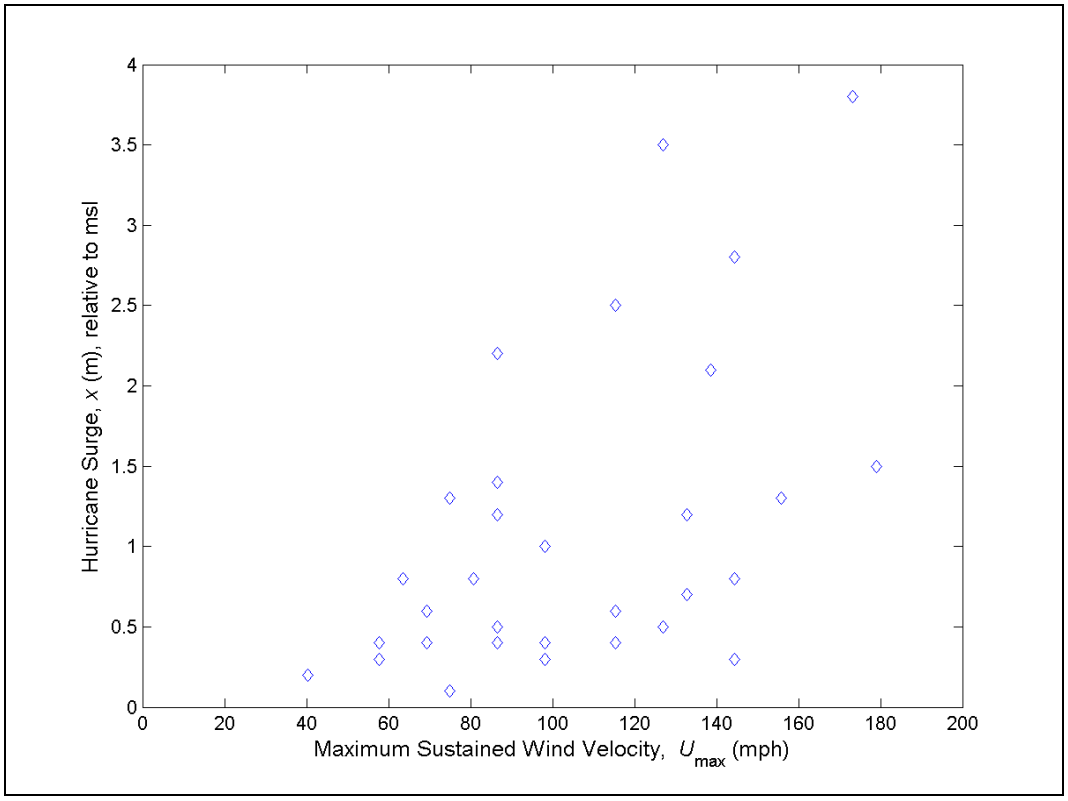

Figure A6. Storm surge data and maximum sustained wind speed.

Maximum wind speed data-fitting and EST analysis

The maximum wind speed is analyzed for the 10-min average wind. The relation between the 10-min average wind speed and the 1-min average wind speed (sustained wind speed) is:

10-min average wind speed = 0.88 * 1-min average wind speed

Figure A7 shows the ascending-order samples and least-square-fit curves of 35 maximum wind speed data (Table A2) for Fisher-Tippett Type I, Weibull, Tanh-power, and Fisher-Tippett Type III functions. The best-fit function is the Fisher-Tippett Type III and is used as the base function for the EST. Figure A8 shows the EST projection and the extension of Fisher-Tippett Type III function for the return periods between 50 and 1,000 years. The best-fit curve of Fisher Type III function indicates an upper limit of $U_{\max}$ = 176 mph for the 10-min average wind speed.

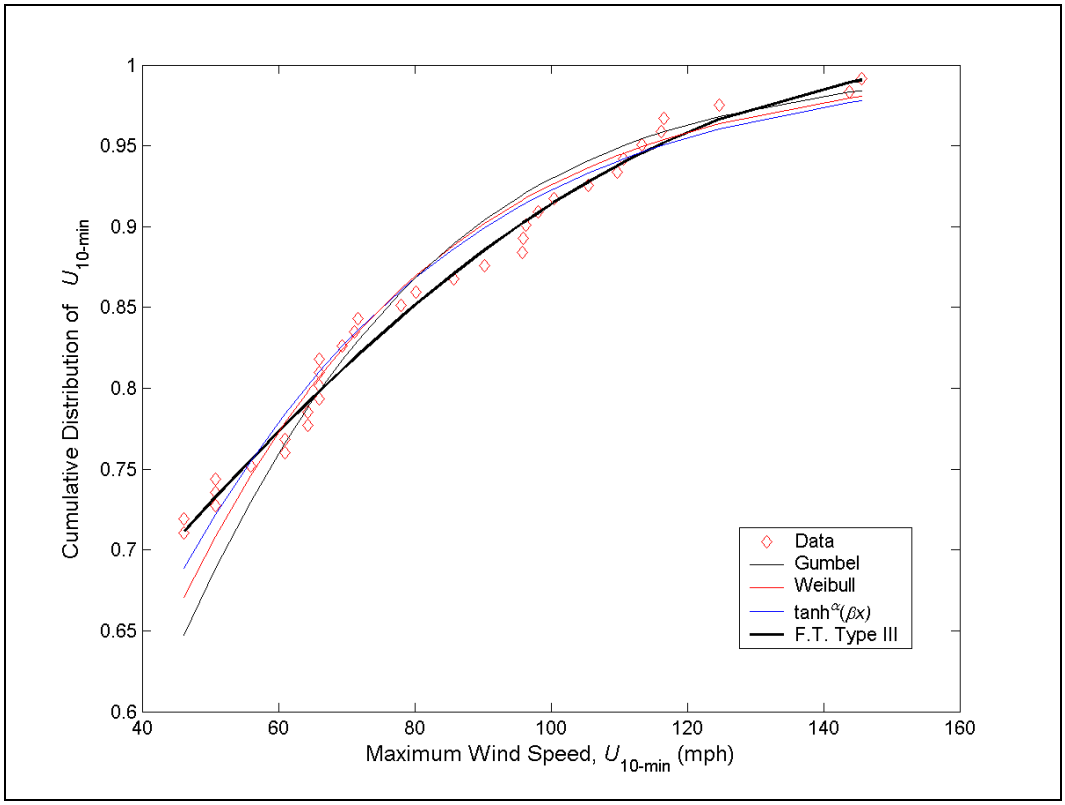

Figure A7. Max wind speeds and Gumbell, Weibull, tanh power, and F.T. Type III functions.

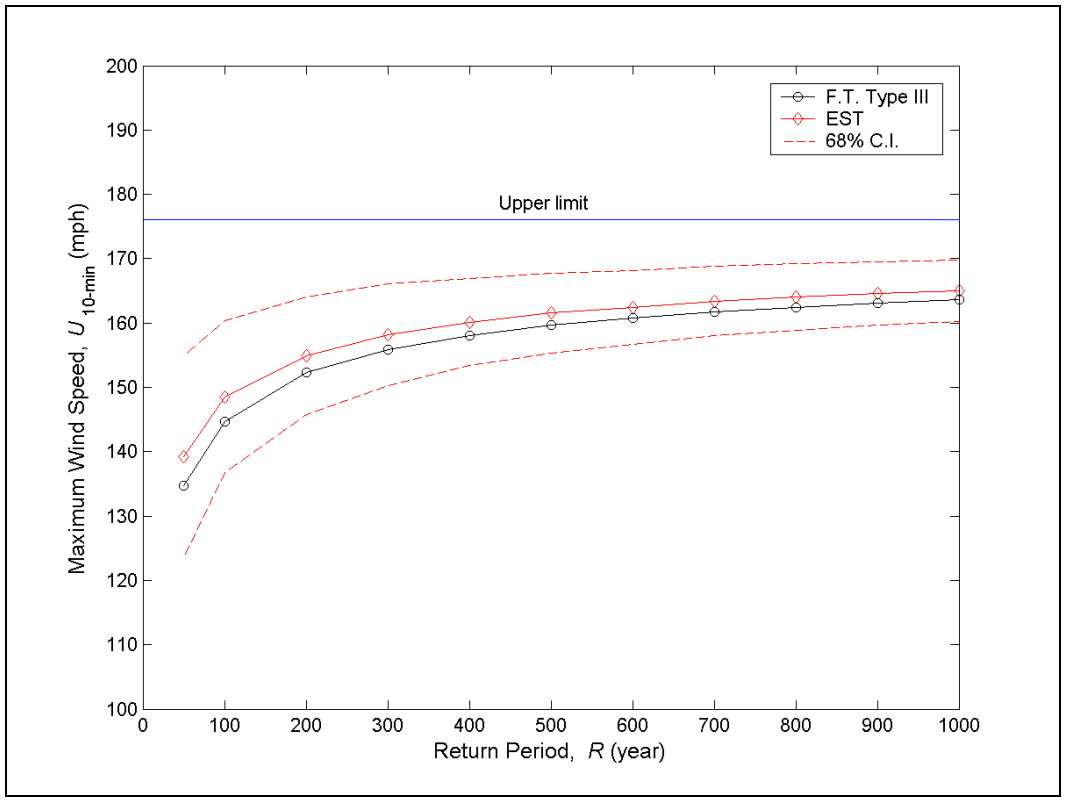

Figure A8. Max wind speed frequencies by F.T. Type III and EST with 60 percent C.I.

Central pressure deficit data-fitting and EST analysis

Figure A9 shows the storm surge data versus the cyclone central pressure deficit. Figure A10 shows the ascending-order samples and least-square-fit curves of 35 central pressure deficit data for Fisher-Tippett Type I, Weibull, and Tanh-power, and Fisher-Tippett Type III functions. The best-fit function is the Fisher-Tippett Type III and is used as the base function for the EST. Figure A10 shows the EST projection and the extension of Fisher-Tippett Type III function for the return periods between 50 and 1,000 years. The best-fit curve of Fisher Type III function indicates an upper limit of central pressure deficit p_n - p_o = 116 mb.

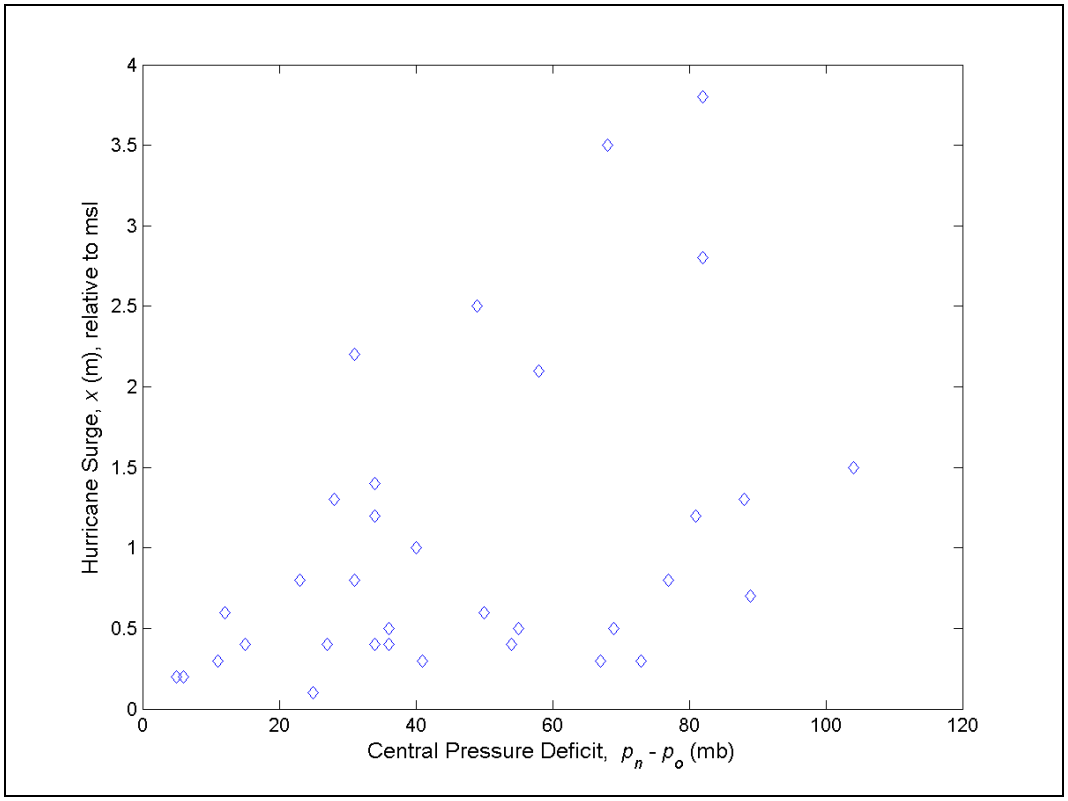

Figure A9. Storm surge data and cyclone central pressure deficit.

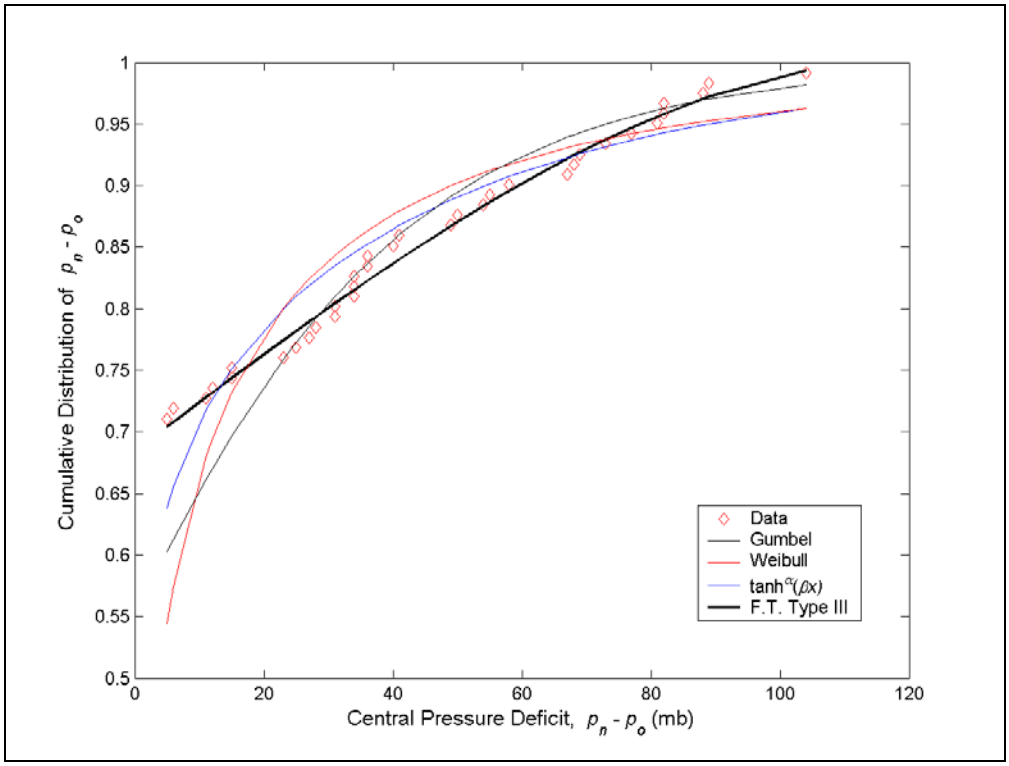

Figure A10. Central pressure deficits and Gumbell, Weibull, tanh power, and F.T. Type III functions.

Using p_n - p_o = 116 mb as the upper limit of the maximum central pressure deficit, the corresponding upper limit of the maximum wind speed can be calculated from three empirical equations:

1. $U_{\max} = 12.24 \cdot (p_n - p_o)^{0.564} = 179$ mph (Atlantic Ocean and Meteorological Lab, Hurricane Research Division, for a moving hurricane).

2. $U_{\max} = 8.33 \cdot (p_n - p_o)^{0.638} = 173$ mph (present study, for a stationary hurricane).

3. $U_{\max} = 15.66 \cdot (p_n - p_o)^{0.5} = 169$ mph (Natarajan and Ramamurthy (1995); for the Indian Ocean; Kumar et al. 2003).

These calculated upper limit values of the maximum wind speed are consistent with the upper limit value determined in the Fisher-Tippett Type III function (Figure A8). Figure A12 shows the plot of the maximum wind speed versus central pressure deficit data for stationary (remove the storm forward speed) and non-stationary cyclones.

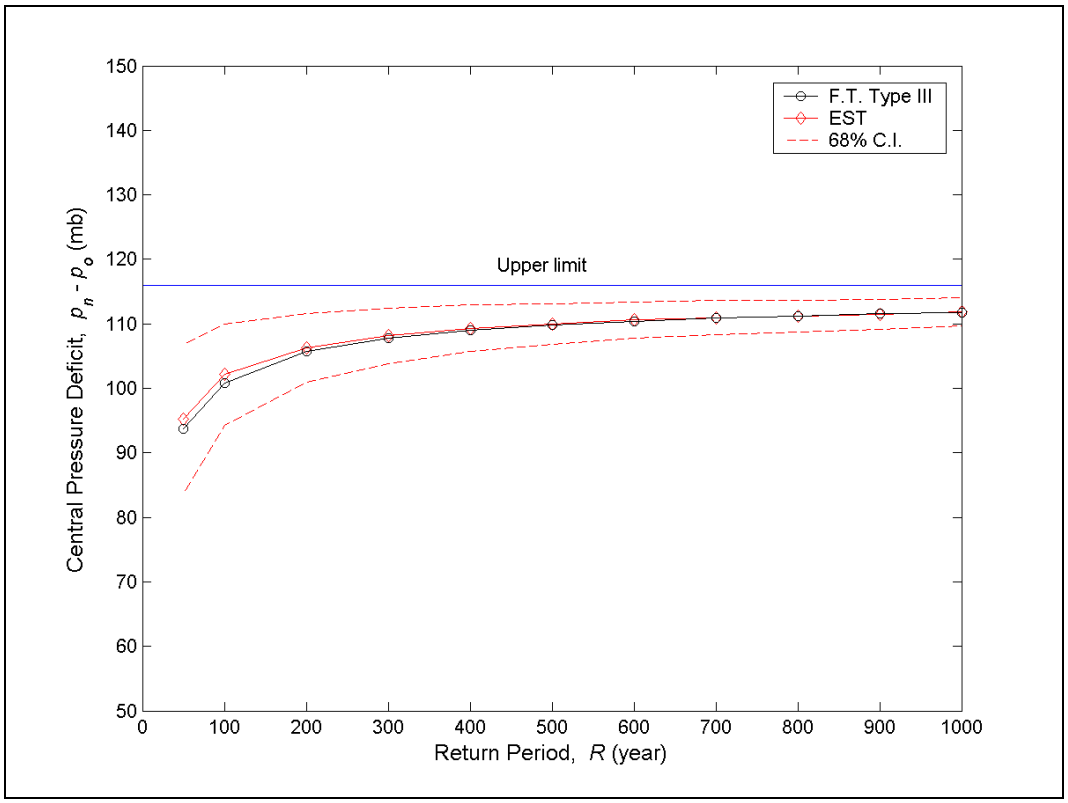

Figure A11. Central pressure deficit frequencies by F.T. Type III, and EST with 60 percent C.I.

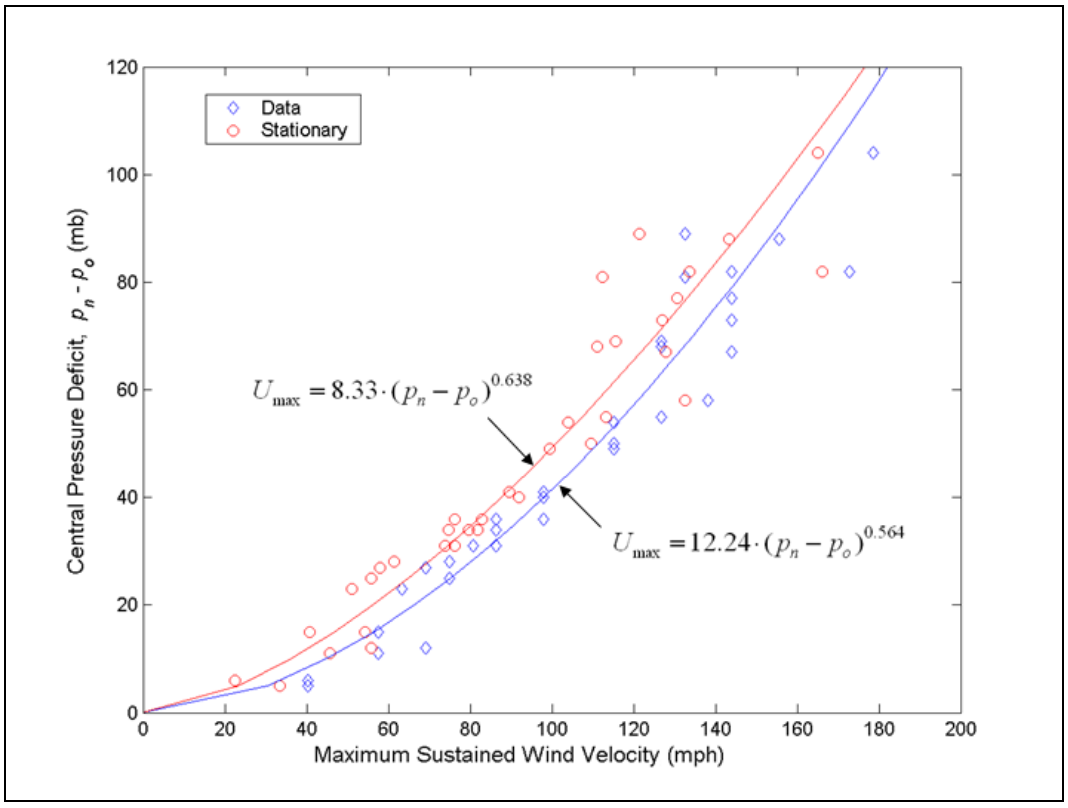

Figure A12. Relation between central pressure deficit and maximum wind speed.

Prediction of hurricane waves

Hurricane waves (significant wave height and wave period) in the deep water can be calculated by simple equations (*Shore Protection Manual* 1984; Young 1988) as:

$$H_s = \frac{U_{\max}^2}{36g} \text{ and } T_p = \frac{2U_{\max}}{g} = 12\sqrt{\frac{H_s}{g}} \leq 9.8\sqrt{\frac{h}{g}}$$

Figure A13 shows the comparison of the deepwater wave height and period relation to the data collected by NDBC buoys within the radius of maximum wind of several major hurricanes that occurred in recent years in the Gulf of Mexico. Table A2 presents the hurricane wave data from NDBC with the maximum wind speed data from the National Hurricane Center. Using the above equations, the deepwater wave height and period corresponding to the life-cycle maximum wind speed can be calculated (Table A3).

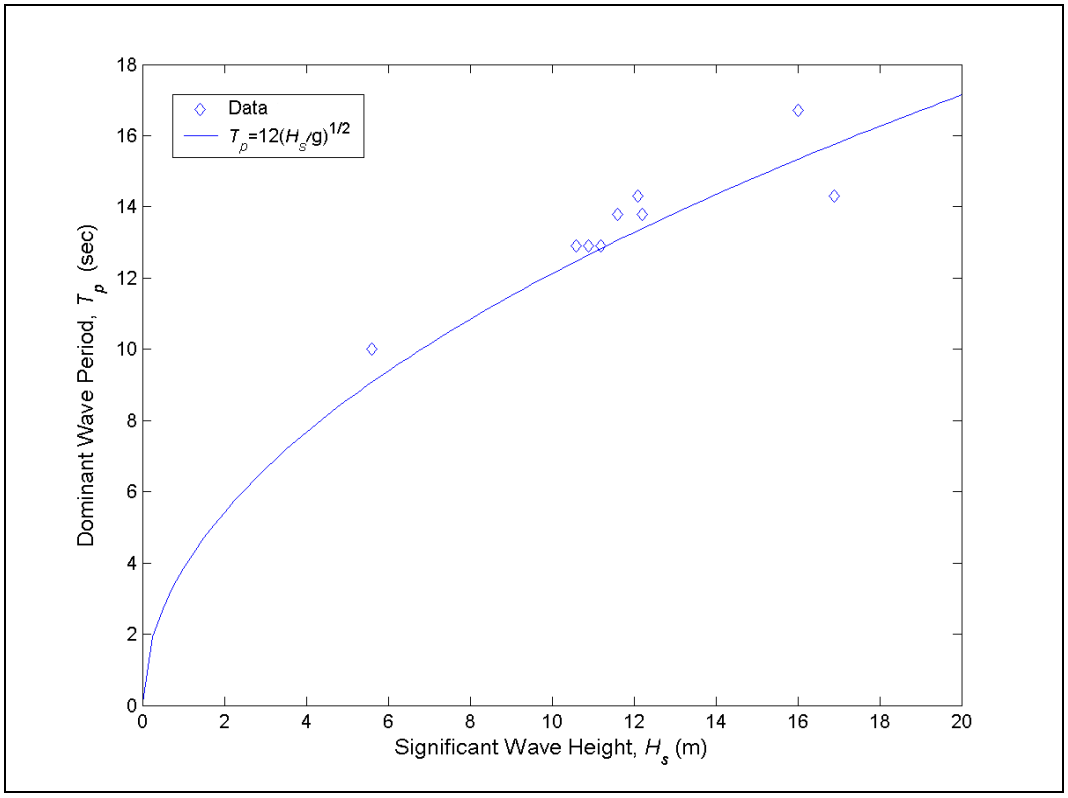

Figure A13. Hurricane deepwater wave height and period relationship.

Table A3. Hurricane surge, maximim wind speed, central pressure deficit, and deepwater wave life-cycle predictions.

Return Period (year)	50	100	200	300	400	500	600	700	800	900	1000
Storm Surge (m)	3.5	4.2	5.0	5.4	5.7	6.0	6.1	6.3	6.5	6.6	6.7
Max Wind Speed* (mph)	139	149	155	158	160	161	162	163	164	165	165
Max Wind Speed** (mph)	151	161	167	170	172	173	174	175	176	177	177
Central Pressure Deficit (mb)	95	102	106	108	109	110	111	111	111	112	112
Sig. Wave Height** (m)	12.9	14.7	15.8	16.4	16.8	17.0	17.1	17.3	17.5	17.6	17.7
Dominant Period** (sec)	13.8	14.7	15.2	15.5	15.7	15.8	15.9	16.0	16.1	16.1	16.1

* Stationary hurricanes.

** Moving hurricanes with an average speed V_F = 12 mph.

Appendix B: Summary of Geotechnical Field and Laboratory Data

Introduction

This summary is provided in eight tables corresponding to the eight borings performed in the field exploratory program. Each table has 15 columns with columns one through eight containing the basic information obtained during the field testing. The basic data includes the sample number, the depth and elevation of the sample, and the obtained blow counts. Laboratory data are presented in columns 9 to 15. The complete field and laboratory data report is found in Rock Engineering and Testing Laboratory (2008).

Standard penetration test data reduction

Tables B1 through B8 contain data obtained from the SPTs performed in each of the eight bore holes. SPTs were performed in borings B-1 to B-8. The locations of these borings are shown on the plan view in Figure 36. Standard engineering practice defines the SPT-N value as the sum of the blow counts between the 6- to 12-in. interval and the 12- to 18-in. interval. An adjustment must be made to each N-value blow count to correct the value to that value which would be obtained if the test were performed at an effective vertical stress of 1.0 tsf. This correction allows SPT N-value blow counts obtained at different depths to be compared on a one-to-one basis for the same material. The corrected blow count is termed $(N_1)_{60}$ and is shown in eighth column. The correction factor C_n depends on the vertical effective stress (overburden pressure) and is determined from the chart on Figure B1. The $(N_1)_{60}$ blow count is determined by multiplying the SPT N-value blow count in the sixth column by C_n. Another correction is made if the sampling depth is less than 10 ft, as shown in the seventh column, by multiplying the SPT N-value blow count by the factor 0.75 to account for the smaller energy losses present in a shorter string of drilling rods.

Table B1. Summary of field and laboratory data for boring B-1.

Field Data								Laboratory Data						
			Blow Count Adjustments											
Sample Number	Depth, ft	Elevation, ft (MSL)	Effective Overburden, ksf	C_n	SPT N value	Rod Length Correction	$(N_1)_{60}$	Unit Weight, pcf	Moisture Content, %	Liquid Limit	Plastic Index	% Passing #200 Sieve	Average S_u, ksf	Classification
	5	*-1*	0.50	2.000				100						
S-1	8	*-4*	0.61	1.807	21	16	28	100	21			7		SP-SM
S-2	18	*-14*	1.39	1.200	32	32	38	140	24			7		SP-SM
S-3	28	*-24*	2.16	0.961	43	43	41	140	36			28		
S-4	38	*-34*	2.84	0.839	21	21	18	130	19			37		
S-5	43	*-39*	3.13	0.800				120	35	66	44	84	1.90	CH
S-6	48	*-44*	3.42	0.765				120	23	21	2	12		SP-SM
S-7	58	*-54*	4.09	0.699	27	27	19	130	24			18		SM
S-8	68	*-64*	4.75	0.649				129	19	45	29	62	1.40	CL
S-9	73	*-69*	5.03	0.630				118	33	70	48	96	1.20	CH
S-10	78	*-74*	5.29	0.615				114	37	83	61	97	2.50	CH
S-11	83	*-79*	5.61	0.597				127	29	56	40	81	1.80	CH
S-12	88	*-84*	5.93	0.581	9	9	5	125	25			48		
S-13	93	*-89*	6.26	0.565				128	22	68	45	68	4.40	CH
S-14	98	*-94*	6.54	0.553				120	18	40	28	63		CL
S-15	108	*-104*	7.27	0.525	38	38	20	135	18			31		
S-16	118	*-114*	7.88	0.504				123	25	53	39	78	3.67	CH
S-17	123	*-119*	8.20	0.494				126	18	41	28	73	3.50	CL
S-18	128	*-124*	8.54	0.484	39	39	19	130	19			23		SM
S-19	138	*-134*	9.21	0.466	32	32	15	130	27			34		
S-20	148	*-144*	9.81	0.451				123	30	58	39	72	1.90	CH
S-21	153	*-149*	10.11	0.445				122	29	66	45	83	1.10	CH
S-22	158	*-154*	10.41	0.438				123	27			94		CH
S-23	163	*-159*	10.73	0.432				127	22	48	29	94	3.60	CL
S-24	168	*-164*	11.04	0.426				124	19	71	49	92	3.40	CH
S-25	173	*-169*	11.35	0.420				124	23	66	41	93	3.80	CH
S-26	178	*-174*	11.65	0.414				124	16	42	26	55		CL
S-27	188	*-184*	12.33	0.403	45	45	18	130	20			54		
S-28	198	*-194*	13.01	0.392	49	49	19	130						

Table B2. Summary of field and laboratory data for boring B-2.

Field Data								Laboratory Data						
			Blow Count Adjustments											
Sample Number	Depth, ft	Elevation, ft (MSL)	Effective Overburden, ksf	C_n	SPT N value	Rod Length Correction	$(N_1)_{60}$	Unit Weight, pcf	Moisture Content, %	Liquid Limit	Plastic Index	% Passing #200 Sieve	Average S_u, ksf	Classification
	7	0	0.70	1.690				100						
S-1	8	-1	0.77	1.614	13	10	16	130	19			4		SP
S-2	18	-11	1.54	1.138	31	31	35	140	19			11		SP-SM
S-3	28	-21	2.32	0.929	35	35	32	140	22			7		SP-SM
S-4	38	-31	3.05	0.810	36	36	29	135	21			6		SP-SM
S-5	48	-41	3.62	0.743				120	24	72	52	56	2.50	CH
S-6	58	-51	4.35	0.678	34	34	23	135	21			9		SP-SM
S-7	68	-61	5.12	0.625	61	61	38	140	12			20		SM
S-8	78	-71	5.65	0.595				115	30	69	49	88	2.70	CH
S-9	88	-81	6.23	0.567				120	23	46	33	56	2.20	CL
S-10	98	-91	6.85	0.540				125	18	23	5	45		SC-SM
S-11	108	-101	7.53	0.515	34	34	18	130	20			50		
S-12	118	-111	8.15	0.495	13	13	6	125	26			60		
S-13	128	-121	8.83	0.476	33	33	16	130	23			51		
S-14	138	-131	9.56	0.457	55	55	25	135	22			15		SM
S-15	148	-141	10.14	0.444				121	28	73	53	88	2.10	CH
S-16	158	-151	10.76	0.431				124	34	73	50	89	2.20	CH
S-17	168	-161	11.38	0.419				125	24	27	12	22		SC

Table B3. Summary of field and laboratory data for boring B-3.

Field Data								Laboratory Data						
			Blow Count Adjustments											
Sample Number	Depth, ft	Elevation, ft (MSL)	Effective Overburden, ksf	C_n	SPT N value	Rod Length Correction	$(N_1)_{60}$	Unit Weight, pcf	Moisture Content, %	Liquid Limit	Plastic Index	% Passing #200 Sieve	Average S_u, ksf	Classification
S-1	3	*4*	0.30	2.582	20	15	39	100	22			*9*		SP-SM
S-2	13	*-6*	1.08	1.363	41	41	56	140	23			5		SP-SM
S-3	23	*-16*	1.80	1.054	19	19	20	135	17			7		SP-SM
S-4	33	*-26*	2.48	0.898	20	20	18	130	22			3		SP
S-5	43	*-36*	3.10	0.803	8	8	6	125	17			5		SP-SM
S-6	53	*-46*	3.83	0.723	29	29	21	135	22			5		SP-SM
S-7	63	*-56*	4.61	0.659	60	60	40	140	21			9		SP-SM
S-8	73	*-66*	5.20	0.620				122	22	54	34	79	2.20	CH
S-9	83	*-76*	5.79	0.588				121	26	60	43	61	2.40	CH
S-10	93	*-86*	6.46	0.556	22	22	12	130	16	29	13	31		SC
S-11	103	*-96*	7.19	0.527	39	39	21	135	17			34		
S-12	113	*-106*	7.92	0.503	42	42	21	135	24			17		SM
S-13	123	*-116*	8.54	0.484	18	18	9	125	17	46	28	84		CL
S-14	133	*-126*	9.27	0.465	45	45	21	135	24			21		SM
S-15	143	*-136*	10.04	0.446	81	81	36	140	20			14		SM
S-16	153	*-146*	10.62	0.434				120	23	71	43	98	2.22	CH
S-17	163	*-156*	11.20	0.423				120	26	47	30	55		CL
S-18	173	*-166*	11.77	0.412	33	33	14	120	24	68	47	99		CH

Table B4. Summary of field and laboratory data for boring B-4.

Field Data								Laboratory Data						
			Blow Count Adjustments											
Sample Number	Depth, ft	Elevation, ft (MSL)	Effective Overburden, ksf	C_n	SPT N value	Rod Length Correction	$(N_1)_{60}$	Unit Weight, pcf	Moisture Content, %	Liquid Limit	Plastic Index	% Passing #200 Sieve	Average S_u, ksf	Classification
S-1	8	*-1*	0.80	1.581	31	23	37	100	*18*			*6*		SP-SM
S-2	18	*-11*	1.53	1.145	25	25	29	135	17			7		SP-SM
S-3	28	*-21*	2.20	0.953	12	12	11	130	16			8		SP-SM
S-4	38	*-31*	2.93	0.826	33	33	27	135	23			5		SP-SM
S-5	48	*-41*	3.55	0.750	12	12	9	125	24			20		SM
S-6	58	*-51*	4.33	0.680	45	45	31	140	24			11		SP-SM
S-7	63	*-56*	4.67	0.655	22	22	14	130	20			8		SP-SM
S-8	68	*-61*	5.03	0.631	36	36	23	135	22			8		SP-SM
S-9	78	*-71*	5.69	0.593				128	19	85	65	58	1.20	CH
S-10	83	*-76*	5.98	0.578				121	33	79	53	95	1.64	CH
S-11	88	*-81*	6.26	0.565				119	29	71	50	77	2.36	CH
S-12	93	*-86*	6.57	0.552				124	25	53	36	88	2.19	CH
S-13	98	*-91*	6.96	0.536	45	45	24	140	22			41		SM
S-14	103	*-96*	7.23	0.526				116	33	77	54	86	2.78	CH
S-15	108	*-101*	7.50	0.517				116	19			13		SM
S-16	118	*-111*	8.22	0.493	30	30	15	135	24			46		
S-17	123	*-116*	8.52	0.484				123	20	35	19	67		CL
S-18	128	*-121*	8.83	0.476				123	33	81	59	73	3.60	CH
S-19	133	*-126*	9.18	0.467				132	19	48	32	63	1.98	CL
S-20	143	*-136*	9.95	0.448	64	64	29	140	25			13		SM
S-21	153	*-146*	10.53	0.436				120	33	71	54	91	1.48	CH
S-22	158	*-151*	10.82	0.430				120	31	76	50	79	0.97	CH
S-23	163	*-156*	11.10	0.424				120	37			76		CH
S-24	168	*-161*	11.39	0.419				120	29	69	47	93		CH
S-25	173	*-166*	11.68	0.414				120	31	77	54	83	2.80	CH
S-26	178	*-171*	11.97	0.409				120	30	70	48	96		CH
S-27	183	*-176*	12.33	0.403	27	27	11	135	26			94		
S-28	193	*-186*	13.06	0.391	35	35	14	135	18			54		

Table B5. Summary of field and laboratory data for boring B-5.

Field Data								Laboratory Data						
			Blow Count Adjustments											
Sample Number	Depth, ft	Elevation, ft (MSL)	Effective Overburden, ksf	C_n	SPT N value	Rod Length Correction	$(N_1)_{60}$	Unit Weight, pcf	Moisture Content, %	Liquid Limit	Plastic Index	% Passing #200 Sieve	Average S_u, ksf	Classification
	6	-1	0.6	1.826				100						
S-1	8	-3	0.75	1.638	18	13.5	22	135	14			1		SP
S-2	18	-13	1.42	1.186	9	9	11	130	23			6		SP-SM
S-3	28	-23	2.20	0.954	45	45	43	140	21			3		SP
S-4	38	-33	2.87	0.834	14	14	12	130	22			6		SP-SM
S-5	48	-43	3.50	0.756	1	1	1	125	22			9		SP-SM
S-6	58	-53	4.13	0.696				125						SM
S-7	63	-58	4.51	0.666	50	50	33	140	17			26		SM
S-8	68	-63	4.83	0.644				125	23	47	31	65		CL
S-9	73	-68	5.14	0.624				125	18	37	22	57		CL
S-10	78	-73	5.42	0.608				118	30	90	77	99	2.30	CH
S-11	83	-78	5.75	0.590	13	13	8	130	22			60		CL
S-12	94	-89	6.55	0.552	38	38	21	135	20			44		SM
S-13	103	-98	7.16	0.528	22	22	12	130	32			96		CH
S-14	108	-103	7.41	0.519				113	30	72	45	97	1.68	CH
S-15	118	-113	8.09	0.497	23	23	11	130	22			75		CL
S-16	128	-123	8.77	0.478	30	30	14	130	20			46		
S-17	138	-133	9.54	0.458	56	56	26	140	23			10		SP-SM
S-18	148	-143	10.12	0.445				120	27	74	52	98		CH
S-19	153	-148	10.41	0.438				120	19	56	36	99		CH
S-20	158	-153	10.69	0.432				120	29	71	45	99	1.56	CH
S-21	163	-158	10.98	0.427				120	25	66	47	99	2.37	CH
S-22	168	-163	11.32	0.420				130	21	53	37	67		CH
S-23	173	-168	11.66	0.414	25	25	10	130	25			95		CH
S-24	178	-173	11.99	0.408				130						
S-25	173	-168	11.63	0.415	35	35	15	135	30			99		CH
S-26	188	-183	12.65	0.398	23	23	9	130	26			99		CL
S-27	198	-193	13.32	0.387	19	19	7	130	26			97		CL

Table B6. Summary of field and laboratory data for boring B-6.

Field Data								Laboratory Data						
			Blow Count Adjustments											
Sample Number	Depth, ft	Elevation, ft (MSL)	Effective Overburden, ksf	C_n	SPT N value	Rod Length Correction	$(N_1)_{60}$	Unit Weight, pcf	Moisture Content, %	Liquid Limit	Plastic Index	% Passing #200 Sieve	Average S_u, ksf	Classification
WT	7	-1	0.7					100						
S-1	8	-2	0.77	1.609	23	17.25	28	135	19			2		SP
S-2	18	-12	1.40	1.196	7	7	8	125	16			1		SP
S-3	28	-22	2.07	0.982	15	15	15	130	17			6		SP-SM
S-4	38	-32	2.70	0.861	8	8	7	125	25			2		SP
S-5	49	-43	3.47	0.760				132	22	32	18	54	1.76	CL
S-6	58	-52	4.12	0.697	40	40	28	135	23			7		SP-SM
S-7	68	-62	4.90	0.639	52	52	33	140	25			15		SM
S-8	78	-72	5.44	0.606				117	12	69	44	93	1.14	CH
S-9	88	-82	5.99	0.578				117	32	59	38	76		CH
S-10	98	-92	6.61	0.550	15	15	8	125	28			54		CL
S-11	108	-102	7.34	0.522	43	43	22	135	20			17		SM
S-12	118	-112	7.97	0.501	12	12	6	125	21			42		SM
S-13	128	-122	8.69	0.480	53	53	25	135	22			50		SC
S-14	138	-132	9.42	0.461	48	48	22	135	21			16		SM
S-15	148	-142	10.14	0.444				135	22					SM
S-16	153	-147	10.47	0.437				128	23	57	37	93	3.61	CH
S-17	163	-157	11.15	0.424				130	19	31	13	20		SC
S-18	173	-167	11.82	0.411	33	33	14	130	24			99		CH

Table B7. Summary of field and laboratory data for boring B-7.

Field Data								Laboratory Data						
			Blow Count Adjustments											
Sample Number	Depth, ft	Elevation, ft (MSL)	Effective Overburden, ksf	C_n	SPT N value	Rod Length Correction	$(N_1)_{60}$	Unit Weight, pcf	Moisture Content, %	Liquid Limit	Plastic Index	% Passing #200 Sieve	Average S_u, ksf	Classification
WT	7	-1	0.7	1.690				100						
S-1	8	-2	0.77	1.609	24	18	29	135	19			4		SP
S-2	18	-12	1.45	1.175	14	14	16	130	15			5		SP-SM
S-3	28	-22	2.07	0.982	8	8	8	125	13			3		SP
S-4	38	-32	2.80	0.845	27	27	23	135	22			9		SP-SM
S-5	48	-42	3.43	0.764				125	29	60	38	92		CH
S-6	58	-52	4.20	0.690	81	81	56	140	20			9		SP-SM
S-7	68	-62	4.88	0.640	30	30	19	130	11			22		SM
S-8	73	-67	5.18	0.622				122	22	65	42	99	2.18	CH
S-9	78	-72	5.46	0.605				119	28	78	50	90	1.92	CH
S-10	83	-77	5.77	0.589				125	37	74	49	81	2.78	CH
S-11	88	-82	6.09	0.573				125	23	60	41	69	1.53	CH
S-12	93	-87	6.40	0.559				125	21	47	32	51		CL
S-13	103	-97	7.12	0.530	48	48	25	135	17			29		SC
S-14	113	-107	7.80	0.506	24	24	12	130	24			51		CL
S-15	123	-117	8.38	0.489				120	22	34	19	48	0.70	SC
S-16	133	-127	9.05	0.470	37	37	17	130	18			22		SM
S-17	143	-137	9.73	0.453	25	25	11	130	28			97		CH
S-18	148	-142	10.03	0.447				123	23			74	2.74	CH
S-19	153	-147	10.33	0.440				123	29	77	53	98		CH
S-20	163	-157	11.01	0.426	25	25	11	130	29			96		CH
S-21	168	-162	11.35	0.420	29	29	12	130	28			99		CH
S-22	173	-167	11.64	0.415				120	27	70	46	96	2.88	CH
S-23	178	-172	11.95	0.409				125	21	34	17	93	1.14	CL
S-24	188	-182	12.63	0.398	24	24	10	130	22			81		CL
S-25	198	-192	13.25	0.388	18	18	7	125	19			64		CL

Table B8. Summary of field and laboratory data for boring B-8.

Field Data								Laboratory Data						
			Blow Count Adjustments											
Sample Number	Depth, ft	Elevation, ft (MSL)	Effective Overburden, ksf	C_n	SPT N value	Rod Length Correction	$(N_1)_{60}$	Unit Weight, pcf	Moisture Content, %	Liquid Limit	Plastic Index	% Passing #200 Sieve	Average S_u, ksf	Classification
S-1	3	1	0.30	2.582	38	29	74	100	13			6		SP-SM
WT	4.5	-1	0.54	1.925	38	29	55	120						SP-SM
S-2	13	-9	1.16	1.315	21	21	28	135	23			9		SP-SM
S-3	23	-19	1.88	1.031	21	21	22	135	22			10		SP-SM
S-4	33	-29	2.61	0.876	33	33	29	135	24			8		SP-SM
S-5	43	-39	3.29	0.780	14	14	11	130	18			13		SM
S-6	53	-49	3.98	0.709				132	33			74		CH
S-7	63	-59	4.71	0.652	37	37	24	135	23			13		SM
S-8	73	-69	5.28	0.615	17	17	10	120	20			76		CH
S-9	83	-79	5.85	0.585				119	31	78	51	89	1.60	CH
S-10	93	-89	6.43	0.558	10	10	6	120	20			72		CH
S-11	103	-99	7.15	0.529	44	44	23	135	24			17		SM
S-12	113	-109	7.83	0.505	27	27	14	130	20			23		SM
S-13	123	-119	8.45	0.486				125	22	30	11	55		CL
S-14	133	-129	9.13	0.468				130	23			16		SM
S-15	143	-139	9.74	0.453				123	27	77	51	92		CH
S-16	153	-149	10.34	0.440	32	32	14	123	19			72		CH
S-17	163	-159	11.12	0.424	78	78	33	140	20			14		SM
S-18	173	-169	11.79	0.412	36	36	15	130	19			86		CH

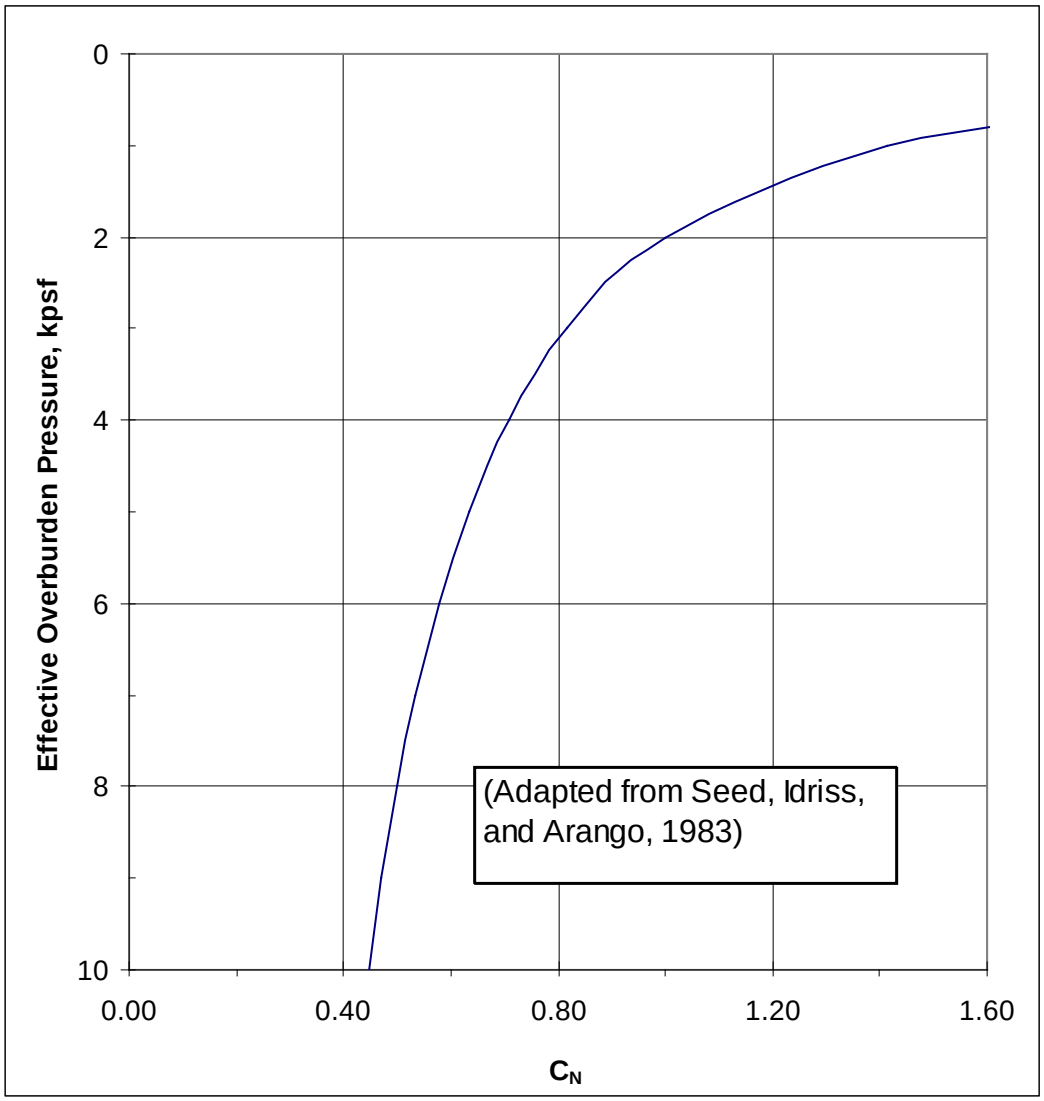

Figure B1. Overburden correction factor, CN, to adjust measured blow counts to overburden stress conditions of 1.0 tsf.

Appendix C: Geotechnical Cross-sections for Analyses

This appendix contains tables of material properties used for the analyses of the eight borings (Tables C1 through C8) and their associated cross-sections used for analysis.

Table C1. Geotechnical cross section for Boring B-1 and properties used for deterministic and probabilistic analyses.

	Deterministic Analysis					Probabilistic Analysis			
			Undrained	Drained			Drained		
Depth, ft	Profile	Unit Weight, pcf	Shear Strength Parameters	Friction Angle, degrees	Cohesion, psf	Profile	Unit Weight, pcf	Friction Angle	Cohesion
5	1 - Sand	130	F=37° c=0 psf	37	0	1 - Sand	130	37	0
8									
18									
28	2 - Sand	130	F=37° c=0 psf	37	0				
38									
43	3 - Clay	120	F=0° c = 1.9 psf	21	140	2 - Clay	120	21	140
48	4 - Sand	130	F=37° c=0 psf	37	0	3 - Sand	130	37	0
58									
68	5 - Clay	124	F=0° c = 1300 psf	22	120	4 - Clay	122	21	135
73									
78	6 - Clay	120	F=0° c = 2150	20	150				
83									
88	7 - Sand	125	F=34° c = 0 psf	34	0	5 - Sand	130	34	0
93	8 - Clay	124	F=0° c= 4200 psf	24	100	6 - Clay	124	24	100
98									
108	9 - Sand	125	F=34° c = 0 psf	34	0	7 - Sand	125	34	0
118	10 - Clay	125	3600	19	150	8 - Clay	125	19	150
123									
128	11 - Sand	125	F=0° c = 34 psf	34	0	9 - Sand	125	34	0
138									
148	12 - Clay	123	F=0° c= 1670	21	120	10 - Clay	124	22	120
153									
158									
163	13 - Clay	125	F=0° c= 3600 psf	22	120				
168									
173									
178									
188									
198	14 - Sand	125	34	34	0	11 - Sand	125	34	V Strong

Table C2. Geotechnical cross section for Boring B-2 and properties used for deterministic and probabilistic analyses.

	Deterministic Analysis				
			Undrained	Drained	
Depth, ft	Profile	Unit Weight, pcf	Shear Strength Parameters	Friction Angle, Degrees	Cohesion, psf
7	1 - Sand	130	F = 38° c = 0 psf	38	0
8					
18					
28	2 - Sand	130	F = 38° c = 0 psf	38	0
38					
48	3 - Clay	120	F = 0° c = 2500 psf	20	150
58	4 - Sand	138	F = 38° c = 0 psf	38	0
68					
78	5 - Clay	117	F = 0° c =2370 psf	22	130
88					
98					
108	6 - Sand	125	F =33 ° c = 0 psf	33	0
118					
128					
138					
148	7 - Clay	123	F = 0 ° c = 2170 psf	20	150
158					
168					

Table C3. Geotechnical cross section for Boring B-3 and properties used for deterministic and probabilistic analyses.

Depth, ft	Deterministic Analysis					Probabilistic Analysis			
			Undrained	Drained			Drained		
	Profile	Unit Weight, pcf	Shear Strength Parameters	Friction Angle, Degrees	Cohesion, psf	Profile	Unit Weight, pcf	Friction Angle	Cohesion
3	1 - Sand	130	F=38° c= 0 psf	38	0	1 - Sand	130	38	0
13									
23	2 - Sand	130	F=38° c= 0 psf	38	0				
33									
43									
53	3 - Sand	130	F=38° c= 0 psf	38	0				
63									
73	4 - Clay	122	F=0° c=2300 psf	22	110	2 - Clay	122	22	110
83									
93	5 - Sand	125	F=35° c=0 psf	35	0	3 - Sand	125	35	0
103									
113									
123	6 - Clay	125	F=0° c=3500 psf	25	80	4 - Clay	125	25	80
133	7- Sand	125	F=35° c = 0 psf	35	0	5 - Sand	125	35	0
143									
153	8 - Clay	120	F=35° c = 2220 psf	22	110	6 - Clay	120	22	110
163									
173									

Table C4. Geotechnical cross section for Boring B-4 and properties used for deterministic and probabilistic analyses.

Depth, ft	Deterministic Analysis				
			Undrained	Drained	
	Profile	Unit Weight, pcf	Shear Strength Parameters	Friction Angle, Degrees	Cohesion, psf
8	1 - Sand	130	F=37° c=0 psf	37	0
18					
28					
38	2 - Sand	130	F=37° c=0 psf	37	0
48					
58	3 - Sand	130	F=37° c=0 psf	37	0
63					
68					
78	4 - Clay	125	F=0° c=1420	19	180
83					
88	5 - Clay	122	F=0° c=2250	20	150
93					
98	6 - Sand	125	F=33° c=0 psf	33	0
103	7 - Clay	116	F=0° c=2780	19	160
108	8 - Sand	125	F=33° c=0 psf	33	0
118					
123	9 - Clay	126	F=0° c=3000	22	120
128					
133					
143	10 - Sand	125	F=33° c=0	33	
153	11 - Clay	120	F=0° c=1140	20	150
158					
163					
168	12 - Clay	120	F=0° c=2800	20	150
173					
178					
183					
193	13 - Sand	125	F=33° c=0 psf	33	0

Table C5. Geotechnical cross section for Boring B-5 and properties used for deterministic and probabilistic analyses.

Depth, ft	Deterministic Analysis				
			Undrained	Drained	
	Profile	Unit Weight, pcf	Shear Strength Parameter	Friction Angle, Degrees	Cohesion, psf
6	1 - Sand	100	F=35 ° c= 0 psf	35	0
8	2 - Sand	130	F=35 ° c= 0 psf	35	0
18					
28					
38					
48	3 - Sand	130	F=35 ° c= 0 psf	35	0
58	4 - Sand	130	F=35 ° c= 0 psf	35	0
63					
68	5 - Clay	125	F=0 ° c= 1250 psf	25	80
73					
78	6 - Clay	118	F=0° c= 2300 psf	18	230
83	7 - Clay	130	F=0° c= 1250 psf	25	80
94	8 - Sand	125	F=36 ° c=0 psf	36	0
103	9 - Clay	113	F=0° c= 1680 psf	21	140
108					
118	10 - Clay	130	F=0° c= 2000 psf	25	80
128					
138	11 - Sand	125	F=36 ° c= 0 psf	36	0
148	12 - Clay	120	F=0° c= 1960 psf	21	140
153					
158					
163					
168	13 - Clay	130	F= 0° c= 2500 psf	21	140
173					
178					
173					
188	14 - Clay	130	F=0° c= 3500 psf	21	140
198					

Table C6. Geotechnical cross section for Boring B-6 and properties used for deterministic and probabilistic analyses.

Depth, ft	Deterministic Analysis				
			Undrained	Drained	
	Profile	Unit Weight, pcf	Shear Strength Parameters	Friction Angle, degrees	Cohesion, psf
7	1 - Sand	130	F=37 ° c = 0 psf	37	0
8					
18					
28	2 - Sand	130	F=37 ° c= 0 psf	37	0
38					
49	3 - Clay	132	F= 0° c=1760 psf	28	60
58	4 - Sand	130	F=37 c=0 psf	37	0
68					
78	5 - Clay	117	F= 0° c=1140 psf	21	100
88					
98	6 - Clay	130	F= 0° c=2000 psf	22	120
108	7 - Sand	125	F=35 ° c=0 psf	35	0
118					
128	8 - Sand	125	F=35 ° c=0 psf	35	0
138	9 - Sand	125	F=35 ° c=0 psf	35	0
148					
153	10 - Clay	131	F= 0° c = 3610 psf	20	150
163					
173					

Table C7. Geotechnical cross section for Boring B-7 and properties used for deterministic and probabilistic analyses.

	Deterministic Analysis					Probabilistic Analysis			
			Undrained	Drained			Drained		
Depth, ft	Profile	Unit Weight, pcf	Shear Strength Parameters	Friction Angle, degrees	Cohesion, psf	Profile	Unit Weight, pcf	Friction Angle, degrees	Cohesion, psf
7	1 - Sand	100	F=35 ^{o} c = 0 psf	35	0	1 - Sand	125	33.5	14
8	2 - Sand	130	F=35 ^{o} c= 0 psf	35	0				
18									
28									
38									
48	3 - Clay	125	F= 0^{o} c= 1900 psf	22	110	2 - Clay	125	22	110
58	4 - Sand	130	F=35 ^{o} C = 0 psf	35	0	3 - Sand	130	35	0
68									
73	5 - Clay	123	F= 0^{o} c= 2100 psf	21	120	4 - Clay	123	21	120
78									
83									
88									
93									
103	6 - Sand	125	F=32 ^{o} c= 0 psf	32	0	5 - Sand	125	32	0
113	7 - Clay	125	F= 0^{o} c =700	24	90	6 - Clay	125	24	90
123									
133	8 - Sand	125	F=32 ^{o} c=0 psf	32	0	7 - Sand	125	32	0
143	9 - Clay	126	F= 0^{o} c= 2800 psf	20	150	8 - Clay	126	24	105
148									
153									
163									
168									
173									
178	10 - Clay	127	F= 0^{o} c=1200 psf	28	60				
188									
198									

Table C8. Geotechnical cross section for Boring B-8 and properties used for deterministic and probabilistic analyses.

Depth, ft	Deterministic Analysis				
			Undrained	Drained	
	Profile	Unit Weight, pcf	Shear Strength Parameters	Friction Angle, degrees	Cohesion, psf
3	1 - Sand	130	F=37° c= 0 psf	37	0
4.5					
13					
23					
33	2 - Sand	130	F=37° c= 0 psf	37	0
43					
53	3 - Clay	132	F=0° c=1800 psf	24	90
63	4 - Sand	130	F=37° c=0 psf	37	0
73	5 - Clay	120	F=0° c=1600 psf	20	150
83					
93					
103	6 - Sand	125	F=35° c= 0 psf	35	0
113					
123	7 - Clay	125	F=0° c=3500 psf	30	40
133	8 - Sand	125	F=35° C= 0 psf	35	0
143	9 - Clay	123	F=0° c= 2740 psf	20	150
153					
163	10 - Sand	125	F=35° c= 0 psf	35	0
173	11 - Clay	130	F=0° c= 3000 psf	21	140

Appendix D: Slope Stability Analysis Results

Introduction

A summary of all undrained and drained slope stability analyses for boring B-1 through B-8 are presented in a graphical format (Figures D1 through D17). There is a figure for each boring that contains the critical failure surface for the three depths analyzed (100, 130, and 150 ft) and an embedded table showing the engineering properties used for each analysis.

Undrained analyses

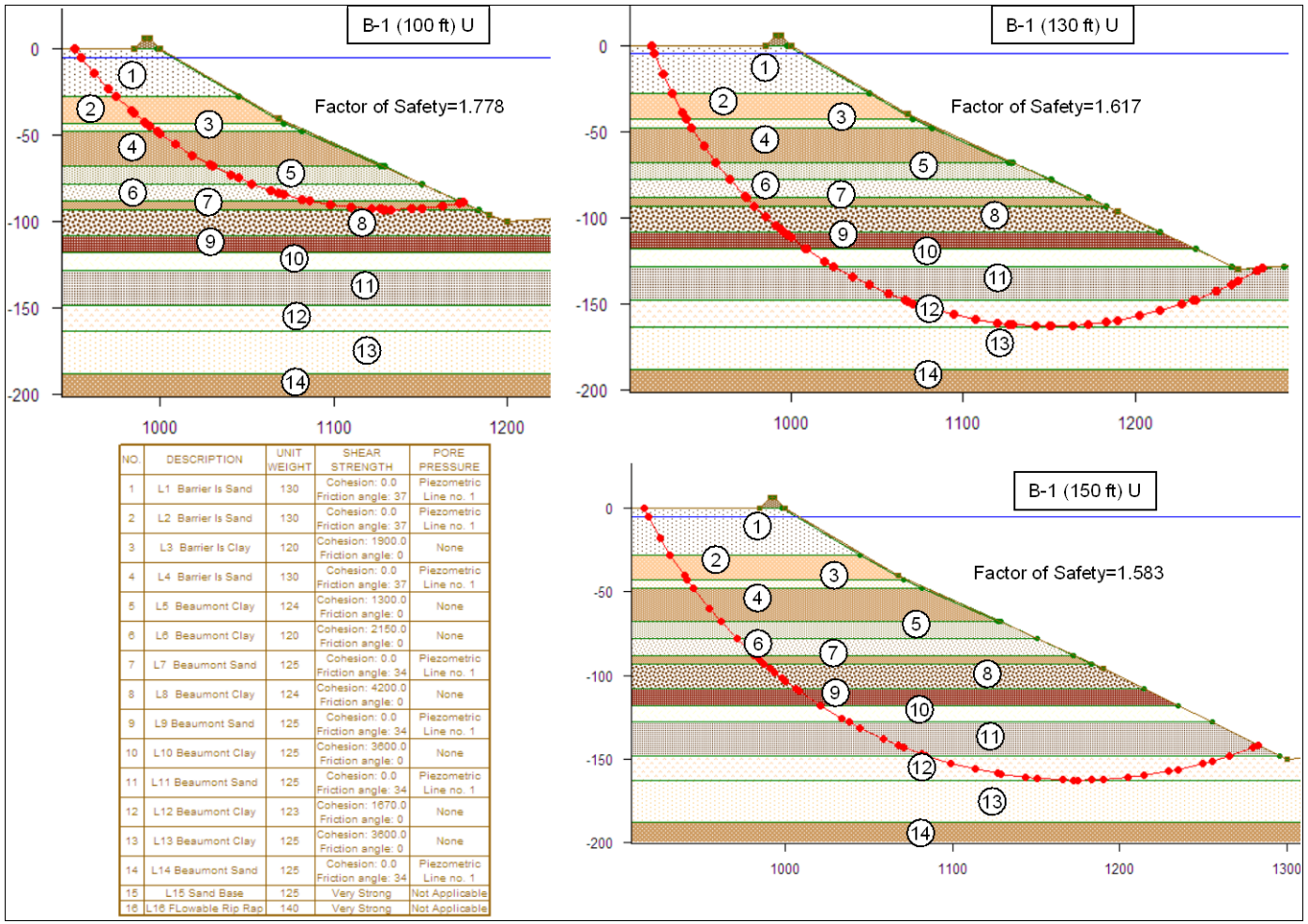

NO.	DESCRIPTION	UNIT WEIGHT	SHEAR STRENGTH	PORE PRESSURE
1	L1 Barrier Is Sand	130	Cohesion: 0.0 Friction angle: 37	Piezometric Line no. 1
2	L2 Barrier Is Sand	130	Cohesion: 0.0 Friction angle: 37	Piezometric Line no. 1
3	L3 Barrier Is Clay	120	Cohesion: 1900.0 Friction angle: 0	None
4	L4 Barrier Is Sand	130	Cohesion: 0.0 Friction angle: 37	Piezometric Line no. 1
5	L5 Beaumont Clay	124	Cohesion: 1300.0 Friction angle: 0	None
6	L6 Beaumont Clay	120	Cohesion: 2150.0 Friction angle: 0	None
7	L7 Beaumont Sand	125	Cohesion: 0.0 Friction angle: 34	Piezometric Line no. 1
8	L8 Beaumont Clay	124	Cohesion: 4200.0 Friction angle: 0	None
9	L9 Beaumont Sand	125	Cohesion: 0.0 Friction angle: 34	Piezometric Line no. 1
10	L10 Beaumont Clay	125	Cohesion: 3600.0 Friction angle: 0	None
11	L11 Beaumont Sand	125	Cohesion: 0.0 Friction angle: 34	Piezometric Line no. 1
12	L12 Beaumont Clay	123	Cohesion: 1670.0 Friction angle: 0	None
13	L13 Beaumont Clay	125	Cohesion: 3600.0 Friction angle: 0	None
14	L14 Beaumont Sand	125	Cohesion: 0.0 Friction angle: 34	Piezometric Line no. 1
15	L15 Sand Base	125	Very Strong	Not Applicable
16	L16 FLowable Rip Rap	140	Very Strong	Not Applicable

Figure.D1. Stability analyses using undrained properties for boring B-1 showing critical failure surface at 100, 130, and 150 ft depths and property table.

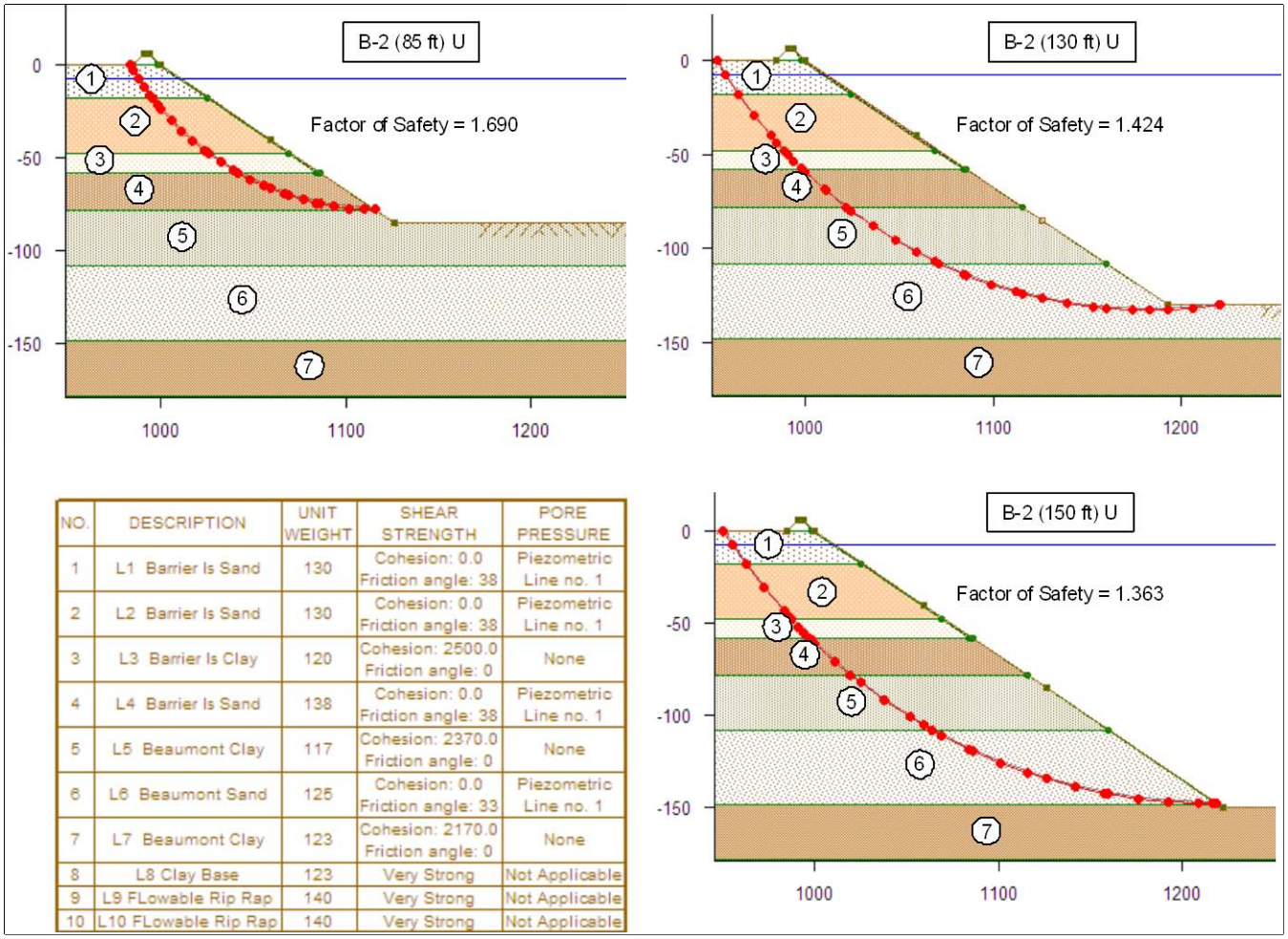

NO.	DESCRIPTION	UNIT WEIGHT	SHEAR STRENGTH	PORE PRESSURE
1	L1 Barrier Is Sand	130	Cohesion: 0.0 Friction angle: 38	Piezometric Line no. 1
2	L2 Barrier Is Sand	130	Cohesion: 0.0 Friction angle: 38	Piezometric Line no. 1
3	L3 Barrier Is Clay	120	Cohesion: 2500.0 Friction angle: 0	None
4	L4 Barrier Is Sand	138	Cohesion: 0.0 Friction angle: 38	Piezometric Line no. 1
5	L5 Beaumont Clay	117	Cohesion: 2370.0 Friction angle: 0	None
6	L6 Beaumont Sand	125	Cohesion: 0.0 Friction angle: 33	Piezometric Line no. 1
7	L7 Beaumont Clay	123	Cohesion: 2170.0 Friction angle: 0	None
8	L8 Clay Base	123	Very Strong	Not Applicable
9	L9 FLowable Rip Rap	140	Very Strong	Not Applicable
10	L10 FLowable Rip Rap	140	Very Strong	Not Applicable

Figure D2. Stability analyses using undrained properties for boring B-2 showing critical failure surface at 100, 130, and 150 ft depths and property table.

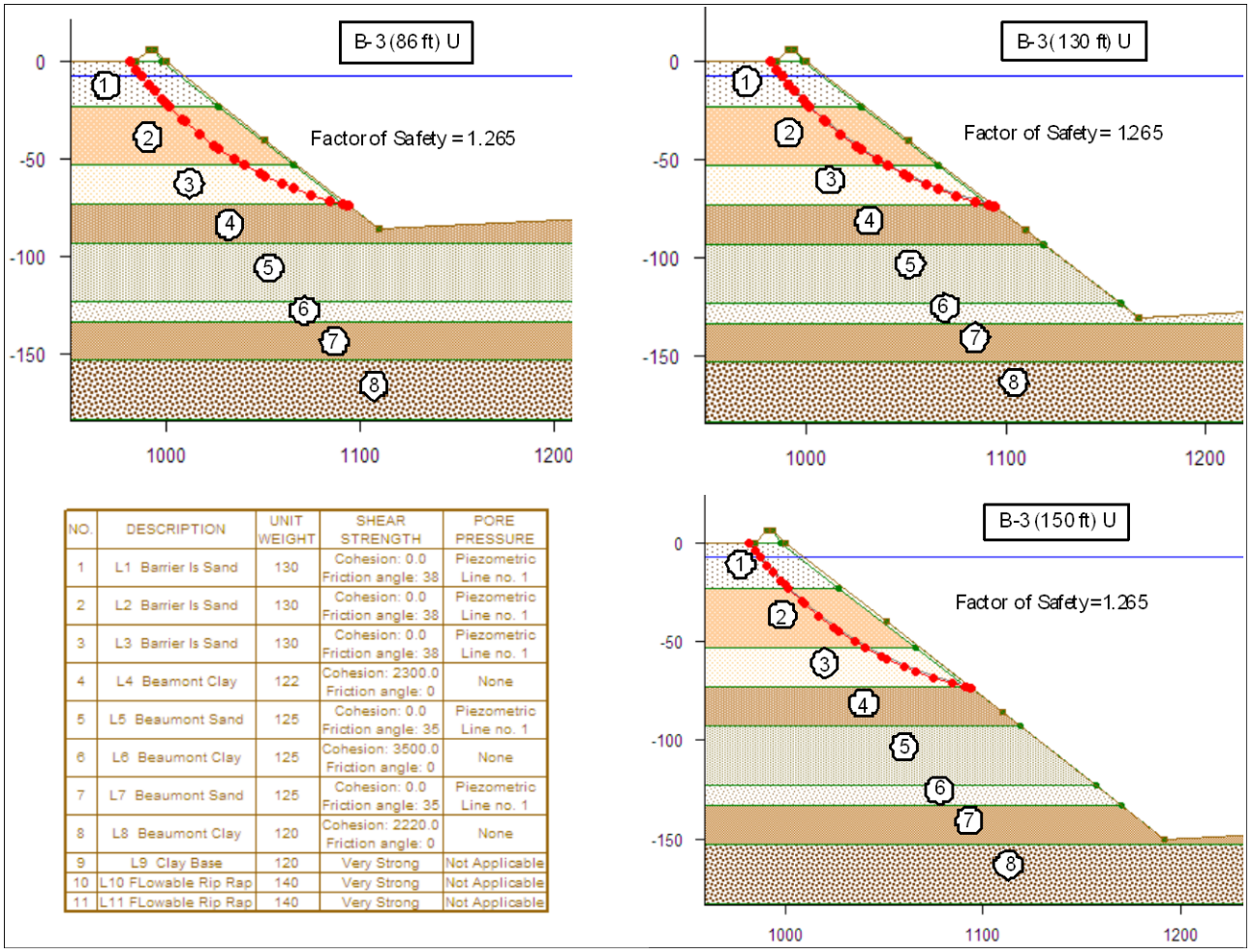

NO.	DESCRIPTION	UNIT WEIGHT	SHEAR STRENGTH	PORE PRESSURE
1	L1 Barrier Is Sand	130	Cohesion: 0.0 Friction angle: 38	Piezometric Line no. 1
2	L2 Barrier Is Sand	130	Cohesion: 0.0 Friction angle: 38	Piezometric Line no. 1
3	L3 Barrier Is Sand	130	Cohesion: 0.0 Friction angle: 38	Piezometric Line no. 1
4	L4 Beamont Clay	122	Cohesion: 2300.0 Friction angle: 0	None
5	L5 Beaumont Sand	125	Cohesion: 0.0 Friction angle: 35	Piezometric Line no. 1
6	L6 Beaumont Clay	125	Cohesion: 3500.0 Friction angle: 0	None
7	L7 Beaumont Sand	125	Cohesion: 0.0 Friction angle: 35	Piezometric Line no. 1
8	L8 Beaumont Clay	120	Cohesion: 2220.0 Friction angle: 0	None
9	L9 Clay Base	120	Very Strong	Not Applicable
10	L10 FLowable Rip Rap	140	Very Strong	Not Applicable
11	L11 FLowable Rip Rap	140	Very Strong	Not Applicable

Figure D3. Stability analyses using undrained properties for boring B-3 showing critical failure surface at 100, 130, and 150 ft depths and property table.

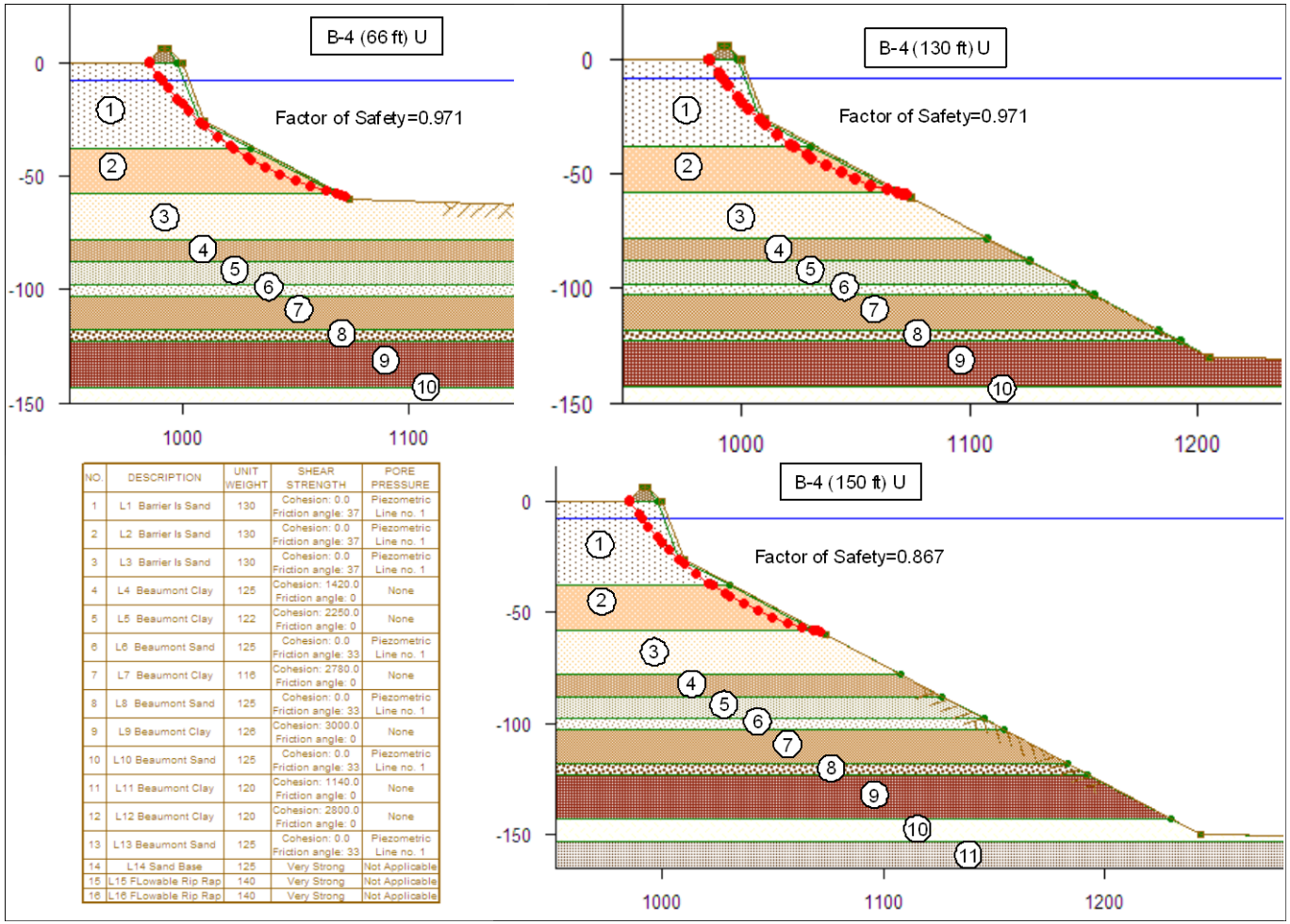

NO.	DESCRIPTION	UNIT WEIGHT	SHEAR STRENGTH	PORE PRESSURE
1	L1 Barrier Is Sand	130	Cohesion: 0.0 Friction angle: 37	Piezometric Line no. 1
2	L2 Barrier Is Sand	130	Cohesion: 0.0 Friction angle: 37	Piezometric Line no. 1
3	L3 Barrier Is Sand	130	Cohesion: 0.0 Friction angle: 37	Piezometric Line no. 1
4	L4 Beaumont Clay	125	Cohesion: 1420.0 Friction angle: 0	None
5	L5 Beaumont Clay	122	Cohesion: 2250.0 Friction angle: 0	None
6	L6 Beaumont Sand	125	Cohesion: 0.0 Friction angle: 33	Piezometric Line no. 1
7	L7 Beaumont Clay	116	Cohesion: 2780.0 Friction angle: 0	None
8	L8 Beaumont Sand	125	Cohesion: 0.0 Friction angle: 33	Piezometric Line no. 1
9	L9 Beaumont Clay	126	Cohesion: 3000.0 Friction angle: 0	None
10	L10 Beaumont Sand	125	Cohesion: 0.0 Friction angle: 33	Piezometric Line no. 1
11	L11 Beaumont Clay	120	Cohesion: 1140.0 Friction angle: 0	None
12	L12 Beaumont Clay	120	Cohesion: 2800.0 Friction angle: 0	None
13	L13 Beaumont Sand	125	Cohesion: 0.0 Friction angle: 33	Piezometric Line no. 1
14	L14 Sand Base	125	Very Strong	Not Applicable
15	L15 FLowable Rip Rap	140	Very Strong	Not Applicable
16	L16 FLowable Rip Rap	140	Very Strong	Not Applicable

Figure D4. Stability analyses using undrained properties for boring B-4 showing critical failure surface at 100, 130, and 150 ft depths and property table.

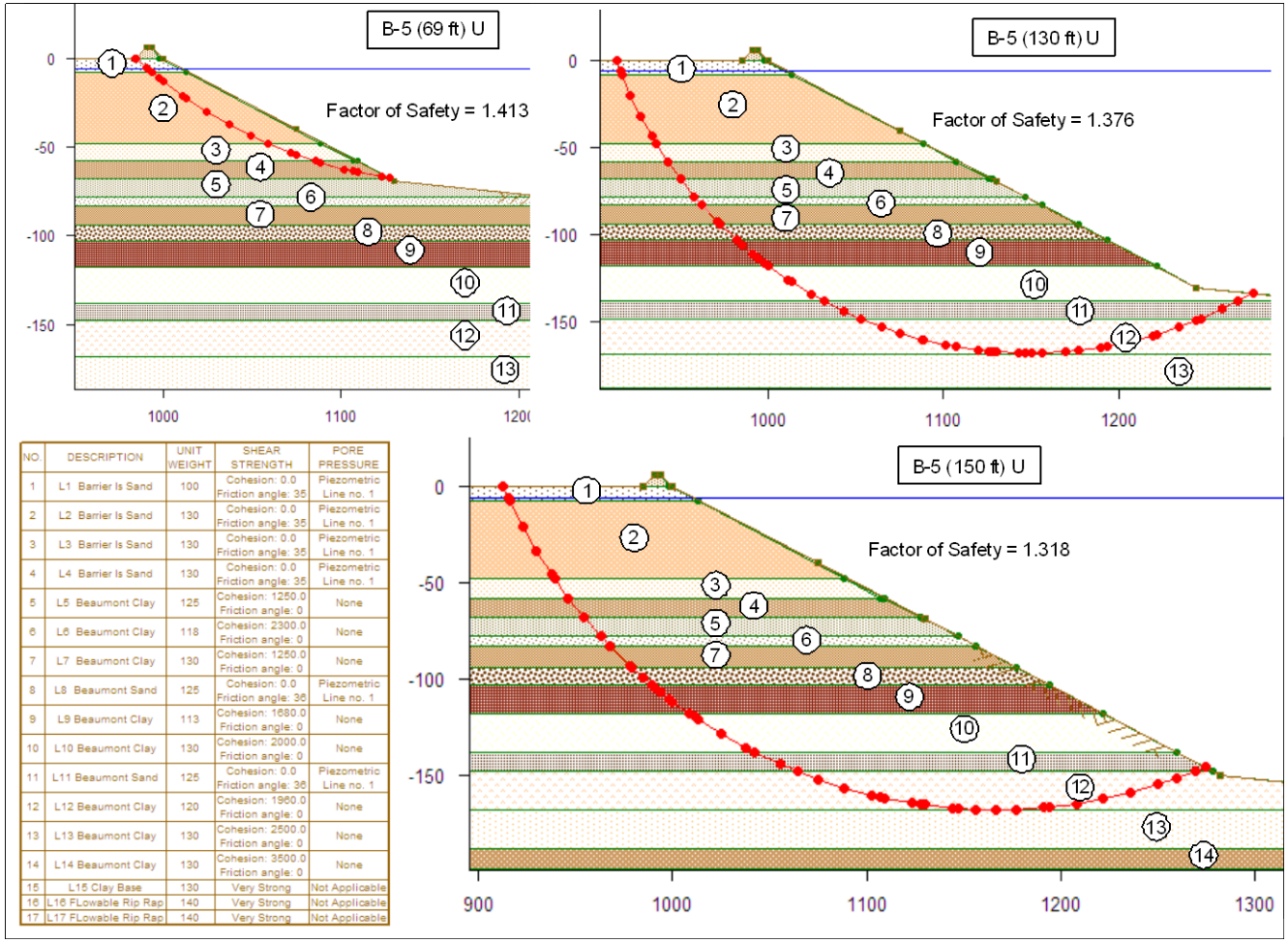

NO.	DESCRIPTION	UNIT WEIGHT	SHEAR STRENGTH	PORE PRESSURE
1	L1 Barrier Is Sand	100	Cohesion: 0.0 Friction angle: 35	Piezometric Line no. 1
2	L2 Barrier Is Sand	130	Cohesion: 0.0 Friction angle: 35	Piezometric Line no. 1
3	L3 Barrier Is Sand	130	Cohesion: 0.0 Friction angle: 35	Piezometric Line no. 1
4	L4 Barrier Is Sand	130	Cohesion: 0.0 Friction angle: 35	Piezometric Line no. 1
5	L5 Beaumont Clay	125	Cohesion: 1250.0 Friction angle: 0	None
6	L6 Beaumont Clay	118	Cohesion: 2300.0 Friction angle: 0	None
7	L7 Beaumont Clay	130	Cohesion: 1250.0 Friction angle: 0	None
8	L8 Beaumont Sand	125	Cohesion: 0.0 Friction angle: 36	Piezometric Line no. 1
9	L9 Beaumont Clay	113	Cohesion: 1680.0 Friction angle: 0	None
10	L10 Beaumont Clay	130	Cohesion: 2000.0 Friction angle: 0	None
11	L11 Beaumont Sand	125	Cohesion: 0.0 Friction angle: 36	Piezometric Line no. 1
12	L12 Beaumont Clay	120	Cohesion: 1960.0 Friction angle: 0	None
13	L13 Beaumont Clay	130	Cohesion: 2500.0 Friction angle: 0	None
14	L14 Beaumont Clay	130	Cohesion: 3500.0 Friction angle: 0	None
15	L15 Clay Base	130	Very Strong	Not Applicable
16	L16 FLowable Rip Rap	140	Very Strong	Not Applicable
17	L17 FLowable Rip Rap	140	Very Strong	Not Applicable

Figure D5. Stability analyses using undrained properties for boring B-5 showing critical failure surface at 100, 130, and 150 ft depths and property table.

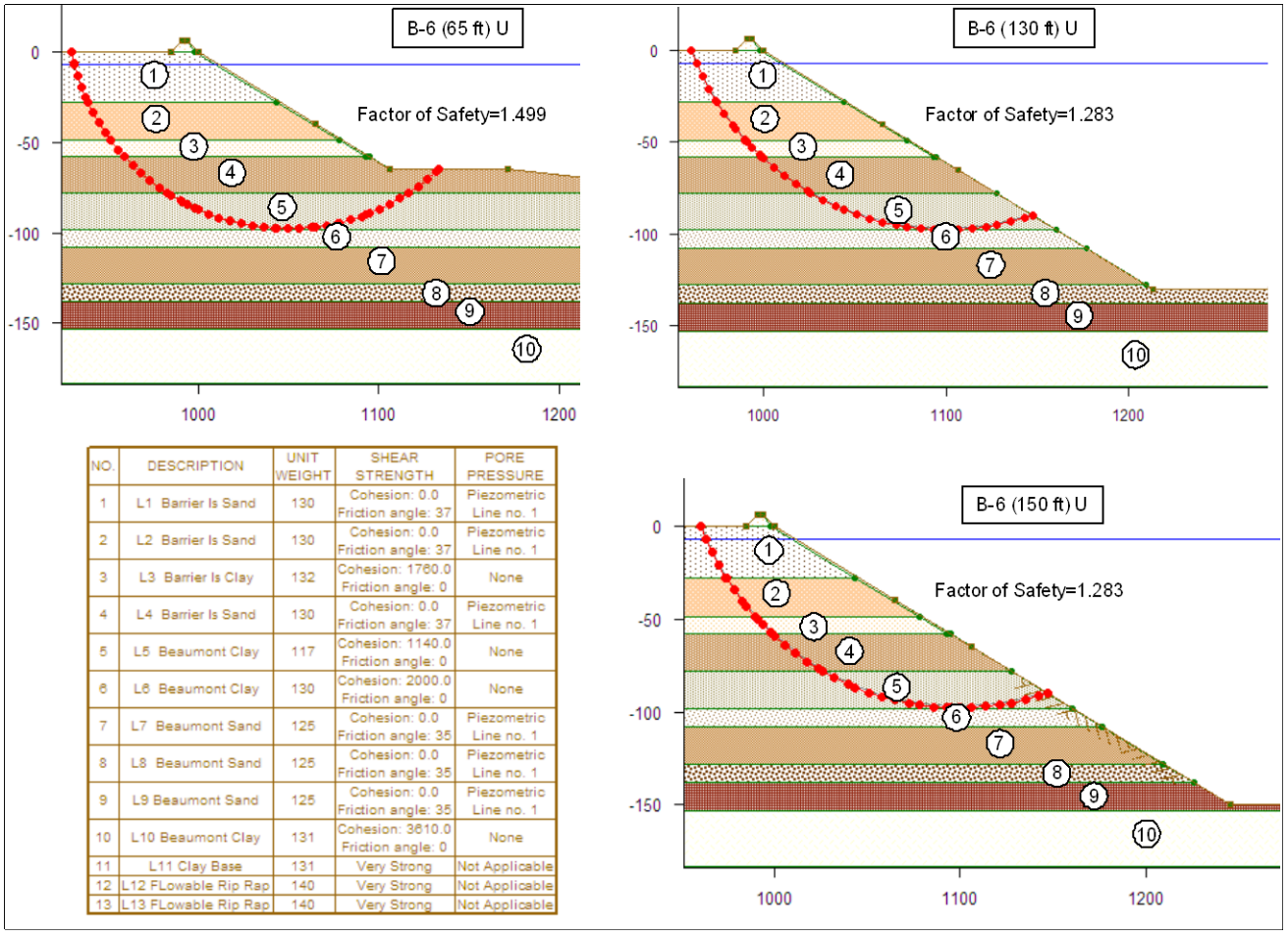

NO.	DESCRIPTION	UNIT WEIGHT	SHEAR STRENGTH	PORE PRESSURE
1	L1 Barrier Is Sand	130	Cohesion: 0.0 Friction angle: 37	Piezometric Line no. 1
2	L2 Barrier Is Sand	130	Cohesion: 0.0 Friction angle: 37	Piezometric Line no. 1
3	L3 Barrier Is Clay	132	Cohesion: 1760.0 Friction angle: 0	None
4	L4 Barrier Is Sand	130	Cohesion: 0.0 Friction angle: 37	Piezometric Line no. 1
5	L5 Beaumont Clay	117	Cohesion: 1140.0 Friction angle: 0	None
6	L6 Beaumont Clay	130	Cohesion: 2000.0 Friction angle: 0	None
7	L7 Beaumont Sand	125	Cohesion: 0.0 Friction angle: 35	Piezometric Line no. 1
8	L8 Beaumont Sand	125	Cohesion: 0.0 Friction angle: 35	Piezometric Line no. 1
9	L9 Beaumont Sand	125	Cohesion: 0.0 Friction angle: 35	Piezometric Line no. 1
10	L10 Beaumont Clay	131	Cohesion: 3610.0 Friction angle: 0	None
11	L11 Clay Base	131	Very Strong	Not Applicable
12	L12 FLowable Rip Rap	140	Very Strong	Not Applicable
13	L13 FLowable Rip Rap	140	Very Strong	Not Applicable

Figure D6. Stability analyses using undrained properties for boring B-6 showing critical failure surface 8at 100, 130, and 150 ft depths and property table.

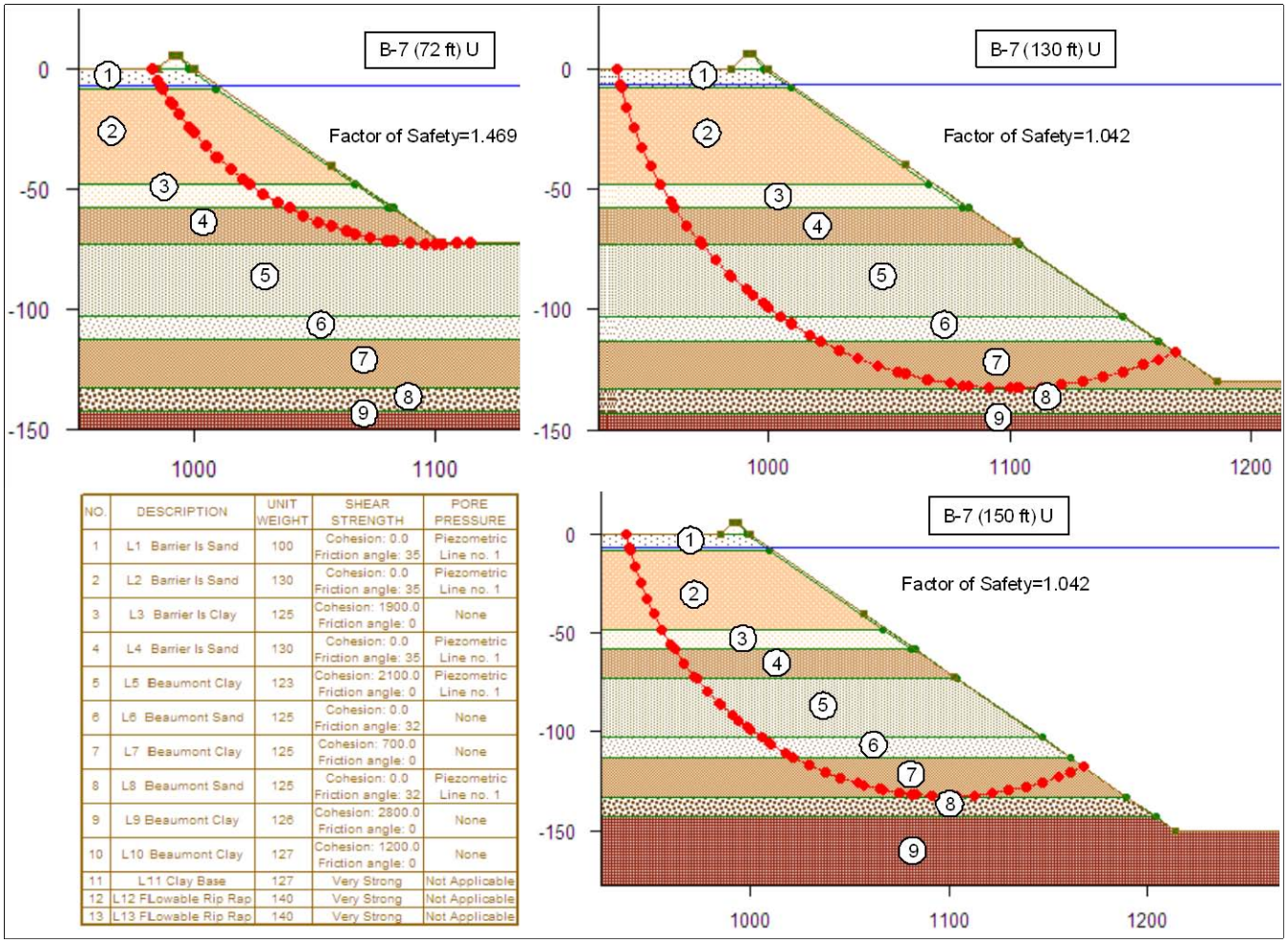

NO.	DESCRIPTION	UNIT WEIGHT	SHEAR STRENGTH	PORE PRESSURE
1	L1 Barrier Is Sand	100	Cohesion: 0.0 Friction angle: 35	Piezometric Line no. 1
2	L2 Barrier Is Sand	130	Cohesion: 0.0 Friction angle: 35	Piezometric Line no. 1
3	L3 Barrier Is Clay	125	Cohesion: 1900.0 Friction angle: 0	None
4	L4 Barrier Is Sand	130	Cohesion: 0.0 Friction angle: 35	Piezometric Line no. 1
5	L5 Beaumont Clay	123	Cohesion: 2100.0 Friction angle: 0	Piezometric Line no. 1
6	L6 Beaumont Sand	125	Cohesion: 0.0 Friction angle: 32	None
7	L7 Beaumont Clay	125	Cohesion: 700.0 Friction angle: 0	None
8	L8 Beaumont Sand	125	Cohesion: 0.0 Friction angle: 32	Piezometric Line no. 1
9	L9 Beaumont Clay	126	Cohesion: 2800.0 Friction angle: 0	None
10	L10 Beaumont Clay	127	Cohesion: 1200.0 Friction angle: 0	None
11	L11 Clay Base	127	Very Strong	Not Applicable
12	L12 FLowable Rip Rap	140	Very Strong	Not Applicable
13	L13 FLowable Rip Rap	140	Very Strong	Not Applicable

Figure D7. Stability analyses using undrained properties for boring B-7 showing critical failure surface at 100, 130, and 150 ft depths and property table.

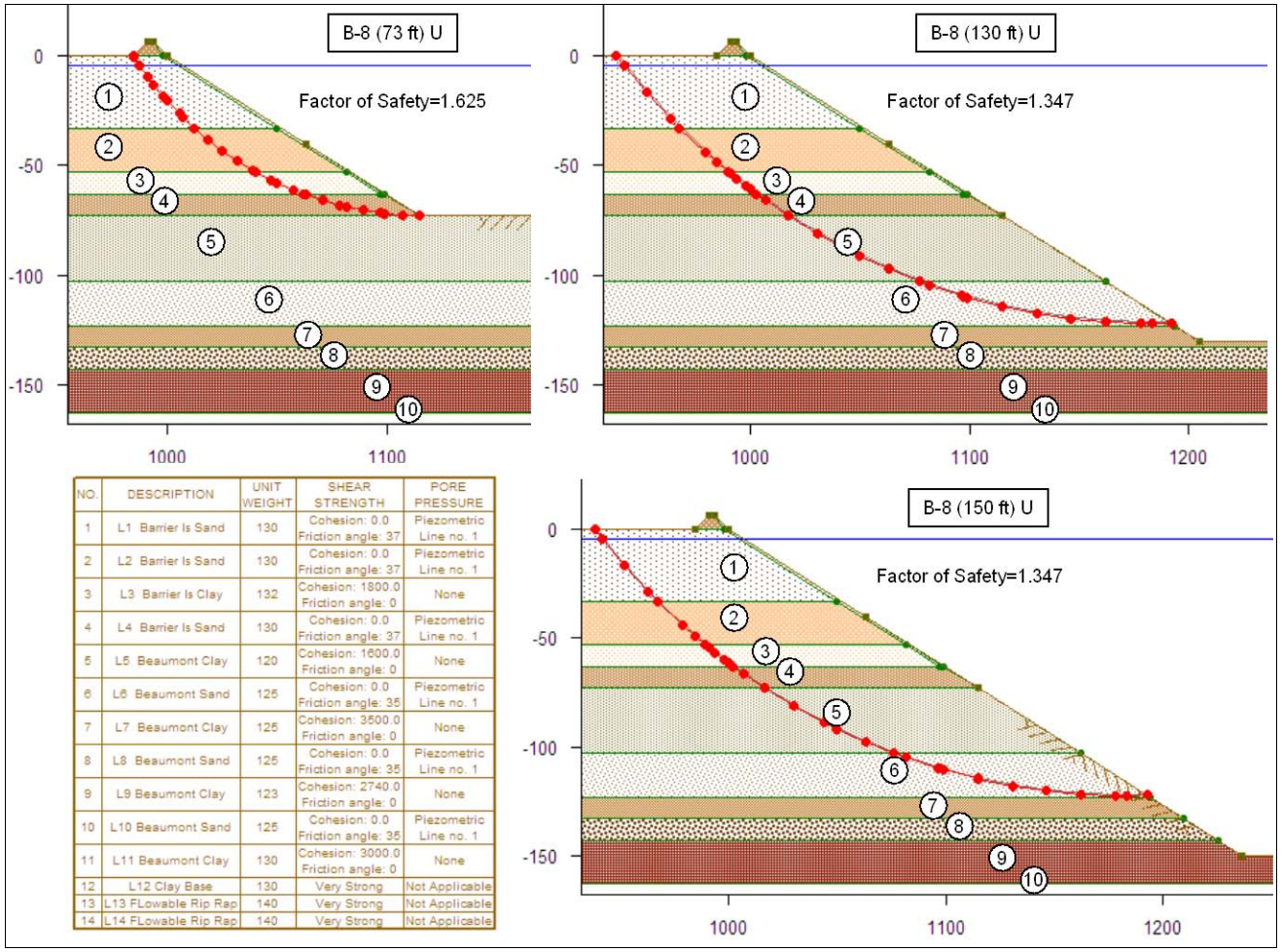

NO.	DESCRIPTION	UNIT WEIGHT	SHEAR STRENGTH	PORE PRESSURE
1	L1 Barrier Is Sand	130	Cohesion: 0.0 Friction angle: 37	Piezometric Line no. 1
2	L2 Barrier Is Sand	130	Cohesion: 0.0 Friction angle: 37	Piezometric Line no. 1
3	L3 Barrier Is Clay	132	Cohesion: 1800.0 Friction angle: 0	None
4	L4 Barrier Is Sand	130	Cohesion: 0.0 Friction angle: 37	Piezometric Line no. 1
5	L5 Beaumont Clay	120	Cohesion: 1600.0 Friction angle: 0	None
6	L6 Beaumont Sand	125	Cohesion: 0.0 Friction angle: 35	Piezometric Line no. 1
7	L7 Beaumont Clay	125	Cohesion: 3500.0 Friction angle: 0	None
8	L8 Beaumont Sand	125	Cohesion: 0.0 Friction angle: 35	Piezometric Line no. 1
9	L9 Beaumont Clay	123	Cohesion: 2740.0 Friction angle: 0	None
10	L10 Beaumont Sand	125	Cohesion: 0.0 Friction angle: 35	Piezometric Line no. 1
11	L11 Beaumont Clay	130	Cohesion: 3000.0 Friction angle: 0	None
12	L12 Clay Base	130	Very Strong	Not Applicable
13	L13 FLowable Rip Rap	140	Very Strong	Not Applicable
14	L14 FLowable Rip Rap	140	Very Strong	Not Applicable

Figure D8. Stability analyses using undrained properties for boring B-8 showing critical failure surface at 100, 130, and 150 ft depths and property table.

Drained analyses

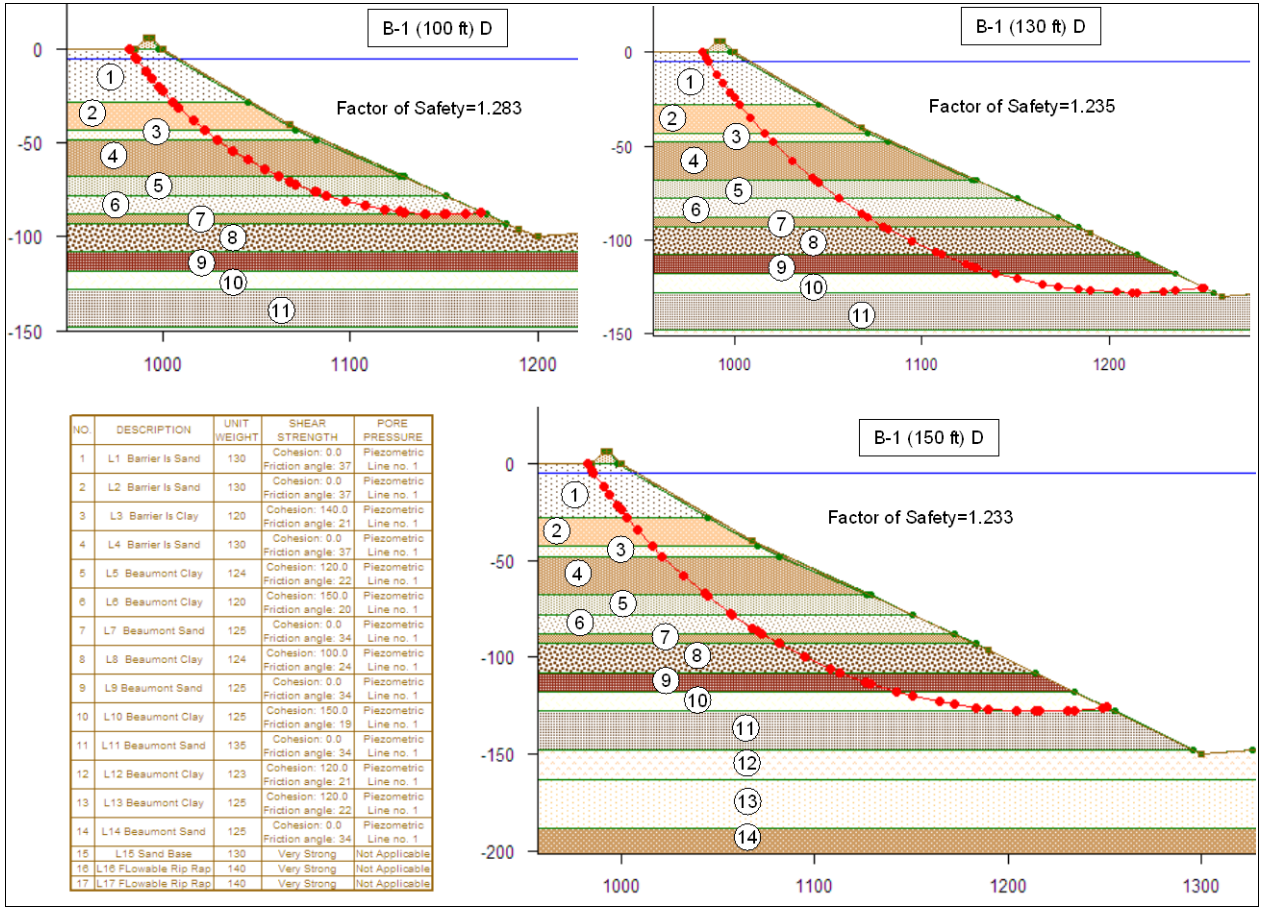

NO.	DESCRIPTION	UNIT WEIGHT	SHEAR STRENGTH	PORE PRESSURE
1	L1 Barrier Is Sand	130	Cohesion: 0.0 Friction angle: 37	Piezometric Line no. 1
2	L2 Barrier Is Sand	130	Cohesion: 0.0 Friction angle: 37	Piezometric Line no. 1
3	L3 Barrier Is Clay	120	Cohesion: 140.0 Friction angle: 21	Piezometric Line no. 1
4	L4 Barrier Is Sand	130	Cohesion: 0.0 Friction angle: 37	Piezometric Line no. 1
5	L5 Beaumont Clay	124	Cohesion: 120.0 Friction angle: 22	Piezometric Line no. 1
6	L6 Beaumont Clay	120	Cohesion: 150.0 Friction angle: 20	Piezometric Line no. 1
7	L7 Beaumont Sand	125	Cohesion: 0.0 Friction angle: 34	Piezometric Line no. 1
8	L8 Beaumont Clay	124	Cohesion: 100.0 Friction angle: 24	Piezometric Line no. 1
9	L9 Beaumont Sand	125	Cohesion: 0.0 Friction angle: 34	Piezometric Line no. 1
10	L10 Beaumont Clay	125	Cohesion: 150.0 Friction angle: 19	Piezometric Line no. 1
11	L11 Beaumont Sand	135	Cohesion: 0.0 Friction angle: 34	Piezometric Line no. 1
12	L12 Beaumont Clay	123	Cohesion: 120.0 Friction angle: 21	Piezometric Line no. 1
13	L13 Beaumont Clay	125	Cohesion: 120.0 Friction angle: 22	Piezometric Line no. 1
14	L14 Beaumont Sand	125	Cohesion: 0.0 Friction angle: 34	Piezometric Line no. 1
15	L15 Sand Base	130	Very Strong	Not Applicable
16	L16 FLowable Rip Rap	140	Very Strong	Not Applicable
17	L17 FLowable Rip Rap	140	Very Strong	Not Applicable

Figure D9. Stability analyses using drained properties for boring B-1 showing critical failure surface at 100, 130, and 150 ft depths and property table.

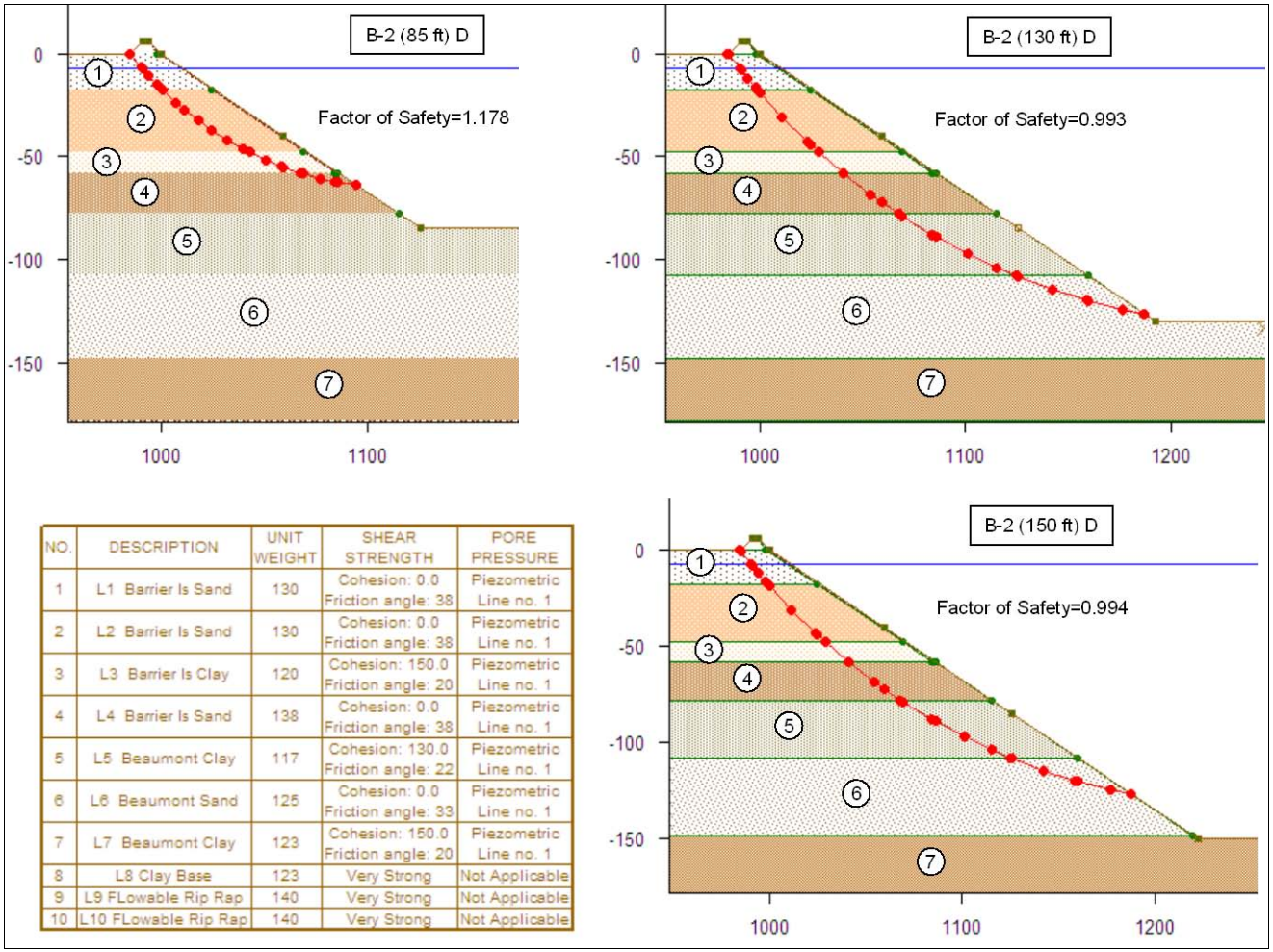

NO.	DESCRIPTION	UNIT WEIGHT	SHEAR STRENGTH	PORE PRESSURE
1	L1 Barrier Is Sand	130	Cohesion: 0.0 Friction angle: 38	Piezometric Line no. 1
2	L2 Barrier Is Sand	130	Cohesion: 0.0 Friction angle: 38	Piezometric Line no. 1
3	L3 Barrier Is Clay	120	Cohesion: 150.0 Friction angle: 20	Piezometric Line no. 1
4	L4 Barrier Is Sand	138	Cohesion: 0.0 Friction angle: 38	Piezometric Line no. 1
5	L5 Beaumont Clay	117	Cohesion: 130.0 Friction angle: 22	Piezometric Line no. 1
6	L6 Beaumont Sand	125	Cohesion: 0.0 Friction angle: 33	Piezometric Line no. 1
7	L7 Beaumont Clay	123	Cohesion: 150.0 Friction angle: 20	Piezometric Line no. 1
8	L8 Clay Base	123	Very Strong	Not Applicable
9	L9 FLowable Rip Rap	140	Very Strong	Not Applicable
10	L10 FLowable Rip Rap	140	Very Strong	Not Applicable

Figure D10. Stability analyses using drained properties for boring B-2 showing critical failure surface at 100, 130, and 150 ft depths and property table.

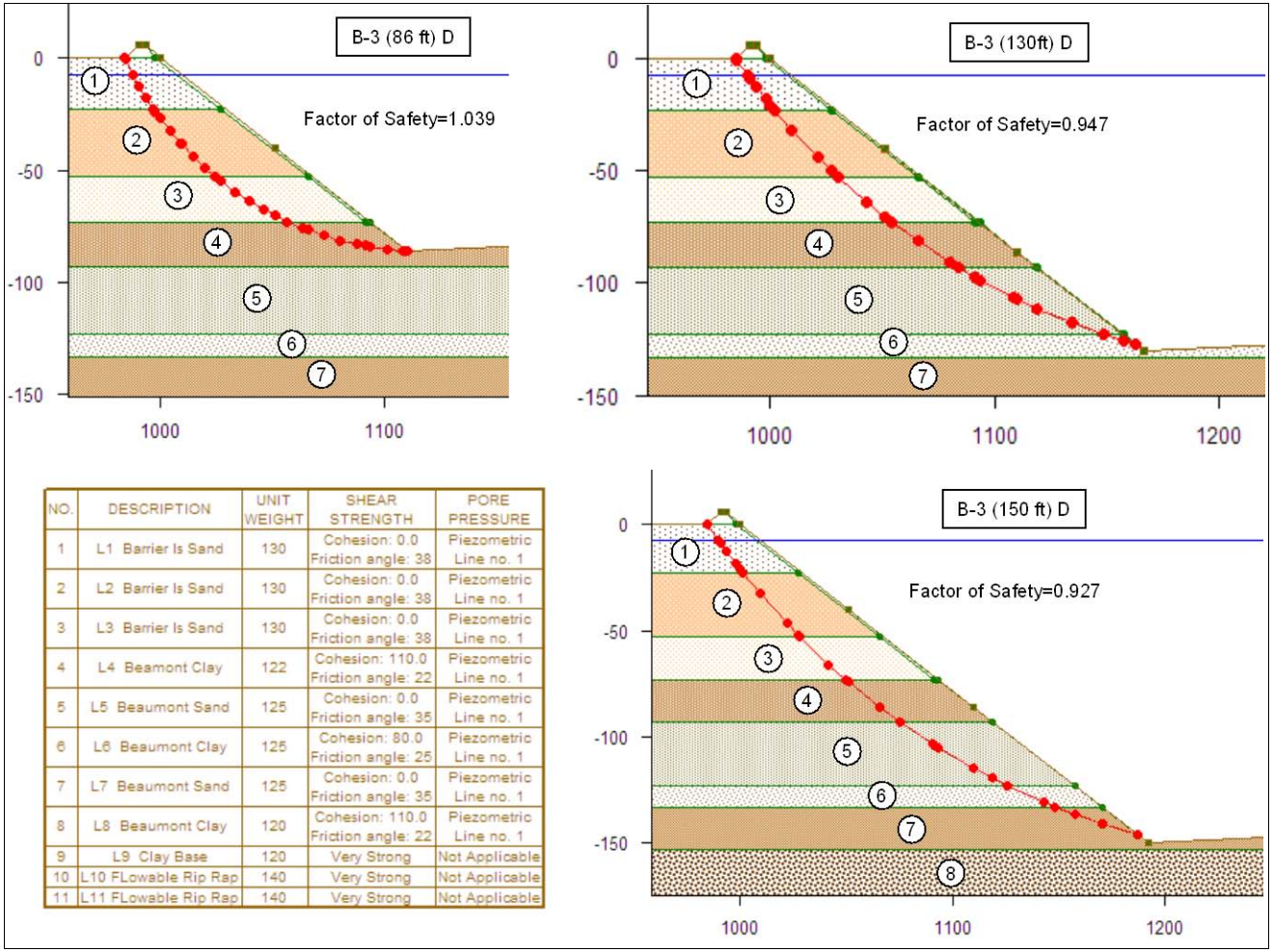

NO.	DESCRIPTION	UNIT WEIGHT	SHEAR STRENGTH	PORE PRESSURE
1	L1 Barrier Is Sand	130	Cohesion: 0.0 Friction angle: 38	Piezometric Line no. 1
2	L2 Barrier Is Sand	130	Cohesion: 0.0 Friction angle: 38	Piezometric Line no. 1
3	L3 Barrier Is Sand	130	Cohesion: 0.0 Friction angle: 38	Piezometric Line no. 1
4	L4 Beamont Clay	122	Cohesion: 110.0 Friction angle: 22	Piezometric Line no. 1
5	L5 Beaumont Sand	125	Cohesion: 0.0 Friction angle: 35	Piezometric Line no. 1
6	L6 Beaumont Clay	125	Cohesion: 80.0 Friction angle: 25	Piezometric Line no. 1
7	L7 Beaumont Sand	125	Cohesion: 0.0 Friction angle: 35	Piezometric Line no. 1
8	L8 Beaumont Clay	120	Cohesion: 110.0 Friction angle: 22	Piezometric Line no. 1
9	L9 Clay Base	120	Very Strong	Not Applicable
10	L10 FLowable Rip Rap	140	Very Strong	Not Applicable
11	L11 FLowable Rip Rap	140	Very Strong	Not Applicable

Figure D11. Stability analyses using drained properties for boring B-3 showing critical failure surface at 100, 130, and 150 ft depths and property table.

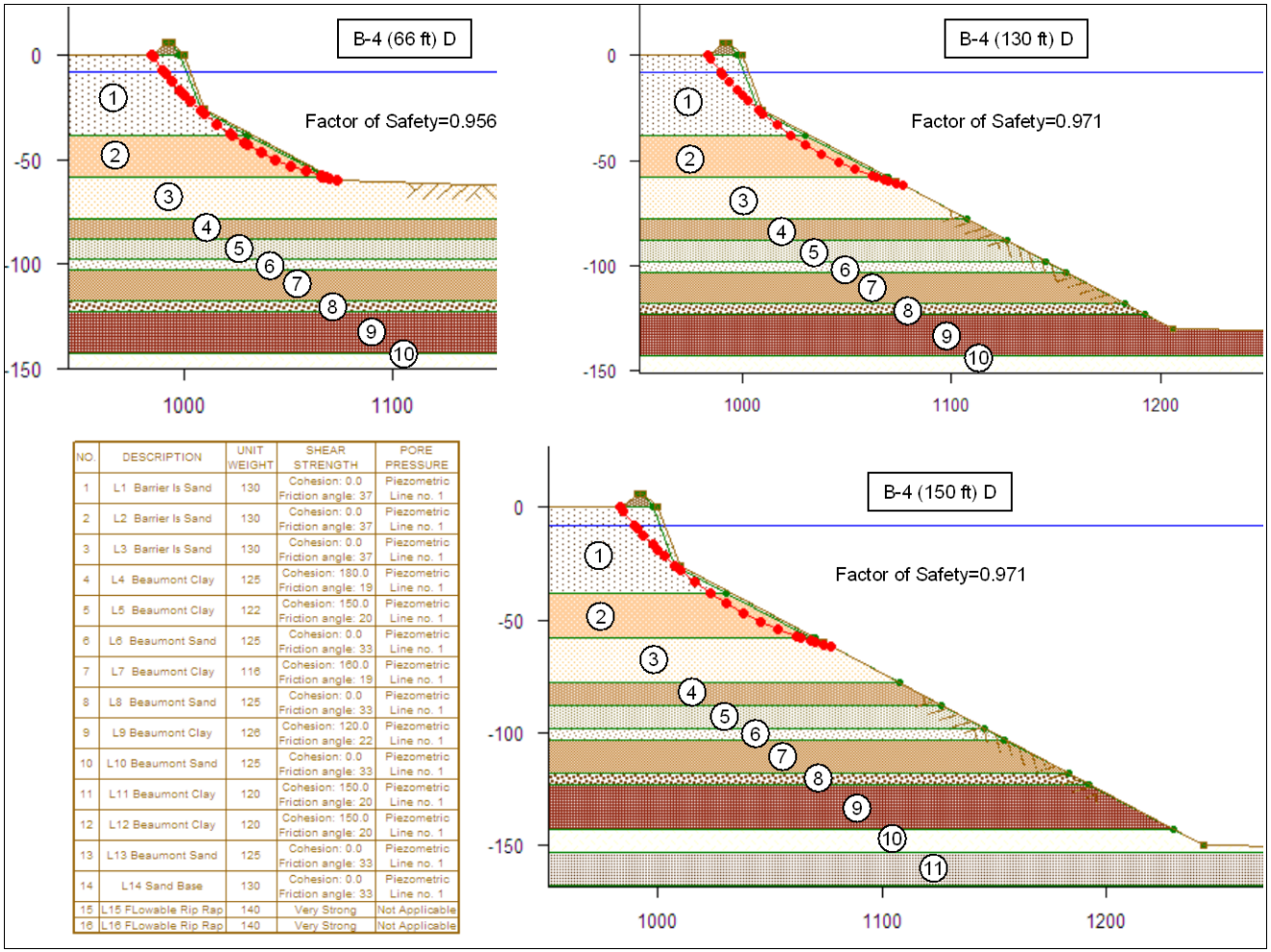

NO.	DESCRIPTION	UNIT WEIGHT	SHEAR STRENGTH	PORE PRESSURE
1	L1 Barrier Is Sand	130	Cohesion: 0.0 Friction angle: 37	Piezometric Line no. 1
2	L2 Barrier Is Sand	130	Cohesion: 0.0 Friction angle: 37	Piezometric Line no. 1
3	L3 Barrier Is Sand	130	Cohesion: 0.0 Friction angle: 37	Piezometric Line no. 1
4	L4 Beaumont Clay	125	Cohesion: 180.0 Friction angle: 19	Piezometric Line no. 1
5	L5 Beaumont Clay	122	Cohesion: 150.0 Friction angle: 20	Piezometric Line no. 1
6	L6 Beaumont Sand	125	Cohesion: 0.0 Friction angle: 33	Piezometric Line no. 1
7	L7 Beaumont Clay	116	Cohesion: 160.0 Friction angle: 19	Piezometric Line no. 1
8	L8 Beaumont Sand	125	Cohesion: 0.0 Friction angle: 33	Piezometric Line no. 1
9	L9 Beaumont Clay	126	Cohesion: 120.0 Friction angle: 22	Piezometric Line no. 1
10	L10 Beaumont Sand	125	Cohesion: 0.0 Friction angle: 33	Piezometric Line no. 1
11	L11 Beaumont Clay	120	Cohesion: 150.0 Friction angle: 20	Piezometric Line no. 1
12	L12 Beaumont Clay	120	Cohesion: 150.0 Friction angle: 20	Piezometric Line no. 1
13	L13 Beaumont Sand	125	Cohesion: 0.0 Friction angle: 33	Piezometric Line no. 1
14	L14 Sand Base	130	Cohesion: 0.0 Friction angle: 33	Piezometric Line no. 1
15	L15 FLowable Rip Rap	140	Very Strong	Not Applicable
16	L16 FLowable Rip Rap	140	Very Strong	Not Applicable

Figure D12. Stability analyses using drained properties for boring B-4 showing critical failure surface at 100, 130, and 150 ft depths and property table.

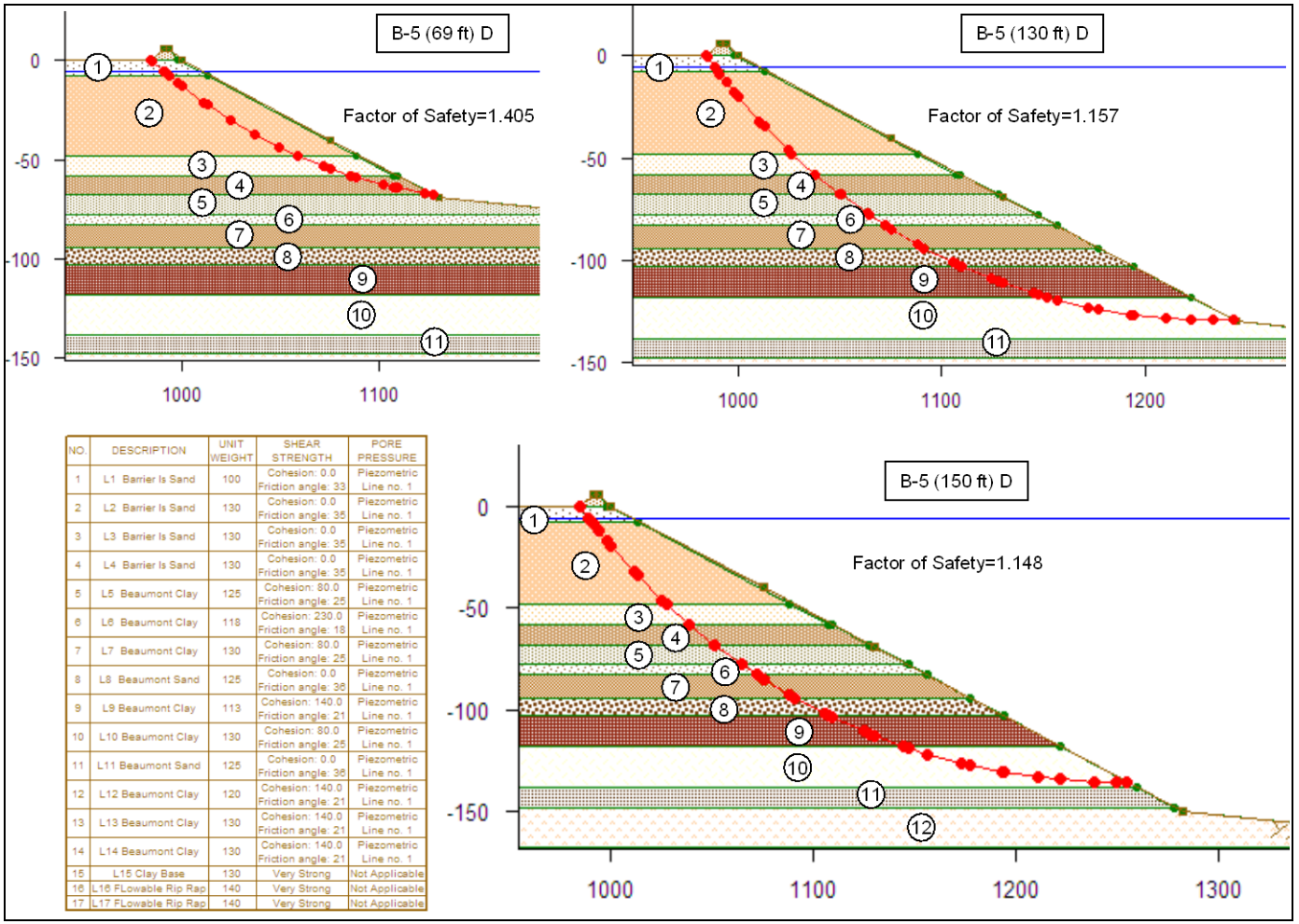

NO.	DESCRIPTION	UNIT WEIGHT	SHEAR STRENGTH	PORE PRESSURE
1	L1 Barrier Is Sand	100	Cohesion: 0.0 Friction angle: 33	Piezometric Line no. 1
2	L2 Barrier Is Sand	130	Cohesion: 0.0 Friction angle: 35	Piezometric Line no. 1
3	L3 Barrier Is Sand	130	Cohesion: 0.0 Friction angle: 35	Piezometric Line no. 1
4	L4 Barrier Is Sand	130	Cohesion: 0.0 Friction angle: 35	Piezometric Line no. 1
5	L5 Beaumont Clay	125	Cohesion: 80.0 Friction angle: 25	Piezometric Line no. 1
6	L6 Beaumont Clay	118	Cohesion: 230.0 Friction angle: 18	Piezometric Line no. 1
7	L7 Beaumont Clay	130	Cohesion: 80.0 Friction angle: 25	Piezometric Line no. 1
8	L8 Beaumont Sand	125	Cohesion: 0.0 Friction angle: 36	Piezometric Line no. 1
9	L9 Beaumont Clay	113	Cohesion: 140.0 Friction angle: 21	Piezometric Line no. 1
10	L10 Beaumont Clay	130	Cohesion: 80.0 Friction angle: 25	Piezometric Line no. 1
11	L11 Beaumont Sand	125	Cohesion: 0.0 Friction angle: 36	Piezometric Line no. 1
12	L12 Beaumont Clay	120	Cohesion: 140.0 Friction angle: 21	Piezometric Line no. 1
13	L13 Beaumont Clay	130	Cohesion: 140.0 Friction angle: 21	Piezometric Line no. 1
14	L14 Beaumont Clay	130	Cohesion: 140.0 Friction angle: 21	Piezometric Line no. 1
15	L15 Clay Base	130	Very Strong	Not Applicable
16	L16 FLowable Rip Rap	140	Very Strong	Not Applicable
17	L17 FLowable Rip Rap	140	Very Strong	Not Applicable

Figure D13. Stability analyses using drained properties for boring B-5 showing critical failure surface at 100, 130, and 150 ft depths and property table.

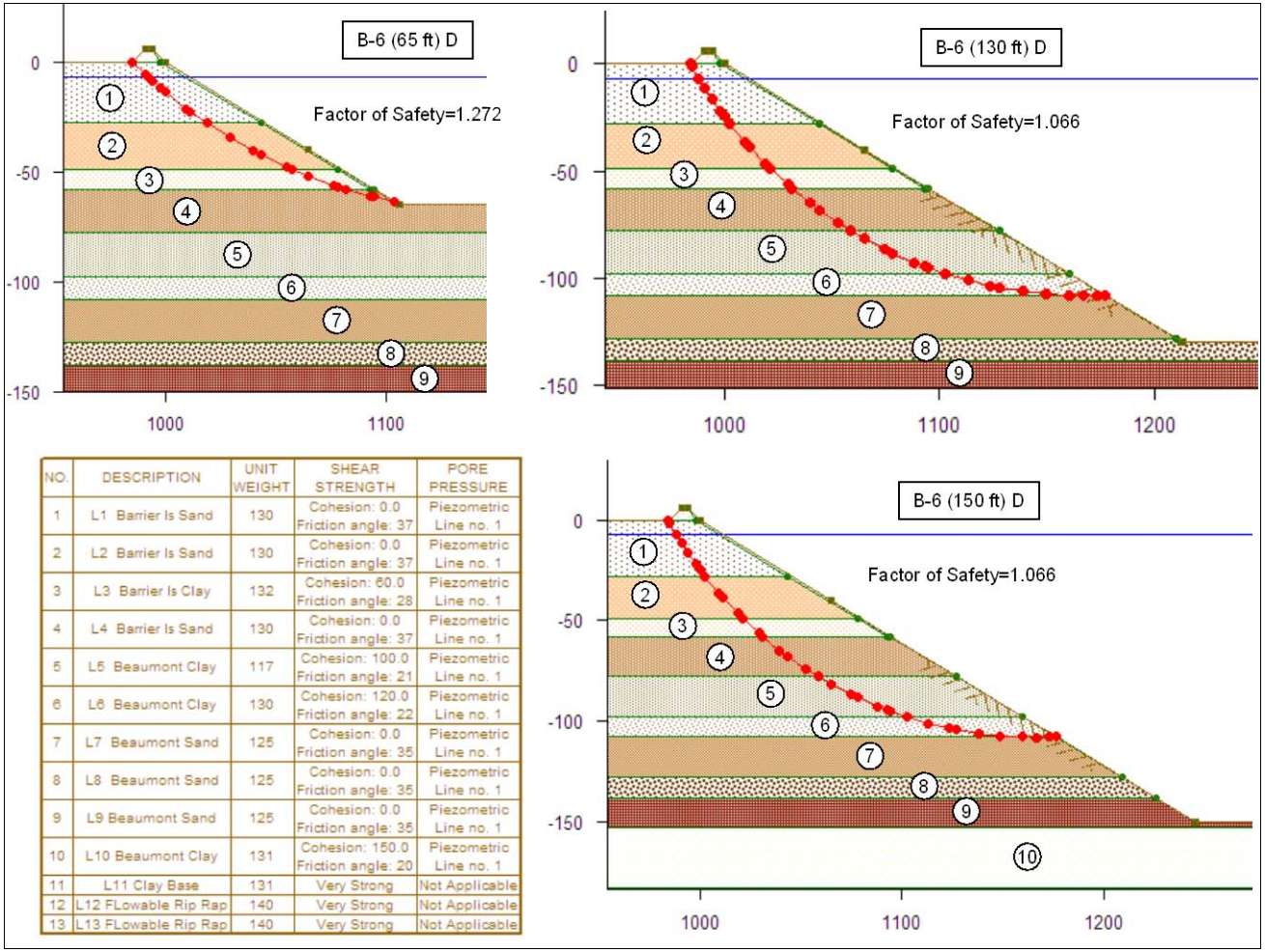

NO.	DESCRIPTION	UNIT WEIGHT	SHEAR STRENGTH	PORE PRESSURE
1	L1 Barrier Is Sand	130	Cohesion: 0.0 Friction angle: 37	Piezometric Line no. 1
2	L2 Barrier Is Sand	130	Cohesion: 0.0 Friction angle: 37	Piezometric Line no. 1
3	L3 Barrier Is Clay	132	Cohesion: 60.0 Friction angle: 28	Piezometric Line no. 1
4	L4 Barrier Is Sand	130	Cohesion: 0.0 Friction angle: 37	Piezometric Line no. 1
5	L5 Beaumont Clay	117	Cohesion: 100.0 Friction angle: 21	Piezometric Line no. 1
6	L6 Beaumont Clay	130	Cohesion: 120.0 Friction angle: 22	Piezometric Line no. 1
7	L7 Beaumont Sand	125	Cohesion: 0.0 Friction angle: 35	Piezometric Line no. 1
8	L8 Beaumont Sand	125	Cohesion: 0.0 Friction angle: 35	Piezometric Line no. 1
9	L9 Beaumont Sand	125	Cohesion: 0.0 Friction angle: 35	Piezometric Line no. 1
10	L10 Beaumont Clay	131	Cohesion: 150.0 Friction angle: 20	Piezometric Line no. 1
11	L11 Clay Base	131	Very Strong	Not Applicable
12	L12 FLowable Rip Rap	140	Very Strong	Not Applicable
13	L13 FLowable Rip Rap	140	Very Strong	Not Applicable

Figure D14. Stability analyses using drained properties for boring B-6 showing critical failure surface at 100, 130, and 150 ft depths and property table.

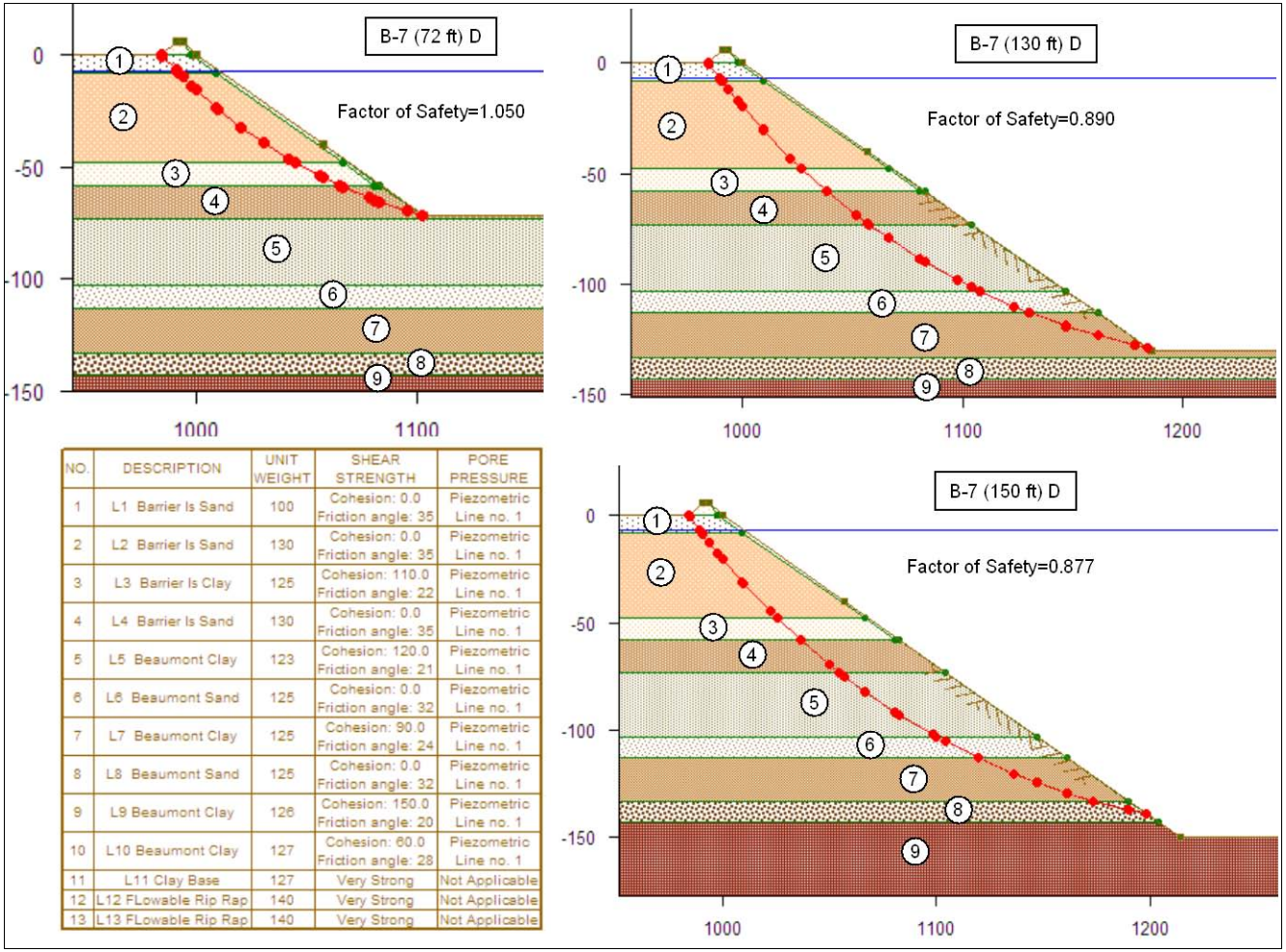

NO.	DESCRIPTION	UNIT WEIGHT	SHEAR STRENGTH	PORE PRESSURE
1	L1 Barrier Is Sand	100	Cohesion: 0.0 Friction angle: 35	Piezometric Line no. 1
2	L2 Barrier Is Sand	130	Cohesion: 0.0 Friction angle: 35	Piezometric Line no. 1
3	L3 Barrier Is Clay	125	Cohesion: 110.0 Friction angle: 22	Piezometric Line no. 1
4	L4 Barrier Is Sand	130	Cohesion: 0.0 Friction angle: 35	Piezometric Line no. 1
5	L5 Beaumont Clay	123	Cohesion: 120.0 Friction angle: 21	Piezometric Line no. 1
6	L6 Beaumont Sand	125	Cohesion: 0.0 Friction angle: 32	Piezometric Line no. 1
7	L7 Beaumont Clay	125	Cohesion: 90.0 Friction angle: 24	Piezometric Line no. 1
8	L8 Beaumont Sand	125	Cohesion: 0.0 Friction angle: 32	Piezometric Line no. 1
9	L9 Beaumont Clay	126	Cohesion: 150.0 Friction angle: 20	Piezometric Line no. 1
10	L10 Beaumont Clay	127	Cohesion: 60.0 Friction angle: 28	Piezometric Line no. 1
11	L11 Clay Base	127	Very Strong	Not Applicable
12	L12 FLowable Rip Rap	140	Very Strong	Not Applicable
13	L13 FLowable Rip Rap	140	Very Strong	Not Applicable

Figure D15. Stability analyses using drained properties for boring B-7 showing critical failure surface at 100, 130, and 150 ft depths and property table.

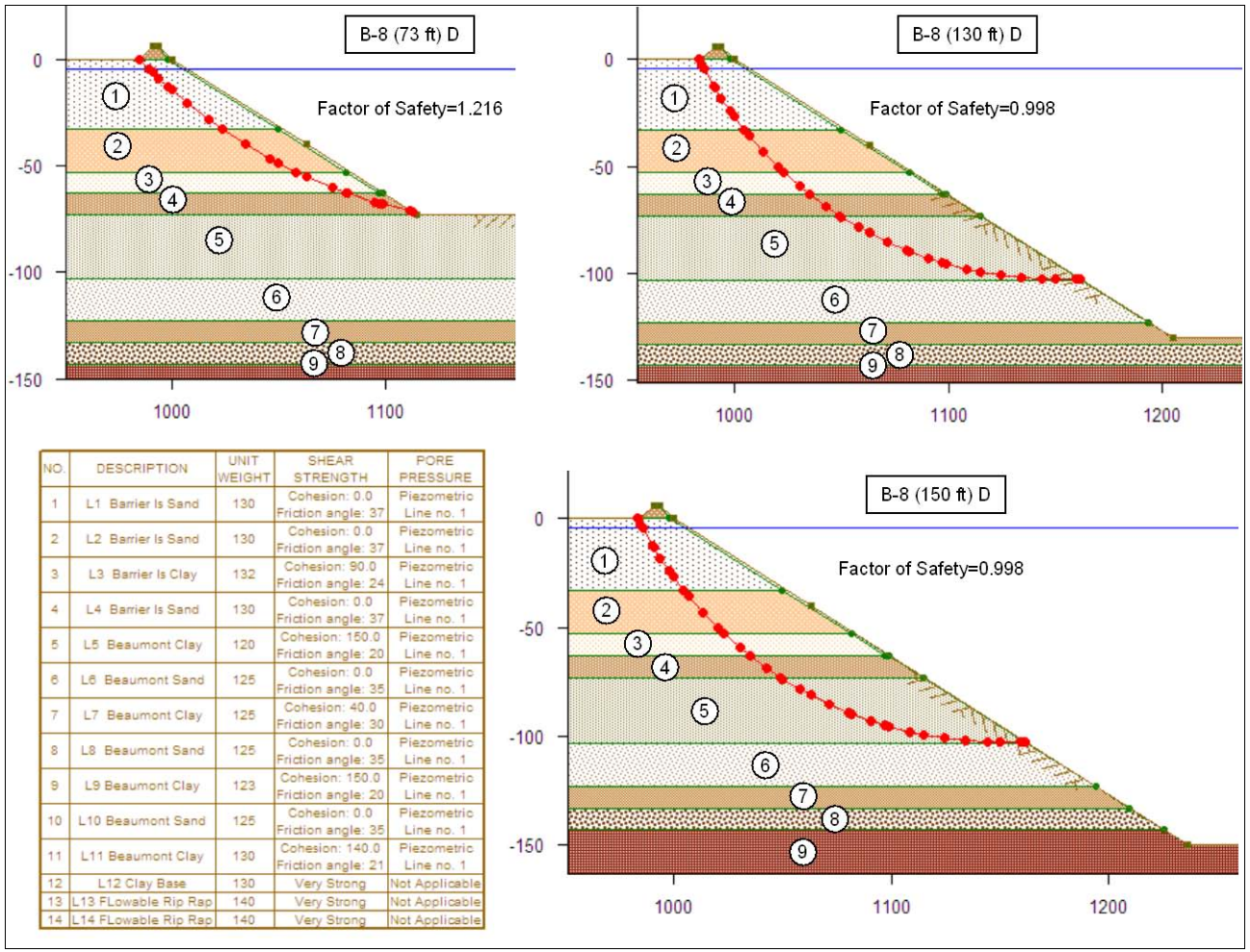

NO.	DESCRIPTION	UNIT WEIGHT	SHEAR STRENGTH	PORE PRESSURE
1	L1 Barrier Is Sand	130	Cohesion: 0.0 Friction angle: 37	Piezometric Line no. 1
2	L2 Barrier Is Sand	130	Cohesion: 0.0 Friction angle: 37	Piezometric Line no. 1
3	L3 Barrier Is Clay	132	Cohesion: 90.0 Friction angle: 24	Piezometric Line no. 1
4	L4 Barrier Is Sand	130	Cohesion: 0.0 Friction angle: 37	Piezometric Line no. 1
5	L5 Beaumont Clay	120	Cohesion: 150.0 Friction angle: 20	Piezometric Line no. 1
6	L6 Beaumont Sand	125	Cohesion: 0.0 Friction angle: 35	Piezometric Line no. 1
7	L7 Beaumont Clay	125	Cohesion: 40.0 Friction angle: 30	Piezometric Line no. 1
8	L8 Beaumont Sand	125	Cohesion: 0.0 Friction angle: 35	Piezometric Line no. 1
9	L9 Beaumont Clay	123	Cohesion: 150.0 Friction angle: 20	Piezometric Line no. 1
10	L10 Beaumont Sand	125	Cohesion: 0.0 Friction angle: 35	Piezometric Line no. 1
11	L11 Beaumont Clay	130	Cohesion: 140.0 Friction angle: 21	Piezometric Line no. 1
12	L12 Clay Base	130	Very Strong	Not Applicable
13	L13 FLowable Rip Rap	140	Very Strong	Not Applicable
14	L14 FLowable Rip Rap	140	Very Strong	Not Applicable

Figure D16. Stability analyses using drained properties for boring B-8 showing critical failure surface at 100, 130, and 150 ft depths and property table.

Appendix E: Probabilistic Analysis Results

Introduction

A summary of the probabilistic analyses for borings B-1, B-3, and B-7 are presented (Figures E1 – E6 and Tables E1 – E17). Five main channel depths were analyzed for each of the cross sections. These fives depths included the current depth and depths deeper than the current depth by 5, 10, 25, and 50 ft. An additional channel depth was analyzed for cross-sections B-3 and B-7 so that all cross sections would have a 150 ft channel depth analysis. Each figure shows the critical failure surface used to determine the most likely value for the factor of safety for the channel depths analyzed for any particular cross section. Each figure also contains an embedded table showing the engineering properties used for that analysis. Following the figures for a particular boring are tables presenting the results of the probabilistic analyses. The cases with the last character labeled as lower-case “a” represent analysis with the strengths decreased by one standard deviation and those labeled as lower-case “b” represent the analysis performed with the strengths increased by one standard deviation.

Results for probabilistic analyses for boring B-1 cross section

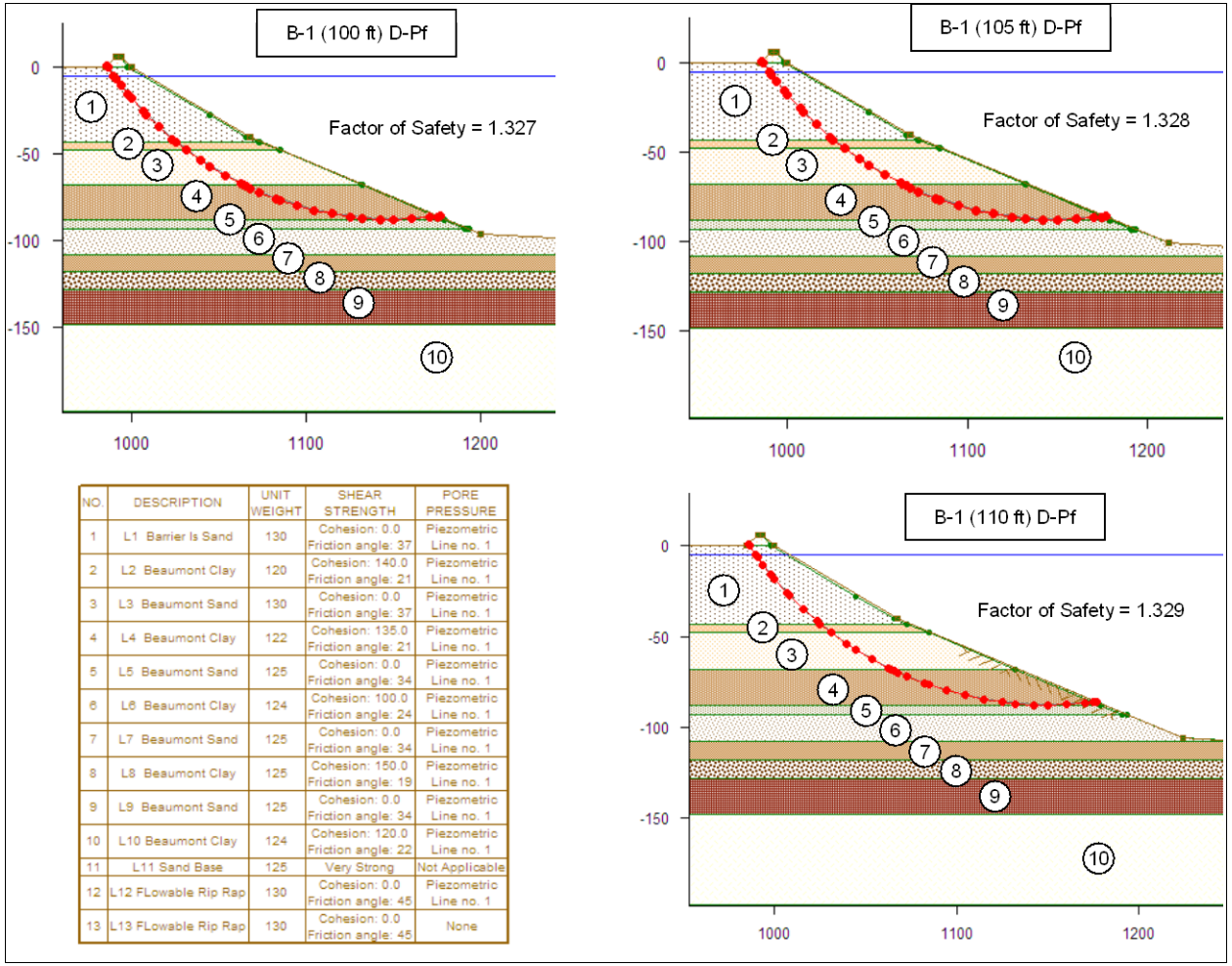

NO.	DESCRIPTION	UNIT WEIGHT	SHEAR STRENGTH	PORE PRESSURE
1	L1 Barrier Is Sand	130	Cohesion: 0.0 Friction angle: 37	Piezometric Line no. 1
2	L2 Beaumont Clay	120	Cohesion: 140.0 Friction angle: 21	Piezometric Line no. 1
3	L3 Beaumont Sand	130	Cohesion: 0.0 Friction angle: 37	Piezometric Line no. 1
4	L4 Beaumont Clay	122	Cohesion: 135.0 Friction angle: 21	Piezometric Line no. 1
5	L5 Beaumont Sand	125	Cohesion: 0.0 Friction angle: 34	Piezometric Line no. 1
6	L6 Beaumont Clay	124	Cohesion: 100.0 Friction angle: 24	Piezometric Line no. 1
7	L7 Beaumont Sand	125	Cohesion: 0.0 Friction angle: 34	Piezometric Line no. 1
8	L8 Beaumont Clay	125	Cohesion: 150.0 Friction angle: 19	Piezometric Line no. 1
9	L9 Beaumont Sand	125	Cohesion: 0.0 Friction angle: 34	Piezometric Line no. 1
10	L10 Beaumont Clay	124	Cohesion: 120.0 Friction angle: 22	Piezometric Line no. 1
11	L11 Sand Base	125	Very Strong	Not Applicable
12	L12 FLowable Rip Rap	130	Cohesion: 0.0 Friction angle: 45	Piezometric Line no. 1
13	L13 FLowable Rip Rap	130	Cohesion: 0.0 Friction angle: 45	None

Figure E1. Probabilistic stability analyses to determine the most likely value for safety factor using drained properties for boring B-1 showing critical failure surface for 100, 105 and 110 ft depths and property table.

NO.	DESCRIPTION	UNIT WEIGHT	SHEAR STRENGTH	PORE PRESSURE
1	L1 Barrier Is Sand	130	Cohesion: 0.0 Friction angle: 37	Piezometric Line no. 1
2	L2 Beaumont Clay	120	Cohesion: 140.0 Friction angle: 21	Piezometric Line no. 1
3	L3 Beaumont Sand	130	Cohesion: 0.0 Friction angle: 37	Piezometric Line no. 1
4	L4 Beaumont Clay	122	Cohesion: 135.0 Friction angle: 21	Piezometric Line no. 1
5	L5 Beaumont Sand	125	Cohesion: 0.0 Friction angle: 34	Piezometric Line no. 1
6	L6 Beaumont Clay	124	Cohesion: 100.0 Friction angle: 24	Piezometric Line no. 1
7	L7 Beaumont Sand	125	Cohesion: 0.0 Friction angle: 34	Piezometric Line no. 1
8	L8 Beaumont Clay	125	Cohesion: 150.0 Friction angle: 19	Piezometric Line no. 1
9	L9 Beaumont Sand	125	Cohesion: 0.0 Friction angle: 34	Piezometric Line no. 1
10	L10 Beaumont Clay	124	Cohesion: 120.0 Friction angle: 22	Piezometric Line no. 1
11	L11 Sand Base	125	Very Strong	Not Applicable
12	L12 FLowable Rip Rap	130	Cohesion: 0.0 Friction angle: 45	Piezometric Line no. 1
13	L13 FLowable Rip Rap	130	Cohesion: 0.0 Friction angle: 45	None

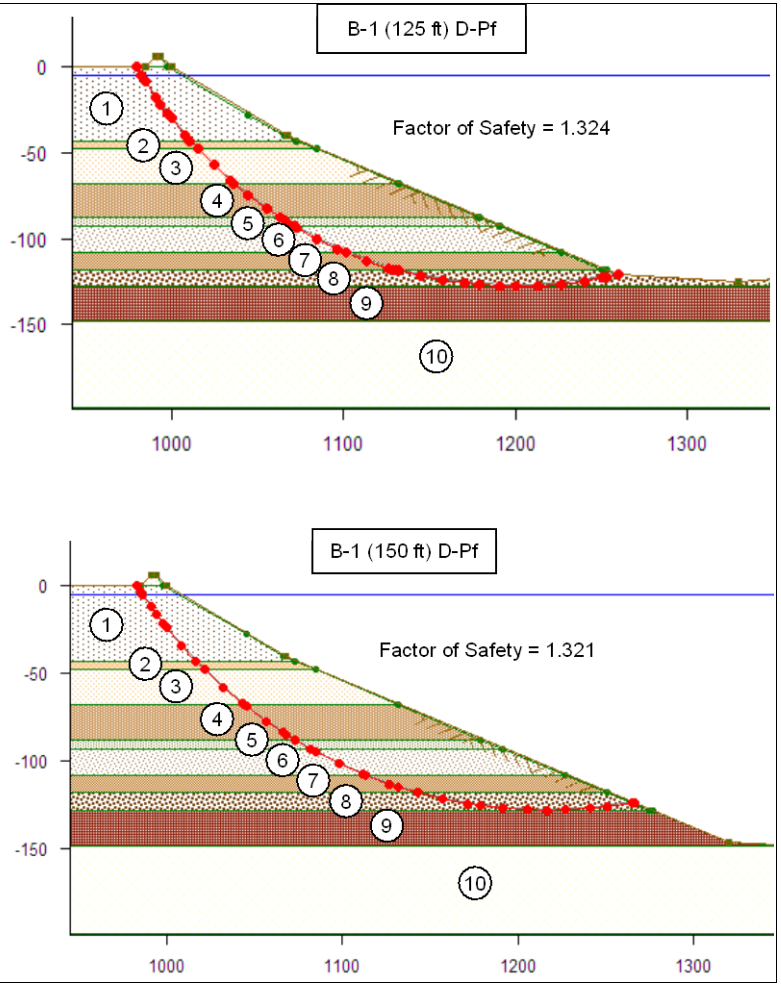

Figure E2. Probabilistic stability analyses to determine the most likely value using drained properties for boring B-1 showing critical failure surface for 125 and 150 ft depths and property table.

Table E1. Probability of failure calculations for boring B-1 at 100 ft depth.

Most Likely Value of FS =				1.327				
Case	**WL**	**Layer #**	**COV**	**FS**	**Delta FS**	**Std Dev of FS**	**COV of FS**	**Prob of failure**
B1-100-1a	5	1	5%	1.275				
B1-100-1b	5	1	5%	1.345	0.07			
B1-100-2a	5	2	30%	1.318				
B1-100-2b	5	2	30%	1.337	0.02			
B1-100-3a	5	3	5%	1.306				
B1-100-3b	5	3	5%	1.349	0.04			
B1-100-4a	5	4	30%	1.171				
B1-100-4b	5	4	30%	1.353	0.18			
B1-100-5a	5	5	5%	1.327				
B1-100-5b	5	5	5%	1.327	0.00			
B1-100-6a	5	6	30%	1.212				
B1-100-6b	5	6	30%	1.327	0.12			
B1-100-7a	5	7	5%	1.327				
B1-100-7b	5	7	5%	1.327	0.00			
B1-100-8a	5	8	30%	1.327				
B1-100-8b	5	8	30%	1.327	0.00			
B1-100-9a	5	9	5%	1.327				
B1-100-9b	5	9	5%	1.327	0.00			
B1-100-10a	5	10	30%	1.327				
B1-100-10b	5	10	30%	1.327	0.00	**0.12**	**8.7%**	**0.07%**

Table E2. Probability of failure calculations for boring B-1 at 105 ft depth.

Most Likely Value of FS =				1.328				
Case	**WL**	**Layer #**	**COV**	**FS**	**Delta FS**	**Std Dev of FS**	**COV of FS**	**Prob of failure**
B1-105-1a	5	1	5%	1.275				
B1-105-1b	5	1	5%	1.346	0.07			
B1-105-2a	5	2	30%	1.320				
B1-105-2b	5	2	30%	1.337	0.02			
B1-105-3a	5	3	5%	1.307				
B1-105-3b	5	3	5%	1.351	0.04			
B1-105-4a	5	4	30%	1.172				
B1-105-4b	5	4	30%	1.353	0.18			
B1-105-5a	5	5	5%	1.328				
B1-105-5b	5	5	5%	1.328	0.00			
B1-105-6a	5	6	30%	1.187				
B1-105-6b	5	6	30%	1.328	0.14			
B1-105-7a	5	7	5%	1.328				
B1-105-7b	5	7	5%	1.328	0.00			
B1-105-8a	5	8	30%	1.328				
B1-105-8b	5	8	30%	1.328	0.00			
B1-105-9a	5	9	5%	1.328				
B1-105-9b	5	9	5%	1.328	0.00			
B1-105-10a	5	10	30%	1.328				
B1-105-10b	5	10	30%	1.328	0.00	**0.12**	**9.2%**	**0.12%**

Table E3. Probability of failure calculations for boring B-1 at 110 ft depth.

Most Likely Value of FS =				1.329				
Case	**WL**	**Layer #**	**COV**	**FS**	**Delta FS**	**Std Dev of FS**	**COV of FS**	**Prob of failure**
B1-110-1a	5	1	5%	1.284				
B1-110-1b	5	1	5%	1.357	0.07			
B1-110-2a	5	2	30%	1.321				
B1-110-2b	5	2	30%	1.338	0.02			
B1-110-3a	5	3	5%	1.308				
B1-110-3b	5	3	5%	1.352	0.04			
B1-110-4a	5	4	30%	1.177				
B1-110-4b	5	4	30%	1.354	0.18			
B1-110-5a	5	5	5%	1.329				
B1-110-5b	5	5	5%	1.329	0.00			
B1-110-6a	5	6	30%	1.190				
B1-110-6b	5	6	30%	1.329	0.14			
B1-110-7a	5	7	5%	1.329				
B1-110-7b	5	7	5%	1.329	0.00			
B1-110-8a	5	8	30%	1.284				
B1-110-8b	5	8	30%	1.329	0.04			
B1-110-9a	5	9	5%	1.329				
B1-110-9b	5	9	5%	1.329	0.00			
B1-110-10a	5	10	30%	1.329				
B1-110-10b	5	10	30%	1.328	0.00	**0.12**	**9.2%**	**0.11%**

Table E4. Probability of failure calculations for boring B-1 at 125 ft depth.

Most Likely Value of FS =				1.324				
Case	**WL**	**Layer #**	**COV**	**FS**	**Delta FS**	**Std Dev of FS**	**COV of FS**	**Prob of failure**
B1-125-1a	5	1	5%	1.284				
B1-125-1b	5	1	5%	1.332	0.05			
B1-125-2a	5	2	30%	1.321				
B1-125-2b	5	2	30%	1.328	0.01			
B1-125-3a	5	3	5%	1.317				
B1-125-3b	5	3	5%	1.332	0.02			
B1-125-4a	5	4	30%	1.175				
B1-125-4b	5	4	30%	1.355	0.18			
B1-125-5a	5	5	5%	1.321				
B1-125-5b	5	5	5%	1.327	0.01			
B1-125-6a	5	6	30%	1.190				
B1-125-6b	5	6	30%	1.332	0.14			
B1-125-7a	5	7	5%	1.310				
B1-125-7b	5	7	5%	1.338	0.03			
B1-125-8a	5	8	30%	1.216				
B1-125-8b	5	8	30%	1.332	0.12			
B1-125-9a	5	9	5%	1.324				
B1-125-9b	5	9	5%	1.324	0.00			
B1-125-10a	5	10	30%	1.324				
B1-125-10b	5	10	30%	1.324	0.00	**0.13**	**9.9%**	**0.26%**

Table E5. Probability of failure calculations for boring B-1 at 150 ft depth.

Most Likely Value of FS =				1.321				
Case	**WL**	**Layer #**	**COV**	**FS**	**Delta FS**	**Std Dev of FS**	**COV of FS**	**Prob of failure**
B1-150-1a	5	1	5%	1.272				
B1-150-1b	5	1	5%	1.330	0.06			
B1-150-2a	5	2	30%	1.317				
B1-150-2b	5	2	30%	1.325	0.01			
B1-150-3a	5	3	5%	1.312				
B1-150-3b	5	3	5%	1.330	0.02			
B1-150-4a	5	4	30%	1.178				
B1-150-4b	5	4	30%	1.354	0.18			
B1-150-5a	5	5	5%	1.317				
B1-150-5b	5	5	5%	1.324	0.01			
B1-150-6a	5	6	30%	1.192				
B1-150-6b	5	6	30%	1.334	0.14			
B1-150-7a	5	7	5%	1.307				
B1-150-7b	5	7	5%	1.336	0.03			
B1-150-8a	5	8	30%	1.220				
B1-150-8b	5	8	30%	1.334	0.11			
B1-150-9a	5	9	5%	1.321				
B1-150-9b	5	9	5%	1.321	0.00			
B1-150-10a	5	10	30%	1.293				
B1-150-10b	5	10	30%	1.321	0.00	**0.13**	**9.9%**	**0.28%**

Results for probabilistic analyses for boring B-3 cross section

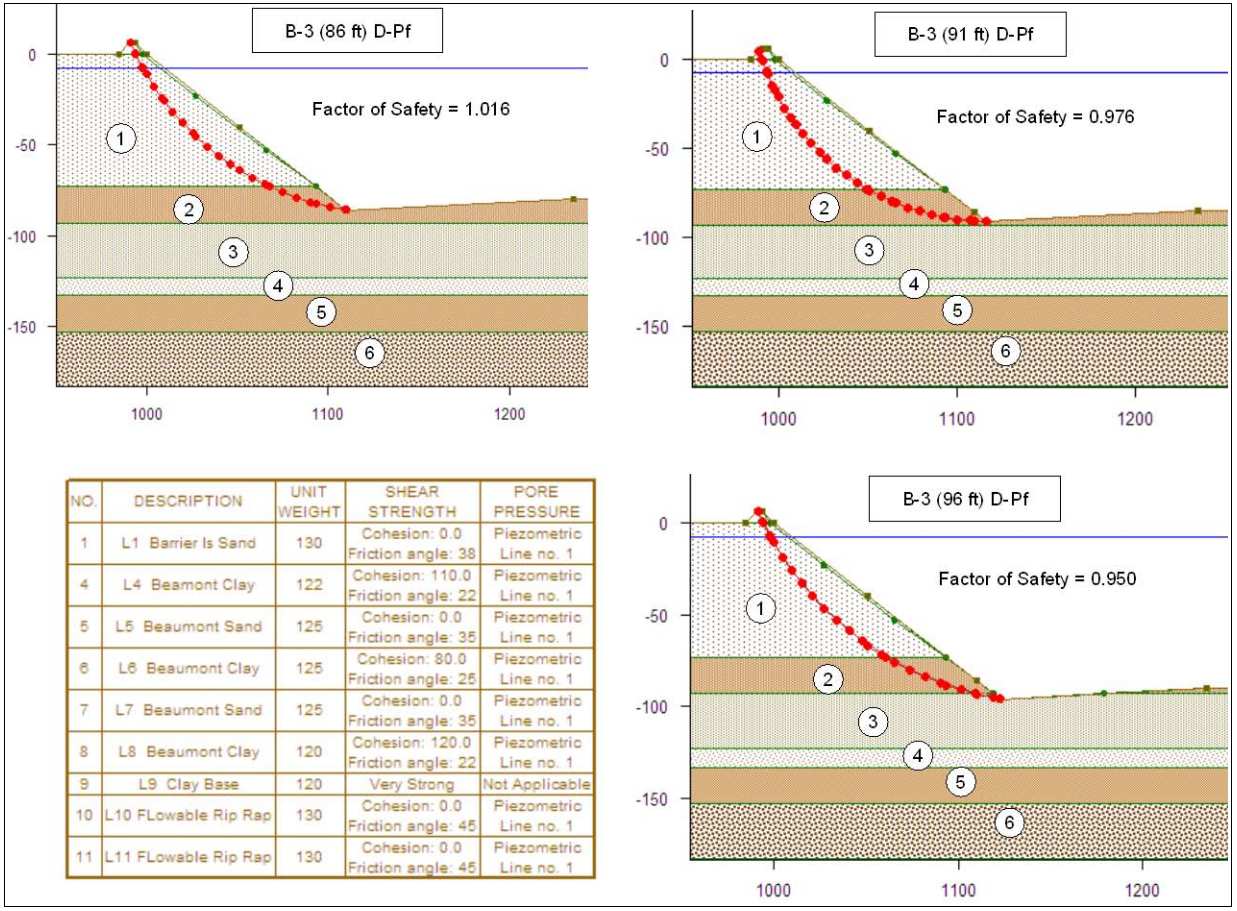

NO.	DESCRIPTION	UNIT WEIGHT	SHEAR STRENGTH	PORE PRESSURE
1	L1 Barrier Is Sand	130	Cohesion: 0.0 Friction angle: 38	Piezometric Line no. 1
4	L4 Beamont Clay	122	Cohesion: 110.0 Friction angle: 22	Piezometric Line no. 1
5	L5 Beaumont Sand	125	Cohesion: 0.0 Friction angle: 35	Piezometric Line no. 1
6	L6 Beaumont Clay	125	Cohesion: 80.0 Friction angle: 25	Piezometric Line no. 1
7	L7 Beaumont Sand	125	Cohesion: 0.0 Friction angle: 35	Piezometric Line no. 1
8	L8 Beaumont Clay	120	Cohesion: 120.0 Friction angle: 22	Piezometric Line no. 1
9	L9 Clay Base	120	Very Strong	Not Applicable
10	L10 FLowable Rip Rap	130	Cohesion: 0.0 Friction angle: 45	Piezometric Line no. 1
11	L11 FLowable Rip Rap	130	Cohesion: 0.0 Friction angle: 45	Piezometric Line no. 1

Figure E3. Probabilistic stability analyses using drained properties for boring B-3 showing critical failure surface for 86, 91, and 96 ft depths and property table.

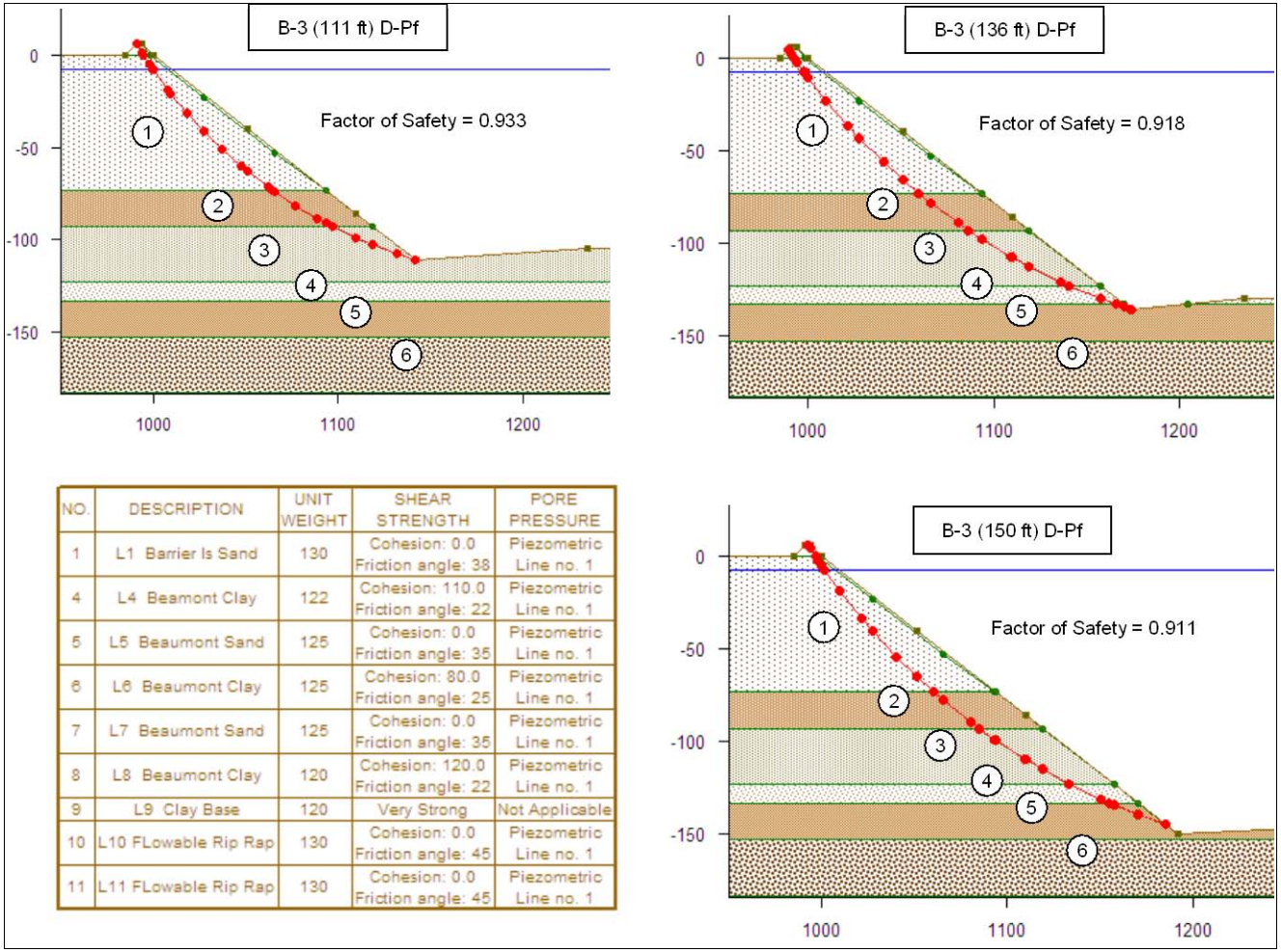

NO.	DESCRIPTION	UNIT WEIGHT	SHEAR STRENGTH	PORE PRESSURE
1	L1 Barrier Is Sand	130	Cohesion: 0.0 Friction angle: 38	Piezometric Line no. 1
4	L4 Beamont Clay	122	Cohesion: 110.0 Friction angle: 22	Piezometric Line no. 1
5	L5 Beaumont Sand	125	Cohesion: 0.0 Friction angle: 35	Piezometric Line no. 1
6	L6 Beaumont Clay	125	Cohesion: 80.0 Friction angle: 25	Piezometric Line no. 1
7	L7 Beaumont Sand	125	Cohesion: 0.0 Friction angle: 35	Piezometric Line no. 1
8	L8 Beaumont Clay	120	Cohesion: 120.0 Friction angle: 22	Piezometric Line no. 1
9	L9 Clay Base	120	Very Strong	Not Applicable
10	L10 FLowable Rip Rap	130	Cohesion: 0.0 Friction angle: 45	Piezometric Line no. 1
11	L11 FLowable Rip Rap	130	Cohesion: 0.0 Friction angle: 45	Piezometric Line no. 1

Figure E4. Probabilistic stability analyses using drained properties for boring B-3 showing critical failure surface for 111, 136, and 150 ft depths and property table.

Table E6. Probability of failure calculations for boring B-3 at 86 ft depth.

Most Likely Value of FS =				1.044				
Case	**WL**	**Layer #**	**COV**	**FS**	**Delta FS**	**Std Dev of FS**	**COV of FS**	**Prob of failure**
B3-86-1a	7.5	1	5%	0.990				
B3-86-1b	7.5	1	5%	1.087	0.10			
B3-86-2a	7.5	2	30%	0.914				
B3-86-2b	7.5	2	30%	1.081	0.17			
B3-86-3a	7.5	3	5%	1.044				
B3-86-3b	7.5	3	5%	1.044	0.00			
B3-86-4a	7.5	4	30%	1.044				
B3-86-4b	7.5	4	30%	1.044	0.00			
B3-86-5a	7.5	5	5%	1.044				
B3-86-5b	7.5	5	5%	1.044	0.00			
B3-86-6a	7.5	6	30%	1.044				
B3-86-6b	7.5	6	30%	1.044	0.00	**0.10**	**9%**	**33%**

Table E7. Probability of failure calculations for boring B-3 at 91 ft depth.

Most Likely Value of FS =				0.993				
Case	**WL**	**Layer #**	**COV**	**FS**	**Delta FS**	**Std Dev of FS**	**COV of FS**	**Prob of failure**
B3-91-1a	7.5	1	5%	0.952				
B3-91-1b	7.5	1	5%	1.034	0.08			
B3-91-2a	7.5	2	30%	0.874				
B3-91-2b	7.5	2	30%	1.061	0.19			
B3-91-3a	7.5	3	5%	0.993				
B3-91-3b	7.5	3	5%	0.993	0.00			
B3-91-4a	7.5	4	30%	0.993				
B3-91-4b	7.5	4	30%	0.993	0.00			
B3-91-5a	7.5	5	5%	0.993				
B3-91-5b	7.5	5	5%	0.993	0.00			
B3-91-6a	7.5	6	30%	0.993				
B3-91-6b	7.5	6	30%	0.993	0.00	**0.10**	**10%**	**55%**

Table E8. Probability of failure calculations for boring B-3 at 96 ft depth.

Most Likely Value of FS =				0.975				
Case	**WL**	**Layer #**	**COV**	**FS**	**Delta FS**	**Std Dev of FS**	**COV of FS**	**Prob of failure**
B3-96-1a	7.5	1	5%	0.932				
B3-96-1b	7.5	1	5%	1.019	0.09			
B3-96-2a	7.5	2	30%	0.866				
B3-96-2b	7.5	2	30%	1.039	0.17			
B3-96-3a	7.5	3	5%	0.971				
B3-96-3b	7.5	3	5%	0.978	0.01			
B3-96-4a	7.5	4	30%	0.978				
B3-96-4b	7.5	4	30%	0.978	0.00			
B3-96-5a	7.5	5	5%	0.978				
B3-96-5b	7.5	5	5%	0.978	0.00			
B3-96-6a	7.5	6	30%	0.978				
B3-96-6b	7.5	6	30%	0.978	0.00	**0.10**	**10%**	**62%**

Table E9. Probability of failure calculations for boring B-3 at 111 ft depth.

Most Likely Value of FS =				0.957				
Case	**WL**	**Layer #**	**COV**	**FS**	**Delta FS**	**Std Dev of FS**	**COV of FS**	**Prob of failure**
B3-111-1a	7.5	1	5%	0.919				
B3-111-1b	7.5	1	5%	0.994	0.08			
B3-111-2a	7.5	2	30%	0.866				
B3-111-2b	7.5	2	30%	1.006	0.14			
B3-111-3a	7.5	3	5%	0.941				
B3-111-3b	7.5	3	5%	0.971	0.03			
B3-111-4a	7.5	4	30%	0.957				
B3-111-4b	7.5	4	30%	0.957	0.00			
B3-111-5a	7.5	5	5%	0.957				
B3-111-5b	7.5	5	5%	0.957	0.00			
B3-111-6a	7.5	6	30%	0.957				
B3-111-6b	7.5	6	30%	0.957	0.00	**0.08**	**8%**	**72%**

Table E10. Probability of failure calculations for boring B-3 at 136 ft depth.

Most Likely Value of FS =				0.941				
Case	**WL**	**Layer #**	**COV**	**FS**	**Delta FS**	**Std Dev of FS**	**COV of FS**	**Prob of failure**
B3-136-1a	7.5	1	5%	0.914				
B3-136-1b	7.5	1	5%	0.959	0.04			
B3-136-2a	7.5	2	30%	0.866				
B3-136-2b	7.5	2	30%	0.959	0.09			
B3-136-3a	7.5	3	5%	0.889				
B3-136-3b	7.5	3	5%	0.968	0.08			
B3-136-4a	7.5	4	30%	0.920				
B3-136-4b	7.5	4	30%	0.949	0.03			
B3-136-5a	7.5	5	5%	0.941				
B3-136-5b	7.5	5	5%	0.941	0.00			
B3-136-6a	7.5	6	30%	0.941				
B3-136-6b	7.5	6	30%	0.941	0.00	**0.07**	**7%**	**82%**

Table E11. Probability of failure calculations for boring B-3 at 150 ft depth.

Most Likely Value of FS =				0.928				
Case	**WL**	**Layer #**	**COV**	**FS**	**Delta FS**	**Std Dev of FS**	**COV of FS**	**Prob of failure**
B3-150-1a	7.5	1	5%	0.908				
B3-150-1b	7.5	1	5%	0.956	0.05			
B3-150-2a	7.5	2	30%	0.866				
B3-150-2b	7.5	2	30%	0.958	0.09			
B3-150-3a	7.5	3	5%	0.888				
B3-150-3b	7.5	3	5%	0.950	0.06			
B3-150-4a	7.5	4	30%	0.904				
B3-150-4b	7.5	4	30%	0.949	0.04			
B3-150-5a	7.5	5	5%	0.919				
B3-150-5b	7.5	5	5%	0.934	0.02			
B3-150-6a	7.5	6	30%	0.928				
B3-150-6b	7.5	6	30%	0.928	0.00	**0.06**	**7%**	**87%**

Results for probabilistic analyses for boring B-7 cross section

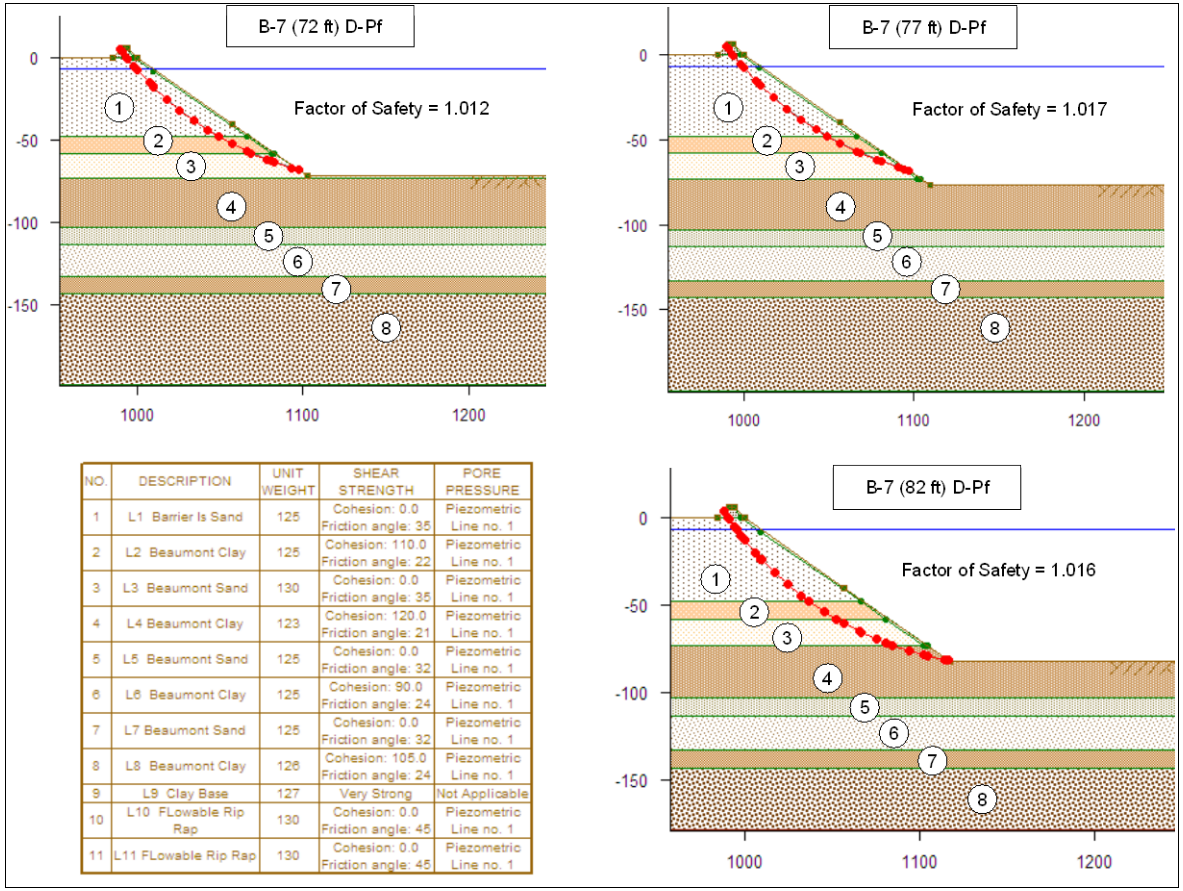

NO.	DESCRIPTION	UNIT WEIGHT	SHEAR STRENGTH	PORE PRESSURE
1	L1 Barrier Is Sand	125	Cohesion: 0.0 Friction angle: 35	Piezometric Line no. 1
2	L2 Beaumont Clay	125	Cohesion: 110.0 Friction angle: 22	Piezometric Line no. 1
3	L3 Beaumont Sand	130	Cohesion: 0.0 Friction angle: 35	Piezometric Line no. 1
4	L4 Beaumont Clay	123	Cohesion: 120.0 Friction angle: 21	Piezometric Line no. 1
5	L5 Beaumont Sand	125	Cohesion: 0.0 Friction angle: 32	Piezometric Line no. 1
6	L6 Beaumont Clay	125	Cohesion: 90.0 Friction angle: 24	Piezometric Line no. 1
7	L7 Beaumont Sand	125	Cohesion: 0.0 Friction angle: 32	Piezometric Line no. 1
8	L8 Beaumont Clay	126	Cohesion: 105.0 Friction angle: 24	Piezometric Line no. 1
9	L9 Clay Base	127	Very Strong	Not Applicable
10	L10 FLowable Rip Rap	130	Cohesion: 0.0 Friction angle: 45	Piezometric Line no. 1
11	L11 FLowable Rip Rap	130	Cohesion: 0.0 Friction angle: 45	Piezometric Line no. 1

Figure E5. Probabilistic stability analyses using drained properties for boring B-7 showing critical failure surface for 72, 77, and 82 ft depths and property table.

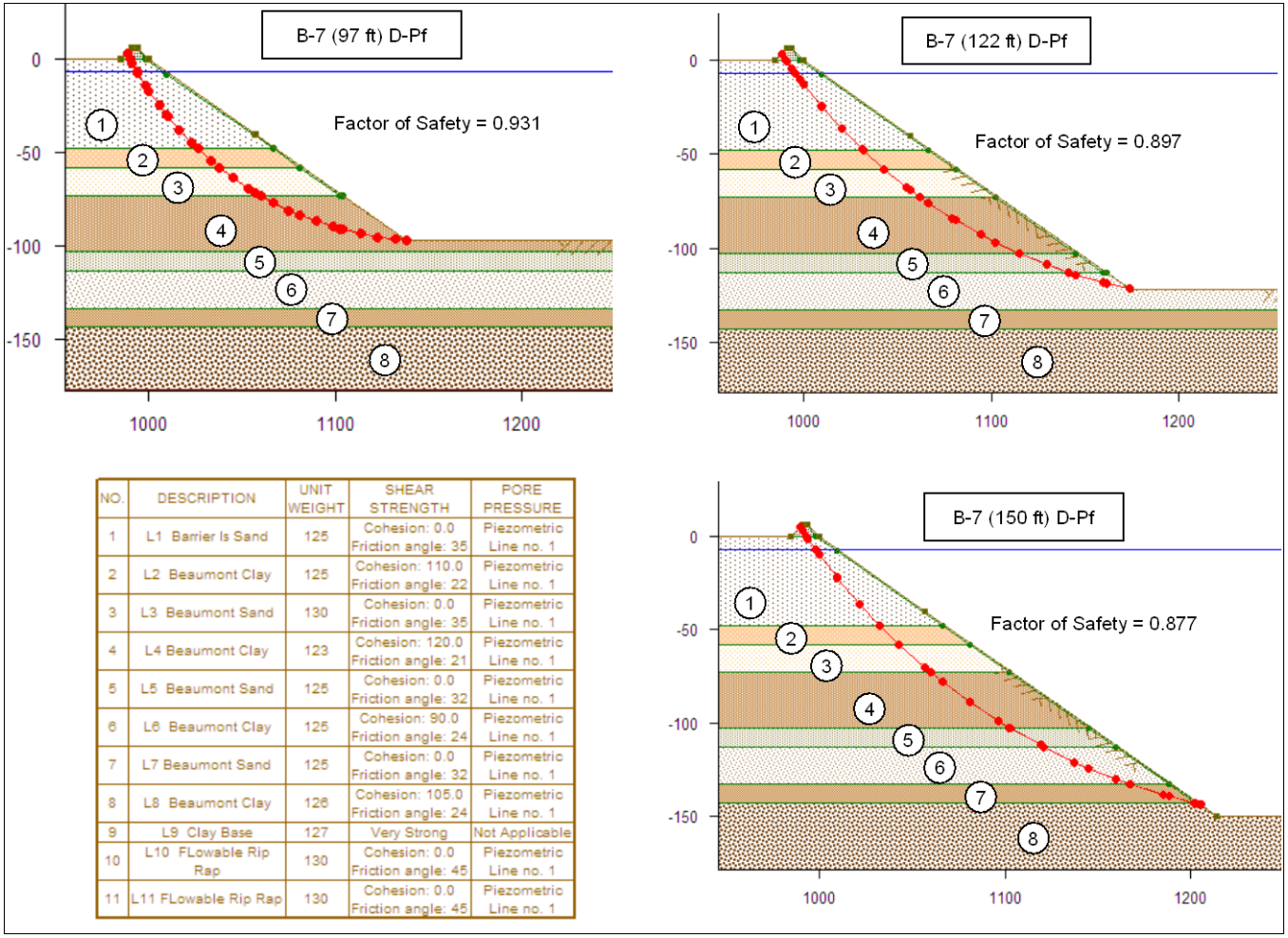

NO.	DESCRIPTION	UNIT WEIGHT	SHEAR STRENGTH	PORE PRESSURE
1	L1 Barrier Is Sand	125	Cohesion: 0.0 Friction angle: 35	Piezometric Line no. 1
2	L2 Beaumont Clay	125	Cohesion: 110.0 Friction angle: 22	Piezometric Line no. 1
3	L3 Beaumont Sand	130	Cohesion: 0.0 Friction angle: 35	Piezometric Line no. 1
4	L4 Beaumont Clay	123	Cohesion: 120.0 Friction angle: 21	Piezometric Line no. 1
5	L5 Beaumont Sand	125	Cohesion: 0.0 Friction angle: 32	Piezometric Line no. 1
6	L6 Beaumont Clay	125	Cohesion: 90.0 Friction angle: 24	Piezometric Line no. 1
7	L7 Beaumont Sand	125	Cohesion: 0.0 Friction angle: 32	Piezometric Line no. 1
8	L8 Beaumont Clay	126	Cohesion: 105.0 Friction angle: 24	Piezometric Line no. 1
9	L9 Clay Base	127	Very Strong	Not Applicable
10	L10 FLowable Rip Rap	130	Cohesion: 0.0 Friction angle: 45	Piezometric Line no. 1
11	L11 FLowable Rip Rap	130	Cohesion: 0.0 Friction angle: 45	Piezometric Line no. 1

Figure E6. Probabilistic stability analyses using drained properties for boring B-7 showing critical failure surface for 97, 122, and 150 ft depths and property table.

Table E12. Probability of failure calculations for boring B-7 at 72 ft depth.

Most Likely Value of FS =				1.012				
Case	**WL**	**Layer #**	**COV**	**FS**	**Delta FS**	**Std Dev of FS**	**COV of FS**	**Prob of failure**
B7-72-1a	7	1	5%	0.974				
B7-72-1b	7	1	5%	1.048	0.07			
B7-72-2a	7	2	30%	0.970				
B7-72-2b	7	2	30%	1.036	0.07			
B7-72-3a	7	3	5%	0.997				
B7-72-3b	7	3	5%	1.022	0.03			
B7-72-4a	7	4	30%	1.012				
B7-72-4b	7	4	30%	1.012	0.00			
B7-72-5a	7	5	5%	1.012				
B7-72-5b	7	5	5%	1.012	0.00			
B7-72-6a	7	6	30%	1.012				
B7-72-6b	7	6	30%	1.012	0.00			
B7-72-7a	7	7	5%	1.012				
B7-72-7b	7	7	5%	1.012	0.00			
B7-72-8a	7	8	30%	1.012				
B7-72-8b	7	8	30%	1.012	0.00	**0.05**	**5%**	**42%**

Table E13. Probability of failure calculations for boring B-7 at 77 ft depth.

Most Likely Value of FS =				1.017				
Case	**WL**	**Layer #**	**COV**	**FS**	**Delta FS**	**Std Dev of FS**	**COV of FS**	**Prob of failure**
B7-77-1a	7	1	5%	0.958				
B7-77-1b	7	1	5%	1.057	0.10			
B7-77-2a	7	2	30%	0.976				
B7-77-2b	7	2	30%	1.032	0.06			
B7-77-3a	7	3	5%	0.996				
B7-77-3b	7	3	5%	1.028	0.03			
B7-77-4a	7	4	30%	1.002				
B7-77-4b	7	4	30%	1.017	0.01			
B7-77-5a	7	5	5%	1.017				
B7-77-5b	7	5	5%	1.017	0.00			
B7-77-6a	7	6	30%	1.017				
B7-77-6b	7	6	30%	1.017	0.00			
B7-77-7a	7	7	5%	1.017				
B7-77-7b	7	7	5%	1.017	0.00			
B7-77-8a	7	8	30%	1.017				
B7-77-8b	7	8	30%	1.017	0.00	**0.06**	**6%**	**40%**

Table E14. Probability of failure calculations for boring B-7 at 82 ft depth.

Most Likely Value of FS =				1.016				
Case	**WL**	**Layer #**	**COV**	**FS**	**Delta FS**	**Std Dev of FS**	**COV of FS**	**Prob of failure**
B7-82-1a	7	1	5%	0.959				
B7-82-1b	7	1	5%	1.043	0.08			
B7-82-2a	7	2	30%	0.996				
B7-82-2b	7	2	30%	1.030	0.03			
B7-82-3a	7	3	5%	0.992				
B7-82-3b	7	3	5%	1.036	0.04			
B7-82-4a	7	4	30%	0.959				
B7-82-4b	7	4	30%	1.017	0.06			
B7-82-5a	7	5	5%	1.016				
B7-82-5b	7	5	5%	1.016	0.00			
B7-82-6a	7	6	30%	1.016				
B7-82-6b	7	6	30%	1.016	0.00			
B7-82-7a	7	7	5%	1.016				
B7-82-7b	7	7	5%	1.016	0.00			
B7-82-8a	7	8	30%	1.016				
B7-82-8b	7	8	30%	1.016	0.00	**0.06**	**6%**	**41%**

Table E15. Probability of failure calculations for boring B-7 at 97 ft depth.

Most Likely Value of FS =				0.931				
Case	**WL**	**Layer #**	**COV**	**FS**	**Delta FS**	**Std Dev of FS**	**COV of FS**	**Prob of failure**
B7-97-1a	7	1	5%	0.916				
B7-97-1b	7	1	5%	0.946	0.03			
B7-97-2a	7	2	30%	0.914				
B7-97-2b	7	2	30%	0.948	0.03			
B7-97-3a	7	3	5%	0.917				
B7-97-3b	7	3	5%	0.945	0.03			
B7-97-4a	7	4	30%	0.816				
B7-97-4b	7	4	30%	1.003	0.19			
B7-97-5a	7	5	5%	0.931				
B7-97-5b	7	5	5%	0.931	0.00			
B7-97-6a	7	6	30%	0.931				
B7-97-6b	7	6	30%	0.931	0.00			
B7-97-7a	7	7	5%	0.931				
B7-97-7b	7	7	5%	0.931	0.00			
B7-97-8a	7	8	30%	0.931				
B7-97-8b	7	8	30%	0.931	0.00	**0.10**	**10%**	**78%**

Table E16. Probability of failure calculations for boring B-7 at 122 ft depth.

Most Likely Value of FS =				0.897				
Case	**WL**	**Layer #**	**COV**	**FS**	**Delta FS**	**Std Dev of FS**	**COV of FS**	**Prob of failure**
B7-122-1a	7	1	5%	0.885				
B7-122-1b	7	1	5%	0.909	0.02			
B7-122-2a	7	2	30%	0.886				
B7-122-2b	7	2	30%	0.908	0.02			
B7-122-3a	7	3	5%	0.888				
B7-122-3b	7	3	5%	0.906	0.02			
B7-122-4a	7	4	30%	0.828				
B7-122-4b	7	4	30%	0.961	0.13			
B7-122-5a	7	5	5%	0.888				
B7-122-5b	7	5	5%	0.906	0.02			
B7-122-6a	7	6	30%	0.871				
B7-122-6b	7	6	30%	0.901	0.03			
B7-122-7a	7	7	5%	0.897				
B7-122-7b	7	7	5%	0.897	0.00			
B7-122-8a	7	8	30%	0.897				
B7-122-8b	7	8	30%	0.897	0.00	**0.07**	**8%**	**92%**

Table E17. Probability of failure calculations for boring B-7 at 150 ft depth.

Most Likely Value of FS =				0.877				
Case	**WL**	**Layer #**	**COV**	**FS**	**Delta FS**	**Std Dev of FS**	**COV of FS**	**Prob of failure**
B7-150-1a	7	1	5%	0.868				
B7-150-1b	7	1	5%	0.884	0.02			
B7-150-2a	7	2	30%	0.869				
B7-150-2b	7	2	30%	0.884	0.02			
B7-150-3a	7	3	5%	0.871				
B7-150-3b	7	3	5%	0.888	0.02			
B7-150-4a	7	4	30%	0.791				
B7-150-4b	7	4	30%	0.922	0.13			
B7-150-5a	7	5	5%	0.870				
B7-150-5b	7	5	5%	0.883	0.01			
B7-150-6a	7	6	30%	0.815				
B7-150-6b	7	6	30%	0.902	0.09			
B7-150-7a	7	7	5%	0.870				
B7-150-7b	7	7	5%	0.879	0.01			
B7-150-8a	7	8	30%	0.871				
B7-150-8b	7	8	30%	0.877	0.01	**0.08**	**9%**	**93%**

Appendix F: Pairwise Comparisons used in Expert Elicitation of Pilots

General

Our goal of these questions is to determine the likelihood or probability of grounding in the MSC entrance under various conditions. For example, we want to know the likelihood of a large deep draft ship going inbound with flood tide in less than 3 knot bottleneck currents compared to a large deep draft ship with flood tide going inbound in greater than 5 knot bottleneck currents. Notice that we only changed one item, the speed of the current. In almost all of the questions you are asked, we will change only one item. Previous studies have shown that this is the most reliable way to obtain knowledge from experts.

We are not asking you how frequently you will ground such as once in every 1,000, 2,000, or 5,000 transits.

We are asking you to compare two situations and tell us which is most likely to result in grounding and by how much is it more likely to do so. We could probably get other people to tell us which of two situations is more important to grounding and get it right some/most of the time. Only you, the pilots, can tell us how much more likely or important one situation is compared to another.

The following example shows the format of the questions.

Example

You want to predict if it will be raining or not raining tomorrow based on today's weather condition. Let us assume today's condition is cloudy and it is a little humid. You and your friends are discussing what is the likelihood of raining tomorrow, or not raining and how much more likely one might be over the other.

Situation 1	**Attribute**	**Situation 2**
Raining	Weather condition	Not raining
What is the likelihood of raining tomorrow?		
9 8 7 6 5 4 3 2 1 2 3 4 5 6 7 8 9		

We give the above form to you and three of your friends. Friend A says not raining is 2 times more likely than raining and circles a 2 on the right side of the scale because that is the side corresponding to not raining. Friend B says it is 3 times more likely to be not raining than raining and circles a 3 on the right side of the scale. Friend C says raining and not raining are equally likely and circles the 1 in the middle of the scale. You believe not raining and raining are close but not raining is slightly more likely. You think not raining is less than 2 times more likely than raining. You can write in any value you want (must be 1 or greater) on the right side of the scale such as 1.5. We can combine your and your friend's opinions in various ways such as simply averaging all of the responses. This results in (2 + 3 + 1 + 1.5)/4 = 1.87. You and your friends, on average, believe that not raining is 1.87 times more likely than raining based on the simple averaging method.

Breakdown of Matagorda ship channel navigation

Reach location

Our study area is the gulf to just north of Sundown Island before you get to the intersection of the south GIWW. This study area was selected because this is the area where navigation safety is most affected by removal of the bottleneck, which is one of the options being studied. We have broken the study area into two reaches. The first is the gulf to the bottleneck (G-B) and the second is the bottleneck to north of Sundown Island (B-SI). The G-B reach has problems associated with the cross currents at the gulf entrance, getting the ship aligned with the channel before reaching the bottleneck, and the high currents in the bottleneck. The B-SI reach has a course change, rapid depth change, cross flow from the effects of Sundown Island, and the effects of high currents in the bottleneck. The two reaches are shown in Figure F1.

Ship direction

The next division of navigation conditions is by ship direction.

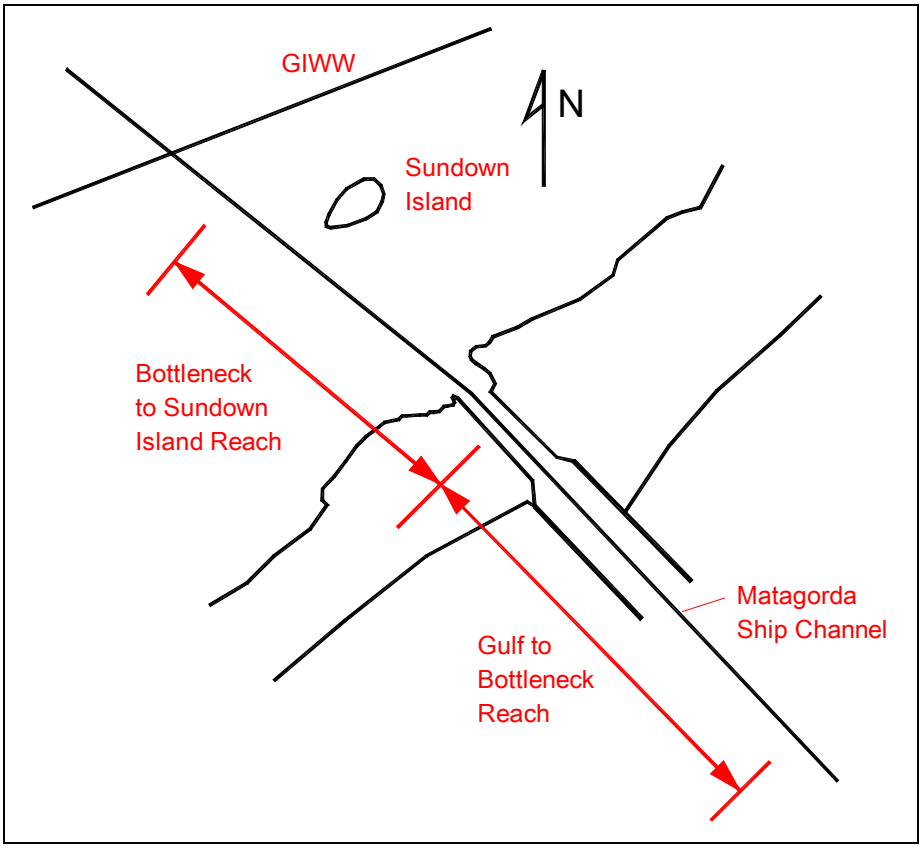

Figure F1. Division of study area into reaches used in expert comparisons.

Tide direction

The next division of navigation conditions is by tide direction.

Attributes

The next division of navigation conditions is divided into attributes describing ship and environmental conditions. For outbound ships in both the G-B reach and the B-SI reach and inbound ships in the B-SI reach, the 3 attributes are tidal current magnitude, ship class, and visibility. For inbound ships in the G-B reach, cross currents are added to the other 3 attributes.

Attribute magnitudes

Each of the attributes was divided into ranges as follows:

1. **Tidal Current Magnitude**. Based on input from the pilots, tidal currents in the bottleneck were divided into light (< 3 knots), medium (3 to < 5 knots), and strong (5 knots and greater).

2. **Ship Class**. Based on the daylight restriction rules, pilot input, and difficulty of nighttime navigation, ships class was divided into four categories: (1) not daylight restricted (during day), (2) not daylight restricted (at night), (3) daylight restricted with draft less than 34 ft, and (4) daylight restricted with draft of 34 ft and greater.

3. **Visibility**. Based on pilot input, visibility was divided into > 1 mile and < = 1 mile for outbound ships and > 3 miles and, < = 3 miles for inbound ships.

4. **Cross Currents**. Cross currents were divided into 3 categories of light, medium, and strong. We are still working on determining numbers to describe the categories of cross currents.

A schematic of the breakdown of the navigation system is shown in Figure F2.

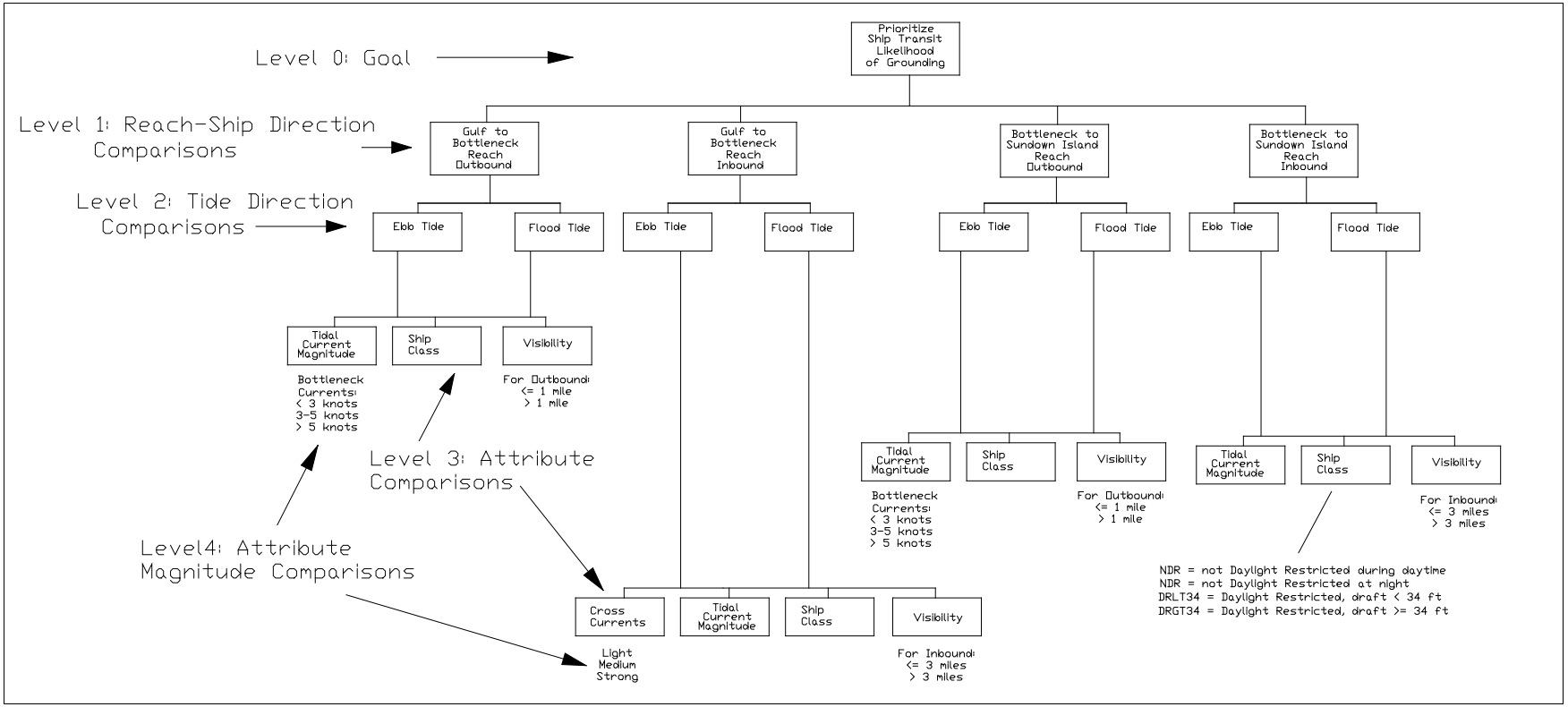

Figure F2. Schematic of breakdown of navigation attributes contributing to likelihood of grounding.

Comparisons

Level 1: Reach-Ship Direction Comparisons. For the following six comparisons of reach location and ship direction, assume you are in difficult transit conditions when you make the comparison. An example would be assuming the ship is going with the tide in both cases when comparing ships going inbound versus outbound.

Table F1.

Situation 1	Attribute	Situation 2
Gulf to Bottleneck - Inbound Ship	Reach Location and Ship Direction	Gulf to Bottleneck - Outbound Ship
What situation is most likely to experience grounding, Inbound Ship in the Gulf to Bottleneck Reach or Outbound Ship in the Gulf to Bottleneck Reach?		
9 8 7 6 5 4 3 2 1 2 3 4 5 6 7 8 9		

Table F2.

Situation 1	Attribute	Situation 2
Bottleneck to Sundown Island - Inbound Ship	Reach Location and Ship Direction	Bottleneck to Sundown Island - Outbound Ship
What situation is most likely to experience grounding, Inbound Ship in the Bottleneck to Sundown Island Reach or Outbound Ship in the Bottleneck to Sundown Island Reach?		
9 8 7 6 5 4 3 2 1 2 3 4 5 6 7 8 9		

Table F3.

Situation 1	Attribute	Situation 2
Gulf to Bottleneck - Inbound Ship	Reach Location and Ship Direction	Bottleneck to Sundown Island - Inbound Ship
What situation is most likely to experience grounding, Inbound Ship in the Gulf to Bottleneck Reach or Inbound Ship in the Bottleneck to Sundown Island Reach?		
9 8 7 6 5 4 3 2 1 2 3 4 5 6 7 8 9		

Table F4.

Situation 1	Attribute	Situation 2
Gulf to Bottleneck - Outbound Ship	Reach Location and Ship Direction	Bottleneck to Sundown Island - Outbound Ship
What situation is most likely to experience grounding, Outbound Ship in the Gulf to Bottleneck Reach or Outbound Ship in the Bottleneck to Sundown Island Reach?		
9 8 7 6 5 4 3 2 1 2 3 4 5 6 7 8 9		

Table F5.

Situation 1	Attribute	Situation 2
Gulf to Bottleneck - Inbound Ship	Reach Location and Ship Direction	Bottleneck to Sundown Island - Outbound Ship
What situation is most likely to experience grounding, Inbound Ship in the Gulf to Bottleneck Reach or Outbound Ship in the Bottleneck to Sundown Island Reach?		
9 8 7 6 5 4 3 2 1 2 3 4 5 6 7 8 9		

Table F6.

Situation 1	Attribute	Situation 2
Gulf to Bottleneck - Outbound Ship	Reach Location and Ship Direction	Bottleneck to Sundown Island - Inbound Ship
What situation is most likely to experience grounding, Outbound Ship in the Gulf to Bottleneck Reach or Inbound Ship in the Bottleneck to Sundown Island Reach?		
9 8 7 6 5 4 3 2 1 2 3 4 5 6 7 8 9		

Level 2: Tide Direction Comparisons. For the next four comparisons of tide direction, note that the reach location and ship direction has been specified in each comparison. Assume you are in difficult transit conditions when you make the comparisons.

Table F7. Outbound Ship in Gulf to Bottleneck Reach.

Situation 1	Attribute	Situation 2
Gulf to Bottleneck- Outbound	Reach Location- Ship Direction	*
Against Ship (Flood)	Tide Direction	With Ship (ebb)
Which situation is more likely to result in grounding in the G-B reach, an outbound ship against a flood tide or an outbound ship with an ebb tide?		
9 8 7 6 5 4 3 2 1 2 3 4 5 6 7 8 9		

* same as situation 1

Table F8. Inbound Ship in Gulf to Bottleneck Reach.

Situation 1	Attribute	Situation 2
Gulf to Bottleneck- Inbound	Reach Location- Ship Direction	*
With Ship (Flood)	Tide Direction	Against Ship (ebb)
Which situation is more likely to result in grounding in the G-B reach, an inbound ship with a flood tide or an inbound ship against an ebb tide?		
9 8 7 6 5 4 3 2 1 2 3 4 5 6 7 8 9		

* same as situation 1

Table F9. Outbound Ship in Bottleneck to Sundown Reach.

Situation 1	Attribute	Situation 2
Bottleneck to Sundown Island- Outbound	Reach Location- Ship Direction	*
Against Ship (Flood)	Tide Direction	With Ship (ebb)
Which situation is more likely to result in grounding in the B-SI reach, an outbound ship against a flood tide or an outbound ship with an ebb tide?		
9 8 7 6 5 4 3 2 1 2 3 4 5 6 7 8 9		

* same as situation 1

Table F10. Inbound Ship in Bottleneck to Sundown Reach.

Situation 1	Attribute	Situation 2
Bottleneck to Sundown Island- Inbound	Reach Location- Ship Direction	*
With Ship (Flood)	Tide Direction	Against Ship (ebb)
Which situation is more likely to result in grounding in the B-SI reach, an inbound ship with a flood tide or an inbound ship against an ebb tide?		
9 8 7 6 5 4 3 2 1 2 3 4 5 6 7 8 9		

* same as situation 1

Level 3: Attribute Comparisons. In the next 15 comparisons of the factors or attributes important to navigation, note that reach location and ship direction has been specified for each comparison. Assume you are in difficult transit conditions when you make the comparisons.

Table F11. Gulf to Bottleneck Reach - Inbound Ship.

Situation 1	Attribute	Situation 2
Gulf to Bottleneck	Location	*
Inbound	Ship Direction	*
Magnitude of Tidal Currents		Ship Class
Which is more important to likelihood of grounding, magnitude of tidal currents or ship class?		
9 8 7 6 5 4 3 2 1 2 3 4 5 6 7 8 9		

* same as situation 1

Table F12. Gulf to Bottleneck Reach - Inbound Ship.

Situation 1	Attribute	Situation 2
Gulf to Bottleneck	Location	*
Inbound	Ship Direction	*
Magnitude of Tidal Currents		Visibility
Which is more important to likelihood of grounding, magnitude of tidal currents or visibility?		
9 8 7 6 5 4 3 2 1 2 3 4 5 6 7 8 9		

* same as situation 1

Table F13. Gulf to Bottleneck Reach - Inbound Ship.

Situation 1	Attribute	Situation 2
Gulf to Bottleneck	Location	*
Inbound	Ship Direction	*
Magnitude of Tidal Currents		Cross currents at jetty entrance
Which is more important to likelihood of grounding, magnitude of tidal currents or cross currents at jetty entrance?		
9 8 7 6 5 4 3 2 1 2 3 4 5 6 7 8 9		

* same as situation 1

Table F14. Gulf to Bottleneck Reach - Inbound Ship.

Situation 1	Attribute	Situation 2
Gulf to Bottleneck	Location	*
Inbound	Ship Direction	*
Ship Class		Visibility
Which is more important to likelihood of grounding, ship class or visibility?		
9 8 7 6 5 4 3 2 1 2 3 4 5 6 7 8 9		

* same as situation 1

Table F15. Gulf to Bottleneck Reach - Inbound Ship.

Situation 1	Attribute	Situation 2
Gulf to Bottleneck	Location	*
Inbound	Ship Direction	*
Cross Currents		Ship Class
Which is more important to likelihood of grounding, cross currents at jetty entrance or ship class?		
9 8 7 6 5 4 3 2 1 2 3 4 5 6 7 8 9		

* same as situation 1

Table F16. Gulf to Bottleneck Reach - Inbound Ship.

Situation 1	Attribute	Situation 2
Gulf to Bottleneck	Location	*
Inbound	Ship Direction	*
Cross currents		Visibility
Which is more important to likelihood of grounding, cross currents at jetty entrance or visibility?		
9 8 7 6 5 4 3 2 1 2 3 4 5 6 7 8 9		

* same as situation 1

Table F17. Gulf to Bottleneck Reach - Outbound Ship.

Situation 1	Attribute	Situation 2
Gulf to Bottleneck	Location	*
Outbound	Ship Direction	*
Magnitude of Tidal Currents		Ship Class
Which is more important to likelihood of grounding, magnitude of tidal currents or ship class?		
9 8 7 6 5 4 3 2 1 2 3 4 5 6 7 8 9		

* same as situation 1

Table F18. Gulf to Bottleneck Reach - Outbound Ship.

Situation 1	Attribute	Situation 2
Gulf to Bottleneck	Location	*
Outbound	Ship Direction	*
Magnitude of Tidal Currents		Visibility
Which is more important to likelihood of grounding, magnitude of tidal currents or visibility?		
9 8 7 6 5 4 3 2 1 2 3 4 5 6 7 8 9		

* same as situation 1

Table F19. Gulf to Bottleneck Reach - Outbound Ship.

Situation 1	Attribute	Situation 2
Gulf to Bottleneck	Location	*
Outbound	Ship Direction	*
Ship Class		Visibility
Which is more important to likelihood of grounding, ship class or visibility?		
9 8 7 6 5 4 3 2 1 2 3 4 5 6 7 8 9		

* same as situation 1

Table F20. Bottleneck to Sundown Reach - Inbound Ship.

Situation 1	Attribute	Situation 2
Bottleneck to Sundown	Location	*
Inbound	Ship Direction	*
Magnitude of Tidal Currents		Ship Class
Which is more important to likelihood of grounding, magnitude of tidal currents or ship class?		
9 8 7 6 5 4 3 2 1 2 3 4 5 6 7 8 9		

* same as situation 1

Table F21. Bottleneck to Sundown Reach - Inbound Ship.

Situation 1	Attribute	Situation 2
Bottleneck to Sundown	Location	*
Inbound	Ship Direction	*
Magnitude of Tidal Currents		Visibility
Which is more important to likelihood of grounding, magnitude of tidal currents or visibility?		
9 8 7 6 5 4 3 2 1 2 3 4 5 6 7 8 9		

* same as situation 1

Table F22. Bottleneck to Sundown Reach - Inbound Ship.

Situation 1	Attribute	Situation 2
Bottleneck to Sundown	Location	*
Inbound	Ship Direction	*
Ship Class		Visibility
Which is more important to likelihood of grounding, ship class or visibility?		
9 8 7 6 5 4 3 2 1 2 3 4 5 6 7 8 9		

* same as situation 1

Table F23. Bottleneck to Sundown Reach - Outbound Ship.

Situation 1	Attribute	Situation 2
Bottleneck to Sundown	Location	*
Outbound	Ship Direction	*
Magnitude of Tidal Currents		Ship Class
Which is more important to likelihood of grounding, magnitude of tidal currents or ship class?		
9 8 7 6 5 4 3 2 1 2 3 4 5 6 7 8 9		

* same as situation 1

Table F24. Bottleneck to Sundown Reach - Outbound Ship.

Situation 1	Attribute	Situation 2
Bottleneck to Sundown	Location	*
Outbound	Ship Direction	*
Magnitude of Tidal Currents		Visibility
Which is more important to likelihood of grounding, magnitude of tidal currents or visibility?		
9 8 7 6 5 4 3 2 1 2 3 4 5 6 7 8 9		

* same as situation 1

Table F25. Bottleneck to Sundown Reach - Outbound Ship.

Situation 1	Attribute	Situation 2
Bottleneck to Sundown	Location	*
Outbound	Ship Direction	*
Ship Class		Visibility
Which is more important to likelihood of grounding, ship class or visibility?		
9 8 7 6 5 4 3 2 1 2 3 4 5 6 7 8 9		

* same as situation 1

Level 4: Attribute Magnitude Comparisons. In the final set of comparisons, you will be comparing the magnitude of each factor or attribute important to navigation.

Table F26. Gulf to Bottleneck Reach - Inbound Ship.

Situation 1	Attribute	Situation 2
Gulf to Bottleneck	Location	*
Inbound	Ship Direction	*
Flood	Tide Direction	*
3-5 knots	Tidal Current Magnitude	*
Daylight restricted, draft 34 ft and greater	Ship Class	*
3 miles	Visibility	*
Light	Cross Currents	Medium
Which is more likely to ground, light cross currents at jetty entrance or medium cross currents at jetty entrance?		
9 8 7 6 5 4 3 2 1 2 3 4 5 6 7 8 9		

* same as situation 1

Table F27. Gulf to Bottleneck Reach - Inbound Ship.

Situation 1	Attribute	Situation 2
Gulf to Bottleneck	Location	*
Inbound	Ship Direction	*
Flood	Tide Direction	*
3-5 knots	Tidal Current Magnitude	*
Daylight restricted, draft 34 ft and greater	Ship Class	*
3 miles	Visibility	*
Medium	Cross Currents	Strong
Which is more likely to ground, light cross currents at jetty entrance or medium cross currents at jetty entrance?		
9 8 7 6 5 4 3 2 1 2 3 4 5 6 7 8 9		

* same as situation 1

Table F28. Gulf to Bottleneck Reach - Inbound Ship.

Situation 1	Attribute	Situation 2
Gulf to Bottleneck	Location	*
Inbound	Ship Direction	*
Flood	Tide Direction	*
3-5 knots	Tidal Current Magnitude	*
Daylight restricted, draft 34 ft and greater	Ship Class	*
3 miles	Visibility	*
Light	Cross Currents	Strong
Which is more likely to ground, light cross currents at jetty entrance or medium cross currents at jetty entrance?		
9 8 7 6 5 4 3 2 1 2 3 4 5 6 7 8 9		

* same as situation 1

Table F29. Gulf to Bottleneck Reach - Inbound Ship.

Situation 1	Attribute	Situation 2
Gulf to Bottleneck	Location	*
Inbound	Ship Direction	*
Flood	Tide Direction	*
Daylight restricted, draft 34 ft and greater	Ship Class	*
3 miles	Visibility	*
Medium	Cross Currents	*
Less than 3 knots	Tidal Current Magnitude	3 knots to less than 5 knots
Which is more likely to ground, < 3 knot tidal currents in the bottleneck or 3 knots to less than 5 knot tidal currents in the bottleneck?		
9 8 7 6 5 4 3 2 1 2 3 4 5 6 7 8 9		

* same as situation 1

Table F30. Gulf to Bottleneck Reach - Inbound Ship.

Situation 1	Attribute	Situation 2
Gulf to Bottleneck	Location	*
Inbound	Ship Direction	*
Flood	Tide Direction	*
Daylight restricted, draft 34 ft and greater	Ship Class	*
3 miles	Visibility	*
Medium	Cross Currents	*
3 knots to less than 5 knots	Tidal Current Magnitude	5 knots and greater
Which is more likely to ground, 3 knots to < 5 knots tidal currents in the bottleneck or 5 knots and greater tidal currents in the bottleneck?		
9 8 7 6 5 4 3 2 1 2 3 4 5 6 7 8 9		

* same as situation 1

Table F31. Gulf to Bottleneck Reach - Inbound Ship.

Situation 1	Attribute	Situation 2
Gulf to Bottleneck	Location	*
Inbound	Ship Direction	*
Flood	Tide Direction	*
Daylight restricted, draft 34 ft and greater	Ship Class	*
3 miles	Visibility	*
Medium	Cross Currents	*
Less than 3 knots	Tidal Current Magnitude	5 knots and greater
Which is more likely to ground, < 3 knot tidal currents in the bottleneck or 5 knots and greater tidal currents in the bottleneck?		
9 8 7 6 5 4 3 2 1 2 3 4 5 6 7 8 9		

* same as situation 1

Table F32. Gulf to Bottleneck Reach - Inbound Ship.

Situation 1	Attribute	Situation 2
Gulf to Bottleneck	Location	*
Inbound	Ship Direction	*
Flood	Tide Direction	*
3-5 knots	Tidal Current Magnitude	*
3 miles	Visibility	*
Medium	Cross Currents	*
Not Daylight Restricted, during daytime	Ship Class	Not Daylight Restricted, at nighttime
Which is more likely to ground, not daylight restricted ship during daytime or not daylight restricted ship at nighttime?		
9 8 7 6 5 4 3 2 1 2 3 4 5 6 7 8 9		

* same as situation 1

Table F33. Gulf to Bottleneck Reach - Inbound Ship.

Situation 1	Attribute	Situation 2
Gulf to Bottleneck	Location	*
Inbound	Ship Direction	*
Flood	Tide Direction	*
3-5 knots	Tidal Current Magnitude	*
3 miles	Visibility	*
Medium	Cross Currents	*
Not Daylight Restricted, during daytime	Ship Class	Daylight Restricted, draft less than 34 ft
Which is more likely to ground, not daylight restricted ship during daytime or daylight restricted ship with draft less than 34 ft?		
9 8 7 6 5 4 3 2 1 2 3 4 5 6 7 8 9		

* same as situation 1

Table F34. Gulf to Bottleneck Reach - Inbound Ship.

Situation 1	Attribute	Situation 2
Gulf to Bottleneck	Location	*
Inbound	Ship Direction	*
Flood	Tide Direction	*
3-5 knots	Tidal Current Magnitude	*
3 miles	Visibility	*
Medium	Cross Currents	*
Not Daylight Restricted, during daytime	Ship Class	Daylight Restricted, draft 34 ft and greater
Which is more likely to ground, not daylight restricted ship during daytime or daylight restricted ship with draft 34 ft and greater?		
9 8 7 6 5 4 3 2 1 2 3 4 5 6 7 8 9		

* same as situation 1

Table F35. Gulf to Bottleneck Reach - Inbound Ship.

Situation 1	Attribute	Situation 2
Gulf to Bottleneck	Location	*
Inbound	Ship Direction	*
Flood	Tide Direction	*
3-5 knots	Tidal Current Magnitude	*
3 miles	Visibility	*
Medium	Cross Currents	*
Not Daylight Restricted, at nighttime	Ship Class	Daylight Restricted, draft less than 34 ft
Which is more likely to ground, not daylight restricted ship at nighttime or daylight restricted ship with draft less than 34 ft?		
9 8 7 6 5 4 3 2 1 2 3 4 5 6 7 8 9		

* same as situation 1

Table F36. Gulf to Bottleneck Reach - Inbound Ship.

Situation 1	Attribute	Situation 2
Gulf to Bottleneck	Location	*
Inbound	Ship Direction	*
Flood	Tide Direction	*
3-5 knots	Tidal Current Magnitude	*
3 miles	Visibility	*
Medium	Cross Currents	*
Not Daylight Restricted, at nighttime	Ship Class	Daylight Restricted, draft 34 ft and greater
Which is more likely to ground, not daylight restricted ship at nighttime or daylight restricted ship with draft 34 ft and greater?		
9 8 7 6 5 4 3 2 1 2 3 4 5 6 7 8 9		

* same as situation 1

Table F37. Gulf to Bottleneck Reach - Inbound Ship.

Situation 1	Attribute	Situation 2
Gulf to Bottleneck	Location	*
Inbound	Ship Direction	*
Flood	Tide Direction	*
3-5 knots	Tidal Current Magnitude	*
3 miles	Visibility	*
Medium	Cross Currents	*
Daylight Restricted, draft less than 34 ft	Ship Class	Daylight Restricted, draft 34 ft and greater
Which is more likely to ground, daylight restricted ship with draft less than 34 ft or daylight restricted ship with draft 34 ft and greater?		
9 8 7 6 5 4 3 2 1 2 3 4 5 6 7 8 9		

* same as situation 1

Table F38. Gulf to Bottleneck Reach - Inbound Ship.

Situation 1	Attribute	Situation 2
Gulf to Bottleneck	Location	*
Inbound	Ship Direction	*
Flood	Tide Direction	*
3-5 knots	Tidal Current Magnitude	*
Medium	Cross Currents	*
Daylight Restricted, draft 34 ft and greater	Ship Class	*
3 miles or less	Visibility	Greater than 3 miles
Which is more likely to ground, visibility of <= 3 miles or visibility of greater than 3 miles?		
9 8 7 6 5 4 3 2 1 2 3 4 5 6 7 8 9		

* same as situation 1

Note to Pilots: End of gulf to bottleneck comparisons.

Note to Pilots: New reach - Bottleneck to Sundown Island.

Table F39. Bottleneck to Sundown Reach - Outbound Ship.

Situation 1	Attribute	Situation 2
Bottleneck to Sundown	Location	*
Outbound	Ship Direction	*
Flood	Tide Direction	*
Daylight restricted, draft 34 ft and greater	Ship Class	*
1 mile	Visibility	*
Less than 3 knots	Tidal Current Magnitude	3 knots to less than 5 knots
Which is more likely to ground, < 3 knot tidal currents in the bottleneck or 3 knots to less than 5 knot tidal currents in the bottleneck?		
9 8 7 6 5 4 3 2 1 2 3 4 5 6 7 8 9		

* same as situation 1

Table F40. Bottleneck to Sundown Reach - Outbound Ship.

Situation 1	Attribute	Situation 2
Bottleneck to Sundown	Location	*
Outbound	Ship Direction	*
Flood	Tide Direction	*
Daylight restricted, draft 34 ft and greater	Ship Class	*
1 mile	Visibility	*
3 knots to less than 5 knots	Tidal Current Magnitude	5 knots and greater
Which is more likely to ground, 3 knots to < 5 knots tidal currents in the bottleneck or 5 knots and greater tidal currents in the bottleneck?		
9 8 7 6 5 4 3 2 1 2 3 4 5 6 7 8 9		

* same as situation 1

Table F41. Bottleneck to Sundown Reach - Outbound Ship.

Situation 1	Attribute	Situation 2
Bottleneck to Sundown	Location	*
Outbound	Ship Direction	*
Flood	Tide Direction	*
Daylight restricted, draft 34 ft and greater	Ship Class	*
1 mile	Visibility	*
Less than 3 knots	Tidal Current Magnitude	5 knots and greater
Which is more likely to ground, < 3 knot tidal currents in the bottleneck or 5 knots and greater tidal currents in the bottleneck?		
9 8 7 6 5 4 3 2 1 2 3 4 5 6 7 8 9		

* same as situation 1

Table F42. Bottleneck to Sundown Reach - Outbound Ship.

Situation 1	Attribute	Situation 2
Bottleneck to Sundown	Location	*
Outbound	Ship Direction	*
Flood	Tide Direction	*
3-5 knots	Tidal Current Magnitude	*
1 mile	Visibility	*
Not Daylight Restricted, during daytime	Ship Class	Not Daylight Restricted, at nighttime
Which is more likely to ground, not daylight restricted ship during daytime or not daylight restricted ship at nighttime?		
9 8 7 6 5 4 3 2 1 2 3 4 5 6 7 8 9		

* same as situation 1

Table F43. Bottleneck to Sundown Reach - Outbound ship.

Situation 1	Attribute	Situation 2
Bottleneck to Sundown	Location	*
Outbound	Ship Direction	*
Flood	Tide Direction	*
3-5 knots	Tidal Current Magnitude	*
1 mile	Visibility	*
Not Daylight Restricted, during daytime	Ship Class	Daylight Restricted, draft less than 34 ft
Which is more likely to ground, not daylight restricted ship during daytime or daylight restricted ship with draft less than 34 ft?		
9 8 7 6 5 4 3 2 1 2 3 4 5 6 7 8 9		

* same as situation 1

Table F44. Bottleneck to Sundown Reach - Outbound ship.

Situation 1	Attribute	Situation 2
Bottleneck to Sundown	Location	*
Outbound	Ship Direction	*
Flood	Tide Direction	*
3-5 knots	Tidal Current Magnitude	*
1 mile	Visibility	*
Not Daylight Restricted, during daytime	Ship Class	Daylight Restricted, draft 34 ft and greater
Which is more likely to ground, not daylight restricted ship during daytime or daylight restricted ship with draft 34 ft and greater?		
9 8 7 6 5 4 3 2 1 2 3 4 5 6 7 8 9		

* same as situation 1

Table F45. Bottleneck to Sundown Reach - Outbound ship.

Situation 1	Attribute	Situation 2
Bottleneck to Sundown	Location	*
Outbound	Ship Direction	*
Flood	Tide Direction	*
3-5 knots	Tidal Current Magnitude	*
1 mile	Visibility	*
Not Daylight Restricted, at nighttime	Ship Class	Daylight Restricted, draft less than 34 ft
Which is more likely to ground, not daylight restricted ship at nighttime or daylight restricted ship with draft less than 34 ft?		
9 8 7 6 5 4 3 2 1 2 3 4 5 6 7 8 9		

* same as situation 1

Table F46. Bottleneck to Sundown Reach - Outbound ship.

Situation 1	Attribute	Situation 2
Bottleneck to Sundown	Location	*
Outbound	Ship Direction	*
Flood	Tide Direction	*
3-5 knots	Tidal Current Magnitude	*
1 mile	Visibility	*
Not Daylight Restricted, at nighttime	Ship Class	Daylight Restricted, draft 34 ft and greater
Which is more likely to ground, not daylight restricted ship at nighttime or daylight restricted ship with draft 34 ft and greater?		
9 8 7 6 5 4 3 2 1 2 3 4 5 6 7 8 9		

* same as situation 1

Table F47. Bottleneck to Sundown Reach - Outbound ship.

Situation 1	Attribute	Situation 2
Bottleneck to Sundown	Location	*
Outbound	Ship Direction	*
Flood	Tide Direction	*
3-5 knots	Tidal Current Magnitude	*
1 mile	Visibility	*
Daylight Restricted, draft less than 34 ft	Ship Class	Daylight Restricted, draft 34 ft and greater
Which is more likely to ground, daylight restricted ship with draft less than 34 ft or daylight restricted ship with draft 34 ft and greater?		
9 8 7 6 5 4 3 2 1 2 3 4 5 6 7 8 9		

* same as situation 1

Table F48. Bottleneck to Sundown Reach - Outbound ship.

Situation 1	Attribute	Situation 2
Bottleneck to Sundown	Location	*
Outbound	Ship Direction	*
Flood	Tide Direction	*
3-5 knots	Tidal Current Magnitude	*
Daylight Restricted, draft 34 ft and greater	Ship Class	*
1 mile or less	Visibility	Greater than 1 mile
Which is more likely to ground, visibility of < = 1 mile or visibility of greater than 1 mile?		
9 8 7 6 5 4 3 2 1 2 3 4 5 6 7 8 9		

* same as situation 1

REPORT DOCUMENTATION PAGE

Form Approved
OMB No. 0704-0188

1. REPORT DATE *(DD-MM-YYYY)*	**2. REPORT TYPE**	**3. DATES COVERED** *(From - To)*
August 2011	Final Report	

4. TITLE AND SUBTITLE

Risks to Navigation at the Matagorda Ship Channel Entrance, Texas, Phase 2: Evaluation of Significant Risk Factors

5a. CONTRACT NUMBER

5b. GRANT NUMBER

5c. PROGRAM ELEMENT NUMBER

6. AUTHOR(S)

Stephen T. Maynord, Lihwa Lin, Nicholas C. Kraus, Dennis W. Webb, Gary Lynch, Ronald E. Wahl, Daniel A. Leavell, Don E. Yule, Joseph B. Dunbar

5d. PROJECT NUMBER

5e. TASK NUMBER

5f. WORK UNIT NUMBER

7. PERFORMING ORGANIZATION NAME(S) AND ADDRESS(ES)

Coastal and Hydraulics Laboratory and Geotechnical and Sturctures Laboratory
U.S. Army Engineer Research and Development Center
3909 Halls Ferry Road
Vicksburg, MS 39180-6199

8. PERFORMING ORGANIZATION REPORT NUMBER

ERDC TR-11-8

9. SPONSORING / MONITORING AGENCY NAME(S) AND ADDRESS(ES)

10. SPONSOR/MONITOR'S ACRONYM(S)

11. SPONSOR/MONITOR'S REPORT NUMBER(S)

12. DISTRIBUTION / AVAILABILITY STATEMENT

Approved for public release; distribution is unlimited.

13. SUPPLEMENTARY NOTES

14. ABSTRACT

The Phase 1 Matagorda study (Maynord et al. 2007) examined eight factors to identify which factors pose a significant risk of disrupting navigation at the Matagorda Ship Channel (MSC) entrance. Three factors were identified that warranted further study of the risk of disrupting navigation. These three factors were flanking of the jetty and slope protection, strong and asymmetric currents on the bay side of the peninsula and in the bottleneck (constricted portion of the entrance channel), and slope failures that constrict the channel, create adverse currents for navigation, or lead to shoaling of the channel. The risk factor of flanking and breaching of the jetty and slope protection was found to have a minimal risk of disrupting navigation because the cross current through the breach is weak compared to the longitudinal current in the navigation channel. The risk factor of slope failure from the continuing scour of the channel bottom will have a minimal risk of disrupting navigation because the size of the slope failures are not large enough to disrupt currents or cause shoaling problems. However, slope failures will increase in frequency and severity due to the continuing scour of the bottleneck. The risk factor of strong and asymmetric currents poses a significant risk of grounding in the existing navigation channel. In the bottleneck, surface currents at the center of the channel equal or exceed 3 knots more than 60 percent of the time and equal or exceed 5 knots 20 percent of the time. Based on expert elicitation of the pilots, the reach between the bottleneck and Sundown Island (B SI) is the reach most likely to experience a powered grounding. A ship simulator was used to evaluate the effects of removal of the bottleneck.

The Phase 2 MSC study recommends use of a "current window" that limits navigation to periods when current in the bottleneck is less than 5 knots. Daylight restricting all deep draft navigation should be considered. If the 5-knot current window and daylight restriction of all navigation cause unacceptable restrictions on navigation, the structural alternative of bottleneck removal will significantly reduce the likelihood of a powered grounding at the MSC Entrance. Relocation of Sundown Island should reduce adverse cross current effects in the bay.

15. SUBJECT TERMS

Asymetric currents
Deep draft navigation channel
Flanking and slope failures
Grounding
Matagorda ship channel
Navigation risk assessment

16. SECURITY CLASSIFICATION OF:			**17. LIMITATION OF ABSTRACT**	**18. NUMBER OF PAGES**	**19a. NAME OF RESPONSIBLE PERSON:**
a. REPORT	**b. ABSTRACT**	**c. THIS PAGE**			**19b. TELEPHONE NUMBER** *(include area code)*
UNCLASSIFIED	UNCLASSIFIED	UNCLASSIFIED		257	